Instanton theory for modelling the effect of tunneling in molecular systems

Eraković, Mihael

Doctoral thesis / Disertacija

2022

Degree Grantor / Ustanova koja je dodijelila akademski / stručni stupanj: **University of Zagreb, Faculty of Science / Sveučilište u Zagrebu, Prirodoslovno-matematički fakultet**

Permanent link / Trajna poveznica: https://urn.nsk.hr/urn:nbn:hr:217:944213

Rights / Prava: In copyright/Zaštićeno autorskim pravom.

Download date / Datum preuzimanja: **2025-01-25**

University of Zagreb
FACULTY OF SCIENCE

Mihael Eraković

INSTANTON THEORY FOR MODELLING THE EFFECT OF TUNNELING IN MOLECULAR SYSTEMS

DOCTORAL DISSERTATION

Supervisor:
Dr. Marko Tomislav Cvitaš

Zagreb, 2022

Sveučilište u Zagrebu

PRIRODOSLOVNO-MATEMATIČKI FAKULTET

Mihael Eraković

TEORIJA INSTANTONA ZA MODELIRANJE UČINKA TUNELIRANJA U MOLEKULARNIM SUSTAVIMA

DOKTORSKI RAD

Mentor:
dr. sc. Marko Tomislav Cvitaš

Zagreb, 2022

I would like to thank:

- my mentor Marko, for the given knowledge, patience and extensive discussions (and all the lessons on real life).

- Ćomo, Nađa and Jovan, for all the 'coffee breaks' and creating a wonderful and inspiring work environment.

- Anja, for always being by my side, finding all the best places to travel to and countless moments that we shared.

- members of the Belec team, for never giving up, despite all the fourth places.

- Kika, for the help with the LaTeX template.

- my mom, dad and uncle, for their endless support.

Contents

Sveučilište u Zagrebu

Doktorska disertacija

Prirodoslovno-matematički fakultet

Kemijski odsjek

SAŽETAK

TEORIJA INSTANTONA ZA MODELIRANJE UČINKA TUNELIRANJA U MOLEKULARNIM SUSTAVIMA

Mihael Eraković

Institut Ruđer Bošković, Bijenička cesta 54, 10 000 Zagreb, Hrvatska

Tuneliranje je kvantnomehanički efekt prolaska valnog paketa kroz regije u prostoru u kojima prema klasičnoj mehanici takav prolazak ne bi bio moguć zbog nedovoljne energije sustava. Tuneliranje uzrokuje pojavu cijepanja vibracijskih nivoa u sustavima koji sadrže nekoliko simetrijski povezanih minimuma. Modeliranje tuneliranja kvantnomehaničkim metodama iznimno je teško zbog velike osjetljivosti na potencijal i oblik valne funkcije. Teorija instantona je poluklasična metoda koja pruža dobar opis tuneliranjem uzrokovanog cijepanja vibracijskih stanja za osnovno vibracijsko i rotacijsko stanje molekula. Cilj ove disertacije je razviti i poboljšati teoriju instantona kako bi bila primjenjiva na pobuđena vibracijska i rotacijska stanja, sustave s asimetričnim potencijalnim jamama te ab initio potencijale. Dodatno, cilj je primijeniti razvijenu metodu kako bi se opisalo tuneliranjem uzrokovano cijepanje u molekuli malonaldehida, malih grozdovima vode te djelomično izotopno supstituiranim sustavima.

University of Zagreb Doctoral Thesis
Faculty of Science
Department of Chemistry

ABSTRACT

INSTANTON THEORY FOR MODELLING THE EFFECT OF TUNNELING IN MOLECULAR SYSTEMS

Mihael Eraković

Ruđer Bošković Institute, Bijenička cesta 54, 10 000 Zagreb, Croatia

Tunneling is a quantum mechanical effect in which wavepacket passes through regions which are classically inaccessible, due to the insufficient energy of the system. Tunneling causes splitting of the vibrational levels in systems which possess several symmetry-related minima. Modelling of tunneling effect using quantum mechanical methods is extremely challenging due to its sensitivity on the potential's and wavefunction's shapes. Instanton theory is a semiclassical method known to provide a good description of tunneling in the ground vibrational state. The goal of this thesis is to develop and improve instanton theory so that it can be applied to vibrationally excited states, systems with asymmetric potential energy wells and used with ab initio potentials. Additionally, the goal is to apply the developed theory to compute tunneling splittings in malonaldehyde and small water clusters, as well as on the molecules in which a part of identical atoms is substituted with different isotopes.

(134 + xxxvi pages, 22 figures, 21 tables, 139 references, original in English)

Sveučilište u Zagrebu   Doktorska disertacija
Prirodoslovno-matematički fakultet
Kemijski odsjek

PROŠIRENI SAŽETAK

Tuneliranje je kvantnomehanička pojava prolaska valnog paketa kroz područja u prostoru u kojima je potencijalna energija veća od njegove energije. Tu je pojavu prvi puta opisao Hund[1] 1927., a danas je poznato kako je tuneliranje uzrok nekoliko efekata značajnih u poljima spektroskopije i kemijske kinetike. Jedan od tih efekata je tuneliranjem uzrokovano cijepanje vibracijskih energijskih nivoa.[2] Ta je pojava prisutna kod molekula koje posjeduju barem dva minimuma povezana simetrijskim operacijama permutacija istovrsnih atoma te inverzije molekule, a koji su odvojeni barijerama potencijalne energije većima od vibracijske energije sustava. Ukoliko tuneliranje ne bi bilo prisutno u sustavu, svaki vibracijski nivo bio bi N-terostruko degeneriran, pri čemu je N broj simetrijski povezanih minimuma, te bi svako svojstveno stanje odgovaralo valnoj funkciji lokaliziranoj u jednom minimumu. Međutim, kao posljedica tuneliranja, postoji interakcija između različitih minimuma, što uzrokuje cijepanje degeneriranih nivoa te delokalizaciju svojstvenih stanja.

Tuneliranjem uzrokovano cijepanje vibracijskih nivoa uzrokuje cijepanje signala u mikrovalnom spektru, što omogućuje eksperimentalno određivanje iznosa cijepanja primjenom metoda mikrovalne spektroskopije visoke rezolucije. Te su metode iskorištene za određivanje cijepanja u grozdovima vode,[3] koji privlače poseban znanstveni interes. Jedan od razloga za navedeno je činjenica da su iznosi cijepanja direktno povezani s vremenskom skalom preslagivanja molekula vode u grozdovima, zbog čega se grozdovi vode koriste kao modelni sustav za istraživanje dinamike preslagivanja mreže vodikovih veza u tekućoj vodi.

Utjecaj tuneliranja može se modelirati kvantnomehaničkim metodama. Tuneliranjem uzrokovano cijepanje vibracijskih nivoa može se kvantificirati direktnim rješavanjem vremenski neovisne nuklearne Schrödingerove jednadžbe ili vremenski ovisnim metodama, kao što je multikonfiguracijska vremenski ovisna Hartreejeva metoda (MCTDH).[4] Međutim, ovakvi pristupi ograničeni su na sustave s malim brojem atoma zbog potrebe za poznavanjem čitave plohe potencijalne energije, čije je određivanje računalno zahtjevno. Također, iznosi cijepanja mogu varirati nekoliko redova veličine, čak unutar istog sustava, što znači da je često potrebno postići veliku točnost u vibracijskim energijama. To zahtijeva uporabu velikih osnovnih skupova te dugih vremena propagacije za vremenski ovisne metode. Vremenski neovisnim metodama određena su iznosi cijepanja za dimer fluorovodične kiseline,[5] dimer vode,[6] vinil radikal[7] i slične sustave, dok je MCTDH metodom određeno cijepanje u malonaldehidu.[8] Tuneliranjem uzrokovano cijepanje može se odrediti i primjenom metode difuzijskog Monte Carla, te je na taj način određeno cijepanje u trimeru vode[9] i u malonaldehidu.[10]

Efekti tuneliranja mogu se kvantificirati i uporabom teorije integrala po stazama (engl. *path integral*). Koristeći formalizam navedene teorije razvijena je metoda molekulske dinamike s prstenastim polimerom (engl. *ring-polymer molecular dynamics*, RPMD)[11] te teorija instantona.[12] Navedene metode omogućavaju aproksimativno određivanje kvantnih efekata uporabom klasične dinamike, što drastično smanjuje zahtjevnost računa te eliminira

potrebu za poznavanjem cijele plohe potencijalne energije. Teorija instantona temelji se na razvoju akcije oko klasične putanje na invertiranom potencijalu (putanje instantona) u Taylorov red do kvadratnog člana te je pokazano da daje izvrsne rezultate iznosa cijepanja u osnovnom vibracijskom stanju, pogotovo u slučajevima dubokog tuneliranja, za koje su kvantnomehaničke metode prezahtjevne. Postoje dvije osnovne varijante teorije instantona. Prva varijanta (engl. *ring-polymer instanton*, RPI)[13] temelji se na diskretizaciji putanje s jednakim razmacima u vremenu te konstrukciji i dijagonalizaciji hesijana akcije za dobivenu diskretizaciju. RPI metoda formulirana je u Kartezijevim koordinatama, što ju čini lako primjenjivom na proizvoljne sustave, te se može koristiti i u slučajevima putanja s asimetričnim profilom potencijalne energije duž putanje. Glavni nedostatci RPI metode su potreba za velikim brojem točaka korištenih za diskretizaciju putanje, što rezultira velikim brojem evaluacija gradijenta potencijalne energije prilikom optimizacije putanje te potreba za dijagonalizacijom hesijana akcije velikih dimenzija. Navedeno čini RPI metodu ograničenom na relativno male sustave za koje su poznate plohe potencijalne energije. Također, još uvijek nije poznato poopćenje RPI metode za tretman vibracijski pobuđenih stanja. Druga varijanta je teorija instantona temeljena na Jakobijevim poljima (engl. *Jacobi field instanton*, JFI)[14,15], unutar koje su izbjegnuti problemi RPI metode diskretizacijom putanje s jednakim razmakom u udaljenosti te svođenjem problema dijagonalizacije hesijana akcije na dijagonalizaciju Jacobijevih polja. Time se drastično smanjuje broj točaka potrebnih za diskretizaciju putanje, kao i broj evaluacija gradijenta potencijala prilikom optimizacije putanje te se izbjegava problem dijagonalizacije hesijana akcije. Navedeno čini JFI metodu pogodnom za određivanje cijepanja u većim sustavima te korištenje s potencijalima računatima u hodu. Međutim, JFI metoda trenutno je formulirana samo za sustave sa simetričnim potencijalom duž putanje instantona. Uz JFI metodu usko je povezana i Wentzel-Kramers-Brillouin (WKB) metoda na putanji instantona, modificirana na način da se energija tretira kao član prvog reda s obzirom na reduciranu Planckovu konstantu. Takvu teoriju razvijali su Mil'nikov i Nakamura[14] te je primijenili na račun cijepanja za hidroperoksilni radikal,[15] malonaldehid[14] i dimer mravlje kiseline.[16] Dodatna prednost ovakvog pristupa je mogućnost poopćenja teorije za tretman vibracijski pobuđenih stanja, što je i napravljeno za slučaj simetričnih putanja.[15]

Iako numerički efikasna, JFI teorija je formulirana isključivo za potencijale koji posjeduju putanje sa simetričnim profilom potencijalne energije. Navedeno ograničava njenu primjenu na sustave s većim brojem simetrijski povezanih minimuma, koji mogu posjedovati i asimetrične putanje. Također, JFI metoda za pobuđena vibracijska stanja ne rezultira odgovarajućim oblikom valne funkcije u blizini minimuma u slučaju putanja koje posjeduju veliku zakrivljenost. Stoga je cilj ove doktorske disertacije izvesti poopćenje navedene metode za tretman opisanih sustava te stvoriti programski paket koji se može korisititi za njegovu primjenu na općenite molekularne sustave. Također, cilj je izvesti i metodu kojom je moguće opisati tuneliranje u sustavima koji posjeduju minimume koji nisu simetrijski povezani te imaju ili različite energije ili različite konstante sila. Konačno, cilj je i proučiti utjecaj pobude u viša rotacijska stanja na iznose tuneliranjem uzrokovanog cijepanja vibracijskih stanja. Nadalje, razvijene metode primijenit će se za računanje iznosa i obrazaca cijepanja u odabranim molekularnim sustavima, koji uključuju malonaldehid, dimer vode i hidroperoksilni radikal.

Kvantnomehaničke metode za određivanje tuneliranjem uzrokovanog cijepanja vibracijskih stanja

Točan opis tuneliranjem uzrokovanog cijepanja vibracijskih stanja može se dobiti kvantnomehaničkim metodama, koje uključuju direktno rješavanje vremenski neovisne Schrödingerove

jednadžbe ili propagaciju valnog paketa opisanu vremenski ovisnom Schrödingerovom jednadžbom.

Metode rješavanja vremenski neovisne Schrödingerove jednadžbe uglavnom se svode na konstrukciju i dijagonalizaciju matrice hamiltonijana u nekoj odabranoj bazi ili osnovnom skupu. Matrica se najčešće konstruira uporabom Rayleigh-Ritzove[17] ili Galerkinove[18] varijacijske metode. U slučaju sustava s više stupnjeva slobode, osnovni skup se često konstruira kao direktni produkt osnovnih funkcija jedne varijable, čime se dobiva konstrukcija za proizvoljan broj stupnjeva slobode. Međutim, broj funkcija u osnovnom skupu konstruiranom na ovakav način eksponencijalno ovisi o broju stupnjeva slobode, što rezultira velikim memorijskim zahtjevima za spremanje i manipulaciju matrice hamiltonijana. Najnoviji razvoji u navedenom području uključuju metode za smanjivanje broja funkcija u osnovnom skupu, u što spadaju, primjerice, metode kontrakcije osnovnog skupa,[19] uporaba tenzorskog zapisa valne funkcije, na koji se može primjeniti efikasna metoda renormalizacijske grupe matrice gustoće (engl. *density matrix renormalization group*, DMRG)[20] te brojne druge. Međutim, sve navedene metode eksponencijalno skaliraju s obzirom na broj stupnjeva slobode molekule, pri čemu popravci smanjuju bazu i prefaktor u navedenoj ovisnosti, što ograničava njihovu primjenu.

Konstrukcija matrice hamiltonijana uključuje i određivanje matričnih elemenata potencijalne energije, što podrazumijeva numeričku evaluaciju višedimenzionalnih integrala. Najučinkovitija metoda za određivanje navedenih integrala jest uporaba kvadrature, kojom se integral evaluira sumom po relativno malom broju točaka u prostoru. Odabir kvadrature moguće je prilagoditi odabiru osnovnog skupa uporabom reprezentacije diskretnih varijabli[21] (engl. *Discrete Variable Representation*, DVR), u kojoj se točke kvadrature određuju kao svojstvene vrijednosti matrice operatora položaja, zapisane u odabranom osnovnom skupu. Međutim, broj točaka potrebnih za evaluaciju matričnih elemenata potencijalne energije je i dalje toliko velik da je potrebno poznavati analitički oblik plohe, kako bi evaluacija potencijala u svakoj točki bila dovoljno brza. Određivanje analitičkog oblika plohe potencijalne energije je numerički zahtjevan i kompleksan problem, što ograničava primjenu na općenite molekularne sustave.

Računalna zahtjevnost rješavanja vremenski neovisne Schrödingerove jednadžbe može se značajno smanjiti reduciranjem broja stupnjeva slobode. U navedenom pristupu identificira se nekoliko koordinata za koje se procijeni da su važne za opis tuneliranja te se jedino one uključuju u hamiltonijan sustava, dok se vrijednosti preostalih koordinata ili fiksiraju, ili reprezentiraju jednostavnim oblikom valne funkcije. Čest odabir koordinata za određivanje tuneliranjem uzrokovanog cijepanja vibracijskih stanja temelji se na određivanju neke putanje koja povezuje dva minimuma, pri čemu se često koriste putanja najmanje energije (engl. *Minimum Energy Path*, MEP) ili linearna interpolacija između geometrije dva minimuma.[22] Koordinate se zatim često biraju kao koordinate okomite na putanju, pri čemu se prema određenom kriteriju bira koje su od njih važne za proces tuneliranja, ili se putanja zapiše u bazi normalnih koordinata, bilo minimuma, bilo prijelazne strukture, te se za bazu odabiru oni normalni modovi koji su važni za opis putanje. Iako numerički efikasne, pokazano je da ograničavanje stupnjeva slobode može imati značajan utjecaj na iznos tuneliranjem uzrokovanog cijepanja vibracijskih stanja, što čini rezultate dobivene ovakvim pristupom upitne točnosti.

Tuneliranjem uzrokovano cijepanje vibracijskih stanja može se odrediti i rješavanjem vremenski ovisne Schrödingerove jednadžbe. Dva česta pristupa koja se koriste u tu svrhu

su difuzijski Monte Carlo (engl. *Diffusion Monte Carlo*, DMC)[23] i multikonfiguracijska vremenski ovisna Hartreejeva metoda (engl. *Multiconfigurational Time-Dependent Hartree*, MCTDH).[24] DMC metoda temelji se na vezi oblika vremenski ovisne Schrödingerove jednadžbe u imaginarnom vremenu i difuzijske jednadžbe. S obzirom na to da su navedene jednadžbe istog oblika, energije i valna funkcija niskoležećih stanja mogu se odrediti uzorkovanjem plohe potencijalne energije nizom 'hodača' (engl. *walker*), čija se početna raspodjela može generirati nasumično ili prema harmoničkoj valnoj funkciji, a čije je gibanje po plohi potencijalne energije definirano difuzijskom jednadžbom. Ovakvim pristupom se izbjegavaju problemi vremenski neovisnih metoda, jer se izbjegava uporaba osnovnog skupa i integriranja čitave plohe potencijalne energije. Međutim, glavni nedostatak ove metode jest taj da se može primijeniti samo za određivanje energijski niskoležećih stanja i njihovog cijepanja.

MCTDH metoda temelji se na propagaciji valnog paketa uporabom vremenski ovisnog varijacijskog načela. Zapis valnog paketa u MCTDH metodi je oblika sume nekoliko Hartreejevih produkata jednodimenzionalnih funkcija, čime se izbjegava konstrukcija velikih osnovnih skupova. Propagacija valnog paketa u realnom vremenu može se iskoristiti za određivanje odabranih svojstvenih stanja hamiltonijana uporabom Lanczosove metode dijagonalizacije, u kojoj je baza za zapis hamiltonijana valni paket u različitim trenutcima propagacije. S obzirom na to da se metoda svodi na dijagonalizaciju matrice hamiltonijana, njenom uporabom moguće je dobiti cijepanje pobuđenih vibracijskih stanja, međutim i dalje zahtijeva određivanje matričnih elemenata potencijalne energije, što povlači potrebu za poznavanjem njenog analitičkog oblika.

Teorija integrala po stazama

Teorija integrala po stazama (engl. *Path Integral*) jedna je od formulacija kvantne mehanike. Njeni začetci mogu se povezati s Diracom,[25] dok je cjelovitu formu postavio Feynman.[26] Za razliku od Schrödingerove formulacije, teorija integrala po stazama postulira postojanje amplitude vjerojatnosti $K(\mathbf{x}_a, t_a; \mathbf{x}_b, t_b)$, čiji kvadrat modula opisuje gustoću vjerojatnosti da se čestica koja se u trenutku t_a nalazila u točki $\mathbf{x}_a$, u trenutku t_b nađe u točki $\mathbf{x}_b$. Feynman je primijetio da takav objekt mora zadovoljavati svojstvo

$$K(\mathbf{x}_a, t_a; \mathbf{x}_b, t_b) = \int K(\mathbf{x}_a, t_a; \mathbf{x}, t) K(\mathbf{x}, t; \mathbf{x}_b, t_b) \mathrm{d}\mathbf{x}, \qquad t_a < t < t_b,$$

čime se amplituda može rastaviti na infinitezimalne pomake u vremenu. Konačno, inspiriran radom od Diraca, Feynman je povezao oblik amplitude za infinitezimalni pomak u vremenu s lagranžijanom

$$K(\mathbf{x}_k, t; \mathbf{x}_{k+1}, t + \delta t) = \exp\left(i\delta t L\left(\frac{\mathbf{x}_{k+1} - \mathbf{x}_k}{\delta t}, \mathbf{x}_a, t \right) \right),$$

čime se ukupna amplituda svodi na zbroj doprinosa po svim mogućim stazama koje povezuju točke $\mathbf{x}_a$ i $\mathbf{x}_b$

$$K(\mathbf{x}_a, t_a; \mathbf{x}_b, t_b) = A \int_{\mathbf{x}(t_a)=\mathbf{x}_a}^{\mathbf{x}(t_b)=\mathbf{x}_b} \mathrm{e}^{iS(\mathbf{x}(t))} \mathscr{D}\mathbf{x},$$

pri čemu je $S(\mathbf{x}(t)) = \int L(\dot{\mathbf{x}}(t), \mathbf{x}(t), t) \mathrm{d}t$ akcija putanje. Navedena teorija ima točan klasični limit, jer za velike vrijednosti akcija, doprinos putanje najmanje akcije postaje dominantan. To je posljedica činjenice da akcija predstavlja fazu doprinosa svake putanje u amplitudi vjerojatnosti, što znači da kod putanja koje nisu stacionarne točke akcije, dolazi do brze

promjene faze za male perturbacije putanje, što uzrokuje destruktivnu interferenciju njihovih doprinosa. S druge strane, putanja najmanje akcije je stacionarna točka, što znači da se akcija sporije mijenja perturbiranjem te putanje te njen doprinos dominira u integralu. Stoga, gibanje klasičnih sustava dobro je opisano putanjom najmanje akcije, što je temelj klasične mehanike.

U slučaju sustava u kojima su prisutni kvantni efekti, potrebno je razmotriti doprinos ne samo putanje najmanje akcije, već i putanja koje su njoj slične. Navedeno se može napraviti uporabom metode stacionarne faze,[27,28] u kojoj se akcija razvija u Taylorov red oko putanje najmanje akcije do kvadratnog člana s obzirom na fluktuaciju putanje. Integral po stazama se u tom slučaju svodi na integral višedimenzionalne Gaussove funkcije, koji se može evaluirati analitički.

Teorija integrala po stazama može se iskoristiti za određivanje tuneliranjem uzrokovanog cijepanja vibracijskih nivoa. Navedeno je moguće napraviti korištenjem činjenice da je amplituda vjerojatnosti u imaginarnom vremenu $\tau = it$ ekvivalentna elementu matrice gustoće pri inverznoj temperaturi[29] $\beta = \tau$

$$\rho(\mathbf{x}_a, \mathbf{x}_b, \beta) = \langle \mathbf{x}_a | e^{-\beta \hat{H}} | \mathbf{x}_b \rangle = K(\mathbf{x}_b, 0; \mathbf{x}_a, it).$$

Prelazak u imaginarno vrijeme transformira integrand iz integrala po stazama u padajuću eksponencijalnu funkciju te mijenja predznak ispred potencijalne energije, što znači da gibanje u imaginarnom vremenu odgovara gibanju po invertiranoj plohi potencijalne energije.[27] Iznos tuneliranjem uzrokovanog cijepanja osnovnog vibracijskog stanja može se odrediti iz omjera elemenata matrice gustoće[12] koja sadrži i koja ne sadrži tuneliranje u limitu temperature nula

$$\lim_{\beta \to +\infty} \frac{\rho(\mathbf{x}^{(1)}, \mathbf{x}^{(2)}, \beta)}{\rho(\mathbf{x}^{(1)}, \mathbf{x}^{(1)}, \beta)} = \lim_{\beta \to +\infty} \tanh \beta h,$$

pri čemu su $\mathbf{x}^{(1)}$ i $\mathbf{x}^{(2)}$ geometrije dva minimuma, a h element matrice tuneliranja, koji je za sustav s dvije potencijalne jame povezan s iznosom tuneliranjem uzrokovanog cijepanja $\Delta = 2h$. U slučaju sustava s više simetrijski povezanih potencijalnih jama, obrazac tuneliranja može se odrediti pomoću omjera matrica gustoća za sve parove minimuma, što su pokazali Matyus i Althorpe.[30] Stoga, za opisati tuneliranjem uzrokovano cijepanje osnovnog vibracijskog stanja, dovoljno je odrediti elemente matrice gustoće, što se može napraviti uporabom teorije integrala po stazama.

Jedan način za određivanje elemenata matrice gustoće je uporaba molekularne dinamike temeljene na teoriji integrala po stazama[31] (engl. *Path Integral Molecular Dynamics*, PIMD), koja podrazumijeva aproksimaciju akcije s određenim brojem točaka jednako udaljenih u imaginarnom vremenu. Svaka točka odgovara geometriji sustava, zbog čega se one nazivaju i replike. Elementi matrice gustoće tada postaju klasične particijske funkcije sustava koji se sastoji od svih replika povezanih u niz harmoničkim potencijalom, čija konstanta sile ovisi o temperaturi i broju replika. Navedene klasične particijske funkcije mogu se evaluirati uzorkovanjem pomoću molekularne dinamike, pri čemu se ne propagira sami sustav, već linearni polimer sastavljen od svih replika povezanih navedenim harmoničkim potencijalom. Navedena metoda ima slične prednosti kao i DMC, s obzirom na to da je potrebno samo uzorkovati plohu potencijalne energije. Međutim, broj evaluacija potrebnih za postizanje konvergencije particijskih funkcija je i dalje velik.

Efikasnija metoda za određivanje elemenata matrice gustoće temelji se na aproksimaciji instantona.[27] U ovoj metodi, particijska funkcija linearnog polimera aproksimira se razvojem akcije u Taylorov red do kvadratnog člana, slično kao u aproksimaciji stacionarne faze. Putanje koje odgovaraju minimumu akcije, u limitu $\beta \to +\infty$ provode većinu vremena u minimumu potencijalne energije, uz sporadične preskoke iz jednog minimum u drugi, koji se odvijaju klasičnim putanjama. S obzirom na to da je imaginarno vrijeme trajanja navedenih skokova infinitezimalno malo u usporedbi s beskonačnim vremenom koje sustav provodi u minimumima, navedeni skokovi nazivaju se instantonima. Teorija koja koristi instantone za određivanje particijskih funkcija naziva se i teorija instantona prstenastih polimera[13] (engl. *Ring-polymer Instanton*, RPI), jer se uobičajeno koristi za evaluaciju dijagonalnih elemenata matrice gustoće, koji odgovaraju prstenastim polimerima. Minimumi akcije odgovaraju različitim brojevima instantona u polimeru, te se particijska funkcija dobiva zbrajanjem po svim mogućim slučajevima. Doprinos okolnih putanja aproksimativno se uzima u obzir pomoću kvadratnog člana, tj. hesijana akcije, te rezultira integralom Gaussove funkcije. Konačni izraz za element matrice tuneliranja u RPI teoriji je

$$h = \sqrt{\frac{S_{\text{kink}} \det(\mathbf{H}_0/\beta_N)}{2\pi \det'(\mathbf{H}_1/\beta_N)}} \mathrm{e}^{-S_{\text{kink}}},$$

u kojemu je $\mathbf{H}_0$ hesijan polimera u kojemu su sve replike u jednom minimumu, dok je $\mathbf{H}_1$ hesijan polimera koji odgovara diskretiziranoj putanji jednog instantona. Navedeni izraz manje je zahtjevan za računanje od uporabe PIMD metode. Umjesto uzorkovanja cijele plohe potencijalne energije, potrebno je samo odrediti putanju najmanje akcije koja spaja dva minimuma te izračunati i dijagonalizirati njen hesijan. Putanja se u okviru RPI metode određuje diskretizacijom s jednakim razmacima u imaginarnom vremenu, čime se dobiva određeni broj replika sustava koje reprezentiraju putanju. Akcija se zatim aproksimira kao suma po navedenim replikama, što svodi određivanje putanje najmanje akcije na minimizaciju funkcije NN_{dof} varijabli, pri čemu je N broj replika, a N_{dof} broj stupnjeva slobode sustava. Hesijan akcije konstruira se iz hesijana potencijala u svakoj replici sustava. Determinantu hesijana potrebno je računati određivanjem njegovih svojstvenih vrijednosti, zbog postojanja jedne (ili 7 u slučaju molekularnih sustava) svojstvene vrijednosti iznosa nula, koju je potrebno izuzeti iz determinante. Navedeni koraci, iako računalno manje zahtjevni od PIMD i kvantnomehaničkih metoda, i dalje zahtijevaju relativno velik broj evaluacija potencijalne energije i hesijana. Navedeno se može dodatno poboljšati korištenjem metode instantona temeljene na Jakobijevim poljima.

Teorija instantona temeljena na Jakobijevim poljima

Teorija instantona temeljena na Jakobijevim poljima[14,15] (engl. *Jacobi Field Instanton*, JFI) smanjuje zahtjevnost RPI metode prelaskom na diskretizaciju putanje s jednakim pomacima s obzirom na udaljenost od jednog minimuma. Na ovaj način se može drastično smanjiti broj replika potreban za reprezentaciju putanje, jer se izbjegava nakupljanje replika u blizini minimuma, koje je prisutno u RPI metodi. Akcija se u ovom slučaju može zamijeniti s Jakobijevom akcijom

$$S_0 = \int_0^S \sqrt{2V(S')} \mathrm{d}S',$$

pri čemu je S udaljenost na putanji od jednog minimuma. Navedeni izraz može se diskretizirati s jednakim razmacima u udaljenosti te se putanja najmanje akcije može odrediti na analogan

način kao u RPI metodi. Omjer determinanti hesijana može se svesti na omjer determinanti Jakobijevih polja

$$\frac{\det(\mathbf{H}_0/\beta_N)}{\det'(\mathbf{H}_1/\beta_N)} = \frac{\det(\mathbf{J}_0)}{\det'(\mathbf{J}_1)}$$

$$\left(\frac{\partial^2}{\partial\tau^2} + \mathbf{V_{xx}}^{(0)}\right)\mathbf{J}_0 = 0, \qquad J_0(0) = 0, \quad \dot{J}_0(0) = 1$$

$$\left(\frac{\partial^2}{\partial\tau^2} + \mathbf{V_{xx}}\right)\mathbf{J} = 0, \qquad \mathbf{J}(0) = 0, \quad \dot{\mathbf{J}}(0) = 1,$$

pri čemu je $\mathbf{V_{xx}}$ hesijan potencijala, a $\mathbf{V_{xx}}^{(0)}$ hesijan potencijala u minimumu. Mil'nikov i Nakamura[14] su pokazali da se omjer determinanti Jakobijevih polja može, u slučaju simetričnih putanja, odrediti propagacijom matrice

$$p_0\frac{\mathrm{d}}{\mathrm{d}S}\mathbf{A} = \mathbf{V_{xx}} - \mathbf{A}^2$$

$$\mathbf{A}^2(S = 0) = \mathbf{V_{xx}}^{(0)},$$

što rezultira izrazom za element matrice tuneliranja

$$h = \sqrt{\frac{\det\mathbf{A}_0}{\pi\det'\mathbf{P}\mathbf{A}(0)\mathbf{P}}}p_0(S_{\text{tot}}/2)\mathrm{e}^{-\int_0^{S_{\text{tot}}} p_0\mathrm{d}S + \int_0^{S_{\text{tot}}/2}(\mathrm{Tr}\mathbf{A}_0 - \mathrm{Tr}\mathbf{A})/p_0\mathrm{d}S},$$

u kojemu operator $\mathbf{P} = \mathbf{I} - \tau_N\tau_N^\top$ odgovara projektoru na ravninu okomitu na sredinu putanje, a količina gibanja na udaljenosti S je $p_0(S) = \sqrt{2V(S)}$.

Mil'nikov i Nakamura[14] također su pokazali da je JFI teorija ekvivalentna uporabi Herringove formule[32] za određivanje elementa matrice tuneliranja, uz uporabu Wentzel-Kramers-Brillouinove (WKB)[33] aproksimacije za lokalizirane valne funkcije

$$h = \frac{\int\left(\phi^{(\mathrm{L})}\frac{\partial}{\partial S}\phi^{(\mathrm{R})} - \phi^{(\mathrm{R})}\frac{\partial}{\partial S}\phi^{(\mathrm{L})}\right)\delta(f(\mathbf{x}))\mathrm{d}\mathbf{x}}{2\int|\phi^{(L)}|^2\mathrm{d}\mathbf{x}}$$

$$\phi^{(\mathrm{L/R})} = \mathrm{e}^{-W_0^{(L/R)}/\hbar - W_1^{(L/R)}},$$

pri čemu se, za razliku od uobičajene WKB teorije, vibracijska energija tretira kao član reda $\hbar^1$, s obzirom na to da je toga reda energija u harmoničkoj aproksimaciji. Ukoliko se funkcija W_0 razvije do kvadratnog člana oko putanje instantona, a funkcija W_1 odredi samo na putanji instantona, dobiju se isti objekti koji se pojavljuju u izrazu određenom putem teorije integrala po stazama

$$W_0 = \int_0^S p_0(S')\mathrm{d}S' + \frac{1}{2}(\mathbf{x} - \mathbf{x}^{(0)}(S))^\top\mathbf{A}\mathbf{x} - \mathbf{x}^{(0)}(S))$$

$$W_1 = -\frac{1}{2}\int_0^S(\mathrm{Tr}\mathbf{A}_0 - \mathrm{Tr}\mathbf{A})/p_0\mathrm{d}S'.$$

Izvod uporabom WKB pristupa otvara mogućnost određivanja elemenata matrice tuneli-

ranja u pobuđenim vibracijskim stanjima. Navedeno su izveli Mil'nikov i Nakamura[15] za sustave sa simetričnim putanjama, odvojeno razmatrajući pobudu moda koji je longitudinalan na putanju u minimumu te pobude modova koji su transverzalni. Energiju pobude tretirali su uvođenjem dodatne funkcije $W_1^{\text{pob}} = W_1 + w$, koja opisuje prefaktor valne funkcije pobuđenog stanja

$$\phi^{\text{pob},\parallel} = \frac{p_0}{\omega_\parallel} e^{\int_0^S \frac{p_0' - \omega_\parallel}{p_0} dS'} \phi^{(0)}$$

$$\phi^{\text{pob},\perp} = \mathbf{U}^\top (\mathbf{x} - \mathbf{x}^0) e^{\int_0^S \frac{\theta - \omega_\perp}{p_0} dS'} \phi^{(0)}$$

$$p_0 \frac{\mathrm{d}}{\mathrm{d}S} \mathbf{U} = \theta \mathbf{U} - \mathbf{A}\mathbf{U}$$

$$\theta = \mathbf{U}^\top \mathbf{A}\mathbf{U},$$

što rezultira izrazima za elemente matrice tuneliranja u pobuđenim stanjima

$$h_\parallel = h_0 \frac{2p_0^2}{\omega_\parallel} e^{2\int_0^S \frac{p_0' - \omega_\parallel}{p_0} dS'}$$

$$h_\perp = \omega_\perp \mathbf{U}^\top (\mathbf{PAP})^{-1} \mathbf{U} e^{\int_0^S \frac{\theta - \omega_\perp}{p_0} dS'} h_0.$$

Navedena metoda daje dobre rezultate u slučaju putanja male zakrivljenosti, no u slučaju putanja koje su jako zakrivljene, oblik valne funkcije blizu minimuma ne odgovara obliku odgovarajućeg harmoničkog oscilatora. To je posljedica nametnutog oblika valne funkcije, koji zahtijeva da u slučaju transverzalne pobude, čvorna ravnina sadrži putanju, što ne mora biti slučaj za zakrivljene putanje.

U okviru ove doktorske disertacije, izvedena su poopćenja JFI metode za opis asimetričnih putanja. U slučaju osnovnog vibracijskog stanja, izraz za element matrice tuneliranja dobiven je konstrukcijom Jakobijevog polja pomoću dva rješenja propagacijske jednadžbe za Jakobijeva polja, s različitim rubnim uvjetima. Konstrukcija s dva različita rješenja rezultira propagacijom dviju različitih matrica $\mathbf{A}^{(\text{L})}$ i $\mathbf{A}^{(\text{R})}$, koje se propagiraju iz dva različita minimuma sve do neke točke spajanja na putanji. Izraz za element matrice tuneliranja s poopćenom metodom postaje

$$h = \sqrt{\frac{\det \mathbf{A}_0^{(\text{L})}}{\pi \det' \mathbf{P} \left(\frac{\mathbf{A}^{(\text{L})} + \mathbf{A}^{(\text{R})}}{2} \right) \mathbf{P}}} \, p_0 e^{-\int_0^{S_{\text{tot}}} p_0 dS' - \frac{1}{2} \int_0^S \text{Tr}\left(\mathbf{A}^{(\text{L})} - \mathbf{A}_0^{(\text{L})} \right) / p_0 dS' - \frac{1}{2} \int_0^{\tilde{S}} \text{Tr}\left(\mathbf{A}^{(\text{R})} - \mathbf{A}_0^{(\text{R})} \right) / p_0 d\tilde{S}'}.$$

Dodatno je pokazano da iznos elementa matrice tuneliranja ne ovisi o odabiru točke spajanja, što je ujedno i potvrda točnosti i konzistentnosti dobivene metode.

Također, izveden je i modificirani izraz za element matrice tuneliranja u pobuđenim vibracijskim stanjima. Umjesto odvojenog promatranja longitudinalnih i transverzalnih pobuda, svi pobuđeni modovi tretirani su s prefaktorom oblika $F + \mathbf{U}^\top (\mathbf{x} - \mathbf{x}^0)$. Propagacijske

jednadžbe za parametere prefaktora pronađene su da zadovoljavaju

$$p_0 \frac{\mathrm{d}}{\mathrm{d}S} F = \omega F$$

$$p_0 \frac{\mathrm{d}}{\mathrm{d}S} \mathbf{U} = \omega \mathbf{U} - \mathbf{A}\mathbf{U}.$$

Prefaktor ovog oblika točno opisuje ponašanje lokalizirane valne funkcije u blizini minimuma, što ga čini prikladnim za opis elemenata matrice tuneliranja i u slučaju zakrivljenih putanja. Modificirani izraz za element matrice tuneliranja dobiven navedenim valnim funkcijama je

$$h = 2\omega \left(F^{(\mathrm{L})} F^{(\mathrm{R})} + \frac{1}{2} \mathbf{U}^{(\mathrm{L})\top} (\mathbf{P}\bar{\mathbf{A}}\mathbf{P})^{-1} \mathbf{U}^{(\mathrm{R})} \right) h_0.$$

Dodatno, pokazano je da se Herringova formula i navedeni oblici lokaliziranih valnih funkcija mogu koristiti za određivanje elemenata matrice tuneliranja između različitih vibracijskih stanja te između minimuma koji nisu povezani simetrijskim operacijama. U tome slučaju matrica tuneliranja odgovara matrici molekularnog hamiltonijana u bazi stanja lokaliziranih u potencijalnim jamama. Dijagonalni elementi navedene matrice odgovaraju energijama lokaliziranih stanja te se mogu aproksimirati s energijama odgovarajućih harmoničkih oscilatora, ili s energijama dobivenima vibracijskom konfiguracijskom interakcijom (engl. *Vibrational Configuration Interaction*, VCI),[34,35] koja opisuje dio anharmoničnosti u sustavu. Svojstvene vrijednosti dobivene matrice hamiltonijana pokazane su da pružaju izvrstan opis energija sustava.

Konačno, izvedena je i korekcija elemenata matrice tuneliranja za pobuđena rotacijska stanja sustava. U tu je svrhu korišten rotacijsko-kontorcijsko-vibracijski molekularni hamiltonijan, u kojemu je kontorcijska koordinata položaj duž putanje najmanje akcije. U navedenom hamiltonijanu zanemaren je doprinos vibracijske kutne količine gibanja i Watsonovog potencijala, te je iskorištena adijabatska rotacijska aproksimacija za tretman rotacijskog dijela lokaliziranih valnih funkcija. Također, primijećeno je da su rotacijske energije reda $\hbar^2$, što omogućuje njihov opis uvođenjem idućeg člana u WKB razvoju, W_2. Tada se može pokazati da prijašnje izvedeni elementi matrice tuneliranja odgovaraju slučaju $J = 0$, dok se za $J > 0$ mogu korigirati kao

$$h_{J_{K_a K_b}} = h_{J=0} \mathrm{e}^{\int_0^{S_{\mathrm{tot}}} \frac{E^{\mathrm{rot}}(J_{K_a K_b}, S') - E^{\mathrm{rot}}(J_{K_a K_b}, \min)}{p_0} \mathrm{d}S'},$$

pri čemu su $E^{\mathrm{rot}}(J_{K_a K_b}, S')$ energije krutog rotora definiranog geometrijom na položaju S' duž putanje.

Modelni sustavi

Razvijene metode za određivanje elemenata matrice tuneliranja testirane su na nekoliko vrsta modelnih potencijala, koji su konstruirani kako bi ispitali točnost njihovih rezultata. Za testiranje metode za pobuđena vibracijska stanja, odabran je niz dvodimenzionalnih potencijala s različitim zakrivljenostima u blizini minimuma, koji se mogu vidjeti na slici I. Tuneliranjem uzrokovano cijepanje osnovnog i jednostruko pobuđenih vibracijskih stanja određeno je dijagonalizacijom matrice hamiltonijana u bazi DVR funkcija,[21] što predstavlja točne vrijednosti, te uporabom JFI metode. Kao što se može vidjeti u tablici I, dobivena JFI
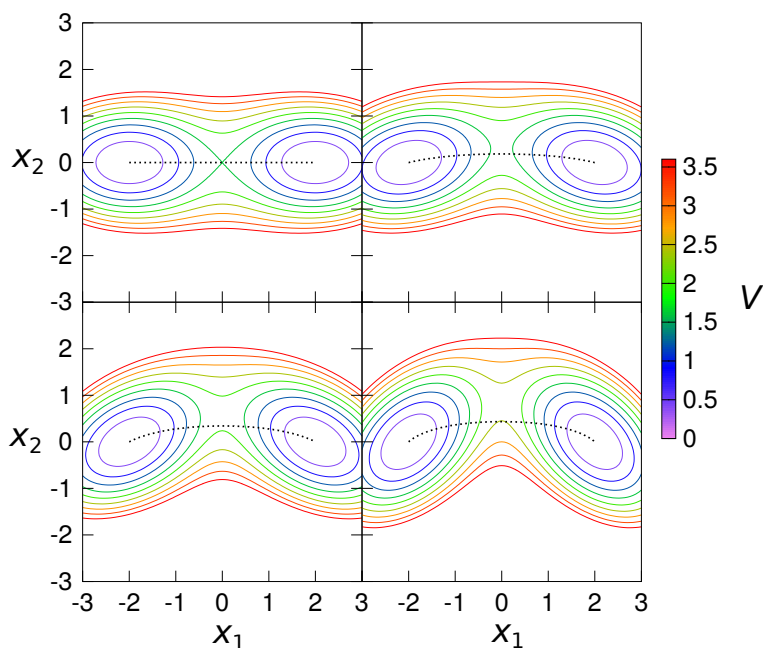
Slika I. Modelni dvodimenzionalni potencijali s različitim zakrivljenostima putanje instantona.

teorija pruža izvrsan opis tuneliranjem uzrokovanog cijepanja vibracijskih stanja, neovisno o zakrivljenosti putanje.

Tablica I. Tuneliranjem uzrokovana cijepanja osnovnog i jednostruko pobuđenih stanja modelnih potencijala prikazanih na slici I. Prikazane su vrijednosti dobivene uporabom samo F člana i uporabom punog $F + U_i(x - x^{(0)})_i$ prefaktora. Točne kvantnomehaničke vrijednosti prikazane su u zagradama.

θ	Δ_0	$\Delta_1(1,0)$	$\Delta_1(0,1)$
		$1.830(-8)$	0.000
0	$2.630(-10)$	$1.830(-8)$	$5.026(-10)$
	$(2.639(-10))$	$(1.811(-8))$	$(5.155(-10))$
		$9.870(-9)$	$5.492(-10)$
$\pi/12$	$1.463(-10)$	$9.882(-9)$	$8.066(-10)$
	$(1.472(-10))$	$(9.858(-9))$	$(8.089(-10))$
		$1.563(-9)$	$4.029(-10)$
$\pi/6$	$2.573(-11)$	$1.571(-9)$	$4.383(-10)$
	$(2.599(-11))$	$(1.583(-9))$	$(4.477(-10))$
		$7.729(-11)$	$5.932(-11)$
$\pi/4$	$1.606(-12)$	$7.827(-11)$	$6.077(-11)$
	$(1.620(-12))$	$(7.879(-11))$	$(6.224(-11))$

Malonaldehid

Razvijena JFI teorija testirana je i na molekuli malonaldehida, koja ima dva simetrijski povezana minimuma koja odgovaraju različitim tautomerima molekule. Za navedenu molekulu dostupni su iznosi cijepanja u osnovnom i pobuđenim vibracijskim stanjima dobiveni MCTDH metodom,[36] što ga čini pogodnim molekularnim sustavom za provjeru točnosti metode. Usporedbom JFI vrijednosti cijepanja s točnim MCTDH vrijednostima, prikazanim u tablici II može se vidjeti da JFI metoda daje izvrsna slaganja s MCTDH rezultatima. Iznimka su prva

dva pobuđena stanja, čiji je iznos cijepanja precijenjen. U slučaju prvog stanja, vjerojatan uzrok leži u nezanemarivom doprinosu anharmoničnosti u ravnini okomitoj na putanju instantona, dok je u slučaju drugog stanja vrijednost cijepanja precijenjena zbog činjenice da je pobuđeni mod longitudinalan, što znači da njegova pobuda smanjuje efektivnu barijeru za tuneliranje. U literaturi je već primijećeno da u slučaju malih efektivnih barijera teorija instanona precjenjuje vrijednosti cijepanja.

Tablica II. Iznosi tuneliranjem uzrokovanog cijepanja osnovnog i jednostruko pobuđenih stanja molekule malonaldehida.

Mode	$\Delta(\text{JFI})/\text{cm}^{-1}$	$\Delta(\text{MCTDH})/\text{cm}^{-1}$
GS	24.60	23.5
1	13.40	6.7
2	88.40	69.9
3	17.06	16.3
4	15.64	18.8
5	24.4	21.1
7	39.5	33.3
8	15.6	14.6

Dobivena JFI metoda za opis energija sustava s minimumima koji nisu povezani operacijama simetrije primijenjena je na djelomično deuterirani malonaldehid, u kojemu je karbonilni vodik supstituiran s deuterijem. Time se razbija simetrija između dva tautomera, te potencijalne jame posjeduju različite vibracijske frekvencije i energije. Uporabom JFI metode određen je uzorak energetskih nivoa dobiven konstrukcijom matrice hamiltonijana s 4 i 8 lokaliziranih stanja u svakoj jami, što je prikazano na slici II. Za navedeni sustav ne postoje poznati teorijski i eksperimentalni podatci za usporedbu, već jedino kut miješanja lokaliziranih osnovnih vibracijskih stanja dvije jame. Pronađeno je da JFI metoda, uz uporabu VCI energija uzrokuje smanjenje kuta miješanja dobivenog RPI metodom s harmoničkim energijama,[37] u kojoj je on bio precijenjen.
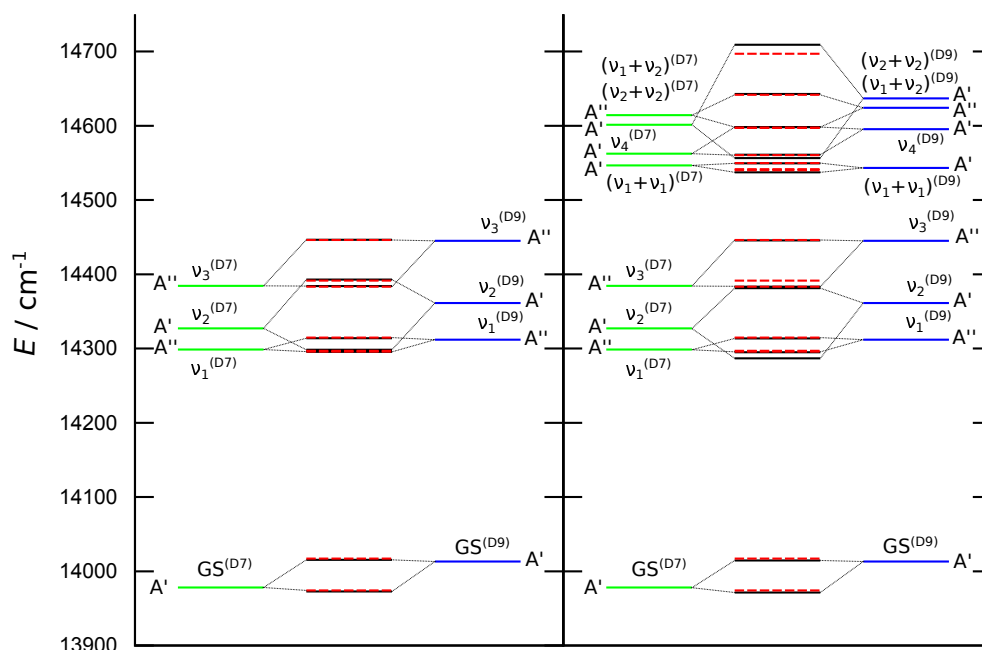
Slika II. Energijske razine djelomično deuteriranog malonaldehida dobivene uporabom 4 i 8 lokaliziranih stanaj u svakoj potencijalnoj jami te razmatranjem 2×2 blokova hamiltonijana (crveno) i pune matrice hamiltonijana (crno). Energije lokaliziranih stanja dvije potencijalne jame dobivene su VCI metodom i prikazane zelenim i plavim crtama.

Grozdovi vode

JFI teorija je iskorištena i za određivanje elemenata matrice tuneliranja u deuteriranom dimeru i djelomično deuteriranom trimeru vode. U slučaju deuteriranog dimera, dostupni su eksperimentalni podatci,[38,39] kao i kvantnomehaničke energije dobivene rješavanjem vremenski neovisne Schrödingerove jednadžbe.[40] Usporedba JFI vrijednosti s njima prikazana je u tablici III. U navedenom sustavu slaganja s eksperimentalnim podatcima lošija su nego u slučaju malonaldehida. Uzrok tome je činjenica da je dimer fleksibilniji od malonaldehida, što uzrokuje veći doprinos anharmoničnosti. Također, preslagivanje akceptora (AT) je gibanje s veoma niskom barijerom, što uzrokuje pogreške u JFI metodi. Međutim, unatoč većim greškama nego u slučaju malonaldehida, sve su dobivene vrijednosti unutar točnog reda veličine.

U slučaju djelomično deuteriranog trimera vode, određeni su elementi matrice tuneliranja za sve moguće putanje te je dobiven obrazac cijepanja u osnovnom vibracijskom stanju. Dobiveni matrični elementi mogu se podijeliti u dvije skupine, koje odgovaraju dvama vrstama preslagivanja. Prva skupina su gibanja u kojima ne dolazi do pucanja prstena vodikovih veza, već samo prebacivanja atoma vodika s jedne strane prstena na drugu. Navedena gibanja karakterizirana su niskim barijerama te velikim vrijednostima elemenata matrice tuneliranja te uzrokuje pojavu seksteta degeneriranih energetskih nivoa. Drugu skupinu gibanja čine bifurkacije, u kojima se zamjenjuje jedan atom vodika iz prstena vodikovih veza. S obzirom na to da u tim gibanjima dolazi do pucanja vodikovih veza, barijere duž putanja su veće i iznosi elemenata matrice tuneliranja manji te uzrokuju cijepanje degeneracije svakog nivoa u sekstetu, što se može vidjeti na slici III.

Tablica III. Elementi matrice tuneliranja deuteriranog dimera vode dobiveni JFI metodom. Prikazane su vrijednosti dobivene uporabom samo F člana i uporabom punog $F + U_i(x_i - x_i^{(0)})$ prefaktora. Točne eksperimentalne i kvantnomehaničke vrijednosti prikazane su u zagradama.

Mode	AT	GI	AI	BT	DE
GS	0.766	9.73(−3)	4.88(−4)	1.83(−4)	3.21(−6)
	(0.45)	(9.4(−3))	(3.7(−4))	(2.3(−4))	(−)
1	−11.8	−4.58(−2)	1.86(−2)	1.43(−9)	2.95(−6)
	−11.1	−5.07(−2)	1.83(−2)	−3.96(−5)	1.12(−5)
	(3.953)	(6.643(−2))	(1.561(−2))	(−)	(−)
	(3.92)	(6.63(−2))	(1.63(−2))	(−)	(−)
2	−0.502	−0.256	4.01(−3)	−6.17(−9)	−5.16(−5)
	−0.509	−0.254	4.98(−3)	−2.28(−4)	−4.38(−5)
	(0.634)	(0.109)	(1.375(−3))	(−)	(−)
	(0.758)	(0.140)	(4.25(−2))	(−)	(−)
3	1.15	0.147	2.13(−2)	5.47(−3)	3.27(−6)
	2.72(−2)	0.141	2.13(−2)	5.42(−3)	2.42(−6)
	(0.442)	(3.033(−2))	(2.427(−3))	(−)	(−)
	(0.45)	(2.88(−2))	(1.25(−3))	(−)	(−)
4	19.5	2.94(−2)	2.64(−2)	2.17(−3)	−2.43(−4)
	8.98	3.20(−2)	2.58(−2)	2.41(−3)	−3.70(−4)
	(−)	(−)	(−)	(−)	(−)
	(1.23)	(0.173)	(7.75(−2))	(−)	(−)

Slika III. Obrazac cijepanja djelomično deuteriranog trimera $D_2O(H_2O)_2$.

Zaključak

U okviru ove doktorske disertacije razvijeno je nekoliko poboljšanja JFI teorije za opis elemenata matrice tuneliranja u molekularnim sustavima. Pronađeno je poopćenje koje može tretirati putanje s asimetričnim profilom potencijalne energije, kao i proširenje teorije za pobuđena vibracijska stanja, koje može tretirati sustave s putanjama velike zakrivljenosti. Također, pronađena je kombinirana JFI/VCI metoda za određivanje energijskih nivoa u sustavima koji posjeduju minimume koji nisu simetrijski povezani, u kojoj se konstruira

matrica hamiltonijana u bazi lokaliziranih stanja. VCI metoda koristi se za određivanje energija lokaliziranih stanja, dok se JFI metoda koristi za točnije određivanje elemenata koji opisuju tuneliranje između stanja različitih jama.

Dobivene metode testirane su na posebno odabranim modelnim potencijalima te je potvrđeno da pružaju dobra slaganja s vrijednostima dobivenim točnim kvantnomehaničkim metodama. Također, razvijene metode primijenjene su i za opis cijepanja u molekuli malonaldehida i djelomično deuteriranog malonaldehida, pri čemu su dobivena dobra slaganja s MCTDH metodom. Konačno, određeni su i elementi matrice tuneliranja u odabranim grozdovima vode, deuteriranom dimeru i djelomično deuteriranom trimeru, za koji je izračunat obrazac cijepanja.

§ 1. INTRODUCTION

Tunneling is a quantum mechanical phenomenon of the passage of a wave packet through regions in space where the potential energy is greater than the energy components of the wave packet. This phenomenon was first described by Hund[1] in 1927, and today it is known that tunneling is the cause of several effects significant in the fields of spectroscopy and chemical kinetics. One of these effects is tunnelling splitting of vibrational states.[2] This phenomenon is present in molecules that possess at least two minima corresponding to different permutations of identical atoms and/or inversion of the molecule, which are separated by potential energy barriers greater than the vibrational energy of the system. If tunneling was not present in the system, each vibrational level would display N-fold degeneracy, with N being the number of symmetry-related minima, and each eigenstate would correspond to a wave packet localized in one of the minima. However, as a consequence of tunneling, states localized in different minima interact, which causes the splitting of degenerate energy levels and delocalization of eigenstates. One of the consequences of tunneling splitting is the splitting of signals in the microwave spectrum, which allows for experimental determination of the magnitude of tunnelling splitting using high-resolution microwave spectroscopy. These methods were used for determination of splittings in water clusters,[3] which are of great scientific interest. One of the reasons for this is the fact that the tunnelling splitting is directly related to the time scale of rearrangements of water molecules in clusters. Thus, tunneling splitting can be used to gain insight into dynamics of water clusters at low temperatures. Furthermore, as splitting pattern can be measured, and is strongly dependent on the height and shape of the potential energy barriers, tunneling splitting in water clusters can be used as an excellent test for the development of new potential energy surfaces.

Tunneling can be modelled using quantum mechanical methods. Tunneling splitting can be computed by solving the time-independent nuclear Schrödinger equation directly, or using time-dependent methods, such as multiconfiguration time-dependent Hartree method (MCTDH)[4]. However, such approaches are limited to small systems with few atoms, because they require analytic potential energy surfaces, which are computationally difficult to obtain. Also, tunnelling splittings can vary over several orders of magnitude, even in the same system, and can be extremely small compared to the vibrational energies. As a consequence, it is often necessary to achieve high accuracy in vibrational energies, necessitating the use of large basis sets and long propagation times in time-dependent methods. Tunneling splittings for hydrofluoric acid dimer[41], water dimer[6], vinyl radical[42] and similar systems have been computed using time-independent methods, while MCTDH has been used to

determine splittings in malonaldehyde.[8] Tunneling splitting can also be determined using diffusion Monte Carlo method, which has been used to compute splittings in water trimer[9] and in malonaldehyde[43], or using path integral theories, such as path integral molecular dynamics (PIMD)[31] or instanton theory.[12] The latter methods allow for the determination of quantum effects using classical dynamics in spaces of increased dimensionality, obtained by introducing N replicas of the system. Though the dimnesionality is increased, the complexity of the calculations is reduced, as classical dynamics is performed, instead of the quantum one.

Instanton theory is based on the Taylor series expansion of action around the classical trajectory on the inverted potential (instanton path) up to the quadratic term, and has been shown to give excellent results for the tunneling splitting in the ground vibrational states. This method works particularly well in cases of deep tunneling, i.e. in cases in which the vibrational energy is significantly lower than the barrier height, for which quantum mechanical methods become computationally intensive.

There are many different variants of instanton theory, two of which have been extensively used to describe molecular systems. The first variant (ring-polymer instanton, RPI)[13] is based on the discretization of the path with points that are equidistant in time and the construction and diagonalization of action Hessian for the discretization used. The RPI method is formulated in Cartesian coordinates, which makes it easily applicable to arbitrary systems, and can also be used for trajectories with asymmetric potential energy profiles. Its disadvantages are the need for a large number of points to discretize the trajectory, resulting in a large number of potential energy evaluations for trajectory optimization, and the need to diagonalize a large action Hessian matrix. This makes RPI method limited to relatively small systems for which analytic potential energy surfaces are known. Additionally, the tunneling splitting obtained using this method has to be converged with respect to two parameters, number of points and total time of trajectory, which requires many repeated calculations. Furthermore, a generalization of the RPI method for vibrationally excited states has not yet been developed.

Formulation of instanton theory via Jacobi fields (Jacobi field instanton, JFI)[14] solves the problems of the RPI method by discretizing the path in terms of its shape in the time-independent form. The diagonalization of action Hessian is replaced by propagation and diagonalization of Jacobi fields. This significantly reduces the number of points required for discretization, as well as the number of potential energy evaluations in path optimization. Furthermore, it also avoids the problem of diagonalization of large action Hessian and the final result depends only on one parameter, the number of points used. This makes JFI method suitable for computation of splittings in larger systems and for the use with on-the-fly potentials. However, the JFI method is currently formulated only for systems with a symmetric potential energy profile along the instanton path. Closely related to the JFI method is the WKB method on the instanton path, modified by treating energy as a first order term

with respect to Planck's constant. Such a theory was used by Mil'nikov and Nakamura to compute splittings for HO_2[15], malonaldehyde[14] and formic acid dimer[16]. The advantage of this approach is the possibility for a generalization to treat vibrationally excited states, which has been formulated for the case of symmetric paths[15].

§ 2.   LITERATURE OVERVIEW

In this chapter, a brief literature overview of the theoretical and experimental methods for the determination of tunneling splittings will be given. First, the quantum-mechanical methods that have been previously used to compute tunneling splittings are described. These methods provide formally exact values, but are computationally intensive and thus limited to small systems. A brief overview of the most recent developments in these methods are presented as well. Next, a brief introduction to the path integral formalism of quantum mechanics is given, as well as efficient semiclassical methods for the computation of tunneling splittings that arise from it, which are ring-polymer instanton theory (RPI) and Jacobi field instanton theory (JFI). This section is followed by a brief description of an alternative method that results in the same equations for the tunneling splitting, but is based on Wentzel-Kramers-Brillouin (WKB) approach. Finally, an overview of experimental methods for tunneling splitting measurements is given, as well as the state-of-the art results for the systems of interest, malonaldehyde and water clusters.

The following conventions will be used in the text that follows. Objects $\mathbf{x}$ will denote N_{dof}-dimensional vectors that describe the geometry of the molecular system. Objects $\vec{\mathbf{x}}$ will denote an N-dimensional array of vectors $\mathbf{x}_1, ..., \mathbf{x}_N$ that will be used to discretize the path integral. Use of atomic units, defined by $\hbar = e = a_0 = m_e = 1$ will be assumed, where $\hbar$ is the reduced Planck constant, a_0 is Bohr radius, e is elementary charge and m_e is the mass of electron. All integrals will be assumed to run over entire range of the variable, unless stated otherwise. Examples will be given on the double-well systems, where labels L ('left') and R ('right') will be used to differentiate between the wells. For multi-well systems, wells will be labeled numerically.

2.1.   Quantum Mechanical Methods for Tunneling Splitting

2.1.1.   Direct Diagonalization Methods

Direct diagonalization methods are both conceptually simplest and computationally the most demanding approaches to computation of tunneling splittings. These methods are based on the computation of approximate eigenvalues E_i and eigenvectors $|\Psi_i\rangle$ of the molecular Hamiltonian $\hat{H}$

$$\hat{H}|\Psi_i\rangle = E_i|\Psi_i\rangle. \tag{2.1}$$

Best approximations are sought by observing the residual vector $|R_i\rangle = (\hat{H} - E_i\hat{I})|\tilde{\Psi}_i\rangle$, where $|\tilde{\Psi}_i\rangle$ is an approximate wavefunction. The most common approach is to approximate

the wavefunction by representing it as a linear combination of N basis functions $\left|\tilde{\Psi}_i\right\rangle = c_j^{(i)}\left|\phi_j\right\rangle$.[17] The best approximation is found by imposing certain conditions on the residual function $|R\rangle$. By far the most commonly used condition relies on the variational principle and consists of minimizing the projection of the residual function onto the approximate solution $\left\langle\tilde{\Psi}_i\right|(\hat{H}-E_i\hat{I})\left|\tilde{\Psi}_i\right\rangle$. Minimization is carried out by variation of coefficients in the linear combination of the basis set, because of which the method is known as the linear variational approach. Another name that appears in the literature is the Rayleigh-Ritz method.[17,44] Alternatively, one can impose a condition that the residual function is orthogonal to the basis set used $\left\langle\phi_j\right|(\hat{H}-E_i\hat{I})\left|\tilde{\Psi}_i\right\rangle = 0$, which is the basis of Galerkin method.[18] In case of eigenvalues and eigenvectors of molecular Hamiltonian, both approaches yield the same system of equation, which is, in essence, the eigenvalue problem for a matrix representation of the Hamiltonian

$$H_{kj}c_j^{(i)} = E_i c_k^{(i)}$$
$$H_{kj} = \langle\phi_k|\hat{H}|\phi_j\rangle = \int \phi_k^* \hat{T}\phi_j \mathrm{d}\mathbf{x} + \int \phi_k^* V(\mathbf{x})\phi_j \mathrm{d}\mathbf{x}, \tag{2.2}$$

where $\hat{T}$ and $\hat{V}$ denote the kinetic and potential energy operators, respectively. A closely related, but less used alternative is to demand that the residual function be orthogonal to a certain set of N position operator eigenvectors $\left\langle\mathbf{x}_j\right|(\hat{H}-E_i\hat{I})\left|\tilde{\Psi}_i\right\rangle = 0$. This constraint is equivalent to choosing the approximate wavefunction so that it satisfies the Schrödinger equation exactly on a certain set of points in space, and results in the collocation method.[45,46] The system of equations that results from this approach also represents an eigenvalue problem, but with a different matrix

$$H_{kj}c_j^{(i)} = E_i c_k^{(i)}$$
$$H_{kj} = \hat{T}\phi_j\big|_{\mathbf{x}_k} + V(\mathbf{x}_k)\phi_j(\mathbf{x}_k). \tag{2.3}$$

The greatest advantage of these methods is the fact that they yield exact quantum-mechanical energy levels, provided that the basis set is sufficiently large. Additionally, higher eigenvalues of the matrices that are diagonalized approximate higher energy levels. If one is interested in tunneling splittings, this means that a single calculation yields splittings of both excited vibrational and rotational states. However, there are serious problems associated with the use of these methods. The greatest problem is the curse of dimensionality. In order to make the method applicable to general molecular systems, basis sets are usually constructed as direct products of one-dimensional functions, one for each degree of freedom. The size of such basis is the product of sizes of one-dimensional bases, meaning that it grows exponentially with respect to the number of degrees of freedom, which limits applicability

to systems with few atoms. Additional problem of the Rayleigh-Ritz method is the fact that matrix elements of the potential energy surface (PES) must be computed. These are multidimensional integrals, that require either the knowledge of the analytical form of the PES, or a very large number of PES evaluations, if one uses numerical integration. By far the most efficient method for the computation of these elements is the use of quadrature.[47] Specific type of quadrature can be used for specific types of basis functions, to ensure that the integrals are approximated with sufficient accuracy. Quadrature points also represent the optimal set of points in the collocation method, which inherently does not require evaluation of the integrals, but requires an ad hoc choice of the points. However, even with the use of quadrature for the computation of potential matrix elements, the number of PES evaluations is generally so large, that it is more feasible to fit the potential energy surface and use its analytic form.

While quadrature points are known for many types of integrals, and as such can be matched with a number of basis set choices, there is no general algorithm for computation of the optimal set of points for arbitrary basis set functions. This limits the types of basis functions that can be used. This is problematic, as basis functions for which quadrature can be used may poorly describe the wavefunctions, meaning that larger basis must be used, which can drastically increase the computational demands. This can be remedied with the use of discrete variable representation (DVR).[21] In this approach, one-dimensional basis set functions are used to construct the matrix of the position operator for the corresponding coordinate. This matrix is then diagonalized and its eigenvectors used to rotate the original basis into the DVR basis. The DVR functions approximate eigenfunctions of the position operator, meaning that they are localized around certain points in space, which correspond to their eigenvalue. Eigenvalues can be used as quadrature points, with weights that can be computed from the elements of the eigenvector. It can be proven that if the basis is chosen so that the position operator matrix is tridiagonal, the quadrature obtained corresponds to the Gaussian quadrature.[48] As DVR provides an efficient method for computation of potential matrix elements in arbitrary basis set, basis functions can be tailored according to the PES that is of interest. Such approach can greatly reduce the number of basis set functions per degree of freedom necessary for a good description of the system, leading to faster convergence with respect to the basis set size. This approach is the basis of potential optimised DVR (PODVR),[49] where one-dimensional functions are constructed as eigenfunctions of one-dimensional potential, defined along some molecular coordinate. These one-dimensional eigenfunctions are in turn computed using ordinary DVR method, which is numerically efficient as the problem treated is one-dimensional. If one-dimensional potentials are carefully chosen, retaining only a few eigenfunctions per degree of freedom results in good convergence.

The size of basis sets can be reduced by suitable choice of coordinates. If coordinates

are chosen so that the coupling between them is minimal, product of eigenfunctions of the one-dimensional potential energy curves associated with them already represents a good description of the molecular wavefunction. Consequently, only few basis functions have to be used to achieve convergence.[50] There is no universal method for choosing the best set of coordinates, and they are mostly selected employing chemical intuition. Intuitively, bond stretching, angle bending and torsions are prototypical motions in molecules. Thus, coordinates are frequently chosen to emulate these motions approximately. Direct use of internal coordinates (bond lengths, bond angles and torsion angles) is uncommon, due to the linear dependence between them and the fact that they are not orthogonal, which results in mixed derivatives in kinetic energy operator. Rather unfortunately, coordinates that provide a good description of motions in the molecule are frequently curvilinear. As a result, kinetic energy operators can have complicated forms and have to be computed for each system separately. This results in the loss of generality of such methods, and makes it difficult to create a 'black box' implementation. Recently, advancements have been made in numerical generation of kinetic energy operators in arbitrary curvilinear coordinates,[50,51] with growing number of applications.

The most recent advances in quantum-mechanical methods are mostly focused on reduction of basis set size and compactification of the wavefunction form. The methods for reduction of basis set size involve use of pruned or energy-selected basis sets, in which only some of the products of one-dimensional functions are retained in the basis set. Pruned basis sets[19] can be obtained by constricting the indices of one-dimensional functions. On the other hand, energy-selected bases[52] are usually constructed from one-dimensional functions that are eigenfunctions of one-dimensional Hamiltonian operators corresponding to certain coordinates in the system, while restricting the total energy of the product below some threshold. The methods for compactification of wavefunction treat coefficients corresponding to basis functions as tensors with the number of indices corresponding to the number of degrees of freedom. These tensors are then decomposed in terms of lower-order tensors, with the type of decomposition differing between different methods. These methods include density matrix renormalization group (DMRG),[20] tree tensor network states (TTNS)[53] and other.

Alternatively, computational demands can be significantly reduced by restricting the degrees of freedom to some subset of all coordinates. Such methods are known as reduced-dimensionality methods.[54] They require extensive a priori assumptions for the system, as coordinates that are restricted and removed from the wavefunction must not influence the properties that are being sought after. Such assumptions can lead to significant errors in case of tunneling splittings, as its magnitude is extremely sensitive to small perturbations of the system. Tunneling splitting is usually computed in this manner by choosing some a priori path that connects the minima, known as the reaction path. The choice of the reaction path is usually

minimum energy path (MEP), linear path that connects the minima, or a linear combination of those two.[22] Coordinates that are taken into account are chosen to be either some set of normal modes that describes the path, or by choosing the position on the path as one coordinate, and selecting several coordinates orthogonal to the path which are deemed important in some manner. Latter choice has a disadvantage of generating a curvilinear set of coordinates if the reaction path has non-zero curvature, resulting in complicated forms of kinetic energy operator. Former choice can be used to determine a set of orthogonal coordinates, with a simple kinetic operator form, but which may not provide adequate description of the tunneling process. Unfortunately, it is known from the instanton theory[14] that the magnitude of tunneling splitting displays exponential dependence on height and width of the barrier along the selected path, as well as on the zero-point energy of the motions orthogonal to selected path. Thus, removal of certain coordinates from the calculation can have severe impact on the splitting obtained. Even if the contribution of every single restricted coordinate is small, cumulative effect of all restricted coordinates can be significant. Richardson[55] demonstrated on the example of formic acid dimer that tunneling splitting slowly converges with the addition of normal modes to the calculation, and that previous results obtained by reducing the system to 4 degrees of freedom resulted in splitting that is roughly 25 % larger than the value obtained in full dimensionality, which agrees with the experiment.

In spite of many difficulties associated with direct diagonalization methods, a number of systems which exhibit tunneling splitting has been modelled using this approach. Several authors[5,41] have studied HF dimer in the ground rotational state $J = 0$ in full dimensionality. Additionally, fully deuterated DF dimer[56,57] and mixed HF-DF dimer[57] have also been computed. Yu et al.[7] have computed tunneling splittings in several rovibrational states of vinyl radical using full-dimensional PODVR basis and obtained quantitative agreement with experimental values. Tunneling splitting in water dimer has been extensively studied, both in reduced dimensionality with rigid monomers[58,59] and in full dimensionality, with fast intramolecular vibrations adiabatically separated from the slow intermolecular motion,[60] and without adiabatic separation.[40]

2.1.2. Diffusion Monte Carlo

Diffusion Monte Carlo is a method for computing energies and wavefunctions of ground state and low-lying excited states using Monte Carlo sampling.[23] It is based on the time-dependent Schrödinger equation in imaginary time $\tau = it$

$$\frac{\partial}{\partial \tau} \Psi(\mathbf{x}, \tau) = (\hat{H} - E_{\text{ref}})\Psi(\mathbf{x}, \tau)$$

$$\Psi(\mathbf{x}, \tau) = \sum_{i=0}^{+\infty} c_i \psi_i(\mathbf{x}) e^{-(E_i - E_{\text{ref}})\tau}. \tag{2.4}$$

From the form of the solution in terms of eigenstates, it can be seen that propagation in imaginary time causes the decay of all states with $E_i > E_{\text{ref}}$, where E_{ref} is some reference energy. If the reference energy is chosen to equal the energy of the ground state, after sufficiently long propagation, components of all higher states decay, leaving only the ground-state component. Imaginary-time Schrödinger equation takes form of the diffusion equation[61] if one identifies diffusion coefficients as $D_i = (2m_i)^{-1}$.

$$\frac{\partial}{\partial \tau}\Psi(\mathbf{x}, \tau) = D_i \frac{\partial^2}{\partial x_i^2}\Psi(\mathbf{x}, \tau) + (V(\mathbf{x}) - E_{\text{ref}})\Psi(\mathbf{x}, \tau), \tag{2.5}$$

with additional term $(V(\mathbf{x}) - E_{\text{ref}})\Psi(\mathbf{x}, \tau)$ that can be interpreted as a source or a sink of particles, for $V(\mathbf{x}) < E_{\text{ref}}$ and $V(\mathbf{x}) > E_{\text{ref}}$ respectively. The idea of DMC method is to represent the ground-state wavefunction as an ensemble of delta functions, which are called walkers, whose positions can be propagated using the Monte Carlo algorithm, while the source/sink term affects their population.[62] Ground-state energy is computed by adjusting the reference energy during the propagation so that the population of the walkers remains constant. When the population of the walkers is stabilized, the reference energy corresponds to the ground-state energy. Improved sampling of the potential energy surface can be obtained by introducing a guide wavefunction $f(\mathbf{x}, \tau) = \Psi(\mathbf{x}, \tau)\Psi_{\text{T}}(\mathbf{x}, \tau)$, an idea similar to the importance sampling.[63,64] This transforms the diffusion equation into

$$\frac{\partial f}{\partial \tau} = D_i \nabla_i^2 f - \frac{1}{m_i}\nabla_i(f\nabla \ln \Psi_{\text{T}}) - (\Psi_{\text{T}}^{-1}\hat{H}\Psi_{\text{T}} - E_{\text{ref}})f, \tag{2.6}$$

where the additional term $-\frac{1}{m_i}\nabla_i(f\nabla \ln \Psi_{\text{T}})$ corresponds to the flux of particles, governed by the force $\mathbf{F} = \nabla \ln \Psi_{\text{T}}$. To get the best results, it is preferable to choose the guiding wavefunction to resemble the ground-state one as much as possible. One possibility is to use unbiased DMC calculation (i.e. the calculation with $\Psi_{\text{T}} = 1$) to construct the trial wavefunction.[65] However, this method becomes prohibitively costly for systems with many degrees of freedom, which are frequently encountered if one considers tunneling in molecules. Another possibility is to represent the trial wavefunction as a product of single-coordinate wavefunctions, which can be computed from one-dimensional potential energy surfaces using variational quantum mechanical methods. When the choice of the guiding wavefunction is made and an ensemble of walkers is generated, the walkers are propagated in time. Propagation is made by finding a short-time solution of the diffusion equation for the δ-function centered at the position of a specific walker as the initial condition. This solution corresponds to the Gaussian distribution

$$U(\mathbf{x}, \tau + d\tau) = \prod_{k=1}^{N_{\text{dof}}}(4\pi D_k(\tau + d\tau))^{-3/2}e^{-\frac{(\mathbf{x}(\tau+d\tau)-\mathbf{x}(\tau))^2}{4D_k(\tau+d\tau)}}. \tag{2.7}$$

From the form of this solution, it is evident that the initial δ-distribution spreads over at later times. This means that for the further propagation, it would be necessary to obtain information on the potential energy surface in the certain region around the position of the walker. To avoid computationally expensive determination of local potential energy surface, new position of the walker is sampled from the distribution (2.7) using the following expression

$$\mathbf{x}_i(\tau + \Delta\tau) = \mathbf{x}_i(\tau) + \text{RAND} + D_i\Delta\tau F_i(\mathbf{x}_i(\tau)), \tag{2.8}$$

where RAND is a random number sampled from the Gaussian distribution with the width $\sqrt{2D_i\Delta\tau}$ and the last term accounts for the motion of the center of Gaussian distribution under influence of guiding force $\mathbf{F}$. After every move, the effect of the source/sink term on the population must be evaluated. There are two common methods for doing this.[23] First relies on assigning weights w_i to every walker, which are updated according to

$$w_i(\tau + \Delta\tau) = w_i(\tau)e^{-(\Psi_T^{-1}\hat{H}\Psi_T - E_{\text{ref}})\Delta\tau}. \tag{2.9}$$

The major downside of this method is that, usually, after the propagation a majority of walkers carry negligible weights, while only few walkers contribute significantly, resulting in poor statistics. Alternative method is branching of the walkers. In this method, all walkers are assigned equal weights, and after every step an integer

$$n_i = \text{INT}\left(e^{-(\Psi_T^{-1}\hat{H}\Psi_T - E_{\text{ref}})\Delta\tau} + \text{RAND}\right) \tag{2.10}$$

is evaluated, with RAND being a random number sampled from uniform distribution on the interval $[0, 1]$. If $n_i = 0$, the walker is annihilated and is not propagated further, while if $n_i > 0$, the walker is split into n_i replicas. As a result, physically significant region of potential energy surface is sampled with greater accuracy, resulting in better statistics. However, the downside is that the number of walkers is not constant during the propagation. There are also methods that combine these two approaches, for example propagating the weights and annihilating the walker if its weight becomes too small, while simultaneously splitting the walker with the greatest weight in two, each with half the weight.[43] This results in the better sampling of the relevant region, while keeping the number of walkers constant.

To obtain tunneling splitting, it is necessary to compute the energy of the first excited state in addition to the ground-state energy. There are two approaches in the DMC that can be used for this purpose. The first requires an *a priori* knowledge of the nodal plane of the excited state wavefunction.[65] Walkers are then propagated in the restricted region of space by imposing the condition that the walker is annihilated if it crosses the nodal plane. This imposes the node in the wavefunction and the DMC propagation results in the energy of

the first excited state. Such approach can be used in symmetric systems, where position of the nodal plane can be deduced from the symmetry considerations. Alternative method, which is widely used for calculation of tunneling splitting is the use of projection operators (POITSE method).[66] This method seeks to extract the excited state energy from the Laplace transformation of the correlation function

$$\kappa(\tau) \propto \langle \Psi | \hat{A} e^{-(\hat{H}-E_{\text{ref}})\tau} \hat{A}^{\dagger} | \Psi \rangle, \tag{2.11}$$

where $\hat{A}$ is a projection operator, i.e. an operator which ideally projects the ground state to the first excited state. Its purpose is to reduce the number of contributions to the correlation function and improve the statistics for the excited state energy. A common choice for projection operator is multiplication with some coordinate that describes tunneling between the two minima, and is expected to be approximately orthogonal to the nodal plane. Correlation function is estimated at every time step using the DMC algorithm described above.

DMC has been used to calculate tunneling splitting in many molecular systems. Viel et al.[43] computed ground state tunneling splitting for both malonaldehyde and malonaldehyde with deuterated hydroxyl group and obtained tunneling splittings within 10 % of experimental values. Wang et al.[10] have done the same calculation on an improved potential energy surface and obtained results comparable with the experiments within the experimental error range. Gregory and Clary[67] computed tunneling splittings in water dimer, using rigid-monomer approximation. They took into consideration three rearrangement motions in the water dimer and obtained quantitative agreement of the tunneling matrix elements with the experimental values for two of them. Quack and Suhm[68] computed tunneling splitting in HF dimer using rigid-monomer approximation as well, and imposing the nodal plane from symmetry requirements. The results they obtained were in an excellent agreement with the quantum-mechanical values obtained on the same potential energy surface. DMC approach is computationally less intensive than direct diagonalization methods and can be used to treat larger systems in full dimensionality. However, the number of potential energy evaluations necessary to obtain converged energies can still be large, meaning that its use is limited to systems with analytic potential energy surface.

2.1.3. Multiconfigurational Time-Dependent Hartree Method

Multiconfigurational time-dependent Hartree (MCTDH)[4,69,70] is a method used for propagation of nuclear wavepackets. The core idea of this method is to represent the wavepackets by the following ansatz

$$\Psi(\mathbf{x}) = \sum_{k_1\dots,k_n} A_{k_1\dots k_n} \phi_{k_1}^{(1)}(x_1) \cdots \phi_{k_n}^{(n)}(x_n) = \sum_K A_K | \Phi_K \rangle, \tag{2.12}$$

where one-dimensional functions ϕ_k^j are analogues of orbitals in electronic structure theory and $K = (k_1, ..., k_n)$. Equation of motion for such ansatz is derived from Dirac-Frenkel variational principle[71,72] and has the following form

$$i\frac{\partial}{\partial t}A_K = \sum_L \langle\Phi_K|\hat{H}|\Phi_L\rangle A_L$$

$$i\frac{\partial}{\partial t}\phi^{(k)} = (1 - \mathbf{P}^{(k)})\left((\boldsymbol{\rho}^{(k)})^{-1}\langle\mathbf{H}\rangle^{(k)}\right)\phi^{(k)}$$

$$\mathbf{P}^{(k)} = \sum_j \left|\phi_j^{(k)}\right\rangle\left\langle\phi_j^{(k)}\right|$$

$$\rho_{jl}^{(k)} = \left\langle\frac{\partial\Psi}{\partial\phi_j^{(k)}}\middle|\middle|\frac{\partial\Psi}{\partial\phi_l^{(k)}}\right\rangle$$

$$\langle\mathbf{H}\rangle_{jl}^{(k)} = \left\langle\frac{\partial\Psi}{\partial\phi_j^{(k)}}\middle|\hat{H}\middle|\frac{\partial\Psi}{\partial\phi_l^{(k)}}\right\rangle. \tag{2.13}$$

One-dimensional functions $\phi_j^{(k)}$ are represented as a linear combination of some basis set functions, which means that the objects that are propagated are coefficients in these linear combinations and elements of the vector $\mathbf{A}$. The propagation equations for the vector $\mathbf{A}$ and one-dimensional functions $\phi_j^{(k)}$ are coupled and non-linear. They can be propagated using multi-purpose integrators, such as Adams-Bashforth-Moulton predictor-corrector[73]. Such propagation, however, requires small time steps, as phases of elements A_K oscillate rapidly, with frequency proportional to the energy expectation value of the corresponding configuration $|\Phi_K\rangle$. A more efficient propagation can be done using the constant mean-field (CMF) approximation. In this approximation, Hamiltonian matrix $\langle\Phi_K|\hat{H}|\Phi_L\rangle$, density matrices $\rho_{jl}^{(k)}$ and mean-field matrices $\langle\mathbf{H}\rangle_{jl}^{(k)}$ are assumed to vary more slowly than the oscillations of the phase of coefficients A_K. They are thus held constant for the duration of a certain time step, which effectively decouples the propagation equation for vector A_K and one-dimensional functions. Propagation equation for A_K becomes linear differential equation and can be propagated using efficient specialized algorithms, such as Lanczos[74] or Chebyshev[75] integrators. Propagation equation for the one-dimensional functions is still non-linear, due to the projector operators $\mathbf{P}^{(k)}$ and must be propagated with general-use integrators, such as Adams-Bashforth-Moulton predictor-corrector or Bulirsch-Stoer extrapolation method[73]. Unlike direct methods, number of objects that is necessary to store the MCTDH wavepacket is much smaller than in the case of direct diagonalization methods, as one-dimensional functions are constructed to optimally represent the wavepacket with a small number of configurations, in contrast to using a predetermined basis set of one-dimensional functions, for which many configurations are necessary. The loss of certain configurations results in the

loss of correlation between different coordinates. However, unlike electronic wavefunctions, nuclear wavepackets are more localized, due to the larger mass of nuclei in comparison to electrons, making the neglected correlation less significant.[24]

Vibrational energy levels can be computed from the MCTDH propagation using Lanczos diagonalization algorithm.[76] This algorithm seeks approximate eigenvalues of a certain operator $\hat{A}$ by constructing an M-dimensional basis in which its matrix is tridiagonal, and can thus be diagonalized using efficient diagonalization schemes. The basis is generated from a 'seed' vector $|v_1\rangle$ as

$$|v_i\rangle = C\left(\hat{A}|v_{i-1}\rangle - \sum_{j=0}^{i-1} \langle v_j|\hat{A}|v_{i-1}\rangle\right), \tag{2.14}$$

where constant C is chosen so that the obtained vector is normalized. The sum in the parentheses amounts to orthogonalization of the obtained $\hat{A}|v_{i-1}\rangle$. In addition to the fact that the matrix in this basis is tridiagonal, additional benefit arises from the fact that the basis is biased towards the largest eigenvalues of $\hat{A}$, as they begin to dominate in the vectors $\hat{A}^k|v_1\rangle$ as k increases. Thus, relatively few vectors can be used to obtain converged eigenvalues. In the MCTDH approach, there are two convenient choices of operator $\hat{A}$ that can be used to compute energy levels[36,77]

$$\hat{A} = e^{-i\Delta t\hat{H}}$$
$$\hat{A} = e^{-\Delta\tau\hat{H}}. \tag{2.15}$$

In both cases, multiplication $\hat{A}|v_{i-1}\rangle$ amounts to the propagation step, either in real or imaginary time, which can efficiently be done in MCTDH formalism. There are both upsides and downsides for both choices of operator $\hat{A}$. In case of the real-time propagator, operator $\hat{A}$ is not Hermitian and maps all energy levels to the interval $2\pi/\Delta t$, meaning that shorts time steps must be used. Furthermore, orthogonalization step gradually removes contributions of the low-lying states, which are usually of interest, while increasing the weight of the higher states. On the other hand, this propagator treats all energy levels in the desired energy range equivalently. In contrast, imaginary-time propagator is Hermitian, but is biased towards low-lying energy states, as they dominate in the vectors $\hat{A}^k|v_1\rangle$. This is convenient if only ground-state energy or splitting are sought, but has negative effects if excited vibrational states are desired. A good compromise between these operators can be found by combining them as

$$\hat{A} = e^{-i\Delta t\hat{H}}e^{-\Delta\tau\hat{H}}. \tag{2.16}$$

Such propagator damps the unwanted high-energy states before application of the real-time propagator, removing them from the basis and alleviating the problem of the real-time operator. Additionally, eigenvalues of such operator provide two estimates of the energies, one from the

norm of the eigenvalues $|\lambda_j| = \exp(-\Delta\tau E_j)$ and one from the phase $\lambda_j/|\lambda_j| = \exp(-i\Delta t E_j)$. Agreement between these eigenvalues can be used as an estimate of the error in their values. A third approach can also be used, which replaces the orthogonal basis with non-orthogonal one of the form $|w_i\rangle = \exp(-\Delta\tau\hat{H})|v_i\rangle$ and solving the generalized eigenvalue problem.[36]

For computation of tunneling splitting, it is advantageous to use more then one seed vector in the Lanczos scheme.[78,79] Each seed vector generates a set of basis vectors and the resulting matrix becomes banded instead of tridiagonal. However, even though the diagonalization of banded matrices is computationally more intensive that diagonalization of tridiagonal matrices, good choice of seed vectors can significantly reduce overall the number of basis vectors necessary to converge the eigenvalues, thus resulting in a more efficient algorithm. For symmetric double-well systems, a good choice for the seed vectors are symmetric and antisymmetric combinations of single-well wavepackets.

As MCTDH approach is based on diagonalization of a function of Hamiltonian, it can be used to compute tunneling splittings in excited vibrational states. Hammer and Manthe[8] have demonstrated that an efficient method for computing tunneling splittings in singly excited vibrational states is obtained by taking the seed vectors to be generated as $\hat{\mu}\left|\Psi^{(\pm)}\right\rangle$, where $\hat{\mu}$ is the dipole moment operator. This operator effectively maps the ground state tunneling doublet to the vibrationally excited states with high transition probability. They used this method to obtain tunneling splittings for several singly-excited states of malonaldehyde in excellent agreement with the experimental values.

As has been mentioned previously, MCTDH calculations are less resource-intensive than the direct diagonalization methods. However, they require analytic potential energy surface. This is due to the fact that potential energy matrix elements must be computed for the MCTDH calculation. Number of elements that have to be computed is usually reduced by representing the potential energy surface as a sum of products of one-dimensional terms, which reduces multidimensional integrals that represent potential energy matrix elements to the combinations of one-dimensional integrals. However, to compute the form of the potential energy surface, it has to be fitted to the aforementioned form first, which requires large number of potential energy evaluations. One-dimensional integrals can then be efficiently computed, either using the analytic expressions tailored for a specific combination of basis set functions and functions used to represent potential energy surface, or using the DVR approach. Due to these requirements, MCTDH calculations are usually either as intensive or more intensive than DMC calculations, but provide the excited-state tunneling splittings as well. Numerical efficiency can be significantly increased using multilayer MCTDH.[80] In this approach, instead of writing the Hartree product of one-dimensional functions, some modes that are strongly correlated may be combined into multidimensional functions, which can be determined using MCTDH as well. Grouping of coordinates can be done on several

levels, resulting in a compact form of the **A** tensor. As a result, systems with an order of magnitude more degrees of freedom may be treated. Finally, need for analytic potential energy surfaces may be removed by replacing the one-dimensional functions with Gaussian functions, whose maximum is time-dependent.[81] Integrals involving potential energy surface can then be evaluated in harmonic approximation around the position of the maximum, for which only potential energy Hessian is necessary, which can be computed on-the-fly.

2.2. Path Integral Formulation of Quantum Mechanics

One of the central objects studied in classical physics is action,[82] defined as a functional of the trajectory of point particles that form the system of interest

$$S(\mathbf{x}) = \int_{t_a}^{t_b} L(\dot{\mathbf{x}}, \mathbf{x}, t) \mathrm{d}t, \tag{2.17}$$

where $L(\dot{\mathbf{x}}, \mathbf{x}, t)$ denotes the Lagrangian of the system, and $\mathbf{x}(t)$ is the trajectory of all the particles. In the absence of magnetic fields, and ignoring the relativistic effects, the Lagrangian takes the form

$$L(\dot{\mathbf{x}}, \mathbf{x}, t) = \frac{1}{2} m_i \dot{x}_i \dot{x}_i - V(\mathbf{x}), \tag{2.18}$$

where $V(\mathbf{x})$ denotes the potential of the system. Transition to mass-scaled coordinates, defined as $x_i^{(\mathrm{mw})} = \sqrt{m_i} x_i$ can be used to absorb the mass term. From this point on, Einstein summation convention will be used, unless mentioned otherwise, and use of mass-scaled coordinates will be assumed. In mass-scaled coordinates, Lagrangian is recast in the form

$$L(\dot{\mathbf{x}}, \mathbf{x}, t) = \frac{1}{2} \dot{\mathbf{x}} \cdot \dot{\mathbf{x}} - V(\mathbf{x}). \tag{2.19}$$

Classical equations of motion can be derived by postulating that the system evolves from the initial point $\mathbf{x}_a$ at t_a to the final point $\mathbf{x}_b$ at t_b along the trajectory for which action is stationary, which is known as the principle of stationary action or Maupertius principle. Equations of motion follow by applying the calculus of variations to the action functional. This is done by observing paths that are close to the classical trajectory, denoting them as

$$\mathbf{x}(t) = \mathbf{x}_{\mathrm{cl}}(t) + \delta \mathbf{x}(t) \tag{2.20}$$

with the condition that $\delta\mathbf{x}(t_a) = \delta\mathbf{x}(t_b) = 0$, which ensures that the initial and final point are fixed. Expanding action to the first order in $\delta\mathbf{x}$ yields

$$S(\mathbf{x}_{\mathrm{cl}} + \delta\mathbf{x}) = \int_{t_a}^{t_b} L(\dot{\mathbf{x}}_{\mathrm{cl}} + \delta\dot{\mathbf{x}}, \mathbf{x}_{\mathrm{cl}} + \delta\mathbf{x}, t)\mathrm{d}t$$

$$S(\mathbf{x}_{\mathrm{cl}} + \delta\mathbf{x}) = \int_{t_a}^{t_b} \left(L(\dot{\mathbf{x}}_{\mathrm{cl}}, \mathbf{x}_{\mathrm{cl}}, t) + \left.\frac{\partial L}{\partial \dot{x}_i}\right|_{\mathbf{x}_{\mathrm{cl}}} \delta\dot{x}_i + \left.\frac{\partial L}{\partial x_i}\right|_{\mathbf{x}_{\mathrm{cl}}} \delta x_i \right)\mathrm{d}t$$

$$S(\mathbf{x}_{\mathrm{cl}} + \delta\mathbf{x}) = S(\mathbf{x}_{\mathrm{cl}}) + \left.\frac{\partial L}{\partial x_i}\delta x_i\right|_{t_a}^{t_b} + \int_{t_a}^{t_b} \left(-\frac{\mathrm{d}}{\mathrm{d}t}\left.\frac{\partial L}{\partial \dot{x}_i}\right|_{\mathbf{x}_{\mathrm{cl}}} + \left.\frac{\partial L}{\partial x_i}\right|_{\mathbf{x}_{\mathrm{cl}}} \right)\delta x_i \mathrm{d}t$$

$$S(\mathbf{x}_{\mathrm{cl}} + \delta\mathbf{x}) = S(\mathbf{x}_{\mathrm{cl}}) + \delta x_i \int_{t_a}^{t_b} \left(-\frac{\mathrm{d}}{\mathrm{d}t}\left.\frac{\partial L}{\partial \dot{x}_i}\right|_{\mathbf{x}_{\mathrm{cl}}} + \left.\frac{\partial L}{\partial x_i}\right|_{\mathbf{x}_{\mathrm{cl}}} \right)\mathrm{d}t. \tag{2.21}$$

For the action to be stationary, the second term must vanish, which can be accomplished by demanding that the classical path satisfies

$$\frac{\mathrm{d}}{\mathrm{d}t}\frac{\partial L}{\partial \dot{x}_i} = \frac{\partial L}{\partial x_i}, \tag{2.22}$$

which is the Lagrange equation of motion.

First formulations of quantum mechanics, made by Heisenberg and Schrödinger, were not given in terms of Lagrangian and action, but were centered on operators, which represent observables, and vectors, which represent the state of the system. First to note the role of Lagrangian in quantum mechanics was Dirac,[25] who considered the unitary transformations corresponding to contact transformations of position eigenstates. This idea was expanded upon by Feynman and developed into the path integral formulation.[26] Feynman considered probability amplitudes, which describe the state of the system in terms of possible outcomes of measurements of certain observable. He noted that, if three consecutive measurements of observables A, B and C (which may be the same) yields results a, b and c, then the probability of obtaining result c after measuring results a and b is given by

$$P_{abc} = P_{ab}P_{bc}, \tag{2.23}$$

where P_{ij} is the probability of obtaining result j after measurement that provided result i. Overall probability of obtaining c after measurement a is given as a sum over all possible results of measurement B

$$P_{ac} = \sum_b P_{ab}P_{bc}. \tag{2.24}$$

However, this statement does not hold for quantum systems. The simplest counterexample is the double-slit experiment, in which the diffraction pattern is not the same if a measurement

that determines through which slit the electron has passed is performed or not. This inconsistency can be remedied by postulating the existence of probability amplitude $K(i,j)$, which is a complex number that satisfies

$$P_{ac} = |K(a,c)|^2$$
$$K(a,c) = \sum_b K(a,b)K(b,c). \tag{2.25}$$

As probability amplitudes are complex numbers, the differences in their phases account for the diffraction pattern produced in the double-slit experiment. Feynman used the properties of (2.25) to assign the probability amplitude to a certain trajectory that system can take to evolve from point $\mathbf{x}_a$ at t_a to the point $\mathbf{x}_b$ at t_b. This is done by discretization of the trajectory at points t_m, which is in literature commonly referred to as time-slicing. Feynman used equally spaced time intervals $t_{m+1} - t_m = \varepsilon$. However, this does not have to be the case. In fact, defining potential-dependent time intervals is the key of Duru-Kleinert transformation,[83,84] which can be used to apply path integral formalism to potentials with singularities, such as the Coulomb potential. The time-sliced probability amplitude for a certain trajectory is then

$$K(\mathbf{x}(t)) = K(\mathbf{x}_a,t_a;\mathbf{x}_1,t_1)K(\mathbf{x}_1,t_1;\mathbf{x}_2,t_2)...K(\mathbf{x}_N,t_N;\mathbf{x}_b,t_b) = \prod_{\substack{m=0 \\ \mathbf{x}_0=\mathbf{x}_a \\ \mathbf{x}_{N+1}=\mathbf{x}_b}}^{N} K(\mathbf{x}_m,t_m;\mathbf{x}_{m+1},t_{m+1})$$

$$\tag{2.26}$$

Finally, the probability amplitude for time evolution from $\mathbf{x}_a$ to $\mathbf{x}_b$ is obtained by summing over all possible intermediate values of positions. As position is a continuous variable, sums are replaced with integrals, which yields

$$K(\mathbf{x}_a,t_a;\mathbf{x}_b,t_b) = \int_{-\infty}^{+\infty} ... \int_{-\infty}^{+\infty} \prod_{\substack{m=0 \\ \mathbf{x}_0=\mathbf{x}_a \\ \mathbf{x}_{N+1}=\mathbf{x}_b}}^{N} K(\mathbf{x}_m,t_m;\mathbf{x}_{m+1},t_{m+1})\mathrm{d}\mathbf{x}_1...\mathrm{d}\mathbf{x}_N. \tag{2.27}$$

Finally, Feynman postulated, based on the previous work by Dirac, that the individual probability amplitudes are connected to the finite-difference Lagrangian as

$$K(\mathbf{x}_m,t_m;\mathbf{x}_{m+1},t_{m+1}) = \exp\left(i\varepsilon L\left(\frac{\mathbf{x}_{m+1}-\mathbf{x}_m}{\varepsilon},\mathbf{x}_m,t_m\right)\right). \tag{2.28}$$

It should be noted that, in presence of vector potentials, one must take the midpoint $(\mathbf{x}_{m+1} + \mathbf{x}_m)/2$ instead of $\mathbf{x}_m$ in the discretization of L. Otherwise, the computed probability amplitude does not correspond to the one obtained from Schrödinger equation.[27] Inserting this expression into (2.27) and taking the limit $\varepsilon \to 0$, one arrives at the central equation of the path integral

formalism

$$K(\mathbf{x}_a, t_a; \mathbf{x}_b, t_b) = A \int_{\mathbf{x}(t_a)=\mathbf{x}_a}^{\mathbf{x}(t_b)=\mathbf{x}_b} e^{iS(\mathbf{x}(t))} \mathscr{D}\mathbf{x}. \tag{2.29}$$

The object on the right-hand side of this equation is the path integral, i.e. the integral over all possible paths that satisfy the correct boundary conditions. The operative definition is given by time-slicing of the path, producing the expression analogous to (2.27) in the limit of $\varepsilon \to 0$. Constant A is added to normalize the overall probability to unity, and will be derived in the following sections. Probability amplitude thus defined is also referred to as the kernel and is proportional to the Green's function of the quantum-mechanical time propagator.[85]

2.2.1. Stationary Phase Approximation

A common method for evaluation of the kernel between two points is the stationary phase approximation.[27,28] The idea of this method is to locate the minimum action path $\mathbf{x}^{(0)}$ (MAP) and expand the action functional up to second order with respect to fluctuations $\delta\mathbf{x}$ around the MAP. The action then becomes

$$\mathbf{x}(t) = \mathbf{x}^{(0)}(t) + \delta\mathbf{x}(t)$$
$$S(\mathbf{x}(t)) \approx S(\mathbf{x}^{(0)}(t)) + \frac{1}{2}\delta\mathbf{x}^\top \mathbf{H}\delta\mathbf{x}, \tag{2.30}$$

where $\mathbf{H}$ denotes the action hessian, which is defined for the time-sliced paths as $H_{ij,kl} = \frac{\partial^2 S}{\partial x_i(t_j)\partial x_k(t_l)}\big|_{\mathbf{x}=\mathbf{x}^{(0)}}$. This reduces the path integral to a Gaussian integral, which can be solved analytically. Restoring the $\hbar$, the kernel becomes

$$K(\mathbf{x}_a, t_a; \mathbf{x}_b, t_b) = A \int_{-\infty}^{+\infty} e^{iS(\mathbf{x}^{(0)}(t))/\hbar + i/(2\hbar)\delta\mathbf{x}^\top \mathbf{H}\delta\mathbf{x}} d\delta\mathbf{x}_1...d\delta\mathbf{x}_N$$
$$K(\mathbf{x}_a, t_a; \mathbf{x}_b, t_b) = A \sqrt{\frac{(2\pi i\hbar)^{NN_{\text{dof}}}}{\det \mathbf{H}}} e^{iS(\mathbf{x}^{(0)}(t))/\hbar}. \tag{2.31}$$

In essence, stationary phase approximation assumes that MAP and paths that are in its neighbourhood account for the largest contribution in the path integral. Intuitively, this is true, as paths that are in the neighbourhood of some non-stationary action path are expected to display large variations in action. This causes destructive interference among them during path integration, as action plays a role of the phase. A more rigorous argument involves evaluation of path integral in the neighbourhood of some non-stationary path $S(\mathbf{x}^{(\text{NS})}(t))$. In this case, one can make a coordinate transformation from Cartesian fluctuations to a set of fluctuations in which the first coordinate q_1 is tangent to the action gradient, while the others are orthogonal to it. In this coordinate system, the action is stationary with respect to

coordinates $\mathbf{q}' = \{q_2, ..., q_{NN_{\text{dof}}}\}$, and can be expanded around them to second order

$$S(\mathbf{x}(t)) = S(q_1) + \frac{1}{2}\mathbf{q}'^{\top}\mathbf{H}'\mathbf{q}'. \tag{2.32}$$

In this case, the kernel becomes

$$K(\mathbf{x}_a, t_a; \mathbf{x}_b, t_b) = A\sqrt{\frac{(2\pi i\hbar)^{NN_{\text{dof}}-1}}{\det\mathbf{H}'}}\int_{-\infty}^{+\infty}e^{iS(q_1)/\hbar}dq_1. \tag{2.33}$$

One can now make another change of variables $z = S(q_1)$ and perform partial integration to arrive at

$$K(\mathbf{x}_a, t_a; \mathbf{x}_b, t_b) = A\frac{\hbar}{i}\sqrt{\frac{(2\pi i\hbar)^{NN_{\text{dof}}-1}}{\det\mathbf{H}'}}\left(\frac{1}{S'(q_1)}e^{iS(q_1)/\hbar}\bigg|_{-\infty}^{+\infty} - \int_{S(-\infty)}^{S(+\infty)}e^{iz/\hbar}\frac{d}{dz}\frac{1}{S'(q_1)}dz\right). \tag{2.34}$$

From this expression, one can see that the contribution of these paths is of the order $\sqrt{\hbar^{NN_{\text{dof}}+1}}$, while the contribution of the paths around MAP is of the order $\sqrt{\hbar^{NN_{\text{dof}}}}$, meaning that they dominate. Correspondence limit follows directly from this fact, as it means that in the classical limit $\hbar \to 0$, MAP dominates the path integral, with the contribution of neighbouring paths decreasing as $S/\hbar$ increases. Thus, classical particles can be taken to propagate only along MAP. If there are several stationary action paths, they all contribute to the path integral, and the expression for kernel becomes

$$K(\mathbf{x}_a, t_a; \mathbf{x}_b, t_b) = A\sqrt{\frac{(2\pi i\hbar)^{NN_{\text{dof}}}}{\det\mathbf{H}_1}}e^{iS(\mathbf{x}_1^{(0)}(t))/\hbar} + A\sqrt{\frac{(2\pi i\hbar)^{NN_{\text{dof}}}}{\det\mathbf{H}_2}}e^{iS(\mathbf{x}_2^{(0)}(t))/\hbar} + ... \tag{2.35}$$

In those cases, interference effects can be observed, which depend on the phase differences of different MAPs, which are $(S(\mathbf{x}_i^{(0)}(t)) - S(\mathbf{x}_j^{(0)}(t)))/\hbar$. The simplest of those cases is the double-slit experiment, in which a particle can arrive at the screen via two classical paths, one through each slit.

2.2.2. Equivalence with Schrödinger Formulation

Path integral formulation can be used to derive the time-dependent Schrödinger equation, which was shown by Feynman.[26,85] First step in the derivation is to provide a definition of a wavefunction. As modulus squared of the wavefunction and the kernel have similar interpretations in terms of probability density, a potential connection would be of the form

$$\Psi(\mathbf{x}, t) = \int f(\mathbf{x}_a)K(\mathbf{x}_a, t_a; \mathbf{x}, t)d\mathbf{x}_a, \tag{2.36}$$

where $f(\mathbf{x}_a)$ is some function that enables one to define an arbitrary wavefunction at $(\mathbf{x}, t)$. At an infinitesimally later moment $t + \delta t$, wavefunction becomes

$$
\begin{aligned}
\Psi(\mathbf{x}, t + \delta t) &= \int f(\mathbf{x}_a) K(\mathbf{x}_a, t_a; \mathbf{x}, t + \delta t) \mathrm{d}\mathbf{x}_a \\
&= \int \int f(\mathbf{x}_a) K(\mathbf{x}_a, t_a; \mathbf{x}', t) K(\mathbf{x}', t; \mathbf{x}, t + \delta t) \mathrm{d}\mathbf{x}_a \mathrm{d}\mathbf{x}' \\
&= \int \Psi(\mathbf{x}', t) K(\mathbf{x}', t; \mathbf{x}, t + \delta t) \mathrm{d}\mathbf{x}'.
\end{aligned}
\tag{2.37}
$$

For an infinitesimal δt, one can introduce a new variable $\mathbf{y}$ so that $\mathbf{x}' = \mathbf{x} + \mathbf{y}$ and expand both the kernel and the wavefunction as

$$
\Psi(\mathbf{x}', t) = \Psi(\mathbf{x}, t) + \frac{\partial \Psi(\mathbf{x}, t)}{\partial x_i} y_i + \frac{1}{2} \frac{\partial^2 \Psi(\mathbf{x}, t)}{\partial x_i \partial x_j} y_i y_j
$$

$$
\Psi(\mathbf{x}, t + \delta t) = \Psi(\mathbf{x}, t) + \frac{\partial}{\partial t} \Psi(\mathbf{x}, t) \delta t
$$

$$
K(\mathbf{x}', t; \mathbf{x}, t + \delta t) = A e^{i/(2\delta t \hbar) y_i y_i - i \delta t V(\mathbf{x})/\hbar}
$$

$$
\approx A e^{i/(2\delta t \hbar) y_i y_i} \left(1 - i \frac{\delta t}{\hbar} V(\mathbf{x})\right).
\tag{2.38}
$$

With these approximations, integrals in (2.37) are all of Gaussian form and can be solved analytically to yield

$$
\Psi(\mathbf{x}, t) + \frac{\partial}{\partial t} \Psi(\mathbf{x}, t) \delta t =
$$
$$
A \sqrt{(2\pi i \delta t \hbar)^{N_{\mathrm{dof}}}} \left(\Psi(\mathbf{x}, t) + \delta t i \frac{\hbar}{2} \frac{\partial^2}{\partial x_i \partial x_i} \Psi(\mathbf{x}, t) - \delta t i \hbar V(\mathbf{x}) \Psi(\mathbf{x}, t) \right), \tag{2.39}
$$

where higher order terms with respect to δt have been neglected. Equating terms of the same order, one arrives at the expressions for the normalization constant A and the wavefunction

$$
A = \frac{1}{\sqrt{(2\pi i \delta t \hbar)^{N_{\mathrm{dof}}}}}
$$
$$
i\hbar \frac{\partial}{\partial t} \Psi(\mathbf{x}, t) = -\frac{\hbar^2}{2} \frac{\partial^2}{\partial x_i \partial x_i} \Psi(\mathbf{x}, t) + V(\mathbf{x}) \Psi(\mathbf{x}, t), \tag{2.40}
$$

which is equivalent to the time-dependent Schrödinger equation. It should be noted that in the presence of vector potentials, which arises if one considers charged particles in magnetic fields, the outlined derivation becomes much more involved, and care must be taken when approximate form of the kernel is written.

Similarly, the expression for the kernel can be derived from the Schrödinger formulation. From the definition, kernel corresponds to the matrix element of time-evolution operator in

the basis of position eigenvectors

$$K(\mathbf{x}_a, t_a; \mathbf{x}_b, t_b) = \langle \mathbf{x}_b | e^{-i(t_b - t_a)/\hbar \hat{H}} | \mathbf{x}_a \rangle. \tag{2.41}$$

The time-evolution operator can be split into $N + 1$ products as

$$K(\mathbf{x}_a, t_a; \mathbf{x}_b, t_b) = \langle \mathbf{x}_b | e^{-i\delta t/\hbar \hat{H}} \ldots e^{-i\delta t/\hbar \hat{H}} | \mathbf{x}_a \rangle, \tag{2.42}$$

with $\delta t = (t_b - t_a)/(N + 1)$. At this point, one can place N resolutions of identity and expand the hamiltonian operator

$$K(\mathbf{x}_a, t_a; \mathbf{x}_b, t_b) = \int \langle \mathbf{x}_b | e^{-i\delta t/\hbar(\hat{T} + \hat{V})} | \mathbf{x}_1 \rangle \ldots \langle \mathbf{x}_N | e^{-i\delta t/\hbar(\hat{T} + \hat{V})} | \mathbf{x}_a \rangle \, d\mathbf{x}_1 \ldots d\mathbf{x}_N. \tag{2.43}$$

Each bracket in this integral can be split using Trotter product formula, which becomes exact in the limit $\delta t \to 0$. The expression thus obtained can be evaluated analytically as follows

$$
\begin{aligned}
\langle \mathbf{x}_i | e^{-i\delta t/\hbar \hat{T}} e^{-i\delta t/\hbar \hat{V}} | \mathbf{x}_{i+1} \rangle &= \int \langle \mathbf{x}_i | e^{-i\delta t/\hbar \hat{T}} | \mathbf{x} \rangle \langle \mathbf{x} | e^{-i\delta t/\hbar \hat{V}} | \mathbf{x}_{i+1} \rangle \, d\mathbf{x} \\
&= \int \langle \mathbf{x}_i | e^{-i\delta t/\hbar \hat{T}} | \mathbf{x} \rangle \langle \mathbf{x} | \mathbf{x}_{i+1} \rangle e^{-i\delta t/\hbar V(\mathbf{x}_{i+1})} \, d\mathbf{x} \\
&= \int \langle \mathbf{x}_i | e^{-i\delta t/\hbar \hat{T}} | \mathbf{x} \rangle \delta(\mathbf{x} - \mathbf{x}_{i+1}) e^{-i\delta t/\hbar V(\mathbf{x}_{i+1})} \, d\mathbf{x} \\
&= \langle \mathbf{x}_i | e^{-i\delta t/\hbar \hat{T}} | \mathbf{x}_{i+1} \rangle e^{-i\delta t/\hbar V(\mathbf{x}_{i+1})} \\
&= \int \langle \mathbf{x}_i | e^{-i\delta t/\hbar \hat{T}} | \mathbf{p} \rangle \langle \mathbf{p} | | \mathbf{x}_{i+1} \rangle e^{-i\delta t/\hbar V(\mathbf{x}_{i+1})} \, d\mathbf{p} \\
&= \int \langle \mathbf{x}_i | \mathbf{p} \rangle e^{-i\delta t/(2\hbar) \mathbf{p} \cdot \mathbf{p}} \langle \mathbf{p} | | \mathbf{x}_{i+1} \rangle e^{-i\delta t/\hbar V(\mathbf{x}_{i+1})} \, d\mathbf{p} \\
&= \frac{1}{(2\pi\hbar)^{N_{\text{dof}}}} \int e^{-i\delta t/(2\hbar) \mathbf{p} \cdot \mathbf{p} + i\mathbf{p} \cdot (\mathbf{x}_{i+1} - \mathbf{x}_i)/\hbar} e^{-i\delta t/\hbar V(\mathbf{x}_{i+1})} \, d\mathbf{p} \\
&= \frac{1}{\sqrt{(2\pi i\hbar \delta t)^{N_{\text{dof}}}}} e^{i(\mathbf{x}_{i+1} - \mathbf{x}_i)^2/(2\delta t)} e^{-i\delta t/\hbar V(\mathbf{x}_{i+1})}.
\end{aligned}
$$

When this expression is inserted into (2.43), equation for the kernel becomes

$$K(\mathbf{x}_a, t_a; \mathbf{x}_b, t_b) = \frac{1}{\sqrt{(2\pi i\hbar \delta t)^{N_{\text{dof}}(N+1)}}} \int e^{i\delta t/\hbar \sum_{i=1}^{N+1} ((\mathbf{x}_i - \mathbf{x}_{i-1})^2/(2\delta t^2) - V(x_i))} \, d\mathbf{x}_1 \ldots d\mathbf{x}_N, \tag{2.44}$$

where we define $\mathbf{x}_0 = \mathbf{x}_b$ and $\mathbf{x}_{N+1} = \mathbf{x}_a$. In the limit $\delta t \to 0$, the sum in the exponent becomes the action of the path, which means that the kernel obtained with this method has the same form as (2.29), with the appropriate normalization constant A. These results demonstrate the equivalence between Schrödinger formulation and the path integral formulation of quantum mechanics.

2.3. Ring Polymer Instanton Theory

One of the many methods for calculation of tunneling splitting relies on the determination of partition functions for the tunneling system and system constrained to one potential energy well. For clarity, it is sufficient to consider a double-well system, while the extension to the multi-well systems will be given at the end of this section.

Double-well system in which the minima are related by a symmetry operator $\hat{P}^{-1}$ and separated by a finite potential energy barrier will exhibit tunneling splitting of vibrational states. The prototypical Hamiltonian for such system is a 2×2 matrix

$$\hat{H} = \begin{pmatrix} E_i & -h_i \\ -h_i & E_i \end{pmatrix}, \tag{2.45}$$

where E_i denotes the energy of the i-th state constrained to one potential energy well, while h_i describes interaction between i-th localized states in each well caused by tunneling. Energy levels for such Hamiltonian are

$$E_i^{(\pm)} = E_i \mp h_i. \tag{2.46}$$

Obtained energy levels can be used to construct partition functions for the tunneling and non-tunneling system in the form

$$Z(\beta) = \sum_i \left(e^{-\beta E_i^{(+)}} + e^{-\beta E_i^{(-)}} \right)$$
$$Z_0(\beta) = 2 \sum_i e^{-\beta E_i}, \tag{2.47}$$

where $\beta = 1/(k_B T)$ denotes the inverse temperature. Interaction element for the ground vibrational state h_0, which shall be called the tunneling matrix element, can be extracted from the zero-temperature limit of the ratio of the partition functions

$$\lim_{\beta \to +\infty} \frac{Z(\beta)}{Z_0(\beta)} = \lim_{\beta \to +\infty} \frac{\sum_i \left(e^{-\beta E_i^{(+)}} + e^{-\beta E_i^{(-)}} \right)}{2 \sum_i e^{-\beta E_i}}$$
$$= \lim_{\beta \to +\infty} \frac{e^{-\beta E_0^{(+)}} + e^{-\beta E_0^{(-)}}}{2 e^{-\beta E_0}}$$
$$= \lim_{\beta \to +\infty} \cosh(\beta h_0), \tag{2.48}$$

which holds because in the limit $\beta \to +\infty$, the terms with the lowest energy dominate the sum. Thus, it is possible to calculate the tunneling matrix elements if low-temperature limits of the tunneling and non-tunneling partition functions are provided.[12] These can be computed using path integral formalism.[13,31]

An alternative, but closely related method for computing tunneling splitting, relies on the properties of density matrix elements

$$\rho(\mathbf{x}_a, \mathbf{x}_b, \beta) = \langle \mathbf{x}_a | \mathrm{e}^{-\beta \hat{H}} | \mathbf{x}_b \rangle. \tag{2.49}$$

This method was discovered and used by Ceperley and Jacucci[86] to compute the exchange frequency in solid ^{3}He. If one of the minima is denoted by $\mathbf{x}^{(0)}$, the diagonal density matrix element can be expanded as

$$\rho(\mathbf{x}^{(0)}, \mathbf{x}^{(0)}, \beta) = \sum_i \left(|\psi_i^{(+)}(\mathbf{x}^{(0)})|^2 \mathrm{e}^{-\beta E_i^{(+)}} + |\psi_i^{(-)}(\mathbf{x}^{(0)})|^2 \mathrm{e}^{-\beta E_i^{(-)}} \right). \tag{2.50}$$

Furthermore, the density matrix element that connects minimum $\mathbf{x}^{(0)}$ with its symmetry-related counterpart $\hat{P}^{-1}\mathbf{x}^{(0)}$ is

$$\rho(\mathbf{x}^{(0)}, \hat{P}^{-1}\mathbf{x}^{(0)}, \beta) = \sum_i \left(|\psi_i^{(+)}(\mathbf{x}^{(0)})|^2 \mathrm{e}^{-\beta E_i^{(+)}} - |\psi_i^{(-)}(\mathbf{x}^{(0)})|^2 \mathrm{e}^{-\beta E_i^{(-)}} \right), \tag{2.51}$$

where the fact that the two eigenfunctions have different symmetry properties with respect to $\hat{P}^{-1}$ has been used, namely $\psi_i^{(\pm)}(\mathbf{x}^{(0)}) = \pm\psi_i^{(\pm)}(\hat{P^{-1}}\mathbf{x}^{(0)})$. The ratio of these elements, in the low-temperature limit becomes

$$\lim_{\beta \to +\infty} \frac{\rho(\mathbf{x}^{(0)}, \hat{P}^{-1}\mathbf{x}^{(0)}, \beta)}{\rho(\mathbf{x}^{(0)}, \mathbf{x}^{(0)}, \beta)} = \lim_{\beta \to +\infty} \tanh\left(\frac{1}{2}\Delta E_0(\beta - \tilde{\beta}_0) \right)$$

$$\tilde{\beta}_0 = \frac{2}{\Delta E_0} \ln\left(\frac{|\psi_0^-(\mathbf{x}^{(0)})|}{|\psi_0^+(\mathbf{x}^{(0)})|} \right), \tag{2.52}$$

where $\Delta E = E_0^{(-)} - E_0^{(+)}$ denotes the ground-state splitting. In the case of deep tunneling, values of both eigenfunctions in one minimum are dominated by the value of the localized basis function of that well, which makes $\tilde{\beta}_0 \approx 0$ a good approximation.

Matyus and Althorpe[30] generalized this approach to treat systems with multiple symmetry-related minima. If symmetry operations $\hat{P}^{(i)}$ that connect the minima form the symmetry

group $\mathbb{G}$, density matrix elements that connect pairs of minima have the following form

$$\rho(\mathbf{x}^{(0)}, (\hat{P}^{(i)})^{-1}\mathbf{x}^{(0)}, \beta) = \sum_n \sum_\lambda \sum_{p=1}^{d_\lambda} \psi_{n\lambda p}^*(\mathbf{x}^{(0)}) \psi_{n\lambda p}((\hat{P}^{(i)})^{-1}\mathbf{x}^{(0)}) e^{-\beta E_{n\lambda}}$$

$$= \sum_n \sum_\lambda \sum_{p=1}^{d_\lambda} \psi_{n\lambda p}^*(\mathbf{x}^{(0)}) (\hat{P}^{(i)} \psi_{n\lambda p})(\mathbf{x}^{(0)}) e^{-\beta E_{n\lambda}}$$

$$= \sum_n \sum_\lambda \sum_{p=1}^{d_\lambda} \sum_{q=1}^{d_\lambda} \Gamma^{(\lambda)}(\hat{P}^{(i)})_{pq} \psi_{n\lambda p}^*(\mathbf{x}^{(0)}) \psi_{n\lambda q}(\mathbf{x}^{(0)}) e^{-\beta E_{n\lambda}}, \quad (2.53)$$

where $\Gamma^{(\lambda)}(\hat{P}^{(i)})$ denotes the matrix of operator $\hat{P}^{(i)}$ in λ-th irreducible representation. Index n labels the n-th excited state manifold, created by combining n-th excited localized wavefunctions from all the symmetry-related minima, while d_λ denotes the degeneracy of the corresponding λ-th irreducible representation formed on that manifold. It is possible to construct linear combinations of these matrix elements in which only one term for each n is nonzero. These combinations are of the form

$$\eta_{\lambda,pq}(\mathbf{x}^{(0)}, \beta) = \sum_i \Gamma^{(\lambda)}(\hat{P}^{(i)})_{pq}^* \rho(\mathbf{x}^{(0)}, (\hat{P}^{(i)})^{-1}\mathbf{x}^{(0)}, \beta)$$

$$= \sum_i \sum_n \sum_{\lambda'} \sum_{p'=1}^{d_n} \sum_{q'=1}^{d_n} \Gamma^{(\lambda)}(\hat{P}^{(i)})_{pq}^* \Gamma^{(\lambda')}(\hat{P}^{(i)})_{p'q'} \psi_{n\lambda' p'}^*(\mathbf{x}^{(0)}) \psi_{n\lambda' q'}(\mathbf{x}^{(0)}) e^{-\beta E_{n\lambda'}}$$

$$= \sum_n \sum_{\lambda'} \sum_{p'=1}^{d_n} \sum_{q'=1}^{d_n} \frac{|\mathbb{G}|}{d_\lambda} \delta_{\lambda\lambda'} \delta_{pp'} \delta_{qq'} \psi_{n\lambda' p'}^*(\mathbf{x}^{(0)}) \psi_{n\lambda' q'}(\mathbf{x}^{(0)}) e^{-\beta E_{n\lambda'}}$$

$$= \sum_n \frac{|\mathbb{G}|}{d_\lambda} \psi_{n\lambda p}^*(\mathbf{x}^{(0)}) \psi_{n\lambda q}(\mathbf{x}^{(0)}) e^{-\beta E_{n\lambda}}, \quad (2.54)$$

where in the second step, the great orthogonality theorem has been used. For nuclear motion, ground state can be shown to always belong to the totally symmetric representation and to be non-degenerate. This makes it a convenient reference point to compute the energy levels of other states belonging to the 0-th manifold, which can be done from the following expression

$$\lim_{\beta \to +\infty} \frac{\eta_{0,pp}(\mathbf{x}^{(0)}, \beta) - \eta_{\lambda,pp}(\mathbf{x}^{(0)}, \beta)}{\eta_{0,pp}(\mathbf{x}^{(0)}, \beta) + \eta_{\lambda,pp}(\mathbf{x}^{(0)}, \beta)} = \lim_{\beta \to +\infty} \frac{|\psi_{00}(\mathbf{x}^{(0)})|^2 e^{-\beta E_{00}} - 1/d_\lambda |\psi_{0p}(\mathbf{x}^{(0)})|^2 e^{-\beta E_{0\lambda}}}{|\psi_{00}(\mathbf{x}^{(0)})|^2 e^{-\beta E_{00}} + 1/d_\lambda |\psi_{0p}(\mathbf{x}^{(0)})|^2 e^{-\beta E_{0\lambda}}}$$

$$(2.55)$$

$$= \lim_{\beta \to +\infty} \tanh\left(\frac{1}{2}(E_{0\lambda} - E_{00})(\beta - \tilde{\beta})\right), \quad (2.56)$$

where $\tilde{\beta} = 2/(E_{0\lambda} - E_{00}) \ln\left(\psi_{0\lambda}(\mathbf{x}^{(0)})/(\sqrt{d_\lambda} \psi_{00}(\mathbf{x}^{(0)}))\right)$. The major disadvantage of both methods presented here is that they can only be used to compute the splitting pattern up to

the energy level of the same symmetry as some lower one. This is a consequence of the fact that the low-temperature limit is used to eliminate contributions of higher energy levels of the same symmetry.

2.3.1. Wick Rotation

Quantum-mechanical partition functions can be computed using a well known connection between quantum dynamics and statistical mechanics. Namely, the central objects of these theories, which are the time-evolution operator and density matrix, can be connected with a transformation from real time to imaginary time $\beta = it$, known as Wick rotation[87]

$$\rho(\mathbf{x}_b, \mathbf{x}_a, \beta) = \langle \mathbf{x}_b | e^{-\beta \hat{H}} | \mathbf{x}_a \rangle$$
$$K(\mathbf{x}_a, t_a; \mathbf{x}_b, t_b) = \langle \mathbf{x}_b | e^{-i(t_b - t_a)\hat{H}} | \mathbf{x}_a \rangle. \tag{2.57}$$

From the equation (2.57), one can see that the density matrix element is equivalent to the kernel, if one makes the propagation in imaginary time. Consequently, partition function $Z = \text{Tr}\,\rho = \int \rho(\mathbf{x}, \mathbf{x}, \beta)\mathrm{d}\mathbf{x}$ can be obtained by integrating imaginary-time kernels over all cyclic paths. To obtain the density matrix elements from the path integral formalism, it is necessary to transform the expression (2.44) from real time to imaginary time. Setting the initial time to $t_a = 0$ for simplicity, this yields the imaginary-time kernel[27]

$$K(\mathbf{x}_a, \mathbf{x}_b, \beta) \equiv \rho(\mathbf{x}_b, \mathbf{x}_a, \beta) = \frac{1}{\sqrt{(2\pi\beta_N)^{N+1}}} \int e^{-\beta_N \sum_{i=1}^{N+1} \left((\mathbf{x}_i - \mathbf{x}_{i-1})^2/(2\beta_N^2) + V(\mathbf{x}_i)\right)} \mathrm{d}\mathbf{x}_1 \dots \mathrm{d}\mathbf{x}_N,$$
$$\tag{2.58}$$

where $\beta_N = t_b/(N+1)$ denotes the imaginary-time interval. The exponent in this expression has the same form as the time-sliced action integral in (2.44), with the significant difference in the sign in front of the potential. Due to the change in sign, the imaginary-time action corresponds to the real-time action on the inverted potential energy surface $-V(\mathbf{x})$. Because of this, it is commonly referred to in literature as the Euclidean action, while its real-time counterpart is referred to as the Minkowski action. This is a consequence of the fact that the transformation from the real time to imaginary time also affects the space-time line element, changing it from Minkowski ($\mathrm{d}s^2 = \mathrm{d}x^2 + \mathrm{d}y^2 + \mathrm{d}z^2 - \mathrm{d}t^2$) to Euclidean ($\mathrm{d}s^2 = \mathrm{d}x^2 + \mathrm{d}y^2 + \mathrm{d}z^2 + \mathrm{d}\beta^2$). Finally, the expression for partition function is obtained by choosing cyclic paths, which is done by setting $\mathbf{x}_a = \mathbf{x}_b = \mathbf{x}_{N+1}$, and integrating over all possible $\mathbf{x}_{N+1}$

$$Z(\beta) = \frac{1}{\sqrt{(2\pi\beta_N)^{N_{\text{dof}}(N+1)}}} \int e^{-\beta_N \sum_{i=1}^{N+1} \left((\mathbf{x}_i - \mathbf{x}_{i-1})^2/(2\beta_N^2) + V(\mathbf{x}_i)\right)} \mathrm{d}\mathbf{x}_1 \dots \mathrm{d}\mathbf{x}_{N+1}. \tag{2.59}$$

2.3.2. Classical Isomorphism

The path integral form of the partition function (2.59) can be used to build an isomorphism between the quantum theory and classical statistical mechanics. This was done by Chandler and Wolynes,[29] who noted that the time-sliced action in the exponent can be treated as the potential energy of an extended system, which is formed by creating $N+1$ replicas of the original quantum system. The potential energy is then a sum of two contributions, the total potential energy of all the replicas, and harmonic two-replica interactions

$$U(\mathbf{x}_1,...,\mathbf{x}_{N+1}) = \sum_{i=1}^{N+1} \left(\frac{(\mathbf{x}_i - \mathbf{x}_{i-1})^2}{2\beta_N^2} + V(\mathbf{x}_i) \right). \tag{2.60}$$

As the path integral form of the partition function involves sum over cyclic paths, the harmonic springs connect the replicas into a ring, which is dubbed the ring-polymer. The force constant of these springs is temperature-dependent and their motion emulates the uncertainty present in the quantum system. At high temperatures, the springs are stiff and the spread of replicas around an average position is small, making the system localized and its motion well described by the classical motion of the average of all replicas, called the centroid. At lower temperatures, the force constant decreases and the replicas move more freely, which emulates the probability distribution of the quantum nuclei. This enables ring-polymer to correctly account for quantum effects at the low temperatures, such as tunneling and zero-point energy. The path integral can be evaluated using any of the sampling methods from the classical statistical mechanics. The most commonly used approaches are molecular dynamics and Monte Carlo sampling.

Molecular dynamics performed on the path integral form of the partition function yields the method of path integral molecular dynamics (PIMD).[88,89] To perform sampling using molecular dynamics, momenta have to be reintroduced into exponent of the integrand in (2.44), which is simply done by rewriting the normalization constant

$$Z(\beta) = \int e^{-\beta_N \sum_{i=1}^{N+1}(\mathbf{p}_i^2/2+(\mathbf{x}_i-\mathbf{x}_{i-1})^2/(2\beta_N^2)+V(\mathbf{x}_i))}\, d\mathbf{x}_1 d\mathbf{p}_1 \ldots d\mathbf{x}_{N+1} d\mathbf{p}_{N+1}. \tag{2.61}$$

In addition to partition function, PIMD can be used to compute thermodynamic averages of a number of observables, such as heat capacities[90,91] or enthalpies,[92,93] by providing an appropriate form of the estimator. Due to the isomorphism with quantum system, averages obtained in this way include the quantum effects of tunneling and zero-point energy. In addition to static properties, path integral molecular dynamics can be used to compute autocorrelation functions as well. From appropriate autocorrelation functions, it is possible to compute both one-dimensional and multidimensional spectra of molecules, as well as the chemical rate constants. Based on the form of autocorrelation functions used, there is a number of PIMD methods developed, which include ring-polymer molecular dynamics (RPMD),[11,94]

centroid molecular dynamics (CMD)[95–98] and Matsubara dynamics,[99] as notable examples.

Thermodynamic integration can be used to accelerate convergence of estimators that are sensitive on the regions of potential energy surface that are poorly explored during MD simulation, such as density matrix elements that connect different minima. This approach has been used by Matyus et al.[31] to compute density matrix ratios (2.52) and determine tunneling splitting in 1D model potential and malonaldehyde. The method is based on representing the density matrix element as a partition function of an open polymer with fixed ends. One end is always fixed at minimum $\mathbf{x}^{(0)}$, while the coordinates of the other end can take any value. This makes it possible to define a free energy $A(\mathbf{x}, \beta_N)$ as a function of the position of the other end as

$$A(\mathbf{x}, \beta_N) = -\frac{1}{\beta_N} \ln \rho(\mathbf{x}^{(0)}, \mathbf{x}, \beta). \tag{2.62}$$

The ratio of density matrix elements can then be computed from the difference in the free energy for the second end located at a symmetry-related minimum and free energy for both ends located at the minimum $\mathbf{x}^{(0)}$, which is performed using thermodynamic integration, by continuously moving the second end from one minimum to the other. The results obtained using this method were shown to be in quantitative agreement with the ones obtained using variational methods for 1D case, and the ones obtained from diffusion Monte Carlo (DMC) for malonaldehyde.[100]

The major drawback of aforementioned methods for the computation of the tunneling splitting is the fact that they are computationally intensive. While they do not necessitate the use of analytic potential energy surfaces, as is the case for quantum-mechanical methods, they still demand a large number of potential energy evaluations. This is due to the fact that, in order to obtain converged results for tunneling splitting, it is necessary to go to the low-temperature limit. In order to obtain converged results in this limit, it is necessary to use a large number of replicas, to correctly describe the quantum behaviour of the system. Since in each step of the computation of the path-integral potential, potential energy has to be evaluated for each bead, this method becomes very expensive even for moderately large systems. Matyus et al.[31] comment on this, stating that their computation of tunneling splitting for malonaldehyde included approximately 10 times more potential energy evaluations than the number used for DMC calculation,[100] while yielding larger error in the splitting. This problem can be mitigated using the instanton approximation, which we explore in the following paragraph.

2.3.3. Instanton Approximation

The path integral form of the partition function (or density matrix element) can be approximated in a way similar to the stationary phase approximation. Derivation in terms of path integral formalism was made by Richardson and Althorpe[13] and is briefly outlined here. From

the form of the integrand, it is obvious that the path for which the imaginary-time action is stationary and paths in its vicinity will give the largest contribution to the integral. As a result, the path integral can be approximated by expanding the action around the minimum action path up to second order and evaluating the resulting Gaussian integral to account for the neighbouring paths.

$$S(\mathbf{x}_1,...,\mathbf{x}_N) = S(\mathbf{x}_1^{(0)},...,\mathbf{x}_N^{(0)}) + \frac{1}{2}\vec{\mathbf{x}}^\top \mathbf{H}\vec{\mathbf{x}}. \tag{2.63}$$

If there is more than one stationary path, all of their contributions are summed. Stationary paths are obtained from the condition

$$\nabla_{\mathbf{x}_i} S(\mathbf{x}_1,...,\mathbf{x}_N) = 0$$
$$\frac{2\mathbf{x}_i^{(0)} - \mathbf{x}_{i-1}^{(0)} - \mathbf{x}_{i+1}^{(0)}}{\beta_N^2} + \nabla_{\mathbf{x}_i} V(\mathbf{x}_i^{(0)}) = 0. \tag{2.64}$$

In the limit $\beta_N \to 0$, which is the correct limit at which the path integral becomes exact, this corresponds to a differential equation of the form

$$\frac{\mathrm{d}^2}{\mathrm{d}\beta^2}\mathbf{x}^{(0)} = \nabla V(\mathbf{x}^{(0)}). \tag{2.65}$$

This equation is equivalent to the equation of motion for classical system, but on the inverted potential energy surface. In order to build the partition function, only paths that are cyclic are sought, which means that they must have turning points either at the minima, or in the region between them. Otherwise, paths can collapse into the region where $V(\mathbf{x}) \to +\infty$ and cannot return to the initial point. From these paths, only the ones with the turning points exactly at the minima contribute significantly. This is due to the fact that, if the turning point is in the region where $\nabla V(\mathbf{x}) \neq 0$, the path will take finite time to complete one cycle. However, as the limit $\beta \to +\infty$ is sought, path can make an infinite number of cycles, each contributing with finite, non-negative action, making their total contribution negligible. Thus, only cyclic classical paths that have turning points at the minima can contribute significantly to the path integral. There is infinite number of such paths, each with a different, even number of 'jumps' or 'kinks' from one minimum to the other, along the classical path that connects them. The classical path that does not move from the minimum has action $S = 0$, which represents the global minimum of action. Other paths have larger actions, which increase cumulatively with the number of kinks that they have. As these paths spend an infinite amount of imaginary time at the minima and kinks happen in finite time intervals, they are virtually instantaneous. For this reason, these kinks are called instantons.

The contribution of a path with $2n$ kinks can be written in the form

$$Z_{2n}(\beta) = \frac{1}{\sqrt{(2\pi\beta_N)^N}} \int e^{-S_{2n}(\mathbf{x}^{(0)}) - \frac{1}{2}\delta\vec{\mathbf{x}}^\top \mathbf{H}_{2n}\delta\vec{\mathbf{x}}} \mathrm{d}\delta\mathbf{x}_1 \dots \mathrm{d}\delta\mathbf{x}_N, \tag{2.66}$$

where fluctuation coordinates $\delta\mathbf{x}_i = \mathbf{x}_i - \mathbf{x}_i^{(0)}$ describe the difference between the considered path and the stationary path. The action Hessian can be obtained by differentiating the time-sliced action twice, which yields a matrix of the following form

$$\mathbf{H}_{2n} = \begin{pmatrix} \beta_N\mathbf{V}_{\mathbf{x}_0\mathbf{x}_0} + \frac{2}{\beta_N}\mathbf{I} & -\frac{1}{\beta_N}\mathbf{I} & 0 & \dots & -\frac{1}{\beta_N}\mathbf{I} \\ -\frac{1}{\beta_N}\mathbf{I} & \beta_N\mathbf{V}_{\mathbf{x}_1\mathbf{x}_1} + \frac{2}{\beta_N}\mathbf{I} & -1\frac{1}{\beta_N}\mathbf{I} & \dots & 0 \\ 0 & -\frac{1}{\beta_N}\mathbf{I} & \beta_N\mathbf{V}_{\mathbf{x}_2\mathbf{x}_2} + \frac{2}{\beta_N}\mathbf{I} & \dots & 0 \\ \vdots & \vdots & \vdots & \ddots & \vdots \\ -\frac{1}{\beta_N}\mathbf{I} & 0 & 0 & \dots & \beta_N\mathbf{V}_{\mathbf{x}_N\mathbf{x}_N} + \frac{2}{\beta_N}\mathbf{I} \end{pmatrix}, \tag{2.67}$$

where $\mathbf{V}_{\mathbf{x}_i\mathbf{x}_i}$ denotes the potential energy Hessian at point $\mathbf{x}_i^{(0)}$ and $\mathbf{I}$ denotes the $N_{\mathrm{dof}} \times N_{\mathrm{dof}}$ identity matrix. The action Hessian is a block-tridiagonal matrix of Hückel type, with additional corner blocks which arise from the cyclic nature of the ring-polymer. The integral (2.66) can be evaluated by coordinate transformation to eigenvectors $\mathbf{U}$ of action Hessian. As the action Hessian is a real, symmetric matrix, its eigenvectors form an orthonormal set, which means that the change to normal coordinates is given by a linear transformation $\mathbf{q} = \mathbf{U}^{-1}\delta\mathbf{x}$ with unit Jacobian. The integral in the normal coordinates can be written as

$$Z_{2n}(\beta) = \frac{1}{\sqrt{(2\pi\beta_N)^N}} e^{-S_{2n}(\mathbf{x}^{(0)})} \int e^{-\frac{1}{2}\lambda_1 q_1^2} \mathrm{d}q_1 \dots \int e^{-\frac{1}{2}\lambda_1 q_{NN_{\mathrm{dof}}}^2} \mathrm{d}q_{NN_{\mathrm{dof}}}, \tag{2.68}$$

where λ_i are the eigenvalues of the action Hessian. As the $2n$-kink ring-polymers that are chosen represent the minima of the action, all of the eigenvalues must be non-negative. For the eigenvalues that are non-zero, corresponding integrals are of Gaussian type and can be solved analytically. However, every $2n$-kink ring-polymer must possess $2n$ eigenvalues which are zero. These correspond to the eigenvectors that have all elements zero, except for those corresponding to one of the kinks, which are proportional to the velocity at the corresponding point

$$U_{ij} = \frac{1}{\sqrt{\beta_N S_{\mathrm{kink}}}}(\mathbf{x}_{i+1}^{(0)} - \mathbf{x}_i^{(0)}) = \sqrt{\frac{\beta_N}{S_{\mathrm{kink}}}}\dot{\mathbf{x}}_i^{(0)}. \tag{2.69}$$

This can be confirmed by observing the action of the Hessian on such vectors, which gives

the components

$$(\mathbf{H}\mathbf{U}_j) = \sqrt{\frac{\beta_N}{S_{\text{kink}}}} \left(\frac{2\dot{\mathbf{x}}_i^{(0)} - \dot{\mathbf{x}}_{i-1}^{(0)} - \dot{\mathbf{x}}_{i+1}^{(0)}}{\beta_N} + \beta_N \mathbf{V}_{\mathbf{x}_i \mathbf{x}_i} \dot{\mathbf{x}}_i^{(0)} \right)$$

$$= \frac{1}{\sqrt{\beta_N S_{\text{kink}}}} \left(-\frac{d^2}{d\beta^2} \dot{\mathbf{x}}^{(0)} + \mathbf{V}_{\mathbf{x}\mathbf{x}} \dot{\mathbf{x}}^{(0)} \right) \beta_N^2. \tag{2.70}$$

The expression in the brackets can be evaluated by differentiating the equation (2.65) and applying the chain rule to the right-hand side

$$\frac{d^3}{d\beta^3} \mathbf{x}^{(0)} = \frac{d}{d\beta} \nabla V(\mathbf{x}^{(0)})$$

$$\frac{d^2}{d\beta^2} \dot{\mathbf{x}}^{(0)} = V_{\mathbf{x}\mathbf{x}} \frac{d\mathbf{x}^{(0)}}{d\beta}. \tag{2.71}$$

This proves that $(\mathbf{H}\mathbf{U}_j) = 0$ for this choice of $\mathbf{U}_j$. Integrals of these variables have to be evaluated separately, which is done by observing their eigenvectors. As can be seen from (2.69), motion along these directions corresponds to temporal translation of the kinks along the ring-polymer. Motion by amount $\sqrt{\beta_N S_{\text{kink}}}$ translates the centre of the kink to the neighbouring bead, which corresponds to the shift in the imaginary time by β_N. This makes it possible to make a change of coordinates from q_j to the positions of kinks in the imaginary time, by noting that in the limit $N \to +\infty$ one can assign $\beta_N \to d\tau$, which means that $dq_j / \sqrt{\beta_N S_{\text{kink}}} = d\tau_j$. To avoid double-counting, boundaries of the integration for the first kink must be set from 0 to β, which is the period of ring-polymer. Consequently, position of the second kink must be placed either before or after the first one, etc. This reduces the $2n$-dimensional integral over zero-frequency modes to the analytically solvable form

$$\int dq_1 \dots dq_{2n} = (\beta_N S_{\text{kink}})^n \int_0^\beta \int_0^{\tau_1} \dots \int_0^{\tau_{2n-1}} d\tau_{2n} \dots d\tau_1 = (\beta_N S_{\text{kink}})^n \frac{\beta^{2n}}{(2n)!}. \tag{2.72}$$

The integration automatically accounts for all possible distributions of the kinks along the ring-polymer. Using this result and solving the remaining Gaussian integrals, one arrives at the result for the $2n$-kink contribution to the partition function

$$Z_{2n}(\beta) = \frac{1}{\sqrt{(2\pi\beta_N)^N}} e^{-S_{2n}(\mathbf{x}^{(0)})} (\beta_N S_{\text{kink}})^n \frac{\beta^{2n}}{(2n)!} \sqrt{\frac{(2\pi)^{N-2n}}{\det' \mathbf{H}_{2n}}}, \tag{2.73}$$

where $\det'$ denotes the product of all non-zero eigenvalues. In case of zero-kink contribution,

---

all eigenvalues are non-zero and action is zero, which simplifies that contribution to

$$Z_0(\beta) = \frac{1}{\sqrt{(2\pi\beta_N)^N}} \sqrt{\frac{(2\pi)^N}{\det \mathbf{H}_0}}.$$ (2.74)

From these contributions, it is intuitive to assign only the zero-kink one to the non-tunneling system, as the ring-polymer does not explore the region of the other minimum in this case. Inserting these contributions in (2.48), the expression for tunneling splitting becomes

$$
\begin{aligned}
\lim_{\beta \to +\infty} \cosh(\beta h_0) &= \lim_{\beta \to +\infty} \left(1 + \frac{Z_2}{Z_0} + ... \right) \\
&= \lim_{\beta \to +\infty} \sum_n (\beta_N S_{\text{kink}})^n \frac{\beta^{2n}}{(2n)!} \sqrt{\frac{\det \mathbf{H}_0}{(2\pi)^{2n} \det' \mathbf{H}_{2n}}} e^{-S_{2n}(\mathbf{x}^{(0)})}.
\end{aligned}
$$ (2.75)

This expression can be recast in terms of a single-kink linear polymer that connects the minima. The action of the ring-polymers is then simply a multiple of the single-kink action $S_{2n}(\mathbf{x}^{(0)}) = 2nS_{\text{kink}}$. Furthermore, Richardson and Althorpe[13] have demonstrated that the ratio of determinants can be expressed as

$$\frac{\det \mathbf{H}_0}{\det' \mathbf{H}_{2n}} = \left(\frac{\det \mathbf{H}_0}{\det' \mathbf{H}_1} \right)^{2n}.$$ (2.76)

The proof involves expansion of determinants and is quite involved, so it is not included here. The final expression for the splitting becomes

$$
\begin{aligned}
\lim_{\beta \to +\infty} \cosh(\beta h_0) &= \lim_{\beta \to +\infty} \left(1 + \frac{Z_2}{Z_0} + ... \right) \\
&= \lim_{\beta \to +\infty} \sum_n \frac{1}{(2n)!} \left(\sqrt{\beta_N S_{\text{kink}}} \beta \sqrt{\frac{\det \mathbf{H}_0}{2\pi \det' \mathbf{H}_1}} e^{-S_{\text{kink}}} \right)^{2n} \\
&= \lim_{\beta \to +\infty} \cosh \left(\beta \sqrt{\frac{S_{\text{kink}} \det(\mathbf{H}_0/\beta_N)}{2\pi \det'(\mathbf{H}_1/\beta_N)}} e^{-S_{\text{kink}}} \right) \\
h_0 &= \sqrt{\frac{S_{\text{kink}} \det(\mathbf{H}_0/\beta_N)}{2\pi \det'(\mathbf{H}_1/\beta_N)}} e^{-S_{\text{kink}}}.
\end{aligned}
$$ (2.77)

2.3.4. Multi-Well Systems

Richardson et al.[101] generalized the above approach to systems with multiple wells. In that case, the ratio of partition functions, in the low temperature limit, is dominated by the energy

levels of split ground state manifold

$$\lim_{\beta \to +\infty} \frac{Z(\beta)}{Z_0(\beta)} = \lim_{\beta \to +\infty} \sum_v \frac{1}{G} e^{-\beta(E_v - E_0)}, \tag{2.78}$$

where G denotes the number of minima and E_0 denotes the energy of a state localized in one minimum. In this case, each n-kink ring-polymer (where n no longer has to be even) can be constructed by choosing a number of sequences of kinks that connect the minima. For a certain sequence of minima $\mu_1 \to \mu_2 \to ... \to \mu_n$, ring-polymer contribution can be factorized in a manner analogous to the one presented previously as

$$\lim_{\beta \to +\infty} \frac{Z_{\mu_1...\mu_n}(\beta)}{Z_0(\beta)} = \frac{\beta^n}{n!} h_{\mu_1 \mu_2} ... h_{\mu_n \mu_1}$$

$$h_{\mu_i \mu_j} = \sqrt{\frac{S_{\text{kink}}(\mu_i \to \mu_j) \det(\mathbf{H}_0 / \beta_N)}{2\pi \det'(\mathbf{H}_{\mu_i \to \mu_j} / \beta_N)}} e^{-S_{\text{kink}}(\mu_i \to \mu_j)}. \tag{2.79}$$

Counting the number of possible paths that lead from one minimum to the other can be done using graph theory, by defining the adjacency matrix $\mathbf{A}$, whose element A_{ij} denotes the number of kinks that connect minima i and j. The number of n-kink paths is then simply a corresponding matrix element of $\mathbf{A}^n$. One can similarly produce all the possible products (2.79) by defining the tunneling matrix as

$$W_{ij} = -A_{ij} h_{ij}. \tag{2.80}$$

The sum of contributions of n-kink ring-polymers that start and end at minimum μ_i is then simply the corresponding diagonal element of $\mathbf{W}^n$. The sum of all possible contributions is given by the trace of $\mathbf{W}^n$, which means that the ratio of partition functions becomes

$$\lim_{\beta \to +\infty} \frac{Z(\beta)}{Z_0(\beta)} = \lim_{\beta \to +\infty} \sum_n \frac{1}{G} \frac{\beta^n}{n!} \text{Tr}(\mathbf{W}^n)$$

$$= \frac{1}{G} \text{Tr}\left(e^{-\beta \mathbf{W}}\right). \tag{2.81}$$

Through comparison of this expression with (2.78), it is clear that the eigenvalues of tunneling matrix represent the energy levels of the split ground state manifold. Furthermore, symmetries of the eigenvectors can be used to describe the symmetry of the corresponding state in the manifold, thus providing all the information about those states.

2.3.5. Asymmetric Systems

Ring-polymer instanton method can also be generalized to treat systems that have wells which are not connected by symmetry, but have the same energy at the minimum. Such

systems possess different vibrational frequencies and, as a result, different zero-point energies. This case can arise in molecular systems in which some of the atoms are substituted with a different isotope. If the substituted atoms are not at the equivalent positions in different minima, normal modes and frequencies will differ. However, potential energy at the minima remains unchanged, as it does not depend on the mass of nuclei. The proof will briefly be presented here for the case of 1D potential, following the paper by Jahr et al.,[37] with the generalization to N_{dof}-D system that is straightforward. Due to different zero-point energies, the prototype Hamiltonian for such systems is a 2×2 matrix

$$\hat{H} = \begin{pmatrix} E_0 - d & -h_0 \\ -h_0 & E_0 + d \end{pmatrix}, \tag{2.82}$$

where $2d$ denotes the zero-point energy difference and E_0 is the mean value of the zero-point energies. Eigenvalues of such system are of the form

$$E_{\pm} = E_0 \mp \sqrt{d^2 + h_0^2}. \tag{2.83}$$

It can be seen from this equation that tunneling causes a shift in the energy levels of the localized states. If the zero-point energy difference is large, compared to the tunneling matrix element h_0, tunneling will have a negligible effect on the system. Thus, only systems with small energy asymmetry d are of interest. To compute the partition function ratio, a convenient choice for the non-tunneling partition function in the denominator is a harmonic mean of the non-tunneling partition functions of the two minima, $Z_g = 2\sqrt{Z^{(\mathrm{L})} Z^{(\mathrm{R})}}$. In that case, the partition function ratio becomes

$$\lim_{\beta \to +\infty} \frac{Z(\beta)}{2\sqrt{Z^{(\mathrm{L})}(\beta) Z^{(\mathrm{R})}(\beta)}} = \lim_{\beta \to +\infty} \cosh\left(\beta \sqrt{d^2 + h_0^2}\right). \tag{2.84}$$

Jahr proposed the expansion of this expression with respect to tunneling matrix element h_0, which yields

$$\lim_{\beta \to +\infty} \frac{Z(\beta)}{2\sqrt{Z^{(\mathrm{L})}(\beta) Z^{(\mathrm{R})}(\beta)}} = \cosh(\beta d) + \frac{\beta h_0^2 \sinh(\beta d)}{2d} + \ldots \tag{2.85}$$

From the comparison with the result obtained for the symmetry-related minima, it is observed that the terms in this expansion should correspond to $2n$-kink contributions. In the derivation of these contributions, an extensive use of the analytic form of the imaginary-time kernel in harmonic potential in the low-temperature limit is used

$$K(x_a, x_b, \tau) = \sqrt{\frac{\omega}{\pi e^{\tau \omega}}} e^{-\frac{1}{2}\omega[(x_b - x_{\min})^2 + (x_a - x_{\min})^2]}. \tag{2.86}$$

Non-tunneling partition functions are obtained by approximating the potential in both wells with a harmonic one. This results in the following solution

$$Z^{(\text{L/R})} = \int K(x_a, x_a, \beta) \mathrm{d}x_a = \mathrm{e}^{-\frac{1}{2}\beta\omega^{(\text{L/R})}}. \tag{2.87}$$

Zero-kink contribution is a sum of non-tunneling partition functions, which yields the following first term in the expansion of the ratio of partition functions

$$\frac{Z_0}{Z_g} = \frac{\mathrm{e}^{-1/2\beta\omega^{(\text{L})}} + \mathrm{e}^{-1/2\beta\omega^{(\text{R})}}}{2\mathrm{e}^{-1/2\beta(\omega^{(\text{L})}+\omega^{(\text{R})})}} = \cosh\left(\frac{1}{4}\beta(\omega^{(\text{R})} - \omega^{(\text{L})})\right). \tag{2.88}$$

From this expression follows the expected relation for the difference in the zero-point energies $2d = 1/2(\omega^{(\text{R})} - \omega^{(\text{L})})$. The 2-kink contribution is computed by cutting the ring-polymer into 4 pieces, with cuts located at the endpoints of kinks

$$Z_2'(\tau_1, \tau_2) = \int K'(x_a, x_b, \tau_k) K(x_b, x_c, \tau_2 - \tau_1 - \tau_k)$$
$$K'(x_c, x_d, \tau_k) K(x_d, x_a, \beta - \tau_2 + \tau_1 - \tau_k) \mathrm{d}x_a \mathrm{d}x_b \mathrm{d}x_c \mathrm{d}x_d, \tag{2.89}$$

where primes indicate that the positions of kinks are fixed at τ_1 and τ_2, while τ_k denotes the duration of one kink. Second and last terms are contributions of beads that fluctuate around first and/or second minimum, so these kernels can be approximated by 2.87. Kernels which include the kink are further expanded around their endpoints, which are set at the minima. Mixed terms of the form $(x_a - x^{(\text{L})})(x_b - x^{(\text{R})})$ are neglected, under assumption that they are small compared with the $(x_{a/b} - x^{(\text{L/R})})^2$ terms, which holds for the case of harmonic oscillator in the low-temperature limit,

$$K'(x_a, x_b, \tau_k) = K'(x^{(\text{L})}, x^{(\text{R})}, \tau_k) \sqrt{\frac{\sqrt{\omega^{(\text{L})}\omega^{(\text{R})}}}{\pi \mathrm{e}^{\frac{1}{2}\tau_k(\omega^{(\text{L})}+\omega^{(\text{R})})}}} \mathrm{e}^{-\frac{1}{2}\omega^{(\text{L})}(x_b-x^{(\text{L})})^2 - \frac{1}{2}\omega^{(\text{R})}(x_b-x^{(\text{R})})^2}. \tag{2.90}$$

Inserting this equation into (2.89) and solving the Gaussian integrals yields the following expression

$$Z'(\tau_1, \tau_2) = \theta^2(\tau_k)\left(\mathrm{e}^{\frac{1}{2}\omega^{(\text{R})}(\tau_2-\tau_1)}\mathrm{e}^{\frac{1}{2}\omega^{(\text{L})}(\beta-\tau_2+\tau_1)} + \mathrm{e}^{\frac{1}{2}\omega^{(\text{L})}(\tau_2-\tau_1)}\mathrm{e}^{\frac{1}{2}\omega^{(\text{R})}(\beta-\tau_2+\tau_1)}\right)$$
$$\theta(\tau_k) = \frac{K'(x^{(\text{L})}, x^{(\text{R})}, \tau_k)}{\sqrt{Z^{(\text{L})}(\tau_k)Z^{(\text{R})}(\tau_k)}}. \tag{2.91}$$

To obtain the final 2-kink contribution, one must sum over all possible positions of kinks

$$Z_2 = \int_0^\beta \int_{\tau_1}^\beta Z_2'(\tau_1, \tau_2)\mathrm{d}\tau_1\mathrm{d}\tau_2 = 2\beta\theta^2(\tau_k)\frac{\mathrm{e}^{-\frac{1}{2}\beta\omega^{(\text{L})}} - \mathrm{e}^{-\frac{1}{2}\beta\omega^{(\text{R})}}}{\omega^{(\text{R})} - \omega^{(\text{L})}}. \tag{2.92}$$

This gives a two-kink contribution to the ratio of partition functions of the form

$$\frac{Z_2}{Z_g} = 2\beta\theta^2(\tau_k)\frac{\sinh\left(\frac{1}{4}\beta(\omega^{(\mathrm{R})} - \omega^{(\mathrm{L})})\right)}{\omega^{(\mathrm{R})} - \omega^{(\mathrm{L})}} = \frac{\beta h_0^2 \sinh(\beta d)}{2d}. \tag{2.93}$$

From this equation, it is clear that the tunneling matrix element is given by

$$h_0 = \theta\tau_k = \frac{K'(x^{(\mathrm{L})}, x^{(\mathrm{R})}, \tau_k)}{\sqrt{Z^{(\mathrm{L})}(\tau_k)Z^{(\mathrm{R})}(\tau_k)}}. \tag{2.94}$$

This ratio can be estimated in the large τ_k limit using the analogous method to the one presented in the previous section. The term in the numerator corresponds to a one-kink linear polymer, while the terms in the denominator correspond to the localized ring-polymers. The final expression takes the following form

$$h_0 = \sqrt{\frac{S_{\mathrm{kink}}\sqrt{\det\left(\mathbf{H}_0^{(\mathrm{L})}/\beta_N\right)\det\left(\mathbf{H}_0^{(\mathrm{R})}/\beta_N\right)}}{2\pi\det'(\mathbf{H}_1/\beta_N)}}e^{-S_{\mathrm{kink}}}. \tag{2.95}$$

2.3.6. Numerical Implementation and Applications

Ring-polymer instanton theory is extremely numerically efficient in comparison with variational and path integral methods. There are two major steps which have to be done in order to obtain the tunneling matrix element using RPI.

First step involves locating the minimum action path and computing the action along it. This can be done by direct optimization of the time-sliced action[13]

$$S(\mathbf{x}_1, ..., \mathbf{x}_{N+1}) = \sum_{i=1}^{N+1}\left(\frac{(\mathbf{x}_i - \mathbf{x}_{i-1})^2}{2\beta_N^2} + V(\mathbf{x}_i)\right). \tag{2.96}$$

Gradient of this object can be computed analytically, provided that the potential energy gradients are available. Thus, any optimization method can be applied for that purpose, the commonly used one being limited-memory Broyden-Fletcher-Goldfarb-Shanno (L-BFGS)[102] algorithm. Additionally, potential energy gradient can be evaluated using on-the-fly *ab initio* methods.

Second step involves computation and diagonalization of action Hessians. This has to be done for two reasons. The first reason is that, in the case of single-kink polymer, zero eigenvalue must be eliminated from the determinant, as integral along the corresponding normal mode is treated separately. As a result, determinant cannot be computed using numerically efficient LU decomposition, as such method would yield zero value. Second

reason is that, even in the case of a non-tunneling polymer, where all eigenvalues are non-zero, the determinant is a diverging quantity, with only the ratio of determinants being convergent. This is due to the $1/\beta_N^2$ terms, which are large in the $\beta_N \to +\infty$ limit that has to be explored and make the determinant proportional to $1/\beta_N^{2N}$. Action Hessians are constructed using potential energy Hessians, which have to be evaluated at every bead on the optimized path. Action Hessian for the non-tunneling polymer does not have to be numerically diagonalized, as its eigenvalues can be constructed from the eigenvalues of the potential energy Hessian at the minimum. This is possible because the Hessian is a block-Hückel matrix, for which there is a known eigenvalue expression

$$\lambda_{ik} = \omega_i^2 + \frac{4}{\beta_N^2} \cos^2\left(\frac{k\pi}{N+1}\right), \qquad k = 1,\ldots N. \tag{2.97}$$

The Hessian of a single-kink polymer must be diagonalized numerically, which is a computationally intensive step, as its dimension is NN_{dof}. However, as it has a structure of a banded matrix, significant savings can be made in storage and diagonalization.

The major disadvantage in the ring-polymer theory is the fact that the final result must be converged in the limit $\beta, N \to +\infty$ and $\beta_N \to 0$.[13] This means that it is necessary to run calculations with a large number of beads N, which increases cost in both the path optimization and Hessian construction, given that gradients and Hessians must be computed at each bead. Furthermore, convergence can be slow, as due to the fact that the minimum action path spends most of the time in the region near the minima (where its velocity is virtually zero), increase in the number of beads results mostly in clustering of the beads near the minima, while the region under the potential energy barrier is explored by a small number of beads. Most of these problems can be solved using the Jacobi field instanton (JFI)[14,15,103] method, which will be presented in the following section.

2.4. Jacobi Field Instanton Theory

Problems that plague RPI method, the dependence of tunneling matrix element on the imaginary-time length of instanton path β and the requirement for a large number of beads in the time-slicing, can both be solved by changing the method for the path slicing. If slicing is done using equidistant points with respect to the distance from the first minimum, one can reduce the number of beads necessary for convergence by roughly an order of magnitude.[104] This is due to the fact that the slicing at equidistant points in distance avoids clustering of beads in the vicinity of minima and places more beads in the relevant region in the barrier. Moving from the time-slicing to the distance-slicing requires a change in variables of all objects in the RPI expression for the tunneling matrix element, the action and the determinant of its Hessian. This transition can be made analytically, and adds a further bonus of providing

a formally exact $\beta \to +\infty$ limit, eliminating parameter β from the calculation. This method is well-known in physics for 1D systems and has been generalized to treat symmetric molecular systems by Mil'nikov and Nakamura.[14] Their derivation will briefly be outlined in this paragraph.

2.4.1. Coordinate Transformation

First step in derivation is transformation of coordinate system from global Cartesian to local coordinates.[14] Local coordinates are denoted by $\{S, \xi_\alpha\}$, where coordinate S denotes the arc-length distance on the trajectory from the first minimum and coordinates ξ_α describe orthogonal shifts from the trajectory. This results in the following equations for the coordinate transformation

$$x_i = x_i^{(0)}(S) + \tau_{i\alpha}(S)\xi_\alpha. \tag{2.98}$$

In this section, indices denoted by Greek letters will be assumed to run from 1 to $N_{\text{dof}} - 1$, while indices denoted by Latin letters will be assumed to run from 1 to N_{dof}. As variables ξ_α denote orthogonal shift from the trajectory, local vectors τ_α must be orthogonal to the tangent vector, which will be denoted by $\tau_N = \frac{\mathrm{d}}{\mathrm{d}S}\mathbf{x}^{(0)}(S)$. Furthermore, without loss of generality, they are assumed to be normalized, which also applies to the tangent vector τ_N due to the definition of S as arc length. Finally, orientation of orthogonal vectors τ_α at different points on the trajectory can be fixed using parallel transport criteria, which requires minimal change in these vectors from one point to another, i.e. it is demanded that the change in τ_α is orthogonal to all other orthogonal vectors. These constraints result in the following set of conditions

$$\tau_{ij}\tau_{ik} = \delta_{jk}$$
$$\tau_{i\beta}\frac{\mathrm{d}}{\mathrm{d}S}\tau_{i\alpha} = 0$$
$$\frac{\mathrm{d}}{\mathrm{d}S}\tau_{i\alpha} = C_\alpha(S)\tau_{iN}, \tag{2.99}$$

where the last equation follows from the parallel transport, with constants C_α defining the curvature at position S. The metric tensor for this coordinate transformation is

$$\mathbf{g} = \begin{pmatrix} \mathbf{I} & 0 \\ 0 & (1 + C_\alpha\xi_\alpha)^2 \end{pmatrix}, \tag{2.100}$$

which makes it a unit matrix on the trajectory, where $\xi_\alpha = 0$. Since metric tensor is diagonal, there are no mixed terms in the classical kinetic energy and Lagrangian takes the form

$$L(S, \xi_\alpha, \tau) = \frac{1}{2}(1 + C_\alpha\xi_\alpha)^2\dot{S}^2 + \frac{1}{2}\dot{\xi}_\alpha\dot{\xi}_\alpha + V(S, \xi_\alpha). \tag{2.101}$$

Next step involves approximating the potential with the second-order series in orthogonal coordinates ξ_α

$$L(S, \xi_\alpha, \tau) = \frac{1}{2}(1 + C_\alpha \xi_\alpha)^2 \dot{S}^2 + \frac{1}{2}\dot{\xi}_\alpha \dot{\xi}_\alpha + V_0(S) + a_\alpha(S)\xi_\alpha + \frac{1}{2}b_{\alpha\beta}(S)\xi_\alpha \xi_\beta. \quad (2.102)$$

Connection between the coordinate $S_0(\tau)$, which defines the classical trajectory, and imaginary time τ can be obtained from Euler-Lagrange equations, taking into account that, by definition, $\xi_\alpha = 0$ at the classical trajectory

$$\frac{d}{d\tau}\left(\frac{\partial}{\partial \dot{S}}L\right) = \frac{\partial}{\partial S}L$$
$$\ddot{S}_0 = V_0'(S_0). \quad (2.103)$$

Integrating this equation and using the fact that the minima are turning points and the velocity at the minima is zero, it is possible to obtain the momentum along the trajectory $p_0 = \dot{S}_0 = \sqrt{2V_0(S_0)}$. The other Euler-Lagrange equations define the curvature of the trajectory

$$\frac{d}{d\tau}\left(\frac{\partial}{\partial \dot{\xi}_\alpha}L\right) = \frac{\partial}{\partial \xi_\alpha}L$$
$$C_\alpha(S_0)\dot{S}_0^2 + a_\alpha(S_0) = 0. \quad (2.104)$$

With the equations for the classical trajectory known, it is possible to define the fluctuation coordinate $s(\tau) = S - S_0$, while ξ_α already depict fluctuation coordinates. As the only fluctuations that need to be taken into account are the ones that leave endpoints at the minima, fluctuation coordinate must satisfy boundary conditions $s(0) = s(\beta) = 0$. Furthermore, since this coordinate transformation is just a shift, metric tensor remains an identity matrix at the trajectory. Lagrangian and action are expanded up to second order with respect to the fluctuation coordinates. Zeroth order term in that case becomes

$$L^{(0)} = \frac{1}{2}\dot{S}_0^2 + V_0(S_0) = 2V_0(S_0). \quad (2.105)$$

This means that the action of the trajectory is

$$S_{\text{kink}} = \int_0^\beta 2V_0 d\tau = \int_0^{S_{\text{tot}}} 2V_0 \frac{d\tau}{dS_0}dS_0 = \int_0^{S_{\text{tot}}} \sqrt{2V_0}dS_0 \quad (2.106)$$

and can be computed without any use of imaginary-time variable. First order term in Lagrangian and the corresponding term in action are

$$\delta L = (C_\alpha \dot{S}_0^2 + a_\alpha)\xi_\alpha + \dot{S}_0 \dot{s} + V_0' s = \dot{S}_0 \dot{s} + V_0' s$$

$$\delta S_{\text{kink}} = \int_0^\beta (\dot{S}_0 \dot{s} + V_0' s)\mathrm{d}\tau = s\dot{S}_0|_0^\beta + \int_0^\beta (-\ddot{S}_0 + V_0')s\mathrm{d}\tau = 0, \qquad (2.107)$$

as expected, given that the fluctuations are taken around MAP. Second order terms take the form

$$\delta^2 L = \frac{1}{2}\dot{s}^2 + 2C_\alpha \dot{S}_0 \xi_\alpha \dot{s} + \frac{1}{2}C_\alpha C_\beta \dot{S}_0^2 \xi_\alpha \xi_\beta + C_\alpha' \dot{S}_0^2 s \xi_\alpha + $$
$$+ \frac{1}{2}\dot{\xi}_\alpha \dot{\xi}_\alpha + \frac{1}{2}V'' s^2 + a_\alpha' s \xi_\alpha + \frac{1}{2}b_{\alpha\beta}\xi_\alpha \xi_\beta. \qquad (2.108)$$

This expression can be simplified by performing yet another coordinate transformation, which is a shift in fluctuation variable s

$$s(\tau) = u(\tau) + \dot{S}_0 v(\tau)$$
$$\dot{v} = -2C_\alpha \xi_\alpha, \qquad (2.109)$$

where new variable u satisfies the same boundary conditions as s. This reduces second order term to a simple form

$$\delta^2 L = \frac{1}{2}\dot{u}^2 + \frac{1}{2}V'' u^2 + \frac{1}{2}\dot{\xi}_\alpha \dot{\xi}_\alpha + \frac{1}{2}(b_{\alpha\beta} - 3\dot{S}_0^2 C_\alpha C_\beta)\xi_\alpha \xi_\beta + \qquad (2.110)$$
$$+ \frac{1}{2}\frac{\mathrm{d}}{\mathrm{d}\tau}(\ddot{S}_0 \dot{S}_0 v^2) + \frac{\mathrm{d}}{\mathrm{d}\tau}(\ddot{S}_0 uv). \qquad (2.111)$$

Upon integration, last two terms vanish due to the boundary conditions. Thus, second order fluctuations of action separate into longitudinal part, which depends only on u, and transversal part, which depends only on ξ_α

$$\delta^2 S = \int \left(\frac{1}{2}\dot{u}^2 + \frac{1}{2}V'' u^2 \right)\mathrm{d}\tau + \int \left(\frac{1}{2}\dot{\xi}_\alpha \dot{\xi}_\alpha + \frac{1}{2}(b_{\alpha\beta} - 3\dot{S}_0^2 C_\alpha C_\beta)\xi_\alpha \xi_\beta \right)\mathrm{d}\tau. \qquad (2.112)$$

This form can then be inserted into the expression for the kernel, time-sliced and integrated analytically to yield the following expression for the ground-state splitting

$$h_0 = \sqrt{\frac{S_{\text{kink}} \det(\mathbf{H}_0/\beta_N)}{2\pi \det'(\mathbf{H}_\parallel/\beta_N) \det(\mathbf{H}_\perp/\beta_N)}} \mathrm{e}^{-\int_0^{S_{\text{tot}}} \sqrt{2V(S')}\mathrm{d}S'}, \qquad (2.113)$$

with the Hessians of the form

$$\mathbf{H}_{\parallel} = \begin{pmatrix} \beta_N V''(\tau_1) + \frac{2}{\beta_N} & -\frac{1}{\beta_N} & \cdots & 0 \\ -\frac{1}{\beta_N} & \beta_N V''(\tau_2) + \frac{2}{\beta_N} & \cdots & 0 \\ \vdots & \vdots & \ddots & \vdots \\ 0 & 0 & \cdots & V''(\tau_N) + \frac{2}{\beta_N} \end{pmatrix}$$

$$\mathbf{H}_{\perp} = \begin{pmatrix} \beta_N \Omega(\tau_1) + \frac{2}{\beta_N}\mathbf{I} & -\frac{1}{\beta_N}\mathbf{I} & \cdots & 0 \\ -\frac{1}{\beta_N}\mathbf{I} & \beta_N \Omega(\tau_2) + \frac{2}{\beta_N}\mathbf{I} & \cdots & 0 \\ \vdots & \vdots & \ddots & \vdots \\ 0 & 0 & \cdots & \Omega^2(\tau_N) + \frac{2}{\beta_N}\mathbf{I} \end{pmatrix}$$

$$\Omega^2_{\alpha\beta} = b_{\alpha\beta} - 3\dot{S}_0^2 C_\alpha C_\beta. \tag{2.114}$$

As seen in the last paragraph, zero-frequency modes of the action Hessian correspond to the velocity along the kinks and movement along them translates the centers of the kinks in time. As this motion is purely longitudinal, only $\mathbf{H}_{\parallel}$ has zero-frequency modes that must be removed. These matrices still include the imaginary-time variable. However, their determinants can be expressed as a solution of a differential equation using the Gelfand-Yaglom formula,[27,105] which will be discussed in the following paragraph. These equations can then be expressed in terms of distance variable S.

2.4.2. Gelfand-Yaglom Formula

Gelfand-Yaglom formula[105] is a method for reducing the determinant of action Hessian to the solution of a differential equation. Derivation for the one-dimensional blocks will be given here, while extension to multidimensional blocks will be commented at the end of the paragraph. Generally, action Hessian is a matrix of the form

$$\mathbf{H}_N = \begin{pmatrix} \beta_N V''(\tau_1) + \frac{2}{\beta_N} & -\frac{1}{\beta_N} & 0 & \cdots & -\frac{1}{\beta_N} \\ -\frac{1}{\beta_N} & \beta_N V''(\tau_2) + \frac{2}{\beta_N} & -\frac{1}{\beta_N} & \cdots & 0 \\ 0 & -\frac{1}{\beta_N} & \beta_N V''(\tau_3) + \frac{2}{\beta_N} & \cdots & 0 \\ \vdots & \vdots & \vdots & \ddots & \vdots \\ -\frac{1}{\beta_N} & 0 & 0 & \cdots & \beta_N V''(\tau_N) + \frac{2}{\beta_N} \end{pmatrix}. \tag{2.115}$$

For the purpose of the derivation, one can define series $J_n = \beta_N^{n+1} \det \mathbf{H}_n$. These determinants can be expanded along the last column to yield recursion formula

$$J_n = \beta_N^2 V''(\tau_n) J_{n-1} + 2J_{n-1} - J_{n-2}. \tag{2.116}$$

In the limit $\beta_N \to 0$, this recursion can be transformed to a differential equation

$$\frac{J_n + J_{n-2} - 2J_{n-1}}{\beta_N^2} = V''(\tau_n)J_{n-1}$$

$$\frac{\mathrm{d}^2}{\mathrm{d}\tau^2}J(\tau) = V''(\tau)J(\tau). \tag{2.117}$$

Initial conditions for this equation can be found by observing

$$J_1 = \beta_N^3 V''(\tau_1) + 2\beta_N$$
$$J_2 = \beta_N^5 V''(\tau_1)V''(\tau_2) + 2\beta_N^3 V''(\tau_1) + 2\beta_N^3 V''(\tau_2) + 3\beta_N. \tag{2.118}$$

In the limit $\beta_N \to 0$ this results in

$$J(\tau = 0) = 0$$
$$\dot{J}(\tau = 0) = \frac{J_2 - J_1}{\beta_N} = 1. \tag{2.119}$$

The sought determinant corresponds to $J_N = J(\beta)$. Thus, it can be seen that the computation of the determinant of action Hessian can be reduced to the propagation of function J.

The proof for the N_{dof}-dimensional case is more involved and was given by Papadopoulos.[106] It involves going back to the Gaussian integral and rewriting the second order fluctuations

$$\frac{1}{2}\sum_{i=0}^{N}\left(\frac{(\xi_{i+1} - \xi_i)^2}{\beta_N} + \beta_N \xi_i^\top \Omega_i^2 \xi_i\right) = \frac{1}{2}\sum_{i=1}^{N}(\xi_i^\top - \xi_{i+1}^\top Q_i^\top)A_i(\xi_i - Q_i\xi_{i+1})$$

$$A_1 = \beta_N \Omega_1^2 + \frac{2}{\beta_N}I$$

$$A_{i+1} + Q_i^\top A_i Q_i = \beta_N \Omega_{i+1}^2 + \frac{2}{\beta_N}I$$

$$A_i Q_i = \frac{1}{\beta_N}I$$

$$Q_i^\top A_i = \frac{1}{\beta_N}I. \tag{2.120}$$

Last two equations imply that matrices Q_i exist only if matrices A_i are symmetric, and in that case correspond to $Q_i = A_i^{-1}/\beta_N$. This requirement is obviously fulfilled, as A_1 is symmetric, and recursion formula involves only additions of symmetric matrices. One can now perform the coordinate transformation $\eta_i = \xi_i - Q_i\xi_{i+1}$. This is a linear transformation, with a Jacobi matrix being upper triangular with 1 on the diagonal. This implies that the Jacobian of the transformation is unity. Solving the Gaussian integral in this form yields the following

equality for the action Hessian determinant

$$\det \mathbf{H}_N = \det(\mathbf{A}_N \mathbf{A}_{N-1} \cdots \mathbf{A}_1). \tag{2.121}$$

One can now define the matrices $\mathbf{J}_i$ that satisfy an analogous recursion relation and differential equation to the 1D case

$$\mathbf{J}_{i+1} = \beta_N^{i+2} \mathbf{A}_{i+1} \cdots \mathbf{A}_1$$
$$\mathbf{J}_{i+1} = \beta_N \mathbf{A}_{i+1} \mathbf{J}_i$$
$$\mathbf{J}_{i+1} = \Omega_{i+1}^2 \beta_N^2 \mathbf{J}_i + 2\mathbf{J}_i - \mathbf{J}_{i-1}$$
$$\frac{\mathrm{d}^2}{\mathrm{d}\tau^2} \mathbf{J}(\tau) = \Omega^2(\tau) \mathbf{J}(\tau). \tag{2.122}$$

From this result, it is clear that the determinant of action Hessian, which is a matrix of size $(NN_{\mathrm{dof}}) \times (NN_{\mathrm{dof}})$, can be reduced to the determinant of $N_{\mathrm{dof}} \times N_{\mathrm{dof}}$ matrix $\mathbf{J}$, which has to be propagated in an analogous fashion to the 1D case. Matrices $\mathbf{J}$ are known as Jacobi fields in literature, and this approach to instanton theory is thus dubbed Jacobi field instantons (JFI).[14] The expression for the tunneling splitting in terms of Jacobi fields is

$$h_0 = \sqrt{\frac{S_{\mathrm{kink}} \det \mathbf{J}_0(\beta) \lambda_0}{2\pi J_\parallel(\beta) \det \mathbf{J}_\perp(\beta)}} \mathrm{e}^{-\int_0^{S_{\mathrm{tot}}} \sqrt{2V(S')} \mathrm{d}S'}, \tag{2.123}$$

where λ_0 denotes the lowest eigenvalue of tunneling action Hessian.

2.4.3. Non-tunneling Determinant

Non-tunneling determinant can be easily evaluated,[14] as the potential Hessian does not change in the imaginary time

$$\frac{\mathrm{d}^2}{\mathrm{d}\tau^2} \mathbf{J}_0(\tau) = \mathbf{V}_{\mathbf{xx}}^{(0)} \mathbf{J}_0(\tau). \tag{2.124}$$

The solution with correct initial conditions is

$$\mathbf{J}_0(\tau) = \mathbf{A}_0^{-1} \sinh(\tau \mathbf{A}_0)$$
$$\mathbf{A}_0^2 = \mathbf{V}_{\mathbf{xx}}^{(0)}. \tag{2.125}$$

Thus, the Jacobi field, in the low-temperature limit, becomes

$$\mathbf{J}_0(\beta) = \frac{1}{2} \mathbf{A}_0^{-1} \mathrm{e}^{\beta \mathbf{A}_0}. \tag{2.126}$$

2.4.4. Longitudinal Determinant

Mil'nikov and Nakamura[14] make several key approximations when deriving the expressions for the longitudinal and transversal determinants. First assumption is that the instanton path is symmetric with respect to some symmetry operation, so that one can take the central point on the path as the origin in time. The position on the path is then antisymmetric function of time $S_0(-\tau) = -S_0(\tau)$. Second assumption, which will be important for the transversal determinant, is that the transversal Hessians are symmetric with respect to time $\Omega^2(-\tau) = \Omega^2(\tau)$. Jacobi field for the longitudinal determinant can be constructed as a linear combination of two linearly independent solutions of equation

$$\frac{\mathrm{d}^2}{\mathrm{d}\tau^2} f(\tau) = V'' f(\tau). \tag{2.127}$$

One solution is the velocity along the instanton path $p_0 = \dot{S}_0$, which follows directly from the classical equations of motion. A linearly independent solution can be constructed using the Wronskian, which, for this form of differential equation, is constant and can be set to unity. Thus, the linearly independent solution $\eta(\tau)$ satisfies

$$p_0(\tau)\dot{\eta}(\tau) - \dot{p}_0(\tau)\eta(\tau) = 1. \tag{2.128}$$

The linearly independent solution can be found by dividing the equation (2.128) with p_0^2 and integrating from the first minimum (which is now at the time $-\beta/2$)

$$\frac{p_0(\tau)\dot{\eta}(\tau) - \dot{p}_0(\tau)\eta(\tau)}{p_0^2(\tau)} = \frac{1}{p_0^2(\tau)}$$
$$\frac{\mathrm{d}}{\mathrm{d}\tau}\left(\frac{\eta(\tau)}{p_0(\tau)}\right) = \frac{1}{p_0^2(\tau)}$$
$$\eta(\tau) = p_0(\tau)\left(\int_{-\beta/2}^{\tau} \frac{1}{p_0^2(\tau')}\mathrm{d}\tau' + \eta(-\beta/2)\right), \tag{2.129}$$

which is known as d'Alembert's construction.[14,27] The Jacobi field created from the linear combination of these solutions is then

$$J_\parallel(\tau) = p_0(-\beta/2)p_0(\tau)\int_{-\beta/2}^{\tau} \frac{1}{p_0^2(\tau')}\mathrm{d}\tau'. \tag{2.130}$$

Since the sought limit $J_\parallel(\beta/2)$ includes regions where instanton goes to minima and p_0 tends to zero, the contribution from these regions dominates the integral, and the integrand can be replaced by the asymptotic behaviour of p_0. In the region near the first minimum, it is simple

to show that

$$V(S) \approx \frac{1}{2}\omega_\parallel^2 \left(S + \frac{S_{\text{tot}}}{2}\right)^2$$

$$p_0(\tau \to -\infty) = \frac{\mathrm{d}S}{\mathrm{d}\tau} = \omega_\parallel \left(S + \frac{S_{\text{tot}}}{2}\right)$$

$$S(\tau \to -\infty) = P\mathrm{e}^{\omega_\parallel \tau} - \frac{S_{\text{tot}}}{2}$$

$$p_0(\tau \to -\infty) = P\omega_\parallel \mathrm{e}^{\omega_\parallel \tau}, \tag{2.131}$$

where S_{tot} is the total path length. Insertion of this asymptotic form into the integral gives the longitudinal Jacobi field

$$J_\parallel(\beta/2) = \frac{1}{\omega_\parallel}. \tag{2.132}$$

Constant P can be obtained by formally solving equations of motion as

$$\tau = \int_{-S_{\text{tot}}/2}^{S} \frac{\mathrm{d}S'}{p_0(S')} + C. \tag{2.133}$$

The integrand in this equation has a singularity at the lower limit, which can be removed by a regularization with the asymptotic behaviour of potential

$$\tau = \int_{-S_{\text{tot}}/2}^{S} \left(\frac{1}{p_0(S')} - \frac{1}{\omega_\parallel(S' + S_{\text{tot}}/2)}\right) \mathrm{d}S' + \frac{1}{\omega_\parallel}\ln\left(S + \frac{S_{\text{tot}}}{2}\right) + C. \tag{2.134}$$

In the region near the first minimum, momentum tends to $p_0 \approx \omega_\parallel(S + S_{\text{tot}}/2)$, meaning that the two terms in the integrand cancel out near the lower limit, removing the singularity. Constant of integration can be obtained from the definition $S(\tau = 0) = 0$

$$C = -\int_{-S_{\text{tot}}/2}^{0} \left(\frac{1}{p_0(S')} - \frac{1}{\omega_\parallel(S' + S_{\text{tot}}/2)}\right) \mathrm{d}S' - \frac{1}{\omega_\parallel}\ln\left(S + \frac{S_{\text{tot}}}{2}\right). \tag{2.135}$$

Finally, (2.134) can be compared with the previously obtained asymptotic form

$$\tau = \frac{1}{\omega_\parallel}\ln\left(S + \frac{S_{\text{tot}}}{2}\right) - \frac{1}{\omega_\parallel}\ln P. \tag{2.136}$$

In the asymptotic regime, the contribution of the first integral in (2.134) tends to zero, so it can be neglected, yielding the constant P as

$$P = \mathrm{e}^{-\omega_\parallel C} = \frac{S_{\text{tot}}}{2}\mathrm{e}^{\int_{-S_{\text{tot}}/2}^{0} \left(\frac{\omega_\parallel}{p_0(S')} - \frac{1}{(S' + S_{\text{tot}}/2)}\right)\mathrm{d}S'}, \tag{2.137}$$

or equivalently, adding and subtracting p_0'/p_0 in the integrand and noting that it has the same asymptotic behaviour as the second term in (2.134)

$$P = \frac{p_0(0)}{\omega_{\parallel}} e^{\int_{-S_{\text{tot}}/2}^0 \left(\frac{\omega_{\parallel}}{p_0(S')} - \frac{1}{p_0} \frac{dp_0}{dS} \right) dS'}, \tag{2.138}$$

Final step in the determination of the longitudinal Jacobi field is calculation of the lowest eigenvalue λ_0. For this purpose, it is necessary to completely specify the second solution by choosing the initial value $\eta(-\beta/2)$. A convenient choice is the one that reflects the symmetry of the trajectory, which is

$$\eta(\tau) = p_0(\tau) \left(\int_{-\beta/2}^{\tau} \frac{1}{p_0^2(\tau')} d\tau' - \frac{1}{2P^2 \omega_{\parallel}^3} e^{\omega_{\parallel}\beta} \right). \tag{2.139}$$

This choice makes η an antisymmetric function with asymptotic behaviour

$$\lim_{\tau \to \pm\beta/2} \eta(\tau) = \pm \frac{1}{2P\omega_{\parallel}^2} e^{\omega_{\parallel}|\tau|}. \tag{2.140}$$

The sought eigenvalue corresponds to a certain eigenfunction $\Psi(\tau)$, which is required to satisfy $\Psi(\pm\beta/2) = 0$ due to the boundary condition on fluctuations. This eigenvector can be constructed from the solution of the homogeneous equation using the Green's function as

$$\Psi(\tau) = \Psi_0(\tau) + \lambda_0 \int_{-\beta/2}^{\tau} (p_0(\tau)\eta(\tau') - p_0(\tau')\eta(\tau))\Psi(\tau')d\tau'. \tag{2.141}$$

As the integral is zero at $\tau = -\beta/2$, for the eigenfunction to satisfy the boundary conditions, solution to the homogeneous equation must satisfy $\Psi_0(-\beta/2) = 0$. Such eigenfunction can be constructed from the known solutions as

$$\Psi_0(\tau) = p_0(\tau) + 2P^2 \omega_{\parallel}^3 e^{-\omega_{\parallel}\beta} \eta(\tau). \tag{2.142}$$

Finally, the eigenvalue λ_0 can be obtained from the second boundary condition $\Psi(\beta/2) = 0$, approximating the eigenfunction in the integral with the leading contribution Ψ_0 and noting

that $\eta(\tau)$ is antisymmetric function, while $p_0(\tau)$ is symmetric

$$
\lambda_0 = -\frac{\Psi_0(\beta/2)}{\int_{-\beta/2}^{\beta/2}(p_0(\tau)\eta(\tau') - p_0(\tau')\eta(\tau))\Psi_0(\tau')\mathrm{d}\tau'}
$$

$$
= -\frac{p_0(\beta/2) + 2P^2\omega_\parallel^3 e^{-\omega_\parallel\beta}\eta(\beta/2)}{\int_{-\beta/2}^{\beta/2}(p_0(\beta/2)\eta(\tau') - p_0(\tau')\eta(\beta/2))(p_0(\tau') + 2P^2\omega_\parallel^3 e^{-\omega_\parallel\beta}\eta(\tau'))\mathrm{d}\tau'} \tag{2.143}
$$

$$
= -\frac{2P\omega_\parallel e^{-\omega_\parallel\beta/2}}{2P^3\omega_\parallel^4 e^{-3\omega_\parallel\beta/2}\int_{-\beta/2}^{\beta/2}\eta^2(\tau')\mathrm{d}\tau' - \left(2P\omega_\parallel^2\right)^{-1}e^{\omega_\parallel\beta/2}\int_{-\beta/2}^{\beta/2}p_0^2(\tau')\mathrm{d}\tau'}. \tag{2.144}
$$

The second integral in the denominator is simply the action of the path, while the first integral is of the order $\exp(\omega_\parallel\beta)$, which means that the first part is exponentially small compared to the second one. Thus, the eigenvalue becomes

$$
\lambda_0 = \frac{4P^2\omega_\parallel^3}{S_{\mathrm{kink}}}e^{-\omega_\parallel\beta}. \tag{2.145}
$$

2.4.5. Transversal Determinant

To compute the transversal determinant,[14] it is necessary to solve the equation for the transversal Jacobi fields with the following initial conditions

$$
\frac{\mathrm{d}^2}{\mathrm{d}\tau^2}\mathbf{J}_\perp(\tau) = \Omega^2(\tau)\mathbf{J}_\perp(\tau)
$$

$$
\mathbf{J}_\perp(-\beta/2) = 0
$$

$$
\dot{\mathbf{J}}_\perp(-\beta/2) = \mathbf{I}. \tag{2.146}
$$

For this purpose, a solution $\boldsymbol{\eta}$ with different boundary conditions is defined

$$
\boldsymbol{\eta}(-\beta/2) = \mathbf{I}
$$

$$
\dot{\boldsymbol{\eta}}(-\beta/2) = \Omega_0. \tag{2.147}
$$

Its asymptotic behaviour at $\tau \to -\beta/2$ is easily determined from the fact that in that region $\Omega \approx \Omega_0$

$$
\boldsymbol{\eta}(\tau) = \frac{1}{2}e^{\Omega_0(\tau+\beta/2)}. \tag{2.148}
$$

It can be seen from the form of this equation that the solution $\boldsymbol{\eta}$ grows exponentially as it is propagated away from the first minimum. Jacobi field can be obtained with a procedure

similar to d'Alambert's construction as

$$\mathbf{J}_\perp(\tau) = \boldsymbol{\eta}(\tau) \int_{-\beta/2}^{\tau} \mathbf{a}(\tau')\mathrm{d}\tau'$$

$$2\dot{\boldsymbol{\eta}}(\tau)\mathbf{a}(\tau) + \boldsymbol{\eta}(\tau)\dot{\mathbf{a}}(\tau) = 0. \tag{2.149}$$

For the initial conditions to be satisfied, one must choose $\mathbf{a}(-\beta/2) = \mathbf{I}$. Matrix $\mathbf{a}$ can be determined in the region $\tau \to -\beta/2$ using asymptotic form of $\boldsymbol{\eta}(\tau)$. If the basis is chosen to correspond to the eigenvectors of $\boldsymbol{\Omega}_0$, differential equation for a becomes

$$2\dot{\eta}_{\alpha\beta}a_{\beta\gamma} + \eta_{\alpha\beta}a_{\beta\gamma} = 0$$

$$\delta_{\alpha\beta}\mathrm{e}^{\omega_\alpha(\tau+\beta/2)}a_{\beta\gamma} + \delta_{\alpha\beta}\frac{\mathrm{e}^{\omega_\alpha(\tau+\beta/2)}}{2\omega_\alpha}\dot{a}_{\beta\gamma} = 0$$

$$\dot{a}_{\alpha\gamma} = -2\omega_\alpha a_{\alpha\gamma}$$

$$a_{\alpha\gamma} = \delta_{\alpha\gamma}\mathrm{e}^{-2\omega_\alpha(\tau+\beta/2)}. \tag{2.150}$$

From this form, it is clear that $\mathbf{a}$ decays exponentially as one moves from the first minimum. Thus, only significant contribution to the integral (2.149) comes from the lower bound, and the determinant of the transversal Jacobi field at $\tau = \beta/2$ becomes

$$\det\mathbf{J}_\perp(\beta/2) = \frac{\det\boldsymbol{\eta}(\beta/2)}{2^{N_{\mathrm{dof}}-1}\det\boldsymbol{\Omega}_0}. \tag{2.151}$$

Next, Mil'nikov and Nakamura[14] claim that the following equality holds

$$\det\boldsymbol{\eta}(\beta/2) = \frac{\det\boldsymbol{\eta}(0)\det\dot{\boldsymbol{\eta}}(0)}{\det\boldsymbol{\Omega}_0}. \tag{2.152}$$

However, they only provide the proof for the two-dimensional case, which is not readily generalizable to the N-dimensional, as in that case matrix $\boldsymbol{\eta}$ is one-dimensional. Detailed proof for more general systems will be given as a part of theoretical methods developed. Determinants in this equation can be computed via their log-derivative matrix

$$\boldsymbol{\Xi} = \dot{\boldsymbol{\eta}}\boldsymbol{\eta}^{-1}$$

$$\boldsymbol{\Xi}(-\beta/2) = \boldsymbol{\Omega}_0$$

$$\dot{\boldsymbol{\Xi}} = \boldsymbol{\Omega}^2 - \boldsymbol{\Xi}^2. \tag{2.153}$$

Determinant of η can be computed by observing its derivation and propagating it from the first minimum

$$\frac{\mathrm{d}}{\mathrm{d}\tau}\det\eta = \det\eta\,\mathrm{Tr}\,\Xi$$
$$\det\eta(\tau) = e^{\int_{-\beta/2}^{\tau}\mathrm{Tr}\,\Xi(\tau')\mathrm{d}\tau'}. \tag{2.154}$$

Finally, using the expression $\det\dot{\eta} = \det\eta\det\Xi$, which follows directly from the definition of log-derivative, the transversal determinant becomes

$$\det\mathbf{J}_{\perp}(\beta/2) = \frac{\det\Xi(0)}{2^{N_{\mathrm{dof}}-1}\det\Omega_0^2}e^{2\int_{-\beta/2}^{0}\mathrm{Tr}\,\Xi(\tau')\mathrm{d}\tau'} \tag{2.155}$$

2.4.6. JFI Expression for Tunneling Matrix Element

Inserting all of the above determinants of Jacobi fields into the expression for tunneling matrix element,[14] and using the fact that $\det\mathbf{A}_0 = \omega_{\parallel}\det\Omega_0$, the formula becomes

$$h_0 = \sqrt{\frac{\det\mathbf{A}_0}{\pi\det\Xi(0)}}\,p_0(0)e^{-\int_0^{S_{\mathrm{tot}}}p_0\mathrm{d}S+\int_0^{S_{\mathrm{tot}}/2}\left(\mathrm{Tr}\,\mathbf{A}_0-\mathrm{Tr}\,\Xi-p_0'\right)/p_0\mathrm{d}S}. \tag{2.156}$$

This equation no longer involves imaginary time variables and does not include β as a parameter. Rather, limit $\beta \to +\infty$ has been taken by demanding that the boundaries of integration run from one minimum to the other. Though all of the objects that appear in this formula can be easily computed, they are formulated in terms of curvilinear coordinates S, ξ_α. Use of these coordinates can be completely avoided, by defining a matrix $\mathbf{A}$

$$\mathbf{A}^{(S,\xi)} = \begin{pmatrix} p_0' & -p_0\mathbf{C}^{\top} \\ -p_0\mathbf{C} & \Xi \end{pmatrix}. \tag{2.157}$$

It is evident that the trace of this matrix is simply $\mathrm{Tr}\,\mathbf{A}^{(S,\xi)} = p_0' + \mathrm{Tr}\,\Xi$, which means that it can be used to replace that expression in the exponent. Furthermore, if one defines a projector operator $\mathbf{P} = \mathbf{I} - \tau_N\tau_N^{\top}$, matrix Ξ can be extracted as

$$\mathbf{P}\mathbf{A}^{(S,\xi)}\mathbf{P} = \begin{pmatrix} 0 & 0 \\ 0 & \Xi \end{pmatrix}. \tag{2.158}$$

Thus, determinant of matrix Ξ can be computed as $\det\Xi = \det'\mathbf{P}\mathbf{A}^{(S,\xi)}\mathbf{P}$, where prime indicates that the determinant represents the product of non-zero eigenvalues. Finally, matrix $\mathbf{A}^{(S,\xi)}$ can be rotated back to the Cartesian coordinates and can be shown to satisfy a simple

Ricatti equation

$$p_0 \frac{\mathrm{d}}{\mathrm{d}S}\mathbf{A} = \mathbf{V_{xx}} - \mathbf{A}^2$$
$$\mathbf{A}_0 = \mathbf{V_{xx}^{\frac{1}{2}}}, \tag{2.159}$$

which can be used to propagate it without any reference to curvilinear coordinates. As both trace and determinant are invariant properties with respect to the change of basis, all of the above equalities can be expressed via $\mathbf{A}$. The tunneling matrix element is then simply

$$h_0 = \sqrt{\frac{\det \mathbf{A}_0}{\pi \det' \mathbf{PA}(0)\mathbf{P}}} p_0(0)\mathrm{e}^{-\int_0^{S_\text{tot}} p_0 \mathrm{d}S + \int_0^{S_\text{tot}/2}(\mathrm{Tr}\,\mathbf{A}_0 - \mathrm{Tr}\,\mathbf{A})/p_0 \mathrm{d}S}. \tag{2.160}$$

2.5. WKB Theory on Instanton Paths

An alternative approach[14] for calculation of tunneling splitting involves the use of Herring formula[32]

$$h_0 = \frac{\int \left(\phi^{(L)} \frac{\partial}{\partial S} \phi^{(R)} - \phi^{(R)} \frac{\partial}{\partial S} \phi^{(L)} \right) \delta(f(\mathbf{x})) \mathrm{d}\mathbf{x}}{2 \int |\phi^{(L)}|^2 \mathrm{d}\mathbf{x}}, \tag{2.161}$$

where $\phi^{(L/R)}$ are wavefunctions localized in two minima. The minima are assumed to be separated by a dividing surface defined by an implicit equation $f(\mathbf{x}) = 0$. S denotes a local coordinate that describes an orthogonal shift from the nearest point on the dividing surface. This formula can easily be proven for systems with two symmetry-related wells. In those cases, eigenfunctons are symmetric and antisymmetric combinations of localized wavefunctions

$$\psi^{(\pm)} = \frac{1}{\sqrt{2}}(\phi^{(L)} \pm \phi^{(R)})$$
$$\hat{H}\psi^{(\pm)} = (E_0 \mp h_0)\psi^{(\pm)}. \tag{2.162}$$

Multiplying the two equations for the eigenvalues with the other eigenfunction, subtracting them and writing the eigenfunctions in terms of localized wavefunctions yields

$$\psi^{(-)}\hat{H}\psi^{(+)} - \psi^{(+)}\hat{H}\psi^{(-)} = -2h_0\psi^{(+)}\psi^{(-)}$$

$$-\frac{1}{4}(\phi^{(L)} - \phi^{(R)})\nabla^2(\phi^{(L)} + \phi^{(R)}) + \frac{1}{4}(\phi^{(L)} + \phi^{(R)})\nabla^2(\phi^{(L)} - \phi^{(R)}) = -h_0\left((\phi^{(L)})^2 - (\phi^{(R)})^2\right)$$

$$\frac{1}{2}\phi^{(R)}\nabla^2\phi^{(L)} - \frac{1}{2}\phi^{(L)}\nabla^2\phi^{(R)} = -h_0\left((\phi^{(L)})^2 - (\phi^{(R)})^2\right)$$

$$\frac{1}{2}\nabla\left(\phi^{(L)}\nabla\phi^{(R)} - \phi^{(R)}\nabla\phi^{(L)}\right) = h_0\left((\phi^{(L)})^2 - (\phi^{(R)})^2\right)$$

$$\frac{1}{2}\int_L \nabla\left(\phi^{(L)}\nabla\phi^{(R)} - \phi^{(R)}\nabla\phi^{(L)}\right)d\mathbf{x} = h_0\int_L\left((\phi^{(L)})^2 - (\phi^{(R)})^2\right)d\mathbf{x},$$

$$(2.163)$$

where integrals are taken over the region of space that contains the first minimum ('left'), and that for one boundary has the dividing surface, while the other boundaries extend to infinity. In case of deep tunneling, which is of interest in this dissertation, the amplitude of $\phi^{(R)}$ in this region is negligible, and its integral can be neglected, while the integral of $\phi^{(L)}$ can be approximated by its norm, as it has a negligible norm outside this region. Finally, one applies the divergence theorem on the left hand side integral, defining the boundaries of the region to be a hemisphere, with radius extending to infinity. As localized wavefunctions decay at the infinity, surface integral over this region vanishes, leaving the only non-zero contribution to be that of the dividing surface, which yields the Herring formula. The expression (2.161) is strictly valid only in cases of deep tunneling, where the probability of finding one localized wavefunction in the other well is negligible. If this condition is not fulfilled, the denominator has to be modified accordingly.

To apply the Herring formula, it is necessary to possess information about the shape and amplitude of both localized wavefunctions at the dividing surface. A numerically efficient method for obtaining this is via Wentzel-Kramers-Brillouin (WKB) approach,[33] where wavefunction is written in exponential form, with exponent expanded in powers of $\hbar$

$$\phi = e^{-\frac{1}{\hbar}(W_0 + W_1\hbar + ...)}. \qquad (2.164)$$

However, unlike the standard WKB method, where energy is treated as a $\hbar^0$ order term, and determined from matching conditions, it is noted that vibrational energy is of the order $\hbar^1$, as in a harmonic approximation. Consequently, it can be moved from the equations that follow

from the $\hbar^0$ order term, to those that are obtained from the $\hbar^1$ order terms

$$\frac{\partial W_0}{\partial x_i}\frac{\partial W_0}{\partial x_i} = 2V(\mathbf{x})$$

$$\frac{\partial W_0}{\partial x_i}\frac{\partial W_1}{\partial x_i} - \frac{1}{2}\frac{\partial^2 W_0}{\partial x_i \partial x_i} + E = 0. \tag{2.165}$$

The first equation depends only on the potential energy surface, and is called Hamilton-Jacobi equation.[14,15] It can be solved using the method of characteristics. In this method, a set of curves, called characteristics, is found, on which the partial differential equation reduces to a set of ordinary differential equations with respect to some variable τ that parameterizes characteristic curves. For this form of differential equation, characteristics are given by equations

$$p_i = \frac{\partial W_0}{\partial x_i}$$

$$p_i = \frac{\mathrm{d}x_i}{\mathrm{d}\tau}$$

$$\frac{\mathrm{d}p_i}{\mathrm{d}\tau} = \frac{\mathrm{d}V}{\mathrm{d}x_i}, \tag{2.166}$$

which are, in essence, the classical equations of motion on the inverted potential energy surface. The total energy of the trajectories is zero, which can be seen from Hamilton-Jacobi equation ($p_i p_i/2 + (-V) = 0$). On the characteristic, Hamilton-Jacobi equation can be solved by a simple integration

$$\frac{\mathrm{d}W_0}{\mathrm{d}\tau} = \frac{\partial W_0}{\partial x_i}\frac{\mathrm{d}x_i}{\mathrm{d}\tau} = p_i p_i = 2V(\mathbf{x})$$

$$W_0(\tau) = W_0(0) + \int_0^\tau 2V \mathrm{d}\tau. \tag{2.167}$$

Value $W_0(0)$ can be freely chosen for a certain reference point, which corresponds to fixing the norm of the wavefunction. For this purpose, a convenient choice for the reference point is the minimum, and the simplest choice is $W_0(0) = 0$. As τ plays the role of the imaginary time for the trajectories with zero total energy, it takes an infinite time to move from minimum to any other point on the surface. To circumvent this inconvenience, one can define the arc-distance variable, analogously to the derivation of JFI theory, with line element

$$\mathrm{d}S = \sqrt{\mathrm{d}x_i \mathrm{d}x_i}. \tag{2.168}$$

Convenient relations follow from this definition

$$\frac{\mathrm{d}S}{\mathrm{d}\tau} = \sqrt{\frac{\mathrm{d}x_i}{\mathrm{d}\tau}\frac{\mathrm{d}x_i}{\mathrm{d}\tau}} = \sqrt{p_i p_i} = |\mathbf{p}| = p_0$$

$$p_0 = \sqrt{2V}$$

$$W_0(S) = \int_0^S \sqrt{V_0(S')}\mathrm{d}S', \tag{2.169}$$

which means that W_0 on the characteristic corresponds to the action in JFI theory. This method can be used to compute the amplitude of the wavefunction at every point on the dividing plane. However, such a method would involve locating classical trajectories for many points, which is computationally unfeasible. Instead, it is possible to define a set of coordinates ξ_α that describe orthogonal shift from the characteristic and expand W_0 function with respect to them

$$W_0(S, \xi_\alpha) = \int_0^S \sqrt{2V_0(S')}\mathrm{d}S' + \frac{1}{2}\Xi_{\alpha\beta}\xi_\alpha\xi_\beta. \tag{2.170}$$

These coordinates can be chosen to correspond to the coordinates used in JFI method, with the same metric tensor. Hamilton-Jacobi equation in these coordinates transforms into

$$\frac{1}{(1+C_\alpha\xi_\alpha)^2}\left(\frac{\partial W_0}{\partial S}\right)^2 + \left(\frac{\partial W_0}{\partial \xi_\alpha}\right)^2 = 2V_0(S) + 2a_\alpha(S)\xi_\alpha + b_{\alpha\beta}(S)\xi_\alpha\xi_\beta + O(\xi_\alpha^3), \tag{2.171}$$

where potential was expanded around the characteristic. Inserting the expansion of W_0, further expanding $(1+C_\alpha\xi_\alpha)^{-2} = 1 - 2C_\alpha\xi_\alpha + 3C_\alpha C_\beta\xi_\alpha\xi_\beta$ and equating the terms of order ξ^2 results in the equation for the matrix Ξ

$$p_0\frac{\mathrm{d}}{\mathrm{d}S}\Xi_{\alpha\beta} = b_{\alpha\beta} - 3p_0^2 C_\alpha C_\beta - \Xi_{\alpha\beta}$$

$$p_0\frac{\mathrm{d}}{\mathrm{d}S}\Xi = \Omega^2 - \Xi^2, \tag{2.172}$$

where Ω^2 denotes the same matrix as in the equation (2.114). It can be noted that the form of equation (2.172) is the same as in the case of transversal Jacobi field (2.153). Thus, Jacobi fields can be interpreted in terms of wavefunction, as the Hessians that determine the width of the wavefunction in the hyperplane orthogonal to the MAP. One can define matrix $A_{ij} = \frac{\partial^2 W_0}{\partial x_i \partial x_j}$, that is completely identical to the corresponding matrix in JFI theory, and propagation can be performed analogously in Cartesian coordinates.

The second WKB equation is called transport equation, and can be solved by integration on the path, which corresponds to expansion of W_1 up to ξ^0 term. As on the path $\mathbf{p}_0 = \nabla W_0$, the first term in the equation can be recognised as a directional derivative, in the direction of the tangent on the path. The second term is simply the trace of previously defined matrix $\mathbf{A}$,

while the energy in harmonic approximation is simply the trace of $\mathbf{A}_0$, the initial matrix $\mathbf{A}$ at a minimum. Thus, W_1 becomes

$$W_1(S) = \int_0^S \frac{\mathrm{Tr}\,(\mathbf{A}(S') - \mathbf{A}_0)}{p_0}\mathrm{d}S'. \tag{2.173}$$

Combining the solutions of WKB equations results in the approximated wavefunction

$$\phi(S, \xi_\alpha) = \mathrm{e}^{-\int_0^S p_0\mathrm{d}S' - \frac{1}{2}\int_0^S (\mathrm{Tr}(\mathbf{A}-\mathbf{A}_0))/p_0\mathrm{d}S' - \frac{1}{2}A_{ij}\tau_{i\alpha}\tau_{j\alpha}\xi_\alpha\xi_\beta}. \tag{2.174}$$

The derivative with respect to S in Herring formula, is evaluated by keeping only terms that arise from W_0, and neglecting contributions of the fluctuation variables. This results in a simple expression

$$\frac{\partial}{\partial S}\phi(S, \xi_\alpha) = -p_0\phi(S, \xi_\alpha). \tag{2.175}$$

Thus, the integrand in Herring formula is proportional to the product $\phi^{(\mathrm{L})}\phi^{(\mathrm{R})}$. The wavefunctions at the dividing surface can be described by an expansion around a point on the surface, by connecting it to both minima with classical trajectories. This expansion will result in the least error if that point is taken so that the product of amplitudes of both wavefunctions is maximal. This is equivalent to choosing that point so that the sum

$$\int_0^{S_{\mathrm{cp}}} p_0^{(L)}\mathrm{d}S' + \int_0^{\tilde{S}_{\mathrm{cp}}} p_0^{(R)}\mathrm{d}\tilde{S}' = \int_0^{S_{\mathrm{tot}}} p_0\mathrm{d}S' \tag{2.176}$$

is minimal, where $\tilde{S}$ denotes the distance from the right minimum, while S denotes the distance from the left minimum. However, this sum is simply the action of the path that connects the two minima and passes through the connection point. It follows that the optimal choice for the connection point is a point that lies on the minimum action path that connects the two minima, which is simply the instanton path. Mil'nikov and Nakamura[14] assume the symmetry of the MAP with respect to the top of the barrier, located at the halfway point, which they choose as the connection point. This results in the convenient relations at the connection point, namely $p_0^{(\mathrm{L})}(S_{\mathrm{cp}}) = p_0^{(\mathrm{R})}(S_{\mathrm{cp}}) = p_0$ and $\mathbf{A}^{(\mathrm{L})}(S_{\mathrm{cp}}) = \mathbf{A}^{(\mathrm{R})}(S_{\mathrm{cp}}) = \mathbf{A}$. Furthermore, as MAP is expected to be smooth, dividing surface can conveniently be chosen to represent the hyperplane orthogonal to it at the connection point, which reduces the integral over the surface to the integral over variables ξ_α. Taking into account everything mentioned here, the integral in the numerator of the Herring formula is of Gaussian type and can be solved analytically to yield

$$\int \left(\phi^{(\mathrm{L})}\frac{\partial}{\partial S}\phi^{(\mathrm{R})} - \phi^{(\mathrm{R})}\frac{\partial}{\partial S}\phi^{(\mathrm{L})} \right) \delta(f(\mathbf{x}))\mathrm{d}\mathbf{x} = 2p_0\sqrt{\frac{\pi^{N_{\mathrm{dof}}-1}}{\det' \mathbf{PAP}}}\mathrm{e}^{-\int_0^{S_{\mathrm{tot}}} p_0\mathrm{d}S' - \int_0^S (\mathrm{Tr}(\mathbf{A}(S')-\mathbf{A}_0))/p_0\mathrm{d}S'}. \tag{2.177}$$

The integral in the denominator of Herring formula is the norm of the localized wavefunction. As the most significant contribution to the norm arises from the vicinity of the minimum, where the amplitude of the ground-state wavefunction is the greatest, $\phi^{(L)}$ can be approximated by a multidimensional harmonic oscillator, with its frequencies given by $\mathbf{A}_0$

$$\phi^{(L)} = e^{-\frac{1}{2}(\mathbf{x}-\mathbf{x}^{(L)})^{\top}\mathbf{A}_0(\mathbf{x}-\mathbf{x}^{(L)})}, \tag{2.178}$$

The prefactor is set to unity so that the value of the approximated wavefunction at $\mathbf{x}^{(L)}$ matches the value of WKB wavefunction. Inserting equation (2.178) into the integral in the denominator results in

$$\int |\phi^{(L)}|^2 d\mathbf{x} = \sqrt{\frac{\pi^{N_{\text{dof}}}}{\det \mathbf{A}_0}}. \tag{2.179}$$

Inserting (2.177) and (2.179) into the Herring formula results in the formula for the tunneling matrix element

$$h_0 = \sqrt{\frac{\det \mathbf{A}_0}{\pi \det' \mathbf{PAP}}} p_0 e^{-\int_0^{S_{\text{tot}}} p_0 dS' - \int_0^S (\text{Tr}(\mathbf{A}(S') - \mathbf{A}_0))/p_0 dS'}, \tag{2.180}$$

which is identical to that obtained from the JFI theory.

2.5.1. WKB Theory on Instanton Paths - Excited States

A major advantage of the WKB approach is the fact that it can readily be generalized to compute tunneling matrix elements in the excited vibrational states. This has been demonstrated by Mil'nikov and Nakamura in a follow-up paper,[15] where they considered singly excited vibrational modes. As Hamilton-Jacobi equation depends only on the potential energy surface, W_0 function is the same for excited states. This represents a great advantage from the computational side, as it means that it is not necessary to recompute MAPs or Hessians along them, which are the most resource-intensive steps. Transport equation, on the other hand, is modified by the excitation energy $E_v = E_0 + \omega_v$. Thus, Mil'nikov and Nakamura propose a correction to the W_1 function for the excited normal mode v

$$W_1^{(v)} = W_1^{(0)} + w$$

$$\frac{\partial W_0}{\partial x_i}\frac{\partial w}{\partial x_i} + \omega = 0. \tag{2.181}$$

They further separate excitation in the longitudinal vibrational mode from the excitations in transversal modes. For the longitudinal mode, they propose to solve the equation for w by a simple integration along the characteristic, neglecting the first and higher order terms with

respect to orthogonal coordinates ξ_α

$$p_0 \frac{\mathrm{d}w}{\mathrm{d}S} = -\omega_\parallel$$

$$w = -\int_0^S \frac{\omega_\parallel}{p_0} \mathrm{d}S' \tag{2.182}$$

$$w = \int_0^S \frac{p_0' - \omega_\parallel}{p_0} \mathrm{d}S' - \ln \frac{p_0}{\omega_\parallel}, \tag{2.183}$$

where regularization of the integral has been performed in the last step. WKB wavefunction for the first excited state then becomes

$$\phi^{(\parallel)} = \frac{p_0}{\omega_\parallel} \mathrm{e}^{-\int_0^S \frac{p_0' - \omega_\parallel}{p_0} \mathrm{d}S'} \phi^{(0)}. \tag{2.184}$$

Such wavefunction has a correct asymptotic behaviour near the minimum, because in that region $p_0 \approx \omega_\parallel S$, and the integral in the exponent tends to zero. The wavefunction becomes

$$\phi^{(\parallel)} \approx S\phi^{(0)}. \tag{2.185}$$

As only W_1 function is modified, the derivative with respect to coordinate S, which appears in the Herring formula, has the same effect of multiplying the wavefunction with p_0 as it has for the ground state. Thus, the longitudinal excitation just scales the integral in the numerator with the same factor by which it scales the wavefunction. For the integral in the denominator, one has to take into account the prefactor S, which is conveniently in the direction of one of the normal modes, meaning that the integral simply picks up a factor of $(2\omega_\parallel)^{-1}$. The expression for the tunneling splitting then becomes

$$h_\parallel = h_0 \frac{2p_0^2}{\omega_\parallel} \mathrm{e}^{2\int_0^S \frac{p_0' - \omega_\parallel}{p_0} \mathrm{d}S'}. \tag{2.186}$$

For the case of the excitations of transversal modes, it is necessary to include first order terms in orthogonal coordinates. Such wavefunctions are expected to have a different shape in the plane orthogonal to MAP, which changes the overlap integral over the dividing plane. Mil'nikov and Nakamura propose the following form for w

$$w = \int_0^S \frac{\theta(S') - \omega}{p_0} \mathrm{d}S' - \ln(U_\alpha(S)\xi_\alpha). \tag{2.187}$$

Inserting this expression into the equation for w yields

$$\frac{\partial W_0}{\partial x_i}\frac{\partial w}{\partial x_i} + \omega = 0$$

$$\left(\frac{\partial W_0}{\partial S}\frac{\partial S}{\partial x_i} + \frac{\partial W_0}{\partial \xi_\alpha}\frac{\partial \xi_\alpha}{\partial x_i}\right)\left(\frac{\partial w}{\partial S}\frac{\partial S}{\partial x_i} + \frac{\partial w}{\partial \xi_\alpha}\frac{\partial \xi_\alpha}{\partial x_i}\right) + \omega = 0$$

$$\left(p_0 J_{Ni}^{-1} + \Xi_{\alpha\beta}\xi_\beta J_{\alpha i}^{-1}\right)\left(\frac{\theta - \omega}{p_0}J_{Ni}^{-1} - \frac{1}{U_\alpha\xi_\alpha}U_\alpha'\xi_\alpha J_{Ni}^{-1} - \frac{1}{U_\alpha\xi_\alpha}U_\alpha J_{\alpha i}^{-1}\right) + \omega = 0, \quad (2.188)$$

where $\mathbf{J}^{-1}$ is the Jacobi matrix for the inverse coordinate transformation. Multiplying out the parentheses and taking into account that rows of $\mathbf{J}^{-1}$ are orthogonal and that $J_{\alpha i}^{-1}J_{\alpha i}^{-1} = 1$ and $J_{Ni}^{-1}J_{Ni}^{-1} = (1 + C_\alpha\xi_\alpha)^{-1} \approx 1 - C_\alpha\xi_\alpha$ yields, up to ξ^1,

$$\left(\theta U_\alpha - p_0 U_\alpha' - \Xi_{\alpha\beta}U_\alpha\right)\xi_\alpha = 0. \quad (2.189)$$

From here, the propagation equation for $\mathbf{U}$ is

$$p_0 U_\alpha' = \theta U_\alpha - \Xi_{\alpha\beta}U_\beta. \quad (2.190)$$

Initial condition follows from matching the wavefunction at minimum to the one of the harmonic oscillator. This gives $\mathbf{U}(0) = \mathbf{U}_\nu$, where the latter is the normal mode that has been excited. Function θ can be chosen arbitrarily, with different choices leading to different norms of vector $\mathbf{U}$. Mil'nikov and Nakamura choose θ so that the norm remains unity over the course of propagation. This corresponds to

$$\mathbf{U}^\top\mathbf{U} = 1. \quad (2.191)$$

Taking the derivative, one obtains

$$2p_0\mathbf{U}^\top\mathbf{U}' = 0$$

$$\theta\mathbf{U}^\top\mathbf{U} - \mathbf{U}^\top\Xi\mathbf{U} = 0$$

$$\theta = \mathbf{U}^\top\Xi\mathbf{U}. \quad (2.192)$$

Finally, they also claim that it is possible to define vector $\tilde{\mathbf{U}}$ in Cartesian coordinates that follows the analogous equation

$$p_0\tilde{\mathbf{U}} = (\tilde{\mathbf{U}}^\top\mathbf{A}\tilde{\mathbf{U}})\tilde{\mathbf{U}} - \mathbf{A}\tilde{\mathbf{U}}, \quad (2.193)$$

for which they claim to have zero component tangential to the path during the entire propagation, and whose other components correspond to vector $\mathbf{U}$. They demonstrate this in

the following way. Due to the initial conditions, at the minimum tangential component is $\tilde{\mathbf{U}}^\top \mathbf{p}_0 = 0$. Furthermore, the derivative of tangential component is

$$p_0 \frac{\mathrm{d}}{\mathrm{d}S} \tilde{\mathbf{U}}^\top \mathbf{p}_0 = \theta \tilde{\mathbf{U}}^\top \mathbf{p}_0 - \tilde{\mathbf{U}}^\top \mathbf{A} \mathbf{p}_0 + \tilde{\mathbf{U}}^\top \mathbf{p}_0'$$

$$= \theta \tilde{\mathbf{U}}^\top \mathbf{p}_0 - \tilde{\mathbf{U}}^\top \mathbf{p}_0' + \tilde{\mathbf{U}}^\top \mathbf{p}_0'$$

$$= \theta \tilde{\mathbf{U}}^\top \mathbf{p}_0 \tag{2.194}$$

$$\tilde{\mathbf{U}}^\top \mathbf{p}_0 = (\tilde{\mathbf{U}}^\top \mathbf{p}_0)(S=0) \mathrm{e}^{\int_0^S \frac{\theta}{p_0} \mathrm{d}S'}, \tag{2.195}$$

where in the second line the directional derivative has been recognised

$$(\mathbf{A} \mathbf{p}_0)_i = \frac{\partial^2 W_0}{\partial x_i \partial x_j} p_{0,j} = p_0 \frac{\partial^2 W_0}{\partial x_i \partial S} = p_0 (p_{0,i})'. \tag{2.196}$$

Finally, due to the initial conditions, pre-exponential factor is zero, which implies that $\tilde{\mathbf{U}}^\top \mathbf{p}_0 = 0$. As vector $\tilde{\mathbf{U}}$ never picks up tangential component, it can easily be seen that the remaining components correspond to $\mathbf{U}$, by writing down all objects in terms of block matrices and block vectors in local coordinates and multiplying out the blocks in propagation equation.

Excited state wavefunction thus becomes

$$\phi^{(\nu)} = U_\alpha \xi_\alpha \mathrm{e}^{2 \int_0^{S_{\mathrm{cp}}} \frac{\theta - \omega}{p_0} \mathrm{d}S'} \phi^{(0)}. \tag{2.197}$$

Inserting this wavefunction into Herring formula results in the integral of the Gaussian function multiplied by a second-order polynomial. This integral can be easily solved by transforming it into normal modes of matrix $\mathbf{A}$ and evaluating one-dimensional integrals of the form $\int q^2 \exp(-\lambda q^2) \mathrm{d}q$. Taking account of the norm in analogous fashion to that of the longitudinal excitations yields the formula for tunneling matrix element

$$h_\nu = \omega \mathbf{U}^\top (\mathbf{P} \mathbf{A} \mathbf{P})^{-1} \mathbf{U} \mathrm{e}^{\int_0^S \frac{\theta - \omega}{p_0} \mathrm{d}S'} h_0, \tag{2.198}$$

where the 'inverse' $(\mathbf{P} \mathbf{A} \mathbf{P})^{-1}$ is defined as a matrix that has the same eigenvectors as $\mathbf{P} \mathbf{A} \mathbf{P}$ and whose nonzero eigenvalues are the inverses of the eigenvalues of $\mathbf{P} \mathbf{A} \mathbf{P}$, while the zero eigenvalues remain zero.

2.6. Experimental Measurement of Tunneling Splitting

High-resolution microwave spectroscopy (HRMS)[107–109] is the most widely used method for experimental determination of ground-state tunneling splittings. It can be applied only on molecules which possess a permanent dipole moment in their ground state, as only those molecules produce signals in microwave spectrum. However, for molecules which do not

possess permanent dipole moment due to symmetry, measurements can be made if one or more atoms are replaced with heavier isotopes.[110] Such substitution breaks the symmetry of the vibrational wavefunction and induces a small dipole moment, which can be sufficient to record microwave spectra. In these cases, however, one must keep in mind that isotopic substitution may have non-negligible effect on tunneling splitting, especially if the atom that is substituted moves significantly during the tunneling rearrangement. Molecules in which tunneling splitting is present have split vibrational ground state, with each split energy level possessing a manifold of rotational states. As different split states usually have similar probability densities, which differ only in the regions of potential energy barriers, where probability density is small, split states have similar rotational constants. As a result, in the absence of coupling between these states, they would all produce signals in the spectrum at similar frequencies. However, rotational states of different split vibrational states interact via Coriolis coupling.[109] Coupling is a consequence of the fact that, along the rearrangement motion path, principal axes of the molecule change. As a result, inverse moment of inertia tensor μ picks up non-diagonal elements $\mu_{ab}(S)$, $\mu_{bc}(S)$ and $\mu_{ac}(S)$ which depend on the position S on the tunneling path. If one considers a system with two wells, for simplicity, which yield two split vibrational states, these elements result in the coupling constants $F_{\alpha\beta} = \left\langle \psi^{(+)} \middle| \mu_{\alpha\beta} \middle| \psi^{(-)} \right\rangle$ between split states, where α and β denote coordinates in the molecular frame. Hamiltonian matrix for the system is then

$$\mathbf{H} = \begin{pmatrix} \mathbf{H}^{(+)} & \mathbf{H}_c \\ \mathbf{H}_c^\top & \mathbf{H}^{(-)} \end{pmatrix}$$

$$\mathbf{H}^{(+)} = \frac{1}{2} \left\langle \psi^{(+)} \middle| \mu_{\alpha\beta} \middle| \psi^{(+)} \right\rangle \hat{J}_\alpha \hat{J}_\beta$$

$$\mathbf{H}^{(-)} = \Delta E + \frac{1}{2} \left\langle \psi^{(-)} \middle| \mu_{\alpha\beta} \middle| \psi^{(-)} \right\rangle \hat{J}_\alpha \hat{J}_\beta$$

$$\mathbf{H}_c = F_{\alpha\beta}(\hat{J}_\alpha \hat{J}_\beta + \hat{J}_\beta \hat{J}_\alpha), \tag{2.199}$$

where ΔE is tunneling splitting and $F_{\alpha\beta}$ denotes coupling. Coupling causes perturbations of rotational energy levels of both manifolds, resulting in the shifts of the peaks in the microwave spectrum, which result in the appearance of doublets. Splitting of the doublets depends on the quantum number J of the corresponding transition. Thus, frequencies of the transitions for a range of J-values hold the information on the magnitude of Coriolis coupling and tunneling splitting. Consequently, if sufficiently many transitions are assigned, values of rotational constants, coupling constants and tunneling splitting are obtained by nonlinear regression, using specialised software.[111] Transitions between states belonging to different rotational manifolds are usually not observed in the microwave spectra, due to the fact that their intensities are weaker.

HRMS has been used to measure tunneling splitting in a number of molecules. Notable examples include malonaldehyde[107] and tropolone,[109] in which splitting is a consequence of intramolecular hydrogen transfer. Additionally, splitting has been measured for a range of carboxylic acid dimers, such as formic acid-benzoic acid dimer[108] and formic acid homodimer,[110] where splitting is a consequence of double intermolecular hydrogen transfer. In the latter case, measurement was made for heterodimer, in which one monomer had hydrogen atom in the C-H bond substituted with deuterium, to induce a dipole moment. Finally, splitting has been measured for a wide range of weakly-bound molecular clusters, such as water dimer.[112]

In addition to HRMS, terahertz spectroscopy is also used to study tunneling splittings. In this method, far infrared region is probed, making it possible to determine tunneling splittings not only of ground vibrational state, but of low-lying vibrational states as well. The method has been used extensively in the study of small water clusters.[113]

2.7. Molecular Systems

2.7.1. Malonaldehyde

Malonaldehyde molecule possesses two symmetry-related minima, which correspond to different positions of hydrogen atom from the OH group. It has been extensively studied using experimental methods. Its ground state splitting was determined using microwave spectroscopy by Baba et al.[107] Furthermore, splittings of low vibrationally excited states was determined using infrared[114,115] and Raman[116] spectroscopy. Additionally, ground state splitting was determined for a range of partially deuterated malonaldehyde molecules, using microwave spectroscopy by Baughcum et al.[117]

Additionally, due to the relatively small number of degrees of freedom, nuclear energy levels of malonaldehyde molecule have been determined using various quantum-mechanical methods, such as MCTDH[36] and DMC.[10,43] Furthermore, several analytic potential energy surfaces are available.[10,118] Additionally, tunneling splitting in malonaldehyde has been determined using several methods based on path integral theory, such as PIMD[31], RPI[37] and JFI[14]. This makes malonaldehyde a convenient benchmark model to test the performance of JFI method developed.

2.7.2. Water Dimer

Water dimer is the smallest water cluster, consisting of two monomers connected by a hydrogen bond in the geometry of the minimum on potential energy surface, shown in Figure 1. Its molecular symmetry group and connectivity of minima was studied by Wales.[119] Minimum energy geometry corresponds to C_s point group. There is a total of $2 \times 2! \times 4!/2 = 48$
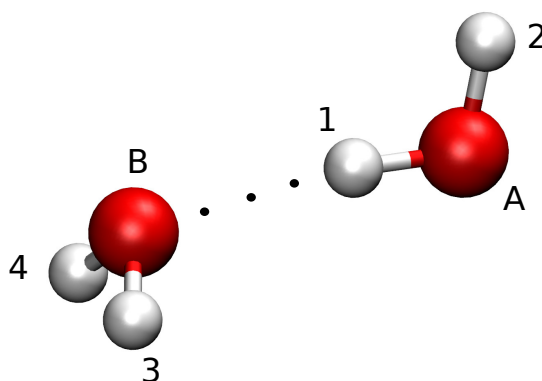
Figure 1. Annotated geometry of global minimum of water dimer.

symmetry-related minima on the potential energy surface, with the first factor of 2 accounting for the inversion symmetry, 2! and 4! accounting for permutations of oxygen and hydrogen atoms, and division by 2 accounting for the C_s symmetry of the minimum geometry. However, as rearrangements that result in the exchange of hydrogen atoms on different oxygen atoms result in covalent bond breaking, corresponding potential energy barriers are large and these motions are not considered feasible. If only rearrangements that do not break covalent bonds are taken into account, the number of connected, symmetry-related minima is reduced to $2 \times 2! \times (2!)^2/2 = 8$, with the first factor of 2 accounting for the inversion symmetry, 2! and $(2!)^2$ accounting for permutations of oxygen atoms and hydrogen atoms bonded with their respective oxygens, and division by 2 accounting for the C_s symmetry of the minimum geometry.

Eight symmetry-related minima of the water dimer are connected by five different pathways,[101,119] listed in Table 1. Acceptor tunneling (AT) path possesses the lowest potential energy barrier and corresponds to the pseudorotation of the acceptor monomer around the axis defined by hydrogen bond. Minima corresponding to this rearrangement are connected by two AT paths, which correspond to the clockwise and counterclockwise rotation of the monomer, and are symmetry-related, making their contributions equal. Geared interchange (GI) and anti-geared interchange (AI) exchange the roles of donor and acceptor monomers, and are characterised by higher potential energy barriers, due to the fact that hydrogen bond is broken along them. Bifurcation tunneling and donor exchange (DE) paths exchange the atom forming hydrogen bond, and possess largest potential energy barriers and, consequently, smallest tunneling matrix elements. Minima corresponding to (12) permutation are connected by 4 DE paths, which is a consequence of the fact that these paths are asymmetric, which means that for one path there exists a symmetry related pair. Furthermore, as this rearrangement involves torsion of the acceptor monomer, which can occur in two directions, there is a total of four equivalent paths with equal contributions.

Table 1. Rearrangement pathways in the water dimer.

Pathway	Permutation
Acceptor tunneling (AT)	(34)
Geared interchange (GI)	(AB)(1324)
Anti-geared interchange (AI)	(AB)(14)(23)
Bifurcation tunneling (BT)	(12)(34)
Donor exchange (DE)	(12)

Tunneling matrix for the water dimer takes the following form

$$
\begin{pmatrix}
0 & h^{\text{BT}} & 4h^{\text{DE}} & 2h^{\text{AT}} & h^{\text{GI}} & h^{\text{GI}} & h^{\text{AI}} & h^{\text{AI}} \\
h^{\text{BT}} & 0 & 2h^{\text{AT}} & 4h^{\text{DE}} & h^{\text{GI}} & h^{\text{GI}} & h^{\text{AI}} & h^{\text{AI}} \\
4h^{\text{DE}} & 2h^{\text{AT}} & 0 & h^{\text{BT}} & h^{\text{GI}} & h^{\text{GI}} & h^{\text{AI}} & h^{\text{AI}} \\
2h^{\text{AT}} & 4h^{\text{DE}} & h^{\text{BT}} & 0 & h^{\text{AI}} & h^{\text{AI}} & h^{\text{GI}} & h^{\text{GI}} \\
h^{\text{GI}} & h^{\text{GI}} & h^{\text{AI}} & h^{\text{AI}} & 0 & h^{\text{BT}} & 4h^{\text{DE}} & 2h^{\text{AT}} \\
h^{\text{GI}} & h^{\text{GI}} & h^{\text{AI}} & h^{\text{AI}} & h^{\text{BT}} & 0 & 2h^{\text{AT}} & 4h^{\text{DE}} \\
h^{\text{AI}} & h^{\text{AI}} & h^{\text{GI}} & h^{\text{GI}} & 4h^{\text{DE}} & 2h^{\text{AT}} & 0 & h^{\text{BT}} \\
h^{\text{AI}} & h^{\text{AI}} & h^{\text{GI}} & h^{\text{GI}} & 2h^{\text{AT}} & 4h^{\text{DE}} & h^{\text{BT}} & 0
\end{pmatrix}.
\tag{2.200}
$$

Eigenvectors of this matrix can be found analytically, using symmetry, with the corresponding eigenvalues

$$
\begin{aligned}
E(B_2^-) &= 2|h^{\text{AT}}| + 2|h^{\text{GI}} - h^{\text{AI}}| - |h^{\text{BT}} - 4h^{\text{DE}}| \\
E(E^-) &= 2|h^{\text{AT}}| + |h^{\text{BT}} - 4h^{\text{DE}}| \\
E(A_2^-) &= 2|h^{\text{AT}}| - 2|h^{\text{GI}} - h^{\text{AI}}| - |h^{\text{BT}} - 4h^{\text{DE}}| \\
E(B_1^+) &= -2|h^{\text{AT}}| + 2|h^{\text{GI}} + h^{\text{AI}}| - |h^{\text{BT}} + 4h^{\text{DE}}| \\
E(E^+) &= -2|h^{\text{AT}}| + |h^{\text{BT}} + 4h^{\text{DE}}| \\
E(B_1^+) &= -2|h^{\text{AT}}| - 2|h^{\text{GI}} + h^{\text{AI}}| - |h^{\text{BT}} + 4h^{\text{DE}}|
\end{aligned}
\tag{2.201}
$$

Taking into account relative magnitudes of tunneling matrix elements, which were found experimentally and theoretically, using RPI, to be $|h^{\text{AT}}| > |h^{\text{GI}}| \approx |h^{\text{AI}}| > |h^{\text{BT}}| > |h^{\text{DE}}|$, it can be seen that AT tunneling path induces splitting into doublet of states, which is further split into two triplets as a consequence of GI and AI paths. Finally, BT and DE perturb the splittings in these triplets. Due to the difference in magnitudes of BT and DE tunneling matrix elements, DE contribution has not been determined experimentally or using quantum-mechanical calculations, but has been estimated with RPI approach.

2.7.3. Water Trimer

Water trimer possesses cyclic structure at the minimum, in which monomers form a three-membered ring of oxygen atoms with one hydrogen atom from each monomer being in the plane of oxygen atoms. Trimer has two types of cyclic minima of different energies, which differ in the position of the remaining hydrogen atoms. Global minimum, shown on Figure 2, corresponds to two hydrogen atoms being on one side of the oxygen plane, and the third one on the opposite, while the local minimum corresponds to all hydrogen atoms on the same side.[120] As is usual in these systems, tunneling motion is considered feasible only if it does not break covalent O-H bonds in the process. Taking this into consideration, there is a total of $3! \times 2 \times 2 \times 2 \times 2 = 96$ symmetry related minima, corresponding to 3! permutations of oxygen atoms, 2! permutations of hydrogen atoms on each oxygen atom, and a factor of 2 accounting for the inversion operation. However, Wales[120,121] has determined that additionally, motion that changes the direction of hydrogen bonds in the ring can also be neglected, a conclusion that was additionally confirmed by Richardson et al.[101] using RPI calculations. Such restriction separates minima into two sets of 48, connected by feasible tunneling motions. As a result, symmetry group for the water trimer is G_{48}, with its character table deduced by Wales.[120] Tunneling motions connecting these minima can be divided into two groups, flip motions and bifurcations.[119–122]
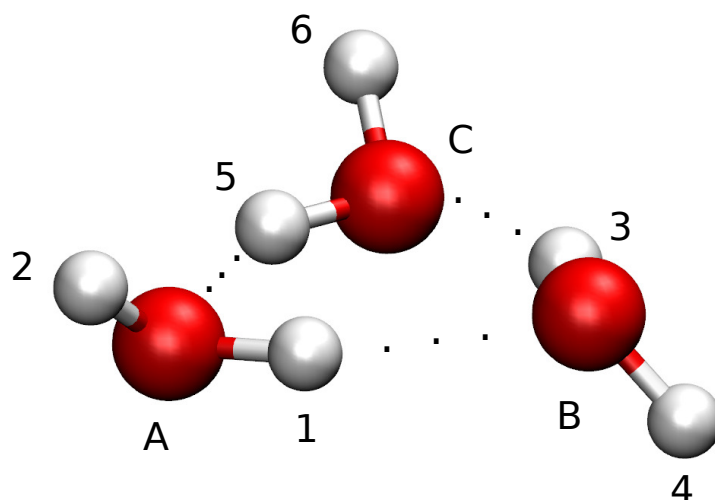
Figure 2. Annotated geometry of global minimum of water trimer.

Flip motions correspond to transfer of one of the hydrogen atoms from one side of the oxygen plane to the other, without breaking of hydrogen bonds. This motion is characterised by low energy barrier, and is virtually over-the-barrier process, corresponding to pseudorotation. As a result, tunneling matrix elements for flips are relatively large and the instanton method results in overestimation by a factor of two. These motions divide minima into cycles

of 6: $uud \rightarrow udd \rightarrow udu \rightarrow ddu \rightarrow duu \rightarrow dud \rightarrow uud$, where u and d denote the side of the oxygen plane on which hydrogen atom is located. There is a total of 8 such cycles, each corresponding to different hydrogen atoms forming hydrogen bonds. Tunneling matrix for flip motion is of the Hückel type, and has the same form as Hückel matrix for benzene

$$
\begin{pmatrix}
0 & h^{F} & 0 & 0 & 0 & h^{F} \\
h^{F} & 0 & h^{F} & 0 & 0 & 0 \\
0 & h^{F} & 0 & h^{F} & 0 & 0 \\
0 & 0 & h^{F} & 0 & h^{F} & 0 \\
0 & 0 & 0 & h^{F} & 0 & h^{F} \\
h^{F} & 0 & 0 & 0 & h^{F} & 0
\end{pmatrix} .
\tag{2.202}
$$

Consequently, flip motion splits the degenerate minima into quartet of states, with corresponding energies $\pm 2h^{F}$, $\pm h^{F}$. Symmetry group for flip states is C_{3h}, which is a direct product of C_3 group, which includes cyclic permutations of monomers, and C_s group, which includes exchange of two monomers.

Bifurcation motions involve permutation of one atom that forms hydrogen bond with the other hydrogen belonging to the same oxygen atom. However, because flip motions are virtually over-the-barrier, the most feasible bifurcation rearrangements may include simultaneous flip motions. Analysis by Walsh and Wales revealed that there are six possible bifurcation motions, which they separated into groups corresponding to bifurcations with 0 or 1 flip (A) and bifurcations with 2 flip motions (B). These paths are listed in Table 2.

Table 2. Bifurcation path for water trimer. Label min corresponds to minority monomer, while don and acc correspond to hydrogen bond donor and acceptor with respect to the minority monomer. For paths that are asymmetric reverse paths are given, separated with backslash.

Label	Pathway
A1	min + acc flip/don + min flip
A2	min + don flip/acc + min flip
A3	don/acc
B1	min + double flip
B2	don + double flip/don + double flip
B3	acc + double flip

RPI calculations by Richardson et al.[101] revealed that B2 path does not correspond to a minimum of action, but to its saddle point. As a result, B2 path does not contribute with a tunneling matrix elements, but decomposes into combination of a flip and an A1 path. As bifurcations involve breaking of hydrogen bonds, the corresponding potential energy barriers are much larger than for the flip motions, resulting in comparatively smaller tunneling matrix elements. As a result, bifurcations induce a fine structure by splitting each of the states formed

by flip motions.

§ 3. THEORETICAL METHODS

In this section, generalizations and improvements of the JFI theory made as a part of this thesis are presented. First generalization is the derivation of the theory for the ground state tunneling matrix elements in systems with asymmetric potential energy profile along the MAP. Next, improvement of the JFI theory for the tunneling matrix elements of excited vibrational states is presented. Finally, generalization of the JFI theory for treatment of non-symmetry related minima and different vibrational states is given, as well as a method for inclusion of the effects of molecular rotation. Furthermore, details of the numerical implementation of the developed methods are presented, along with the numerical parameters used.

3.1. Jacobi Field Instanton Method for Asymmetric Paths

JFI theory is derived by Mil'nikov and Nakamura[14] under assumption that the MAP is symmetric with respect to the symmetry operation that relates the minima. However, this does not have to be the case. A counterexample is donor exchange path in the water dimer,[101] which is evidently asymmetric in the potential energy profile along the path. Thus, a generalization of the JFI theory which can handle such cases has been developed as a part of this research thesis.[103]

Derivation of the generalized JFI parallels the one of Mil'nikov and Nakamura up until the application of Gelfand-Yaglom formula. Due to the lack of symmetry, there is no obvious choice for the placement of the origin of imaginary time. Thus, an arbitrary point is chosen so that the trajectory starts at some time $-T_1$ and ends at T_2, with $T_1 + T_2 = \beta$. The equations for the longitudinal and transversal Jacobi fields are analogous to the ones for the symmetric case

$$
-\frac{\partial^2}{\partial \tau^2} J_\parallel(\tau) = V''(\tau) J_\parallel(\tau)
$$
$$
-\frac{\partial^2}{\partial \tau^2} \mathbf{J}_\perp(\tau) = \Omega^2(\tau) \mathbf{J}_\perp(\tau), \tag{3.1}
$$

with initial conditions

$$
J_\parallel(-T_1) = 0 \qquad \dot{J}_\parallel(-T_1) = 1
$$
$$
\mathbf{J}_\perp(-T_1) = \mathbf{0} \qquad \dot{\mathbf{J}}_\perp(-T_1) = \mathbf{I}. \tag{3.2}
$$

Longitudinal Jacobi field is constructed using two linearly independent solutions $p_0(\tau)$ and $\eta(\tau)$, as in the symmetric case. However, due to lack of symmetry, their asymptotic behaviours

are different

$$\lim_{\tau \to -T_1} p_0(\tau) = P\mathrm{e}^{\omega_1 \tau} \qquad\qquad \lim_{\tau \to T_2} p_0(\tau) = Q\mathrm{e}^{-\omega_2 \tau}$$

$$\lim_{\tau \to -T_1} \eta(\tau) = -\frac{1}{2\omega_1 P}\mathrm{e}^{-\omega_1 \tau} \qquad\qquad \lim_{\tau \to T_2} \eta(\tau) = \frac{1}{2\omega_2 Q}\mathrm{e}^{\omega_2 \tau}. \tag{3.3}$$

Constants P and Q can be computed either by formally solving the equations of motion, as has been done in the symmetric case, or by observing the following relation

$$\frac{\mathrm{d}}{\mathrm{d}\tau}\ln p_0(\tau) = \frac{1}{p_0}\frac{\mathrm{d}p_0}{\mathrm{d}\tau} = \frac{\mathrm{d}p_0}{\mathrm{d}S}$$

$$\ln\frac{p_0(\tau_2)}{p_0(\tau_1)} = \int_{\tau_1}^{\tau_2}\frac{\mathrm{d}p_0}{\mathrm{d}S}\mathrm{d}\tau$$

$$p_0(\tau_2) = p_0(\tau_1)\mathrm{e}^{\int_{\tau_1}^{\tau_2}\frac{\mathrm{d}p_0}{\mathrm{d}S}\mathrm{d}\tau}. \tag{3.4}$$

Using this expression, P and Q can be expressed using the potential at $\tau = 0$ by setting $\tau_1 = 0$ and $\tau_2 = -T_1, T_2$

$$P = p_0(0)\mathrm{e}^{\int_{-T_1}^{0}\left(\omega_1 - \frac{\mathrm{d}p_0}{\mathrm{d}S}\right)\mathrm{d}\tau} \tag{3.5}$$

$$Q = p_0(0)\mathrm{e}^{\int_{0}^{T_2}\left(\omega_2 + \frac{\mathrm{d}p_0}{\mathrm{d}S}\right)\mathrm{d}\tau}. \tag{3.6}$$

Longitudinal Jacobi field that satisfies the correct initial conditions can be written as a linear combination

$$J_{\parallel}(\tau) = -\eta(-T_1)p_0(\tau) + p_0(-T_1)\eta(\tau) \tag{3.7}$$

$$J_{\parallel}(T_2) = \frac{2\omega_2 Q^2\mathrm{e}^{-2\omega_2 T_2} + 2\omega_1 P^2\mathrm{e}^{-2\omega_1 T_1}}{4\omega_1\omega_2 PQ\mathrm{e}^{-\omega_1 T_1 - \omega_2 T_2}}. \tag{3.8}$$

Lowest eigenvalue λ is constructed analogously to the symmetric case, but using different asymptotic behaviours

$$\lambda = \frac{p_0(T_2) + 2\omega_1 P^2\mathrm{e}^{-2\omega_1 T_1}\eta(T_2)}{\eta(T_2)\int_{-T_1}^{T_2}p_0^2(\tau)\mathrm{d}\tau}$$

$$= \frac{1}{S_0}\left(2\omega_2 Q^2\mathrm{e}^{-2\omega_2 T_2} + 2\omega_1 P^2\mathrm{e}^{-2\omega_1 T_1}\right), \tag{3.9}$$

which leads to the following ratio

$$\frac{\lambda}{J_{\parallel}} = \frac{4\omega_1\omega_2 PQ}{S_0}\mathrm{e}^{-\omega_1 T_1 - \omega_2 T_2}. \tag{3.10}$$

Transversal Jacobi field determinant is constructed from two solutions with different boundary conditions

$$\boldsymbol{\eta}(-T_1) = \mathbf{I} \qquad\qquad \tilde{\boldsymbol{\eta}}(T_2) = \mathbf{I}$$
$$\dot{\boldsymbol{\eta}}(-T_1) = \boldsymbol{\Omega}_1 \qquad\qquad \dot{\tilde{\boldsymbol{\eta}}}(T_2) = -\boldsymbol{\Omega}_2. \qquad (3.11)$$

As in the symmetric case, transversal Jacobi field determinant can be shown to satisfy

$$\det \mathbf{J}_\perp(T_2) = \frac{\det \boldsymbol{\eta}(T_2)}{2^{N_{\text{dof}}-1} \det \boldsymbol{\Omega}_1}. \qquad (3.12)$$

Determinant $\det \boldsymbol{\eta}(T_2)$ can be evaluated by reducing the Jacobi field equation to the first order differential equation, which is achieved by constructing a 2×2 block matrix of the following form

$$\mathbf{Y}(\tau) = \begin{pmatrix} \boldsymbol{\eta}(\tau) & \tilde{\boldsymbol{\eta}}(\tau) \\ \dot{\boldsymbol{\eta}}(\tau) & \dot{\tilde{\boldsymbol{\eta}}}(\tau) \end{pmatrix}. \qquad (3.13)$$

The matrix $\mathbf{Y}$ satisfies the following first order propagation equation

$$\frac{\mathrm{d}}{\mathrm{d}\tau} \begin{pmatrix} \boldsymbol{\eta}(\tau) & \tilde{\boldsymbol{\eta}}(\tau) \\ \dot{\boldsymbol{\eta}}(\tau) & \dot{\tilde{\boldsymbol{\eta}}}(\tau) \end{pmatrix} = \begin{pmatrix} \mathbf{0} & \mathbf{I} \\ \boldsymbol{\Omega}^2(\tau) & \mathbf{0} \end{pmatrix} \begin{pmatrix} \boldsymbol{\eta}(\tau) & \tilde{\boldsymbol{\eta}}(\tau) \\ \dot{\boldsymbol{\eta}}(\tau) & \dot{\tilde{\boldsymbol{\eta}}}(\tau) \end{pmatrix}$$
$$\frac{\mathrm{d}}{\mathrm{d}\tau} \mathbf{Y}(\tau) = \mathbf{B}\mathbf{Y}(\tau). \qquad (3.14)$$

Next, the determinant of matrix $\mathbf{Y}$ is shown to be constant, using Jacobi's formula

$$\frac{\mathrm{d}}{\mathrm{d}\tau} \det \mathbf{Y} = \det \mathbf{Y} \operatorname{Tr} \dot{\mathbf{Y}} \mathbf{Y}^{-1} = \det \mathbf{Y} \operatorname{Tr} \mathbf{B} = 0. \qquad (3.15)$$

Thus, the desired determinant $\det \boldsymbol{\eta}(T_2)$ can be obtained by evaluating $\det \mathbf{Y}$ at two points in time, $\tau = 0, T_2$. Using a well-known identity for the determinant of a 2×2 block matrix, and the fact that in the region $\tau \to T_2$ exponential terms dominate in $\boldsymbol{\eta}$, and $\dot{\boldsymbol{\eta}}(\tau) \approx \boldsymbol{\eta}(\tau)\boldsymbol{\Omega}_2$, one obtains

$$\det \mathbf{Y}(T_2) = (-2)^{N_{\text{dof}}-1} \det \boldsymbol{\Omega}_2 \det \boldsymbol{\eta}(T_2)$$
$$\det \mathbf{Y}(0) = \det \boldsymbol{\eta}(0) \det \left(\dot{\tilde{\boldsymbol{\eta}}}(0)\tilde{\boldsymbol{\eta}}^{-1} - \dot{\boldsymbol{\eta}}(0)\boldsymbol{\eta}^{-1} \right) \det \tilde{\boldsymbol{\eta}}(0)$$
$$= \det \boldsymbol{\eta}(0) \det \left(\tilde{\boldsymbol{\Xi}}(0) - \boldsymbol{\Xi}(0) \right) \det \tilde{\boldsymbol{\eta}}(0)$$
$$\det \boldsymbol{\eta}(T_2) = \det \left(\frac{\boldsymbol{\Xi}(0) - \tilde{\boldsymbol{\Xi}}(0)}{2} \right) \frac{\det \boldsymbol{\eta}(0) \det \tilde{\boldsymbol{\eta}}(0)}{\det \boldsymbol{\Omega}_2}, \qquad (3.16)$$

where $\boldsymbol{\Xi}$ and $\tilde{\boldsymbol{\Xi}}$ are log-derivatives of $\boldsymbol{\eta}$ and $\tilde{\boldsymbol{\eta}}$. Determinants $\det \boldsymbol{\eta}(0) \det$ and $\tilde{\boldsymbol{\eta}}(0)$ can be

expressed in terms of these log-derivatives using the same procedure as in the symmetric case

$$\det \boldsymbol{\eta}(0) = e^{-\frac{1}{2} \int_{-T_1}^{0} \mathrm{Tr}\,\boldsymbol{\Xi}\,\mathrm{d}\tau}$$

$$\det \tilde{\boldsymbol{\eta}}(0) = e^{\frac{1}{2} \int_{0}^{T_2} \mathrm{Tr}\,\tilde{\boldsymbol{\Xi}}\,\mathrm{d}\tau}. \tag{3.17}$$

Again, the usage of curvilinear coordinates can be avoided by introducing matrices $\mathbf{A}$ and $\tilde{\mathbf{A}}$ that satisfy

$$\frac{\mathrm{d}}{\mathrm{d}\tau} \mathbf{A} = \mathbf{V_{xx}} - \mathbf{A}^2$$

$$\frac{\mathrm{d}}{\mathrm{d}\tau} \tilde{\mathbf{A}} = \mathbf{V_{xx}} - \tilde{\mathbf{A}}^2$$

$$\mathbf{A}(-T_1) = \mathbf{V_{xx}}^{\frac{1}{2}}(T_1)$$

$$\tilde{\mathbf{A}}(T_2) = -\mathbf{V_{xx}}^{\frac{1}{2}}(T_2). \tag{3.18}$$

Inserting all the obtained expressions into the formula for tunneling matrix element and taking the limits $T_1 \to +\infty$ and $T_2 \to +\infty$ results in the equation

$$h = \sqrt{\frac{\det \mathbf{A}_0}{\pi \det \mathbf{P} \left(\frac{\mathbf{A}(0) - \tilde{\mathbf{A}}(0)}{2} \right) \mathbf{P}}} \, p(0) e^{-S_0 - \frac{1}{2} \int_{-\infty}^{0} (\mathrm{Tr}\,\mathbf{A}_0 - \mathrm{Tr}\,\mathbf{A})\mathrm{d}\tau - \frac{1}{2} \int_{0}^{+\infty} (\mathrm{Tr}\,\mathbf{A}_0 + \mathrm{Tr}\,\tilde{\mathbf{A}})\mathrm{d}\tau}, \tag{3.19}$$

where $\mathbf{P}$ is a projector operator that has been defined in the symmetric case. As in that case, all quantities that appear in the expression can be propagated with respect to arc length distance, avoiding the use of time variable and parameter β.

The expression for tunneling matrix element can be obtained via the WKB approach as well. As the minima are assumed to be symmetry-related, even though the path does not possess the symmetry, Herring formula holds for the tunneling matrix element. Localized wavefunctions can be obtained using the method of characteristics, as in the symmetric case,

$$\phi^{(\mathrm{L})}(S, \xi_\alpha) = e^{-\int_0^S p_0 \mathrm{d}S' - \frac{1}{2} \int_0^S \mathrm{Tr}\left(\mathbf{A}^{(\mathrm{L})} - \mathbf{A}_0^{(\mathrm{L})}\right)/p_0 \mathrm{d}S' - \frac{1}{2} A_{ij}^{(\mathrm{L})} \tau_{i\alpha} \tau_{j\alpha} \xi_\alpha \xi_\beta}$$

$$\phi^{(\mathrm{R})}(\tilde{S}, \xi_\alpha) = e^{-\int_0^{\tilde{S}} p_0 \mathrm{d}\tilde{S}' - \frac{1}{2} \int_0^{\tilde{S}} \mathrm{Tr}\left(\mathbf{A}^{(\mathrm{R})} - \mathbf{A}_0^{(\mathrm{R})}\right)/p_0 \mathrm{d}\tilde{S}' - \frac{1}{2} A_{ij}^{(\mathrm{R})} \tau_{i\alpha} \tau_{j\alpha} \xi_\alpha \xi_\beta}, \tag{3.20}$$

where $\tilde{S}$ denotes arc length for a curve which begins at the right minimum, and S denotes arc length for a curve which begins at the left. Inserting these wavefunctions into Herring formula and keeping only p_0 term in the preexponential part of the wavefunction derivative, it can be seen that, as in the symmetric case, the leading term in the exponent is the sum $\int_0^S p_0 \mathrm{d}S' + \int_0^{\tilde{S}} p_0 \mathrm{d}\tilde{S}'$. Thus, the best approximation to the integrand is obtained when connection point is chosen so that this sum is minimal, which means that the candidates are all points on

the MAP that connects the minima. If the path is assumed to be the MAP, arc length distances are connected as $\tilde{S} = S_{\text{tot}} - S$. Furthermore, as MAP is smooth for smooth potential energy surfaces, vectors τ_α can be chosen to coincide at the connection point. Inserting the wavefunctions into the Herring formula, using the aforementioned facts and noting that $\det \mathbf{A}_0^{(\text{L})} = \det \mathbf{A}_0^{(\text{R})}$ results in

$$
\begin{aligned}
h &= \sqrt{\frac{\det \mathbf{A}_0^{(\text{L})}}{\pi^{N_{\text{dof}}}}} \, p_0 e^{-\int_0^{S_{\text{tot}}} p_0 dS' - \frac{1}{2}\int_0^{S_{\text{cp}}} \text{Tr}\left(\mathbf{A}^{(\text{L})} - \mathbf{A}_0^{(\text{L})}\right)/p_0 dS' - \frac{1}{2}\int_0^{\tilde{S}_{\text{cp}}} \text{Tr}\left(\mathbf{A}^{(\text{R})} - \mathbf{A}_0^{(\text{R})}\right)/p_0 d\tilde{S}'} \\
&\quad \int e^{\frac{1}{2}\left(A_{ij}^{(\text{L})} + A_{ij}^{(\text{R})}\right)\tau_{i\alpha}\tau_{j\alpha}\xi_\alpha\xi_\beta} d\boldsymbol{\xi} \\
&= \sqrt{\frac{\det \mathbf{A}_0^{(\text{L})}}{\pi \det' \mathbf{P}\left(\frac{\mathbf{A}^{(\text{L})} + \mathbf{A}^{(\text{R})}}{2}\right)\mathbf{P}}} \, p_0 e^{-\int_0^{S_{\text{tot}}} p_0 dS' - \frac{1}{2}\int_0^{S_{\text{cp}}} \text{Tr}\left(\mathbf{A}^{(\text{L})} - \mathbf{A}_0^{(\text{L})}\right)/p_0 dS' - \frac{1}{2}\int_0^{\tilde{S}_{\text{cp}}} \text{Tr}\left(\mathbf{A}^{(\text{R})} - \mathbf{A}_0^{(\text{R})}\right)/p_0 d\tilde{S}'},
\end{aligned}
$$

$$(3.21)$$

which is the same as the expression obtained using JFI theory, if one defines new time variable $\tilde{\tau} = T_2 - \tau$ and notes that $\tilde{\mathbf{A}}(\tilde{\tau}) = -\mathbf{A}(T_2 - \tau)$. Due to the equivalence of the JFI and WKB approach, from this point on, JFI will be used as an umbrella term for both methods.

The expression for tunneling matrix element obtained using JFI is invariant with respect to the choice of the connection point. This can be proven by differentiating the formula (3.21) with respect to S_{cp}

$$
\frac{dh}{dS_{\text{cp}}} = \frac{h}{2p_0}\left(2\frac{dp_0}{dS_{\text{cp}}} - \frac{p_0}{\det' \mathbf{P}\bar{\mathbf{A}}\mathbf{P}}\frac{d}{dS_{\text{cp}}}\det'\bar{\mathbf{A}} - \text{Tr}\left(\mathbf{A}^{(\text{L})} - \mathbf{A}_0^{(\text{L})}\right) + \text{Tr}\left(\mathbf{A}^{(\text{R})} - \mathbf{A}_0^{(\text{R})}\right)\right),
$$

$$(3.22)$$

where $\bar{\mathbf{A}} = (\mathbf{A}^{(\text{L})} + \mathbf{A}^{(\text{R})})/2$. Tangent vector is an eigenvector of matrix $\bar{\mathbf{A}}$ at all points on the trajectory, which is seen by taking the derivative of Hamilton-Jacobi equation

$$
\frac{\partial^2 W_0}{\partial x_j \partial x_i}\frac{\partial W_0}{\partial x_i} + \frac{\partial W_0}{\partial x_i}\frac{\partial^2 W_0}{\partial x_j \partial x_i} = 2\frac{\partial V}{\partial x_j}
$$

$$
2A_{ji}^{(\text{L})}p_{0i} = 2\frac{\partial V}{\partial x_j}
$$

$$
2A_{ji}^{(\text{R})}p_{0i} = -2\frac{\partial V}{\partial x_j}
$$

$$
\left(\mathbf{A}^{(\text{L})} + \mathbf{A}^{(\text{R})}\right)\mathbf{p}_0 = 0,
$$

$$(3.23)$$

where the different sign for the (R) equation follows from the fact that propagation from minimum (R) is done in the opposite direction than propagation from the minimum (L). Thus, projector operator $\mathbf{P}$ does not have to be included in formula (3.21). In numerical calculations, however, the inclusion of projector operator removes the numerical noise that accumulates

in the course of propagation of matrices $\mathbf{A}$. Furthermore, if minima are symmetry related, their frequencies are the same and $\mathrm{Tr}\mathbf{A}_0^{(\mathrm{L})} = \mathrm{Tr}\mathbf{A}_0^{(\mathrm{R})}$. Derivative of the determinant can be determined using the Jacobi's formula, which results in

$$\frac{\mathrm{d}h}{\mathrm{d}S_{\mathrm{cp}}} = \frac{h}{2p_0}\left(2\frac{\mathrm{d}p_0}{\mathrm{d}S_{\mathrm{cp}}} - \mathrm{Tr}\left(\bar{\mathbf{A}}^{-1}p_0\frac{\mathrm{d}}{\mathrm{d}S_{\mathrm{cp}}}\bar{\mathbf{A}}\right) + \mathrm{Tr}\left(\mathbf{A}^{(\mathrm{R})} - \mathbf{A}^{(\mathrm{L})}\right)\right). \tag{3.24}$$

Next, the derivative of matrix $\bar{\mathbf{A}}$ can be expanded as

$$\begin{aligned}
p_0\frac{\mathrm{d}}{\mathrm{d}S_{\mathrm{cp}}}\bar{\mathbf{A}} &= \frac{1}{2}\left(p_0\frac{\mathrm{d}}{\mathrm{d}S_{\mathrm{cp}}}\mathbf{A}^{(\mathrm{L})} + p_0\frac{\mathrm{d}}{\mathrm{d}S_{\mathrm{cp}}}\mathbf{A}^{(\mathrm{R})}\right) \\
&= \frac{1}{2}\left(\mathbf{V}_{\mathbf{xx}} - \left(\mathbf{A}^{(\mathrm{L})}\right)^2 - \mathbf{V}_{\mathbf{xx}} + \left(\mathbf{A}^{(\mathrm{R})}\right)^2\right) \\
&= \frac{1}{2}\bar{\mathbf{A}}\left(\mathbf{A}^{(\mathrm{R})} - \mathbf{A}^{(\mathrm{L})}\right) + \frac{1}{2}\left(\mathbf{A}^{(\mathrm{R})} - \mathbf{A}^{(\mathrm{L})}\right)\bar{\mathbf{A}}.
\end{aligned} \tag{3.25}$$

Furthermore, since the tangent vector is the eigenvector corresponding to the eigenvalue zero for both $\bar{\mathbf{A}}$ and, by definition, pseudoinverse $\bar{\mathbf{A}}^{-1}$, the following relations hold

$$\begin{aligned}
\bar{\mathbf{A}}\mathbf{P} &= \mathbf{P}\bar{\mathbf{A}} = \bar{\mathbf{A}} \\
\bar{\mathbf{A}}^{-1}\mathbf{P} &= \mathbf{P}\bar{\mathbf{A}}^{-1} = \bar{\mathbf{A}}^{-1}.
\end{aligned} \tag{3.26}$$

Thus, the trace in equation (3.24) can be rewritten, using its cyclic property, as

$$\begin{aligned}
\mathrm{Tr}\left(\bar{\mathbf{A}}^{-1}p_0\frac{\mathrm{d}}{\mathrm{d}S_{\mathrm{cp}}}\bar{\mathbf{A}}\right) &= \mathrm{Tr}\left(\mathbf{P}\bar{\mathbf{A}}^{-1}\mathbf{P}p_0\frac{\mathrm{d}}{\mathrm{d}S_{\mathrm{cp}}}\bar{\mathbf{A}}\right) \\
&= \mathrm{Tr}\left(\bar{\mathbf{A}}^{-1}\mathbf{P}p_0\frac{\mathrm{d}}{\mathrm{d}S_{\mathrm{cp}}}(\bar{\mathbf{A}})\mathbf{P}\right) \\
&= \mathrm{Tr}\mathbf{P}\left(\mathbf{A}^{(\mathrm{R})} - \mathbf{A}^{(\mathrm{L})}\right)\mathbf{P} \\
&= \mathrm{Tr}\left(\mathbf{A}_\perp^{(\mathrm{R})} - \mathbf{A}_\perp^{(\mathrm{L})}\right)
\end{aligned} \tag{3.27}$$

Inserting this expression into (3.24) and using the fact that $\mathrm{Tr}\mathbf{A}^{(\mathrm{L})} = p_0' + \mathrm{Tr}\mathbf{A}_\perp^{(\mathrm{L})}$ and $\mathrm{Tr}\mathbf{A}^{(\mathrm{R})} = -p_0' + \mathrm{Tr}\mathbf{A}_\perp^{(\mathrm{L})}$, which can be seen from equation (2.157) results in

$$\frac{\mathrm{d}h}{\mathrm{d}S_{\mathrm{cp}}} = 0, \tag{3.28}$$

proving that the tunneling splitting element obtained using JFI is invariant with respect to the position of the chosen connection point.

3.2. JFI Theory for Vibrationally Excited States

Generalization of the JFI method for singly excited vibrational states, which correctly describes the curvature effects, has been developed.[123] Instead of separating the longitudinal and transversal excitations, the new approach treats all normal modes equivalently. As in the derivation by Mil'nikov and Nakamura,[15] the starting point is the equation for the correction function w which accounts for the energy of excitation

$$\frac{\partial W_0}{\partial x_i} \frac{\partial w}{\partial x_i} + \omega = 0. \tag{3.29}$$

The function w is chosen to have the form

$$w = -\ln(F(S) + U_\alpha(S)\xi_\alpha). \tag{3.30}$$

Such form can correctly describe the position of the nodal plane of the singly-excited wavefunction, with the vector $\mathbf{U}$ describing direction of the normal to the nodal plane, and scalar F containing the information on the distance to the nodal plane. Inserting this form into the equation for w yields, up to ξ^1,

$$\left(\frac{\partial W_0}{\partial S} \frac{\partial S}{\partial x_i} + \frac{\partial W_0}{\partial \xi_\alpha} \frac{\partial \xi_\alpha}{\partial x_i} \right) \left(\frac{\partial w}{\partial S} \frac{\partial S}{\partial x_i} + \frac{\partial w}{\partial \xi_\alpha} \frac{\partial \xi_\alpha}{\partial x_i} \right) + \omega = 0$$

$$\left(p_0 J_{Ni}^{-1} + \Xi_{\alpha\beta} \xi_\beta J_{\alpha i}^{-1} \right) \frac{1}{F + U_\alpha \xi_\alpha} \left(-F' J_{Ni}^{-1} - U_\alpha' \xi_\alpha J_{Ni}^{-1} - U_\alpha J_{\alpha i}^{-1} \right) + \omega = 0$$

$$p_0 F' + p_0 U_\alpha' + \Xi_{\alpha\beta} U_\beta \xi_\alpha - \omega F - \omega U_\alpha \xi_\alpha - p_0 F' C_\alpha \xi_\alpha = 0. \tag{3.31}$$

Equating the terms of the same order with respect to ξ_α results in the propagation equations

$$p_0 F' = \omega F$$

$$p_0 U_\alpha' = \omega U_\alpha - \Xi_{\alpha\beta} U_\beta + p_0 C_\alpha F'. \tag{3.32}$$

Initial conditions can be determined by matching the wavefunction in the vicinity of the minimum to the harmonic oscillator wavefunction. For this purpose, it is convenient to choose a point on the path at a small distance $S = \varepsilon$ from the minimum. The prefactor of the harmonic oscillator wavefunction at this point will be $\mathbf{U}_0^\top (\mathbf{x}^{(0)}(\varepsilon) - \mathbf{x}_{\min})$, with $\mathbf{U}_0$ being the excited normal mode at the minimum. If this value is to match the WKB wavefunction, one must choose

$$F(\varepsilon) = \mathbf{U}_0^\top (\mathbf{x}^{(0)}(\varepsilon) - \mathbf{x}_{\min}). \tag{3.33}$$

The orthogonal projection of the normal mode is simply

$$U_\alpha = U_{0,i}\tau_{i\alpha}. \tag{3.34}$$

The use of curvilinear coordinates can again be avoided. Taylor expansion up to first order is made around the point S_0 on the path, which yields $w = -\ln(F(S_0) + F'(S_0)dS + U_\alpha d\xi_\alpha)$. From this expansion, it is evident that both F and U_α can be extracted from the gradient $\tilde{\mathbf{U}} = \nabla \exp(-w)$ as

$$F(S) = \int_0^S \tilde{U}_i(S')\tau_{iN}(S')dS'$$
$$U_\alpha(S) = \tilde{U}_i(S)\tau_{i\alpha}. \tag{3.35}$$

Finally, propagation equation for $\tilde{\mathbf{U}}$ can be obtained by taking a derivative of the propagation equation for w and recognizing the directional derivative that appears

$$\frac{\partial^2 W_0}{\partial x_j \partial x_i}\frac{\partial w}{\partial x_i} + \frac{\partial W_0}{\partial x_i}\frac{\partial^2 w}{\partial x_i \partial x_j} = 0 \quad / - e^{-w}$$
$$A_{ji}\tilde{U}_i - p_0\frac{\partial^2 w}{\partial S \partial x_j}e^{-w} = 0$$
$$A_{ji}\tilde{U}_i - p_0\frac{\partial}{\partial S}\left(\frac{\partial w}{\partial x_j}e^{-w}\right) + p_0\frac{\partial w}{\partial S}\frac{\partial w}{\partial x_j}e^{-w} = 0. \tag{3.36}$$

From (3.29), directional derivative can be identified, resulting in $p_0\frac{\partial w}{\partial S} = -\omega$. Inserting this into (3.36) and noting that, from definition, $\tilde{U}_j = -\frac{\partial w}{\partial x_j}\exp(-w)$ results in

$$A_{ji}\tilde{U}_i + p_0\tilde{U}_j' - \omega\tilde{U}_j = 0$$
$$p_0\tilde{\mathbf{U}}' = \omega\tilde{\mathbf{U}} - \mathbf{A}\tilde{\mathbf{U}}, \tag{3.37}$$

which is the same equation that Mil'nikov and Nakamura obtained in their consideration. However, they argue that, if initial $\tilde{\mathbf{U}}$ is a transversal normal mode (i.e. if its projection onto the tangent direction is zero), it cannot pick up a tangential component during the propagation, as such component must be given by

$$\tilde{\mathbf{U}}^\top\mathbf{p}_0 = (\tilde{\mathbf{U}}^\top\mathbf{p}_0)(S=0)e^{\int_0^S \frac{\theta}{p_0}dS'} \tag{3.38}$$

and for transversal modes $(\tilde{\mathbf{U}}^\top\mathbf{p}_0)(S=0) = 0$. However, the integral in the exponent has a singularity at the lower limit, as potential in the vicinity of the minimum behaves as $p_0 \approx \omega_\parallel S$. Furthermore, near the minimum, the frequency θ equals the frequency of the excited mode, making it constant and non-zero. Thus, the integral in the exponent is of the form $\int_0^S 1/S'dS'$,

which diverges for any $S > 0$. As a result, the expression for the tangential component is undetermined, and the argument does not hold. The existence of the non-zero tangential component is essential for the accurate description of the excited state, as this component gives rise to F, which is necessary to describe the position of the nodal plane if it moves away from the MAP.

Localized wavefunctions can thus be propagated from both minima, as in the case of the ground-state splitting calculation. Using the correct form of the localized wavefunctions results in the following expression for the tunneling matrix element

$$h_v = 2\omega \left(F^{(\mathrm{L})} F^{(\mathrm{R})} + \frac{1}{2} \mathbf{U}^{(\mathrm{L})\top} (\mathbf{P}\bar{\mathbf{A}}\mathbf{P})^{-1} \mathbf{U}^{(\mathrm{R})} \right) h_0, \tag{3.39}$$

with $\bar{\mathbf{A}} = (\mathbf{A}^{(\mathrm{L})} + \mathbf{A}^{(\mathrm{R})})/2$. Projector $\mathbf{P}$ projects out the tangential component and the inverse is assumed to be defined as a matrix with the same eigenvectors, all non-zero eigenvalues reciprocal and zero eigenvalues remaining zero.

Similarly to the ground state case, the dependence of the excited state tunneling matrix elements on the position of the connection point can be determined by taking the derivative with respect to S_{cp}

$$\begin{aligned} \frac{\mathrm{d}h_v}{\mathrm{d}S_{\mathrm{cp}}} =& \frac{2\omega h_0}{p_0} \left(p_0 \frac{\mathrm{d}F^{(\mathrm{L})}}{\mathrm{d}S_{\mathrm{cp}}} F^{(\mathrm{R})} + F^{(\mathrm{L})} p_0 \frac{\mathrm{d}F^{(\mathrm{R})}}{\mathrm{d}S_{\mathrm{cp}}} + \right. \\ & \frac{1}{2} \left(p_0 \frac{\mathrm{d}}{\mathrm{d}S_{\mathrm{cp}}} \mathbf{U}^{(\mathrm{L})\top} \right) \bar{\mathbf{A}}^{-1} \mathbf{U}^{(\mathrm{R})} + \frac{1}{2} \mathbf{U}^{(\mathrm{L})\top} \left(p_0 \frac{\mathrm{d}}{\mathrm{d}S_{\mathrm{cp}}} \bar{\mathbf{A}}^{-1} \right) \mathbf{U}^{(\mathrm{R})} + \\ & \left. \frac{1}{2} \mathbf{U}^{(\mathrm{L})\top} \bar{\mathbf{A}}^{-1} \left(p_0 \frac{\mathrm{d}}{\mathrm{d}S_{\mathrm{cp}}} \mathbf{U}^{(\mathrm{R})} \right) \right). \end{aligned} \tag{3.40}$$

Propagation equations (3.18) and (3.32) can be used to transform this expression into

$$\begin{aligned} \frac{\mathrm{d}h_v}{\mathrm{d}S_{\mathrm{cp}}} =& \frac{2\omega h_0}{p_0} \left(-\frac{1}{2} \mathbf{U}^{(\mathrm{L})\top} \mathbf{A}^{(\mathrm{L})} \bar{\mathbf{A}}^{-1} \mathbf{U}^{(\mathrm{R})} + \frac{1}{2} \mathbf{U}^{(\mathrm{L})\top} \bar{\mathbf{A}}^{-1} \mathbf{A}^{(\mathrm{R})} \mathbf{U}^{(\mathrm{R})} + \right. \\ & \left. \frac{1}{2} \mathbf{U}^{(\mathrm{L})\top} \left(p_0 \frac{\mathrm{d}}{\mathrm{d}S_{\mathrm{cp}}} \bar{\mathbf{A}}^{-1} \right) \mathbf{U}^{(\mathrm{R})} \right). \end{aligned} \tag{3.41}$$

Furthermore, the following relation holds

$$p_0 \frac{\mathrm{d}}{\mathrm{d}S_{\mathrm{cp}}} \bar{\mathbf{A}}^{-1} = \mathbf{P}\mathbf{A}^{(\mathrm{L})} \bar{\mathbf{A}}^{-1} - \bar{\mathbf{A}}^{-1} \mathbf{A}^{(\mathrm{R})} \mathbf{P}, \tag{3.42}$$

which can be proven from the fact that $\bar{\mathbf{A}}\bar{\mathbf{A}}^{-1} = \mathbf{P}$ and $\mathbf{A}^{(\mathrm{L}/\mathrm{R})} p_0 = \pm p_0 \mathbf{p}'_0$. Inserting (3.42)

into (3.41) results in

$$\frac{\mathrm{d}h_\nu}{\mathrm{d}S_{\mathrm{cp}}} = \frac{2\omega h_0}{p_0} \left(-\frac{1}{2} \left(\mathbf{U}^{(\mathrm{L})} - \mathbf{P}\mathbf{U}^{(\mathrm{L})} \right)^\top \mathbf{A}^{(\mathrm{L})} \bar{\mathbf{A}}^{-1} \mathbf{U}^{(\mathrm{R})} + \frac{1}{2} \mathbf{U}^{(\mathrm{L})\top} \bar{\mathbf{A}}^{-1} \mathbf{A}^{(\mathrm{R})} \left(\mathbf{U}^{(\mathrm{R})} - \mathbf{P}\mathbf{U}^{(\mathrm{R})} \right) \right).$$
(3.43)

It can be seen that the excited state tunneling matrix elements, in general, depend on the position of the dividing surface. The cause for this dependence can be traced to the form of the correction function $w = -\ln(F + U_\alpha \xi_\alpha)$ used. For nonzero values of $\mathbf{U}$, function w contains higher-order terms with respect to the variables ξ_α. These terms appear in the equations for the higher-order functions W_i, which are not taken into account in JFI theory. It can be shown that contributions from W_2 function cancel out this dependence. However, for the determination of higher-order functions, it is necessary to compute higher-order derivatives of the potential energy surface, which causes a significant increase in computational complexity and is considered not feasible. On the other hand, as the dependence on the position of the dividing plane arises from higher-order functions, it is expected to be small in comparison with terms considered in JFI. Furthermore, there are two cases in which the dependence vanishes. The first case involves neglecting the $\mathbf{U}$ contribution in the tunneling matrix element. Such approximation works well for modes with significant projection onto MAP near minima, as in those cases F-term is dominant. The second case represent modes that are exactly orthogonal to the MAP, for which $\mathbf{U} - \mathbf{P}\mathbf{U}$ vanishes. This case can arise from the symmetry constraints and is present in malonaldehyde molecule, in which all geometries on the MAP are planar, which causes all out-of-plane modes to be orthogonal to the MAP.

3.3. JFI Theory for Multiple Wells and Multiple States

Herring formula can be used to compute tunneling matrix elements between different pairs of wells, as well as between different vibrational states. The latter generalization can also be used to compute tunneling matrix elements between non-symmetry related wells, which may have different energies of localized wavefunctions. First it is noted that the tunneling matrix is essentially the matrix of Hamiltonian, represented in the basis of localized wavefunctions. Thus, action of the Hamiltonian on a wavefunction localized in well i and corresponding to either the ground state ($\nu = 0$) or a singly excited mode ν is

$$\hat{H}\phi_\nu^{(i)} = E_\nu^{(i)}\phi_\nu^{(i)} + \sum_{j\neq i} h_{\nu\nu'}^{(ij)}\phi_{\nu'}^{(j)},$$
(3.44)

where summation convention for well indices i and j is not used. Localized wavefunctions are defined to be the wavefunctions that are locally eigenfunctions of the Hamiltonian, i.e. that satisfy $\left\langle \phi_\nu^{(i)} \middle| \hat{H} \middle| \phi_{\nu'}^{(i)} \right\rangle = \delta_{\nu\nu'}$. Next, the entire space is partitioned into regions that correspond to each well. This can be done, for example, by assigning all points for which following the

steepest descend path leads to that well. Similarly to the double well case, region of the well i is assumed to contain the entire norm of the wavefunctions localized in that well, while the integrals that contain two wavefunctions from the other wells are assumed to be negligible in that region. Integrals containing one wavefunction from i and one from another well will also be neglected, but, as will be shown, this approximation introduces an error in the splitting. All wavefunctions can be assumed to be real. Focusing on the pair of wavefunctions $\phi_v^{(i)}$ and $\phi_{v'}^{(j)}$, it can easily be shown, from equation (3.44), that

$$\int_{(i)} \phi_{v'}^{(j)} \hat{H} \phi_v^{(i)} \mathrm{d}\mathbf{x} = E_v^{(i)} \int_{(i)} \phi_{v'}^{(j)} \phi_v^{(i)} \mathrm{d}\mathbf{x} + \sum_{j' \neq i} h_{vv''}^{(ij')} \int_{(i)} \phi_{v''}^{(j')} \phi_{v'}^{(j)} \mathrm{d}\mathbf{x}$$
$$= E_v^{(i)} \int_{(i)} \phi_{v'}^{(j)} \phi_v^{(i)} \mathrm{d}\mathbf{x}. \tag{3.45}$$

Similarly, focusing on the $\phi_{v'}^{(j)}$, it can be shown that

$$\int_{(i)} \phi_v^{(i)} \hat{H} \phi_{v'}^{(j)} \mathrm{d}\mathbf{x} = E_{v'}^{(j)} \int_{(i)} \phi_{v'}^{(j)} \phi_v^{(i)} \mathrm{d}\mathbf{x} + \sum_{j' \neq j} h_{v'v''}^{(jj')} \int_{(i)} \phi_{v''}^{(j')} \phi_v^{(i)} \mathrm{d}\mathbf{x}$$
$$= E_{v'}^{(j)} \int_{(i)} \phi_{v'}^{(j)} \phi_v^{(i)} \mathrm{d}\mathbf{x} + h_{v'v''}^{(ji)} \int_{(i)} \phi_{v''}^{(i)} \phi_v^{(i)} \mathrm{d}\mathbf{x}$$
$$= E_{v'}^{(j)} \int_{(i)} \phi_{v'}^{(j)} \phi_v^{(i)} \mathrm{d}\mathbf{x} + h_{v'v''}^{(ji)} \delta_{vv''}$$
$$= E_{v'}^{(j)} \int_{(i)} \phi_{v'}^{(j)} \phi_v^{(i)} \mathrm{d}\mathbf{x} + h_{v'v}^{(ji)}. \tag{3.46}$$

Subtracting these two equations and reducing the integral over the region i to the surface integral results in the formula for the tunneling matrix element

$$h_{v'v}^{(ji)} = h_{vv'}^{(ij)} = \frac{1}{2} \int \left(\phi_{v'}^{(j)} \frac{\partial}{\partial S} \phi_v^{(i)} - \phi_v^{(i)} \frac{\partial}{\partial S} \phi_{v'}^{(j)} \right) \delta(f(\mathbf{x})) \mathrm{d}\mathbf{x} + \left(E_v^{(i)} - E_{v'}^{(j)} \right) \int_{(i)} \phi_{v'}^{(j)} \phi_v^{(i)} \mathrm{d}\mathbf{x}. \tag{3.47}$$

In the case of same vibrational states of the symmetry-related minima, or two states in resonance, the second term vanishes exactly. In other cases, it will be neglected, but it will be shown to introduce an error in the values of the tunneling matrix elements, which is in most cases negligible. In this derivation, localized wavefunctions were assumed to be normalized. If that is not the case, the Herring formula becomes

$$h_{v'v}^{(ji)} = h_{vv'}^{(ij)} = \frac{\int \left(\phi_{v'}^{(j)} \frac{\partial}{\partial S} \phi_v^{(i)} - \phi_v^{(i)} \frac{\partial}{\partial S} \phi_{v'}^{(j)} \right) \delta(f(\mathbf{x})) \mathrm{d}\mathbf{x}}{2 \sqrt{\int \left| \phi_v^{(i)} \right|^2 \mathrm{d}\mathbf{x} \int \left| \phi_{v'}^{(j)} \right|^2 \mathrm{d}\mathbf{x}}}. \tag{3.48}$$

As can be seen, Herring formula can be used to compute tunneling matrix elements between different states and can be applied to multi-well systems. If one is interested only in tunneling manifold of a certain vibrational state of a multi-well system, energies of all localized states are the same, and can be set to 0 when constructing tunneling matrix/Hamiltonian matrix. However, if one wishes to include different vibrational states, or treat non-symmetry related minima, the energies of localized states differ, and must be computed and included on the diagonal of the tunneling matrix. As exact values of these energies can be obtained only using quantum mechanical calculations, an approximation is necessary to keep the method feasible. The simplest approximation is to replace the full potential energy surface of a single well with an approximate one. The approximate surface can be taken to be either harmonic potential, or an n-mode expansion[124,125] of the full potential. The former yields analytical energies, which do not include the anharmonicity effects, while the latter includes anharmonicity, but its eigenstates must be computed numerically. This can be done relatively efficiently using VSCF[34,125] and VCI[34,35] methods, which are especially suited for that particular form of potential energy surface. The overall energy pattern depends only on the differences of the localized energies, which converge faster than their absolute values, with respect to the accuracy of PES approximation and basis set size. Thus, less accurate VSCF and VCI methods can yield satisfactory values.

3.4. JFI Method for Asymmetric Wells and Different Vibrational States

JFI localized wavefunctions can be used to compute the tunneling matrix elements between different vibrational states, and between non-symmetry related minima. Wavefunctions are constructed via the WKB approach as previously mentioned

$$\phi_v^{(i)} = \left(F_v^{(i)} + U_{v,\alpha}^{(i)}\xi_\alpha\right) e^{-\int_0^S p_0^{(i)}(S')\mathrm{d}S' - \frac{1}{2}\int_0^S \mathrm{Tr}\left(\mathbf{A}^{(i)} - \mathbf{A}_0^{(i)}\right)/p_0^{(i)}\mathrm{d}S' - \frac{1}{2}A_{jk}^{(i)}\tau_{j\alpha}\tau_{k\beta}\xi_\alpha\xi_\beta}, \qquad (3.49)$$

where, to obtain a closed-form expression, we define for the ground state wavefunction terms $F_{\mathrm{GS}} = 1$ and $\mathbf{U}_{\mathrm{GS}} = \mathbf{0}$. As characteristics for the Hamilton-Jacobi equation are defined to be classical trajectories with zero energy with respect to the minimum, momenta in different wells are $p_0^{(i)} = \sqrt{2(V - V_{\min}^{(i)})}$. Thus, in case the minima of two wells do not have the same energy, one does not seek MAP that connects them, but rather a path that minimises

$$\int_0^{S_{\mathrm{cp}}} \sqrt{2(V(S') - V_{\min}^{(i)})}\mathrm{d}S' + \int_0^{\tilde{S}_{\mathrm{cp}}} \sqrt{2(V(\tilde{S}') - V_{\min}^{(j)})}\mathrm{d}S'$$
$$= \int_0^{S_{\mathrm{tot}}} \sqrt{2(V(S') - V_{\min}^{(i)} + \Theta(S' - S_{\mathrm{cp}})(V_{\min}^{(i)} - V_{\min}^{(j)}))}\mathrm{d}S', \quad (3.50)$$

where $\Theta(S - S_{cp})$ is Heaviside's step function. If minimum i is chosen to have the lower energy, which is set as the reference, this expression can be interpreted as action on the modified potential energy surface $\tilde{V}(S) = V(S) - \Theta(S - S_{cp})V_{min}^{(j)}$. Thus, the instanton path in that case becomes MAP on the modified surface $\tilde{V}$. Unlike the case of minima at same energies, the shape of the MAP depends on the choice of connection point, which has to be made *a priori* to the path optimization. Additionally, due to the discontinuity in the step function, the MAP obtained is not smooth, but possesses a kink at the connection point, as the momentum vectors $\mathbf{p}_0^{(i)}$ and $\mathbf{p}_0^{(j)}$ differ. As momentum vectors are tangent to the path, the consequence is the discontinuity in the tangent vector. As a result, the dividing plane cannot be taken as the plane orthogonal to the path at the connection point. Instead, normal of the dividing plane is chosen to eliminate the gradient of the exponent in the plane. Expanding functions W_0 of both wavefunctions around the connection point leads to

$$\int_0^{S_{cp}} p_0^{(i)} dS' + \int_0^{\tilde{S}_{cp}} p_0^{(j)} dS' + (\mathbf{p}_0^{(i)} - \mathbf{p}_0^{(j)})^\top (\mathbf{x} - \mathbf{x}_{cp}^{(0)}) + (\mathbf{x} - \mathbf{x}_{cp}^{(0)})^\top \frac{\mathbf{A}^{(i)} + \mathbf{A}^{(j)}}{2} (\mathbf{x} - \mathbf{x}_{cp}^{(0)}),$$
(3.51)

making $\mathbf{p}_0^{(i)} - \mathbf{p}_0^{(j)}$ a convenient choice for the normal. Inserting the obtained wavefunctions into the Herring formula results in the expression for the tunneling matrix elements between arbitrary ground or singly excited vibrational states

$$h_{vv'}^{(ij)} = \sqrt{\frac{\sqrt{\det \mathbf{A}_0^{(i)} \det \mathbf{A}_0^{(j)}}}{\pi \det' \mathbf{P}\bar{\mathbf{A}}\mathbf{P}} \frac{p_0^{(i)} + p_0^{(j)}}{2}} \sqrt{(2\omega_v)^{1-\delta_{v0}}(2\omega_{v'})^{1-\delta_{v'0}}}$$

$$\left(F^{(i)} F^{(j)} + \frac{1}{2} \mathbf{U}^{(i)\top} (\mathbf{P}\bar{\mathbf{A}}\mathbf{P})^{-1} \mathbf{U}^{(j)} \right) e^{-\int_0^{S_{cp}} p_0^{(i)} dS' - \int_0^{\tilde{S}_{cp}} p_0^{(j)} dS'}$$

$$e^{-\frac{1}{2}\int_0^S \text{Tr}\left(\mathbf{A}^{(i)} - \mathbf{A}_0^{(i)}\right)/p_0^{(i)} dS' - \frac{1}{2}\int_0^{\tilde{S}} \text{Tr}\left(\mathbf{A}^{(j)} - \mathbf{A}_0^{(j)}\right)/p_0^{(j)} dS'}.$$
(3.52)

Dependence of the tunneling matrix element on the position of the dividing plane is again determined by differentiating the equation (3.52) with respect to S_{cp}. However, unlike the previous cases, MAP for the non-symmetry-related minima is not necessarily a smooth curve. This is because for the minima that do not have the same energies, the position of the dividing plane has to be given prior to the MAP calculation and the MAP has a kink at its position. However, it can be proven that the dependence of the shape of the MAP on the position S_{cp} depends on the ratio of energy difference and potential energy barrier. As a result, for small asymmetries in energy, the shape of MAP can be assumed not to change significantly. For this purpose, it is observed that moving the dividing plane corresponds to a shift in the center of the step function in equation (3.50). The shift corresponds to addition of function $f(S)$ to

the potential energy surface, which is of the form

$$f(S) = \begin{cases} -V_{\min}^{(j)} & S_{\mathrm{cp}} - \varepsilon < S < S_{\mathrm{cp}} \\ +V_{\min}^{(j)} & S_{\mathrm{cp}} < S < S_{\mathrm{cp}} + \varepsilon \\ 0 & \text{elsewhere} \end{cases} , \tag{3.53}$$

where ε corresponds to the shift in S_{cp}. The equation for characteristic for initial choice of S_{cp} is

$$\frac{d^2}{d\tau^2}\mathbf{x}(\tau) = \nabla \tilde{V}$$
$$\frac{dS}{d\tau} = p_0 = \sqrt{2\tilde{V}}. \tag{3.54}$$

Next, it is possible to define a new imaginary time variable as

$$d\tilde{\tau} = \frac{d\tau}{\sqrt{1 - \frac{f(S)}{V}}}, \tag{3.55}$$

which transforms the equation for characteristic to

$$\frac{d^2}{d\tilde{\tau}^2}\mathbf{x}(\tilde{\tau}) = \nabla(V - f(S)) + \frac{f(S)}{V(S)}\left(\frac{\mathbf{p}_0}{p_0}\frac{d}{dS}V - \nabla V\right),$$
$$\frac{d^2}{d\tilde{\tau}^2}\mathbf{x}(\tilde{\tau}) = \nabla\tilde{V} - \frac{f(S)}{V(S)}\left(\nabla V\right)_\perp. \tag{3.56}$$

The second term in this equation is proportional to the ratio $\frac{f(S)}{V(S)}$, which, if the barrier height is sufficiently larger than the energy difference of minima, can be neglected. In that case, characteristic for the initial choice of S_{cp} satisfies the equation for the modified position, with the only change being in the imaginary time variable. Thus, for the purpose of differentiation of tunneling matrix element, it can be assumed that in the cases of interest, the shape of the MAP is invariant with respect to S_{cp}. Furthermore, for sufficiently high barriers, the following approximation can be used

$$p_0^{(i)} \approx p_0^{(j)} \approx \bar{p}_0 \tag{3.57}$$

Differentiation of tunneling matrix element in equation (3.52) with respect to S_{cp} results

in

$$\frac{\mathrm{d}}{\mathrm{d}S_{\mathrm{cp}}}h^{(ij)}_{\nu\nu'} = \frac{h^{(ij)}_{\nu\nu'}}{\bar{p}_0}\left[2\frac{\mathrm{d}\bar{p}_0}{\mathrm{d}S_{\mathrm{cp}}} + \omega_\nu\delta_{\nu,1} - \omega_{\nu'}\delta_{\nu',1} + \right.$$
$$\left.\bar{p}_0(p_0^{(j)} - p_0^{(i)}) + \frac{1}{2}\mathrm{Tr}\left(\mathbf{A}_\perp^{(i)} - \mathbf{A}_\perp^{(j)}\right) - \right.$$
$$\left.\frac{1}{2}\mathrm{Tr}\left(\mathbf{A}^{(i)} - \mathbf{A}^{(j)}\right) + \frac{1}{2}\mathrm{Tr}\left(\mathbf{A}_0^{(i)} - \mathbf{A}_0^{(j)}\right)\right]$$

$$\frac{\mathrm{d}}{\mathrm{d}S_{\mathrm{cp}}}h^{(ij)}_{\nu\nu'} = \frac{h^{(ij)}_{\nu\nu'}}{\bar{p}_0}\left[\omega_\nu\delta_{\nu,1} - \omega_{\nu'}\delta_{\nu',1} + \right.$$
$$\left.\frac{1}{2}\left(p_0^{(j)2} - p_0^{(i)2}\right) + \frac{1}{2}\mathrm{Tr}\left(\mathbf{A}_0^{(i)} - \mathbf{A}_0^{(j)}\right)\right]$$

$$\frac{\mathrm{d}}{\mathrm{d}S_{\mathrm{cp}}}h^{(ij)}_{\nu\nu'} = \frac{h^{(ij)}_{\nu\nu'}}{\bar{p}_0}\left[\omega_\nu\delta_{\nu,1} + \frac{1}{2}\mathrm{Tr}\,\mathbf{A}_0^{(i)} - \omega_{\nu'}\delta_{\nu',1}\right.$$
$$\left. -V_{\min}^{(j)} - \frac{1}{2}\mathrm{Tr}\,\mathbf{A}_0^{(j)}\right]$$

$$\frac{\mathrm{d}}{\mathrm{d}S_{\mathrm{cp}}}h^{(ij)}_{\nu\nu'} = \frac{h^{(ij)}_{\nu\nu'}}{\bar{p}_0}\left(E_\nu^{(i)} - E_{\nu'}^{(j)}\right). \tag{3.58}$$

Thus, the tunneling matrix element is not invariant with respect to the position of the dividing plane, unless the two states that are considered are in resonance. The origin of the dependence can be traced back to the neglected term proportional to $\phi_\nu^{(i)}\phi_{\nu'}^{(j)}$ in the derivation of Herring formula. Its contribution to the tunneling matrix element is of the form

$$\Delta h^{(ij)}_{\nu\nu'} = (E^{(j)} - E^{(i)})\int_{(i)}\phi_\nu^{(i)}\phi_{\nu'}^{(j)}d\mathbf{x}. \tag{3.59}$$

Differentiation of this expression with respect to S_{cp} corresponds to the increase of the region of space (i) over which the integral is taken. Thus, the following equation holds

$$\frac{\mathrm{d}}{\mathrm{d}S_{\mathrm{cp}}}\Delta h^{(ij)}_{\nu\nu'} = (E^{(j)} - E^{(i)})\int\phi_\nu^{(i)}\phi_{\nu'}^{(j)}\delta f(\mathbf{x})d\mathbf{x}$$
$$= \frac{h^{(ij)}_{\nu\nu'}}{\bar{p}_0}\left(E_{\nu'}^{(j)} - E_\nu^{(i)}\right), \tag{3.60}$$

where $f(\mathbf{x}) = 0$ is the implicit equation of the dividing plane. It can be seen that this contribution cancels out the dependence of the tunneling matrix element on S_{cp} exactly. To take this contribution into account, it would be necessary to compute the overlap between functions localized in different wells. Unfortunately, WKB wavefunctions cannot be used for this purpose. The reason for this is the fact that they become nonphysical as one moves away from the barrier and into the other potential energy well. Nonphysical behaviour is caused by

W_0 function, which may become complex when wavefunction corresponding to the higher minimum approaches the lower minimum, and by W_1 function, which diverges in the region near the other minimum. However, an estimate for the magnitude of the neglected terms can be made by computing the overlap of the localized harmonic oscillator wavefunctions, and using that value instead. Algorithm for the computation of these overlaps has been reported in literature.[126] However, as long as the energy difference is sufficiently small in comparison with the barrier height and the connection point is chosen near the top of the barrier, dependence caused by neglecting this term is small and JFI expression for the tunneling matrix element provides accurate splitting patterns.

3.5. JFI Theory for Rotationally Excited States

The effects of rotational excitation can partially be included in JFI theory. For this purpose, it is convenient to choose rotation-contortion-vibration Hamiltonian[127,128] as a starting point. Contortion coordinate represents a large amplitude motion of the molecule, which corresponds to the coordinate S in JFI theory. Restoring the use of $\hbar$ momentarily, to keep track of the contributions in the WKB wavefunction, Hamiltonian takes the form

$$\hat{H} = -\frac{\hbar}{2}\frac{\partial^2}{\partial \xi_\alpha^2} + \frac{1}{2}\mu^{1/4}(\hat{J}_i - \hat{\pi}_i)\mu^{-1/2}\mu_{ij}^{(0)}(S)(\hat{J}_j - \hat{\pi}_j)\mu^{1/4} + V_W(S, \xi_\alpha) + V(S, \xi_\alpha), \quad (3.61)$$

where $i, j = x, y, z, S$. Operators $\hat{J}_a$, $\hat{J}_b$, $\hat{J}_c$ are angular momentum component operators in body-fixed frame. Operator $\hat{J}_S$ is, by definition

$$\hat{J}_S = -i\frac{\partial}{\partial S}. \quad (3.62)$$

μ is the determinant of $\mu^{(0)}$, which is a 4×4 matrix defined as an inverse of generalized moment of inertia matrix $\mathbf{I}^{\text{mom}}$, whose elements are

$$\begin{aligned}
I_{\alpha\alpha}^{\text{mom}} &= x_{i,\beta}^2 + x_{i,\gamma}^2, & \alpha, \beta, \gamma = a, b, c \\
I_{\alpha\beta}^{\text{mom}} &= -x_{i,\alpha}x_{i,\beta}, & \alpha \neq \beta = a, b, c \\
I_{\alpha S}^{\text{mom}} &= x_{i\gamma}x_{i\beta}' - x_{i\beta}x_{i\gamma}' \\
I_{SS}^{\text{mom}} &= (x_{ia}')^2 + (x_{ib}')^2 + (x_{ic}')^2,
\end{aligned} \quad (3.63)$$

where $i = 1, ..., N_{\text{atoms}}$. Operators $\hat{\pi}_i$ are vibrational angular momentum operators, defined as

$$\hat{\pi}_i = -i\hbar \zeta_{\alpha\beta}^i \xi_\alpha \frac{\partial}{\partial \xi_\beta}$$

$$\zeta_{\alpha\beta}^a = \sum_{n=1}^{N_{\text{atoms}}} \varepsilon_{abc} \tau_{nb,\alpha} \tau_{nc,\beta} \qquad a, b, c = x, y, z$$

$$\zeta_{\alpha\beta}^S = \frac{\mathrm{d}\tau_{i\alpha}}{\mathrm{d}S} \tau_{i\beta} = C_\alpha \tau_{iN} \tau_{i\beta} = 0, \tag{3.64}$$

where $\zeta_{\alpha\beta}^i$ are Coriolis coupling terms, which vanish exactly for the contortional coordinate. Finally, V_{W} is Watson potential term, which is of the order $\hbar^2$ and does not depend on the rotational state, meaning that it can be neglected in these considerations.

MAP has a convenient property that the geometries $\mathbf{x}^{(0)}(S)$ and $\mathbf{x}^{(0)}(S + \mathrm{d}S)$ are aligned so that the distance between them is minimal. This can easily be proven by contradiction, i.e. by assuming that in the MAP there are two geometries for which this does not hold. Action can be discretised as

$$S_0 = \sqrt{2V(\mathbf{x}^{(0)}(S_i))} |\mathbf{x}^{(0)}(S_{i+1}) - \mathbf{x}^{(0)}(S_i)| \tag{3.65}$$

with $S_{i+1} - S_i = \mathrm{d}S$. If geometries $\mathbf{x}^{(0)}(S_{i+1})$ and $\mathbf{x}^{(0)}(S_i)$ are not aligned so that the distance is minimal, one can define a rotation operator $\hat{R}$ which rotates $\mathbf{x}^{(0)}(S_{i+1})$ and minimizes the distance. However, if that operator is applied to all $\mathbf{x}^{(0)}(S_{j>i})$, distance $|\hat{R}\mathbf{x}^{(0)}(S_{i+1}) - \mathbf{x}^{(0)}(S_i)|$ will become smaller, while distances $|\hat{R}\mathbf{x}^{(0)}(S_{j+1}) - \hat{R}\mathbf{x}^{(0)}(S_j)|, j > i$ will be unchanged. Due to the reduction in distance $|\hat{R}\mathbf{x}^{(0)}(S_{i+1}) - \mathbf{x}^{(0)}(S_i)|$, the action decreases, which is in contradiction with the assumption that $\mathbf{x}^{(0)}(S)$ is a MAP. Furthermore, it has been proven[129] that geometries that are aligned so that the distance between them is minimal also satisfy the Eckart condition

$$x_i^{(0)}(S) \times (x_i^{(0)}(S + \mathrm{d}S) - x_i^{(0)}(S)) = 0, \tag{3.66}$$

which means that on the MAP, elements $I_{\alpha S}^{\text{mom}} = 0$. From the definition of local coordinates, it follows that $I_{SS}^{\text{mom}} = (1 + C_\alpha \xi_\alpha)^2$, which means that the matrix μ takes the form

$$\mu = \begin{pmatrix} \mu^{\text{RR}} & \mathbf{0} \\ \mathbf{0} & (1 + C_\alpha \xi_\alpha)^{-2} \end{pmatrix}, \tag{3.67}$$

where $\mu^{\text{RR}}(S)$ is the inverse of the moment of inertia matrix for the rigid rotor at the geometry

$\mathbf{x}^{(0)}(S)$. Such form of the matrix $\boldsymbol{\mu}$ neatly reduces Hamiltonian to

$$\hat{H} = -\frac{\hbar^2}{2}\frac{\partial^2}{\partial \xi_\alpha^2} - \frac{\hbar^2}{2}\mu^{1/4}\frac{\partial}{\partial S}\mu^{-1/2}\frac{1}{(1+C_\alpha \xi_\alpha)^2}\frac{\partial}{\partial S}\mu^{1/4}+$$
$$\frac{1}{2}\mu^{1/4}(\hat{J}_a - \hat{\pi}_a)\mu^{-1/2}\mu^{\mathrm{RR}}_{ab}(\hat{J}_b - \hat{\pi}_b)\mu^{1/4} + V(S,\xi_\alpha). \qquad (3.68)$$

Next, it can be assumed that matrix $\boldsymbol{\mu}^{\mathrm{RR}}$ depends only on the coordinate S. The dependence on coordinates ξ_α can be considered by expansion into Taylor series, from which one can see that all terms that include ξ_α will contribute to terms of higher order in ξ_α in the WKB equations, which are not taken into consideration in the JFI theory, making the approximation justified. This approximation reduces Hamiltonian to

$$\hat{H} = \frac{i\hbar}{2}\mu^{\mathrm{RR}}_{ab}\left(\zeta^a_{\alpha\beta}\hat{J}_b + \zeta^b_{\alpha\beta}\hat{J}_a\right)\xi_\alpha\frac{\partial}{\partial \xi_\beta} + \frac{\hbar^2}{(1+C_\alpha \xi_\alpha)^3}C'_\alpha \xi_\alpha\frac{\partial}{\partial S} + \frac{1}{2}\mu^{\mathrm{RR}}_{ab}\hat{J}_a\hat{J}_b$$
$$- \frac{\hbar^2}{2}\mu^{\mathrm{RR}}_{ab}\zeta^a_{\alpha\alpha'}\zeta^b_{\beta\beta'}\xi_\alpha \xi_\beta\frac{\partial^2}{\partial \xi_{\alpha'}\partial \xi_{\beta'}} - \frac{\hbar^2}{2(1+C_\alpha \xi_\alpha)^2}\frac{\partial^2}{\partial S^2} - \frac{\hbar^2}{2}\frac{\partial^2}{\partial \xi_\alpha^2} + V(S,\xi_\alpha) \quad (3.69)$$

First two terms contain only first derivatives, and are both of the order $\hbar^1$, as angular momentum operators give rise to terms of the order $\hbar$. Thus, in WKB formulas they do not contribute to the W_0 function, but only to the higher order functions W_1, W_2 etc. Furthermore, their contribution is of the order ξ^1, which was not included in the W_1 equation, and can thus be neglected in JFI approximation. Third term contributes to W_2 and higher order functions, and represents the influence of the change in the rotational energy along the MAP, which slightly modifies the effective barrier for tunneling. Fourth term contributes in the equation for Ξ, accounting for the curvature of the $(3N_{\mathrm{atoms}} - 6)$-dimensional space. However, as matrix Ξ is obtained from propagation of matrix $\mathbf{A}$, which is done in full $3N_{\mathrm{atoms}}$, this contribution is already accounted for. Remaining terms are analogues of the terms in the previous JFI theory derivations.

Two methods for the inclusion of the rotational excitation effects have been attempted as a part of this research. First method included adiabatic rotational approximation, in which S-dependent rigid-rotor eigenfunctions are added to the vibrational part of the wavefunction

$$\phi^{(i)}_{vJ_{K_aK_b}} = \phi^{(i)}_{vJ=0}e^{-W_2(J_{K_aK_b},S)}\left|J_{K_aK_b},S\right\rangle, \qquad (3.70)$$

where $\phi^{(i)}_{vJ=0}$ is expanded in terms of W_0 and W_1 functions. Rigid-rotor eigenfunctions are

defined as

$$\hat{H}^{\mathrm{RR}} |J_{K_a K_b}, S\rangle = E^{\mathrm{RR}}(J_{K_a K_b}, S) |J_{K_a K_b}, S\rangle$$
$$\hat{H}^{\mathrm{RR}} = \frac{1}{2} \mu_{ab}^{\mathrm{RR}}(S) \hat{J}_a \hat{J}_b. \tag{3.71}$$

This wavefunction is inserted into Schrödinger equation and terms of the same order in $\hbar$ are grouped. The contribution of non-adiabatic terms of the form $\frac{\partial}{\partial S} |J_{K_a K_b}, S\rangle$ and $\frac{\partial^2}{\partial S^2} |J_{K_a K_b}, S\rangle$ are neglected. Equations for W_0 and W_1 that are obtained are of the same form as in the previous JFI derivations, while the equation for W_2 contains rotational contribution and is of the form

$$p_0 \frac{\partial W_2}{\partial S} + E^{\mathrm{RR}}(J_{K_a K_b}, S) = E^{\mathrm{RR}}(J_{K_a K_b}, \min)$$
$$W_2 = \int_0^S \frac{E^{\mathrm{RR}}(J_{K_a K_b}, \min) - E^{\mathrm{RR}}(J_{K_a K_b}, S')}{p_0} \mathrm{d}S'. \tag{3.72}$$

This results in tunneling matrix elements for a certain rotational state of the form

$$h_{\nu\nu', J_{K_a K_b}}^{(ij)} = h_{\nu\nu', J=0}^{(ij)} \mathrm{e}^{\int_0^{S_{\mathrm{tot}}} \frac{E^{\mathrm{RR}}(J_{K_a K_b}, S') - E^{\mathrm{RR}}(J_{K_a K_b}, \min)}{p_0} \mathrm{d}S'}. \tag{3.73}$$

The second method attempted was to neglect the contribution of rotational energies on the splitting elements and consider the non-adiabatic effects that arise from the change in the principal axes along the MAP. Even though the neighbouring points on the MAP satisfy Eckart conditions, these conditions are not transitive, meaning that there can be a significant change in the orientation of principal axes in the two connected minima. Effects of this change can be accounted for by constructing $(4J + 2)$-dimensional Hamiltonian matrices for each value J of interest, which are represented in the basis of the form

$$\phi_{\nu J K}^{(i)} = \phi_{\nu J=0}^{(i)} |J K\rangle. \tag{3.74}$$

The Hamiltonian matrix is of the form

$$\begin{pmatrix} \mathbf{H}^{\mathrm{RR},\,(1)} & h_{\nu\nu'}^{(12)} \mathbf{I} \\ h_{\nu\nu'}^{(12)} \mathbf{I} & \mathbf{H}^{\mathrm{RR},\,(2)} \end{pmatrix}. \tag{3.75}$$

Due to the difference in principal axes, the eigenvectors of rigid-rotor Hamiltonians $\mathbf{H}^{\mathrm{RR},\,(1)}$ and $\mathbf{H}^{\mathrm{RR},\,(2)}$ are not mutually orthogonal, meaning that if these blocks are diagonalized, off-diagonal coupling block $h_{\nu\nu'}^{(12)} \mathbf{I}$ becomes non-diagonal and accounts for the changes in the splittings of different rotational states. Rotation-tunneling pattern is obtained simply by

diagonalizing the Hamiltonian matrix.

3.6. Numerical Implementation of Generalized JFI Theory

There are several steps involved in the computation of vibration-rotation-tunneling states of a molecule using JFI theory. The general flow of the calculation is the following:

1. Determining all minima of interest on the potential energy surface. If one is interested in symmetry-related minima, they can be constructed from one minimum by applying all possible permutations of equivalent atoms, with or without the application of inversion operator. The set of all of these operators form the complete nuclear permutation-inversion (CNPI) group.[130] However, in most cases, not all rearrangements between different minima are feasible. Rearrangements that include covalent bond-breaking can, in some cases, pass through very large barriers, making their tunneling matrix elements negligible. Thus, some permutations may be eliminated from the CNPI group, leading to the so-called molecular symmetry group.

2. Locating MAPs between all pairs of minima. In most cases, even for molecules with multiple minima, the number of different types of paths will be much smaller than the number of pairs. Thus, only pairs of minima connected with different types of paths need to be considered, while paths between other pairs can be deduced from symmetry considerations. Details of the MAP optimization between a pair of minima will be given in the following section.

3. Computing Hessians along each path and interpolating their elements, as well as geometries and potential energy.

4. Propagating matrices **A** and vectors **U** for the states of interest.

5. Computing rotational corrections, if one is interested in states with $J > 0$.

6. Constructing the tunneling matrix elements from the propagated objects and computing localized energies if different states are taken into consideration, or if non-symmetry-related minima are chosen.

7. Finding the eigenvalues and eigenvectors of tunneling matrix and determining the symmetry of each eigenvector.

Source code that was used in this thesis can be found on `https://github.com/merakovic/JFI`.

3.6.1. Minimum Action Path Optimization

Minimum action path was optimized using string method.[104] The basis of this method lies in discretization of abbreviated action in terms of equidistant points on the path

$$S_0 \approx \sum_{i=0}^{N} \bar{p}_0(S_i, S_{i+1}) \, |\mathbf{x}(S_{i+1}) - \mathbf{x}(S_i)| \,, \tag{3.76}$$

where $\mathbf{x}(S_0) = \mathbf{x}^{(\mathrm{L})}$ and $\mathbf{x}(S_{N+1}) = \mathbf{x}^{(\mathrm{R})}$. The discretized action can be treated as a function of N positions, or 'beads', which has a minimum that corresponds to the discretized MAP. The mean momentum on the segment (S_i, S_{i+1}) can be obtained from the observation of the total energy, which is equal to zero,

$$\frac{1}{2}\bar{p}_0^2(S_i, S_{i+1}) - \bar{V}(S_i, S_{i+1}) = 0$$

$$\frac{1}{2}\bar{p}_0^2(S_i, S_{i+1}) - \frac{1}{2}(V(S_i) + V(S_{i+1})) = 0$$

$$p_0(S_i, S_{i+1}) = \sqrt{V(S_i) + V(S_{i+1})}, \tag{3.77}$$

which results in the discretized action of the form

$$S_0(\vec{\mathbf{x}}) = \sum_{i=0}^{N} \sqrt{V(S_i) + V(S_{i+1})} \, |\mathbf{x}(S_{i+1}) - \mathbf{x}(S_i)| \,. \tag{3.78}$$

Gradient of the discretized action can be computed from the gradients of potential energy at each bead

$$\frac{\partial S_0}{\partial x_j(S_i)} = \frac{|\mathbf{x}(S_i) - \mathbf{x}(S_{i-1})|}{2\sqrt{V(S_i) + V(S_{i-1})}} \frac{\partial V(S_i)}{\partial x_j(S_i)} + \frac{|\mathbf{x}(S_{i+1}) - \mathbf{x}(S_i)|}{2\sqrt{V(S_i) + V(S_{i+1})}} \frac{\partial V(S_i)}{\partial x_j(S_i)} +$$
$$\frac{\sqrt{V(S_i) + V(S_{i-1})}}{|\mathbf{x}(S_i) - \mathbf{x}(S_{i-1})|} (x_j(S_i) - x_j(S_{i-1})) + \frac{\sqrt{V(S_i) + V(S_{i+1})}}{|\mathbf{x}(S_{i+1}) - \mathbf{x}(S_i)|} (x_j(S_i) - x_j(S_{i+1})). \tag{3.79}$$

As the gradient of the discretized action can easily be computed from the geometries and gradients of potential energy, gradient-based methods for optimization can be used to locate MAP. In this research, limited-memory Broyden-Fletcher-Goldfarb-Shanno (L-BFGS) algorithm[102] has been used. This algorithm belongs to the family of quasi-Newton methods, in which optimization step is made so that it leads to the minimum on the approximate quadratic

surface as

$$S_0^q(\vec{\mathbf{x}}) = S_0(\vec{\mathbf{x}}^{(i)}) + \mathbf{G}(\vec{\mathbf{x}} - \vec{\mathbf{x}}^{(i)}) + \frac{1}{2}\left(\vec{\mathbf{x}} - \vec{\mathbf{x}}^{(i)}\right)^{\top}\mathbf{H}\left(\vec{\mathbf{x}} - \vec{\mathbf{x}}^{(i)}\right)$$

$$\vec{\mathbf{x}}^{(i+1)} = \vec{\mathbf{x}}^{(i)} - \mathbf{H}^{-1}\mathbf{G}. \tag{3.80}$$

Instead of computing the action Hessian in each step, which would drastically increase computational demands, the Hessian is approximated. In L-BFGS method, approximate Hessian is constructed from an initial guess, which in our case was taken to be the identity matrix, and adding to it a correction so that the corrected Hessian correctly describes the change in gradients in the previous M steps. Furthermore, as such correction is not uniquely defined, a constraint demanding that the norm of the correction is minimal is placed. Such Hessian updating scheme has two major advantages. First advantage is that it has modest memory requirements, as the only information that needs to be saved in each step are the previous M geometries and gradients. Second advantage is that the updating scheme can be directly applied on the inverse of Hessian, which bypasses a computationally intensive step of computing the inverse of an $(NN_{\text{dof}}) \times (NN_{\text{dof}})$ matrix in each step. Additionally, updating scheme can be used to directly compute the step $\mathbf{H}^{-1}\mathbf{G}$, meaning that the inverse of the Hessian never has to be stored or explicitly constructed. In all calculations in this thesis, value $M = 5$ was used.

The initial guess for the optimization is obtained by a linear interpolation between the minima. In case of molecular systems, the orientation of the geometry of minima is arbitrary. Thus, to accelerate the convergence, minima are aligned so that the distance between them is minimal before the linear interpolation is made. Alignment is made using the method based on quaternions.[131,132] Total distance S_{tot} is computed as the distance between the aligned minima and divided into $N + 1$ segments for the purpose of the interpolation. During path optimization, action gradient is computed in each step and its tangential component eliminated at each bead. This reduces the change in distances between adjacent beads in each step, as the final goal is to obtain a discretized MAP with equidistant points. After each step, both minima are aligned with respect to their neighbouring beads, which allows for their reorientation during optimization, and total lengths S_i are computed as

$$S_0 = 0$$

$$S_{i+1} = S_i + |\mathbf{x}(S_{i+1}) - \mathbf{x}(S_i)|. \tag{3.81}$$

Furthermore, after each step, bead geometries are reinterpolated so that the distances $S_{i+1} - S_i$ remain constant. Optimization is carried out until the maximal component of the action gradient perpendicular to the path is $\max\left(\frac{\partial S_0}{\partial x_j(S_i)}\right) < 10^{-7}$a.u.

After MAP has been optimized, Hessians of the potential are computed at each bead, using finite difference method. Geometries, potential and Hessian matrix elements are interpolated along the path using natural cubic splines,[73] with arc distance S being the parameter for interpolation, and used for propagation of $\mathbf{A}$ and, optionally, $\mathbf{U}$.

3.6.2. Propagation of Matrices $\mathbf{A}$ and Vectors $\mathbf{U}$

Propagation equations for both $\mathbf{A}$ and $\mathbf{U}$ have a singularity at the initial point, caused by the fact that $p_0(S=0)=0$. Thus, in both cases, an initial 'jump' is made to the distance ε. For matrix $\mathbf{A}$, the jump is made by linearizing all quantities on the interval $[0, \varepsilon]$

$$p_0 \approx p^{(1)}S$$
$$\mathbf{H} \approx \mathbf{H}_0 + \mathbf{H}^{(1)}S$$
$$\mathbf{A} \approx \mathbf{A}_0 + \mathbf{A}^{(1)}S. \tag{3.82}$$

Inserting these approximations into the propagation equation yields, up to S^1

$$p^{(1)}\mathbf{A}^{(1)}S = \mathbf{H}_0 + \mathbf{H}^{(1)}S - \mathbf{A}_0^2 - \mathbf{A}_0\mathbf{A}^{(1)}S - \mathbf{A}^{(1)}\mathbf{A}_0 S$$
$$\mathbf{A}_0^2 = \mathbf{H}_0$$
$$p^{(1)}\mathbf{A}^{(1)} + \mathbf{A}_0\mathbf{A}^{(1)} + \mathbf{A}^{(1)}\mathbf{A}_0 = \mathbf{H}^{(1)}, \tag{3.83}$$

where the last two equations are obtained by equating terms next to the same powers of S. First equation corresponds to the initial condition for matrix $\mathbf{A}$, while the second equation can be solved by transforming to the basis of eigenvectors of $\mathbf{A}_0$

$$p^{(1)}\tilde{\mathbf{A}}^{(1)} + \tilde{\mathbf{A}}_0\tilde{\mathbf{A}}^{(1)} + \tilde{\mathbf{A}}^{(1)}\tilde{\mathbf{A}}_0 = \tilde{\mathbf{H}}^{(1)}$$
$$p^{(1)}\tilde{A}_{ij}^{(1)} + \omega_i\delta_{ik}\tilde{A}_{kj}^{(1)} + \tilde{A}_{ik}^{(1)}\omega_j\delta kj = \tilde{H}_{ij}^{(1)}$$
$$p^{(1)}\tilde{A}_{ij}^{(1)} + \omega_i\tilde{A}_{ij}^{(1)} + \tilde{A}_{ij}^{(1)}\omega_j = \tilde{H}_{ij}^{(1)}$$
$$\tilde{A}_{ij}^{(1)} = \frac{\tilde{H}_{ij}^{(1)}}{p^{(1)} + \omega_i + \omega_j}, \tag{3.84}$$

where tilde denotes vectors and matrices in the basis of eigenvectors of $\mathbf{A}_0$. Thus, at the $S=\varepsilon$, value of $\mathbf{A}$ is simply $\mathbf{A}(\varepsilon) = \mathbf{A}_0 + \mathbf{A}^{(1)}\varepsilon$. The integral in the exponent can also be divided into intervals $[0, \varepsilon]$ and $[\varepsilon, S_{\text{cp}}]$. On the first interval, its value is simply

$$\int_0^\varepsilon \frac{\text{Tr}(\mathbf{A} - \mathbf{A}_0)}{p_0}dS = \int_0^\varepsilon \frac{\text{Tr}\,\mathbf{A}^{(1)}}{p^{(1)}}dS = \frac{\text{Tr}\,\mathbf{A}^{(1)}}{p^{(1)}}\varepsilon. \tag{3.85}$$

On the interval $[\varepsilon, S_{\text{cp}}]$ propagation can be made using any integrator for non-linear differential equations. In this research, fourth-order Runge-Kutta integrator[73] was used, with fixed step $\Delta S = 10^{-3}$a.u.. The integral in the exponent was computed using finite-difference approximation after each propagation step. Values of matrices $\mathbf{A}$ at the geometries of each bead were stored and its matrix elements interpolated using natural cubic splines after the propagation. Positions of the connection point S_{cp} and initial jump ε varied from system to system, and will be listed for each case in the Results chapter. At the connection point, projector operator was constructed using eigenvectors that correspond to translations, rotations and tangent to the plane as $\mathbf{P} = \mathbf{I} - \mathbf{u}_k \mathbf{u}_k^\top$ and used to project out these modes from $\bar{\mathbf{A}} = (\mathbf{A}^{(\text{L})} + \mathbf{A}^{(\text{R})})/2$ in equation (3.52).

Vector $\mathbf{U}$ is propagated analogously on the two intervals. A minor difference is that on the interval $[0, \varepsilon]$, vector $\mathbf{U}$ is expanded beyond linear term as

$$\mathbf{U} = \sum_{i=0}^{M} \mathbf{U}^{(i)} S^i. \tag{3.86}$$

Inserting this expression into the propagation equation for $\mathbf{U}$ and equating terms of the same power S^i results in the recursion relation

$$\mathbf{A}_0 \mathbf{U}^{(0)} = \omega \mathbf{U}^{(0)}$$
$$\mathbf{U}^{(i)} = -(\mathbf{A}_0 + (ip^{(1)} - \omega)\mathbf{I})^{-1} \mathbf{A}^{(1)} \mathbf{U}^{(i-1)}. \tag{3.87}$$

Terms $\mathbf{U}^{(i)}$ have been added until the change in the norm of vector $\mathbf{U}(\varepsilon)$ dropped below 10^{-12}. On the interval $[\varepsilon, S_{\text{cp}}]$, propagation was performed using the exponential propagator

$$\mathbf{U}(S + \Delta S) = e^{(\omega \mathbf{I} - \mathbf{A}(S))\Delta S / p_0} \mathbf{U}(S). \tag{3.88}$$

The most stable method for propagating F was found to be via the tangent component of vector $\mathbf{U}$ as

$$F' = \mathbf{U}^\top \tau_N$$
$$\frac{\omega}{p_0} F = \frac{\mathbf{U}^\top \mathbf{p}_0}{p_0} \tag{3.89}$$
$$F(S) = \frac{\mathbf{U}^\top \mathbf{p}_0}{\omega} \tag{3.90}$$

After propagation to S_{cp}, translational and rotational normal modes, as well as tangent component, were projected out from the vector $\mathbf{U}$ as $\mathbf{PU}$, with the projector being the same as for the matrix $\mathbf{A}$.

3.6.3. Computation of Rotational Contribution

Rotational contribution can be computed by constructing the matrices of operators $\hat{J}_\alpha$ for the desired value of J. The most convenient basis is the one of simultaneous eigenfunctions of operators $\hat{J}^2$ and $\hat{J}_a$, denoted as $|J,K\rangle$. Matrix elements in this basis are

$$
\begin{aligned}
(J_a)_{K_1K_2} &= K_1\delta_{K_1K_2} \\
(J_b)_{K_1K_2} &= \frac{1}{2}\sqrt{J(J+1)-K_1(K_1\pm 1)}\,\delta_{K_1\pm 1,K_2} \\
(J_c)_{K_1K_2} &= \mp\frac{i}{2}\sqrt{J(J+1)-K_1(K_1\pm 1)}\,\delta_{K_1\pm 1,K_2}.
\end{aligned} \tag{3.91}
$$

These matrices are used to construct the rigid-rotor Hamiltonian at select geometries along the path as

$$
\mathbf{H}^{\mathrm{RR}}(S) = \mu_{\alpha\beta}(S)\mathbf{J}_\alpha\mathbf{J}_\beta. \tag{3.92}
$$

For the method that employs adiabatic rotation approximation, rigid-rotor Hamiltonian is constructed and diagonalized at the minimum and at the distance $S = \varepsilon$. Overlap matrix for eigenvectors at $S = 0$ and $S = \varepsilon$ is constructed and eigenvalues at $S = \varepsilon$ and 0 are matched with the maximum overlap criteria for their eigenvectors. Integrals for the rotational contribution of each rotational state on the interval $[0,\varepsilon]$ are computed under linear approximation

$$
\begin{aligned}
E^{\mathrm{rot}}(J_{K_1K_2},S) &\approx E^{\mathrm{rot}}(J_{K_1K_2},\mathrm{min}) + \frac{E^{\mathrm{rot}}(J_{K_1K_2},\varepsilon) - E^{\mathrm{rot}}(J_{K_1K_2},\mathrm{min})}{\varepsilon}S \\
W_{2,J_{K_1K_2}}(\varepsilon) &= \int_0^\varepsilon \frac{E^{\mathrm{rot}}(J_{K_1K_2},\varepsilon) - E^{\mathrm{rot}}(J_{K_1K_2},\mathrm{min})}{\varepsilon p^{(1)}}\,\mathrm{d}S = \frac{E^{\mathrm{rot}}(J_{K_1K_2},\varepsilon) - E^{\mathrm{rot}}(J_{K_1K_2},\mathrm{min})}{p^{(1)}}.
\end{aligned} \tag{3.93}
$$

Integration on the interval $[\varepsilon, S_{\mathrm{cp}}]$ is approximated as a sum with step size $\Delta S = 10^{-3}$a.u., Rigid rotor energies and eigenvectors are computed after each step and matched with the previous step with the maximum overlap criteria for their eigenvectors.

For the method that accounts for the change in the principal axes, rigid-rotor Hamiltonians are constructed for both minima and used to construct $(4J+2)$-dimensional Hamiltonian matrix. This matrix is then diagonalized and splittings are computed from its eigenvalues.

3.6.4. Vibrational Self-Consistent Field and Configuration Interaction

For systems in which several different vibrational states were included in Hamiltonian matrix and for systems with non-symmetry related minima, energies of the localized states must be computed, in addition to the tunneling matrix elements. Computationally least expensive approximation is the use of harmonic energies, which are obtained at no additional cost, as Hessian matrix must be computed at the minima for the JFI calculation. However, anhar-

monicity of the potential energy well may be non-negligible when compared to the tunneling matrix elements, resulting in poor estimates of energy levels. To remedy this, anharmonicity has been partially included using vibrational self-consistent field (VSCF)[34,125] and vibrational configuration interaction (VCI)[34,35] methods.

As the desired energies are those of the localized wavefunctions, VSCF and VCI calculations were made on an approximate potential energy surface of a single well of interest. Potential energy surface was approximated using n-mode representation[124] truncated at the two-mode term as

$$V(\mathbf{q}) = \sum_{i=1}^{N_{\text{dof}}} V_i^{(1\text{M})}(q_i) + \sum_{i=1}^{N_{\text{dof}}-1} \sum_{j=i+1}^{N_{\text{dof}}} V_{ij}^{(2\text{M})}(q_i, q_j), \tag{3.94}$$

where q_i is the i-th normal mode coordinate. One-mode and two-mode potentials were represented as N_{pol}-th order polynomials

$$V_i^{(1\text{M})}(q_i) = \sum_{j=2}^{N_{\text{pol}}} C_j^{(i)} q_i^j$$

$$V_{ij}^{(2\text{M})}(q_i, q_j) = \sum_{k=1}^{N_{\text{pol}}-1} \sum_{l=1}^{N_{\text{pol}}-k} C_{kl}^{(ij)} q_i^k q_j^l. \tag{3.95}$$

Coefficients for the polynomials were obtained using multilinear regression. Points at which potential energy was computed for multilinear regression were chosen to be Gauss-Hermite DVR points for the harmonic oscillator with the frequency of the corresponding normal mode. Such choice ensures a balanced sampling for modes of different frequencies. Number of DVR points used varied from system to system and will be given in the Results section. Points for the fit of two-mode coefficients were chosen as all possible combinations of respective points used for the one-mode fit.

Vibrational self-consistent field is a method that is used to approximate vibrational eigenfunctions of a system. The ground-state vibrational wavefunction is assumed to be a product of one-mode functions

$$\psi(\mathbf{q}) = \phi_0^{(1)}(q_1)...\phi_0^{N_{\text{dof}}}(q_{N_{\text{dof}}}). \tag{3.96}$$

Optimal one-mode functions are obtained using variational principle, which results in the system of coupled equations

$$-\frac{1}{2}\frac{\mathrm{d}^2}{\mathrm{d}q_i^2}\phi^{(i)}(q_i) + \left(V_i(q_i) + \sum_{\substack{j=1 \\ j \neq i}}^{N_{\text{dof}}} \left\langle \phi_0^{(j)}(q_j) \middle| V_{ij}^{(2\text{M})} \middle| \phi_0^{(j)}(q_j) \right\rangle \right) \phi^{(i)}(q_i) = \varepsilon_i \phi^{(i)}(q_i). \tag{3.97}$$

This system of equations can be solved using self-consistent field approach. For this approach, all one-mode functions are represented as a linear combination of some basis set functions

$$\phi^{(i)}(q_i) = \sum_{j=1}^{N_{\text{basis}}} \alpha_j^{(i)} \chi_j^{(i)}(q_i). \tag{3.98}$$

An initial guess is made for the coefficients $\alpha_j^{(i)}$ and used to construct matrix Hamiltonian for each equation in (3.97). These matrix Hamiltonians are then diagonalized and the eigenvectors corresponding to the lowest eigenvalues used to construct new matrix Hamiltonians. The entire procedure is repeated until the change in the ground-state energy and one-mode functions drops below a preset threshold. For the purpose of this research, basis set functions were chosen to be harmonic oscillator functions centered at the minimum. Frequencies of these harmonic oscillators, however, were not taken to correspond to the frequencies of the minimum. This was due to the fact that some low-frequency modes possess significant anharmonicity, which causes a steep increase in potential energy for displacements larger than a certain value. Thus, using the frequency of the minimum results in a basis set which penetrates far into the region of high energy, making it necessary to increase the basis set size to obtain good VSCF energies. Instead, for each one-mode potential, eigenfunctions and eigenvalues were found using a sine DVR basis and the frequency for the basis set was taken to be $\omega^{(i)} = E_1^{(i)} - E_0^{(i)}$. Such frequencies yield basis set functions whose widths are similar to the widths of one-mode eigenfunctions. Initial guess for VSCF calculations was taken to be the product of ground state harmonic oscillators from the basis set. Using the harmonic oscillator eigenfunctions as basis set is convenient not only due to the fact that these functions generally already provide a good description of one-mode functions, but because potential energy matrix elements can efficiently be computed using analytic formulae. For this purpose, matrices $\mathbf{Q}_i^{(n)}$ of operators q_i^n are computed and stored, which can be done efficiently using a recursion formula

$$\left\langle \chi_j^{(i)} \middle| q_i^0 \middle| \chi_k^{(i)} \right\rangle = \delta_{jk}$$

$$\left\langle \chi_j^{(i)} \middle| q_i^n \middle| \chi_k^{(i)} \right\rangle = \frac{1}{\sqrt{2\omega_i}} \left\langle \chi_j^{(i)} \middle| q_i^{n-1}(\hat{a}_i + \hat{a}_i^\dagger) \middle| \chi_k^{(i)} \right\rangle$$

$$= \sqrt{\frac{k}{2\omega_i}} \left\langle \chi_j^{(i)} \middle| q_i^{n-1} \middle| \chi_{k-1}^{(i)} \right\rangle + \sqrt{\frac{k+1}{2\omega_i}} \left\langle \chi_j^{(i)} \middle| q_i^{n-1} \middle| \chi_{k+1}^{(i)} \right\rangle. \tag{3.99}$$

VSCF procedure generates N_{basis} one-mode functions for each normal mode, of which only the ground states are used for the ground-state VSCF wavefunction. Higher, or virtual, one-mode functions can be used in VCI procedure. In this method, a set of vibrational wavefunctions is generated by replacing a certain number of ground-state one-mode functions in

the VSCF product with virtual ones. This set of functions is used to construct the Hamiltonian matrix as

$$H_{IJ} = \left\langle \phi_{i_1}^{(1)}...\phi_{i_{N_{\text{dof}}}}^{(N_{\text{dof}})} \left| \hat{H} \right| \phi_{j_1}^{(1)}...\phi_{j_{N_{\text{dof}}}}^{(N_{\text{dof}})} \right\rangle. \tag{3.100}$$

Eigenvectors and eigenvalues of this matrix represent estimates of the vibrational energies of both the ground state and the excited vibrational states of the system. The lowest eigenvalue is a better estimate of the ground-state energy than the VSCF value, as the form of the wavefunction accounts for a part of correlation between normal modes. In this research, VCISD calculations have been performed. It should be noted that this is the highest order of configuration interaction that can be made for the selected approximate PES. Additionally, to reduce the computational demands, the highest excitation in each mode was limited to $N_{\text{exc}} = 6$.

3.6.5. Symmetry Determination

As symmetry group for the partially deuterated water trimer has not been reported in literature, the corresponding character table was determined. For this purpose, a program based on Burnside-Dixon algorithm[133–135] was developed. The input for the determination of character table using this program are the permutation-inversion operations that are deemed feasible. Next, a subroutine for multiplication of permutation-inversion operators is used to compute the multiplication table and identify different conjugacy classes. Following Burnside-Dixon algorithm, characters are determined from simultaneous eigenvectors of a set of matrices $\mathbf{M}_k$, whose matrix elements are defined as

$$(M_k)_{ij} = c_{R_k R_i R_j}, \tag{3.101}$$

with coefficients $c_{R_k R_i R_j}$ being the number of pairs $(a,b) \in R_k \times R_i$ that satisfy $ab = c$ for a fixed $c \in R_j$, where R_i, R_j and R_k are conjugacy classes. These matrix elements can easily be determined from the multiplication table. Set of simultaneous eigenvectors is found as follows. First, matrix $\mathbf{M}_1$ is diagonalized. For each eigenvalue, its degree of degeneracy is determined. Non-degenerate eigenvectors are stored, while each set of degenerate eigenvectors is used to construct a matrix of operator $\mathbf{M}_2$. These matrices are diagonalized, and the above procedure repeated, until there are no degenerate eigenvectors remaining. Elements of simultaneous eigenvectors are given by

$$\begin{pmatrix} \chi(R_1)|R_1| \\ \vdots \\ \chi(R_N)|R_N| \end{pmatrix}, \tag{3.102}$$

where $\chi(R_i)$ is the character of conjugacy class R_1 for the irreducible representation corresponding to this eigenvector. Using the fact that character of identity operator must be equal

to unity, each eigenvector is scaled with the appropriate constant. Finally, characters for each irreducible representation are computed from the elements of the eigenvectors by dividing them with the known size of each conjugacy class.

From the character table and multiplication table, it is possible to construct projection operators for each irreducible representation, defined as

$$\hat{P}^a = \frac{n_a}{h} \sum_R \chi^a(R)^* \hat{R}, \tag{3.103}$$

where the sum goes over all symmetry operators $\hat{R}$, a denotes the irreducible representation, n_a its dimension and h the number of representations. These projection operators are used to determine symmetry of eigenvectors obtained by diagonalization of tunneling matrix. Every projection operator is applied on each eigenvector and the norm of the result is computed. If the norm is close to unity, the eigenvector corresponds to that irreducible representation.

§ 4. RESULTS AND DISCUSSION

4.1. Model Systems

Several types of two-dimensional model systems were used to test the accuracy of developed JFI methods. For the JFI generalization to excited vibrational states, the following potential was used

$$V(\mathbf{x}) = \frac{V_1 V_2}{V_1 + V_2},$$

$$V_1(\mathbf{x}) = \frac{1}{2}\left(\mathbf{x} - \mathbf{x}^{(1)}\right)^\top \mathbf{U}_1 \begin{pmatrix} \alpha_1^2 & 0 \\ 0 & \alpha_2^2 \end{pmatrix} \mathbf{U}_1^\top \left(\mathbf{x} - \mathbf{x}^{(1)}\right),$$

$$V_2(\mathbf{x}) = \frac{1}{2}\left(\mathbf{x} - \mathbf{x}^{(2)}\right)^\top \mathbf{U}_2 \begin{pmatrix} \alpha_1^2 & 0 \\ 0 & \alpha_2^2 \end{pmatrix} \mathbf{U}_2^\top \left(\mathbf{x} - \mathbf{x}^{(2)}\right),$$

$$\mathbf{U}_1 = \begin{pmatrix} \cos\theta & -\sin\theta \\ \sin\theta & \cos\theta \end{pmatrix},$$

$$\mathbf{U}_2 = \begin{pmatrix} -\cos\theta & \sin\theta \\ \sin\theta & \cos\theta \end{pmatrix},$$

$$\mathbf{x}^{(1,2)} = (0, \pm\beta)^\top, \tag{4.1}$$

in which coordinates $\mathbf{x}$ are not mass-scaled. The plot of this potential is shown in Figure 3. It possesses two minima, located at $\mathbf{x}^{(1/2)}$. Potential energy near the minima is approximately harmonic, with the normal modes given by $\mathbf{U}_{1/2}$. Parameters α_1^2 and α_2^2 represent force constants at minima. Parameter θ can be used to vary the angle between the first normal mode and x-axis, which simultaneously varies the angle between normal modes of the two minima. The form of the potential has been chosen to test the ratio of contributions of F and $\mathbf{U}$ terms in the expression for the tunneling splitting. The symmetry group for such PES is D_1 for a general value of θ, while in cases $\theta = 0, \pi/2$, the symmetry group is D_2. The parameters were set to $\beta = 2.0$, $\alpha_1 = 1.265$ and $\alpha_2 = 2.0$ in all calculations. In order to test the accuracy of JFI method, benchmark quantum-mechanical calculations were performed for this potential energy surface. Energy levels have been determined using direct diagonalization of the matrix Hamiltonian, which was constructed in the basis of direct product of one-dimensional sine DVR functions. The grid was chosen to extend over the region $[-6.0, 6.0]$ in both dimensions, which was found to be sufficient to eliminate the boundary effects. The number of DVR functions in each dimension was 150, which was found to provide converged results for all energy levels of interest.
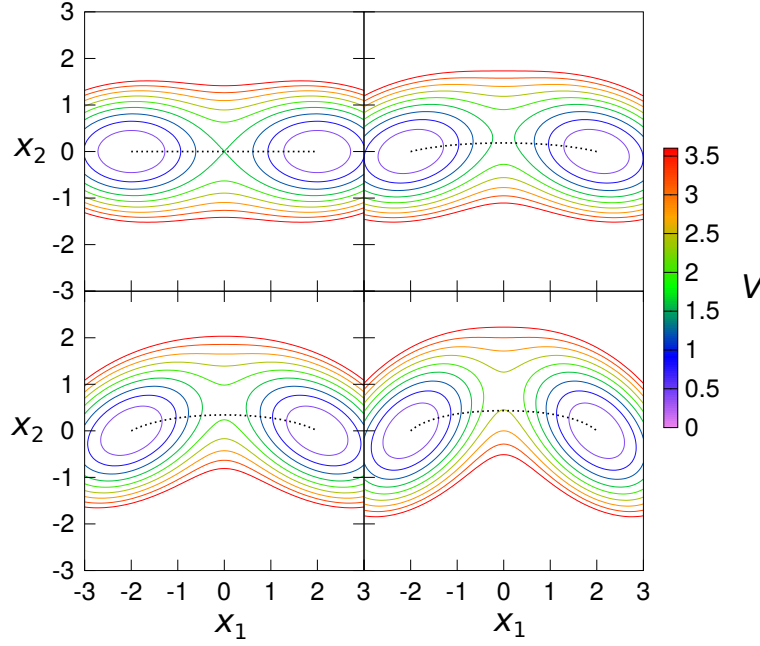
Figure 3. Model PES described with equation (4.1) for different values of angle θ (0, $\pi/12$, $\pi/6$ and $\pi/4$, respectively). MAP is shown as a dotted black line.

In the first set of calculations, mass of the system was taken to be $m = 27.0$, while the angle θ was varied to study the effects of curvature on different terms in the tunneling matrix element. Number of beads used for MAP optimization was $N = 600$, and the distance for the initial 'jump' $\varepsilon = 0.1$ a.u. In case of $\theta = 0$, MAP is a straight line that connects the minima and curvature is zero along the path. For $0 < \theta < \pi/4$, trajectory becomes curved, with the curvature being larger as the angle increases. Cases of $\theta > \pi/4$ are the same as the ones for $0 < \theta < \pi/4$ with force constants exchanged, and were thus not considered. As the curvature of the path near a minimum increases, the projection η of the normal mode on the displacement along the MAP, at some small distance ε changes, as shown in Table 1.

$$\eta(v) = \mathbf{U}_0^{(v),\top}(\mathbf{x}^{(0)}(\varepsilon) - \mathbf{x}^{(1)})/\varepsilon. \tag{4.2}$$

Table 1. Displacement η at $\varepsilon = 0.1$ for the two normal modes, (1,0) and (0,1), of the 2D symmetric potential in (4.1). Fractional contribution of the $F^{(\text{L})}F^{(\text{R})}$ term in equation (3.52) to the tunneling splitting of the singly excited mode is given in parentheses.

θ	$\eta(1,0)$	$\eta(0,1)$
0	1.00000 (1.000)	0.00000 (0.000)
$\pi/12$	0.99998 (0.999)	0.00664 (0.681)
$\pi/6$	0.99989 (0.995)	0.01488 (0.919)
$\pi/4$	0.99962 (0.987)	0.02774 (0.976)

As has been shown previously, the projection η is related to the magnitude of the F contribution in the tunneling matrix element. Even though the projection of the mode (0, 1) at

Table 2. Tunneling splittings in the ground and first two vibrationally excited states for the model potential at various angles θ obtained using instanton theory. Values reported are obtained using either only F term, or full $F + U_\alpha \xi_\alpha$ prefactor. The exact quantum-mechanical results are given in parentheses.

θ	Δ_0	$\Delta_1(1,0)$	$\Delta_1(0,1)$
		$1.830(-8)$	0.000
0	$2.630(-10)$	$1.830(-8)$	$5.026(-10)$
	$(2.639(-10))$	$(1.811(-8))$	$(5.155(-10))$
		$9.870(-9)$	$5.492(-10)$
$\pi/12$	$1.463(-10)$	$9.882(-9)$	$8.066(-10)$
	$(1.472(-10))$	$(9.858(-9))$	$(8.089(-10))$
		$1.563(-9)$	$4.029(-10)$
$\pi/6$	$2.573(-11)$	$1.571(-9)$	$4.383(-10)$
	$(2.599(-11))$	$(1.583(-9))$	$(4.477(-10))$
		$7.729(-11)$	$5.932(-11)$
$\pi/4$	$1.606(-12)$	$7.827(-11)$	$6.077(-11)$
	$(1.620(-12))$	$(7.879(-11))$	$(6.224(-11))$

the distance ε is small, for small values of angle θ, F contribution quickly begins to dominate the tunneling splitting element, with its contribution being over 90% for $\theta > \pi/6$. This result is significant for two reasons. First, it demonstrates that it is necessary to include F term in the tunneling splitting even for small curvatures of the MAP, where it would seem that a separate calculation for the longitudinal and transversal excitations should provide good results. However, as the contribution of F term rises exponentially with respect to the MAP length, it can in fact dominate the magnitude of the splitting. Secondly, as F term is, in essence, obtained by a direct integration of the equation for the w correction function along the MAP, it can be computed for multiple excitations of a normal mode as well. It is then simply

$$F_{(v,0)} = F_{(1,0)}^v. \tag{4.3}$$

Thus, even though the shape of the multiply-excited wavefunction does not match the shape of the corresponding harmonic oscillator function near minima, a large part of the tunneling matrix element may be accounted for using this estimate.

To test the accuracy of the JFI theory for the case of larger zero-point energies, the mass of the system was varied in range $1.0 < m < 27.0$, for a fixed value of angle $\theta = \pi/12$. For each value of the mass, the effective barrier for tunneling was computed, using the following

formulae

$$V_{\text{eff}}^{(0,0)} = V_0 + \frac{1}{2}(\lambda_2 - \omega_1 - \omega_2)$$

$$V_{\text{eff}}^{(1,0)} = V_{\text{eff}}^{(0,0)} - \omega_1 \tag{4.4}$$

$$V_{\text{eff}}^{(0,1)} = V_{\text{eff}}^{(0,0)} - \omega_2 + \lambda_2, \tag{4.5}$$

where V_0 is the potential energy at the center of the MAP, $\omega_{1/2} = \alpha_{1/2}/\sqrt{m}$ are frequencies at minima and λ_2 is the non-zero frequency of the matrix $\bar{\mathbf{A}}$, defined previously. Frequency λ_2 defines the width, and thus the energy of the Gaussian along the direction orthogonal to the MAP at the top of the barrier. As can be seen in Table 3, JFI provides excellent agreement with the quantum-mechanical values in the deep tunneling regime, i.e. when the effective barrier is large. As the effective barrier decreases, JFI method overestimates the tunneling matrix elements. As can be seen in the case of $m = 1.5$, when the effective barrier is approximately zero, tunneling matrix element is overestimated by approximately 60%, while for the negative barriers, i.e. over-the-barrier motion, overestimation is approximately by a factor of 2. Such overestimation is a known feature of instanton method, and has been noticed in the case of acceptor tunneling motion in the water dimer.[101] Thus, results on the model potential indicate that the generalized JFI method for the tunneling matrix elements between excited vibrational states provides excellent agreement with the quantum-mechanical values in the deep-tunneling regime, while it can be used to provide an upper-limit estimate for the case of shallow tunneling or over-the-barrier motion.

Performance of the JFI method for tunneling matrix elements between excited states was also tested on the model potential with four minima connected by asymmetric MAPs. The form of the chosen potential is given by

$$V_1 = \frac{1}{2}\alpha_1^2(x_1 + \beta)^2 + \frac{1}{2}\alpha_2^2(x_2 + \beta)^2,$$

$$V_2 = \frac{1}{2}\alpha_2^2(x_1 - \beta)^2 + \frac{1}{2}\alpha_1^2(x_2 + \beta)^2,$$

$$V_3 = \frac{1}{2}\alpha_1^2(x_1 - \beta)^2 + \frac{1}{2}\alpha_2^2(x_2 - \beta)^2,$$

$$V_4 = \frac{1}{2}\alpha_2^2(x_1 + \beta)^2 + \frac{1}{2}\alpha_1^2(x_2 - \beta)^2,$$

$$V = \frac{V_1 V_2 V_3 V_4}{V_1 V_2 V_3 + V_1 V_2 V_4 + V_1 V_3 V_4 + V_2 V_3 V_4}, \tag{4.6}$$

where x_i are not mass scaled. The parameters were set to $\beta = 2.0$, $\alpha_1 = 1.265$ and $\alpha_2 = 2.0$, while the mass of the system was set at $m = 27.0$. Parameters of the DVR and JFI calculations were set to same values as in the previously described example. Symmetry group for this potential is C_4 and there are two types of MAPs between the minima. First type is the MAP

Table 3. Tunneling splittings in the ground (Δ_0) and first two vibrationally excited states (Δ_1) for the potential at $\theta = \pi/12$ and various masses m obtained using instanton theory. The excited-state splittings are, top to bottom, obtained using the F and $F + U_\alpha \xi_\alpha$ prefactors, respectively. The exact quantum-mechanical results are given in parentheses. For each excitation, the effective barrier heights V_{eff} on the MAP are given.

m	Δ_0	$\Delta_1(1,0)$	$V_{\text{eff}}^{(1,0)}$	$\Delta_1(0,1)$	$V_{\text{eff}}^{(0,1)}$
		9.870(-9)		5.492(-10)	
27.0	1.463(-10)	9.882(-9)	1.273	8.066(-10)	1.428
	(1.472(-10))	(9.858(-9))		(8.089(-10))	
		4.156(-3)		2.312(-4)	
5.0	1.431(-4)	4.168(-3)	0.731	4.831(-4)	1.091
	(1.435(-4))	(3.921(-3))		(4.979(-4))	
		0.214		1.191(-2)	
1.7	1.264(-2)	0.215	0.051	3.416(-2)	0.668
	(1.231(-2))	(0.146)		(3.080(-2))	
		0.297		1.649(-2)	
1.5	1.865(-2)	0.298	-0.055	4.932(-2)	0.603
	(1.802(-2))	(0.188)		(4.157(-2))	
		0.740		0.041	
1.0	5.696(-2)	0.745	-0.445	0.141	0.360
	(5.300(-2))	(0.361)		(0.102)	

that connects minima related with symmetry operator $\hat{C}_4$, while the second connects minima connected with operator $\hat{C}_2$. The latter path is both longer and possesses a larger barrier, making its tunneling matrix elements negligible in comparison with the former ones. From
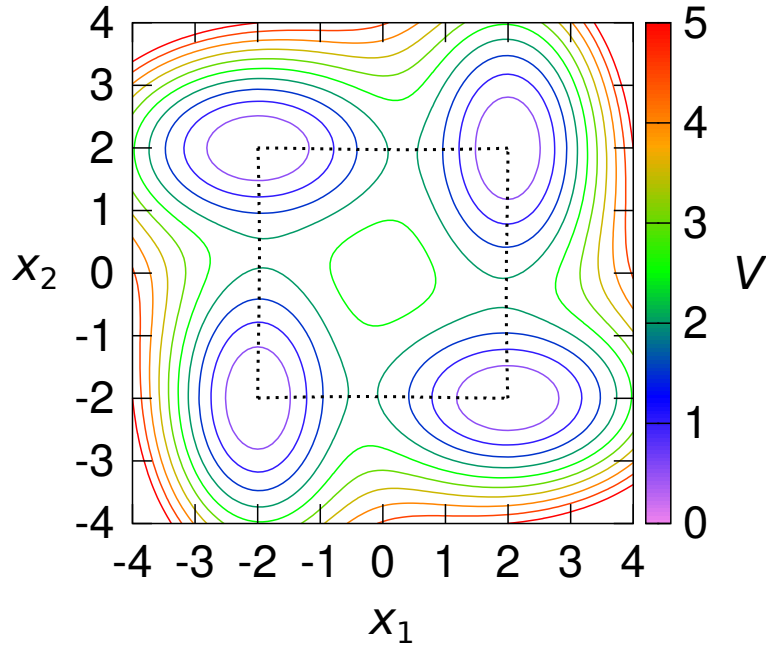
Figure 4. Model PES described by equation (4.6) with MAPs that correspond to significant tunneling matrix elements shown as a dotted black lines.

the shape of MAPs shown on the Figure 5, it appears as if each MAP enters its minima along different normal modes. In reality, MAP enters both minima along the normal mode of lower frequency. However, the curvature of the path near one end is extremely large, resulting in its immediate turn towards the normal mode of higher frequency. Such potential is precisely where the previously known JFI method provides a poor description, as in the case of excited states nodal plane turns immediately as the MAP turns, resulting in a wavefunction whose shape does not match the one of the harmonic oscillator of the well in question. Comparison with the quantum-mechanical results, given in Table 4, shows a good agreement of JFI values with the exact ones, with the ground-state splitting being within 3% of the exact value and the splitting of the lower excited mode being within 25%. The worst agreement is in the splitting of the higher excited mode, which is underestimated by a factor of 2. However, the obtained value is far closer to the exact result than the one that would be obtained with the existing JFI method, which yields splitting $7.9(-13)$, merely 1% of the exact value. The cause for the discrepancies probably lies in the anharmonicity in the plane orthogonal to the MAP, which is neglected in the JFI calculation. This could also explain why the disagreement is larger for the excited mode of higher frequency. In that case wavefunction penetrates deeper into the region where anharmonicity is large.

Table 4. Tunneling splittings in first two vibrationally excited states (Δ_1) for the potential described by equation (4.6) obtained using instanton theory. QM denotes the exact quantum-mechanical results. Displacements, η are given for the left, $(-\beta, -\beta)$, and the right, $(\beta, -\beta)$, minimum. The ground-state splitting obtained using the JFI method is $\Delta_0 = 9.129(-12)$, while the exact result is $\Delta_0 = 8.887(-12)$.

	$\Delta_1(1,0)$	$\Delta_1(0,1)$
	$1.304(-11)$	$2.979(-11)$
instanton	$1.340(-11)$	$3.058(-11)$
QM	$1.775(-11)$	$6.531(-11)$
$\eta^{(\mathrm{L})}$	0.13442	0.99092
$\eta^{(\mathrm{R})}$	1.00000	0.00008

A third type of model potential was used to test JFI method for computation of tunneling

matrix elements in systems with non-symmetry related wells. This potential was given by

$$V(\mathbf{x}) = \frac{\gamma_1 V^{(\mathrm{L})}(\gamma_2 V^{(\mathrm{R})} + d)}{\gamma_1 V^{(\mathrm{L})} + \gamma_2 V^{(\mathrm{R})}},$$

$$V^{(\mathrm{L})}(\mathbf{x}) = \frac{1}{2}\Delta\mathbf{x}^{(\mathrm{L})\top}\mathbf{U}_0^{(\mathrm{L})}\begin{pmatrix} \alpha_{1,\mathrm{L}} & 0 \\ 0 & \alpha_{2,\mathrm{L}} \end{pmatrix}\mathbf{U}_0^{(\mathrm{L})\top}\Delta\mathbf{x}^{(\mathrm{L})},$$

$$V^{(\mathrm{R})}(\mathbf{x}) = \frac{1}{2}\Delta\mathbf{x}^{(\mathrm{R})\top}\mathbf{U}_0^{(\mathrm{R})}\begin{pmatrix} \alpha_{1,\mathrm{R}} & 0 \\ 0 & \alpha_{2,\mathrm{R}} \end{pmatrix}\mathbf{U}_0^{(\mathrm{R})\top}\Delta\mathbf{x}^{(\mathrm{R})},$$

$$\mathbf{U}_0^{(\mathrm{L})} = \begin{pmatrix} \cos\theta & -\sin\theta \\ \sin\theta & \cos\theta \end{pmatrix}, \qquad \mathbf{U}_0^{(\mathrm{R})} = \begin{pmatrix} -\cos\theta & \sin\theta \\ \sin\theta & \cos\theta \end{pmatrix},$$

$$\Delta\mathbf{x}^{(\mathrm{L/R})} = \mathbf{x} - \mathbf{x}^{(\mathrm{L})}, \qquad \mathbf{x}^{(\mathrm{L/R})} = (\pm\beta, 0)^\top,$$

$$\gamma_1 = \frac{1 + \frac{d^2}{V^{(\mathrm{L})}(\mathbf{x}^{(\mathrm{R})})V^{(\mathrm{R})}(\mathbf{x}^{(\mathrm{L})})}}{1 + \frac{d}{V^{(\mathrm{R})}(\mathbf{x}^{(\mathrm{L})})}}, \quad \gamma_2 = \frac{1 + \frac{d^2}{V^{(\mathrm{L})}(\mathbf{x}^{(\mathrm{R})})V^{(\mathrm{R})}(\mathbf{x}^{(\mathrm{L})})}}{1 - \frac{d}{V^{(\mathrm{L})}(\mathbf{x}^{(\mathrm{R})})}}, \tag{4.7}$$

where coordinates x_i are not mass scaled. This potential possesses two minima, near which the surface is approximately harmonic, with force constants $\alpha_{1/2,\mathrm{L/R}}$ and normal modes $\mathbf{U}^{(\mathrm{L/R})}$, all of which are adjustable parameters, similarly to the case of the first model potential considered. Additionally, parameter d can be used to vary the energy at the minimum (R) relative to the minimum (L). This form of the potential was used to study the accuracy of JFI
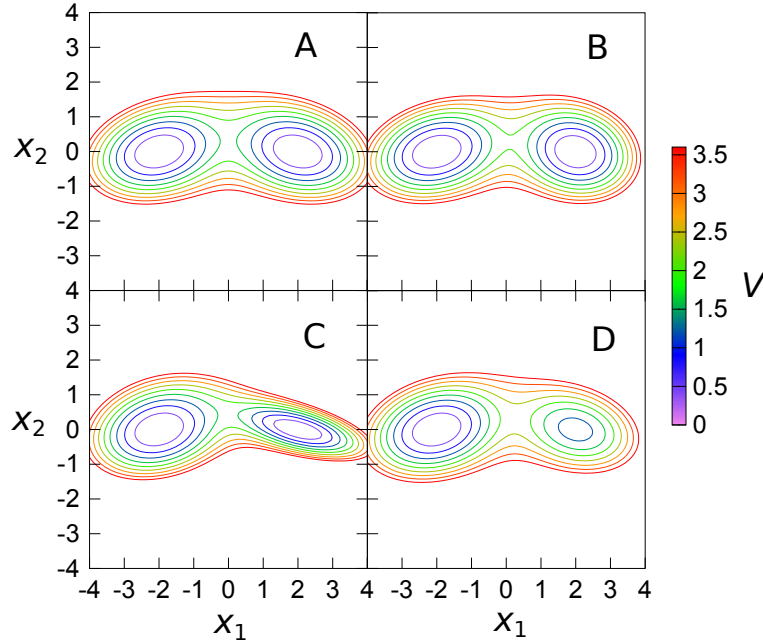
Figure 5. Potential energy surface given by (4.7). Top left panel corresponds to the symmetric potential, top right to $\omega_{1,(\mathrm{R})} > \omega_{1,(\mathrm{L})}$, bottom left to $\omega_{2,(\mathrm{R})} > \omega_{2,(\mathrm{R})}$, and bottom right to $d > 0$, with other parameters set equal to the symmetric case.

theory for the asymmetric systems, with the asymmetry being in either the frequency of one

of the normal modes, or in the difference of the energies of the two minima. The parameters of the potential were set to $\beta = 2.0$, $\theta = \pi/12$, while the mass of the system was taken to be $m = 3.5$ in both dimensions. Furthermore, parameters of minimum (L) were kept constant at values $\alpha_{1,L} = 1.6$, $\alpha_{2,L} = 4.0$. The parameters of minimum (R) were varied, one at a time, with the others being fixed at the same values as in minimum (L). Parameters of the DVR and instanton calculations were the same as in the case of previous model potentials, while in the case of $d \neq 0$, the position of the dividing point was chosen to be on the central bead. Furthermore, to obtain Hamiltonian matrix, energies of the localized states were computed using VCI approach, described previously. Number of Gauss-Hermite DVR points used to fit the potential energy surface was $N_{fit} = 8$, while the order of polynomials used for the fit was $N_{pol} = 8$. For the purpose of VSCF calculation, $N_{basis} = 7$ basis set functions were chosen for each normal mode. VCI calculation was performed with the highest excitation in each mode limited to $N_{exc} = 6$, as described previously.

In the first test, the force constant of the lower mode was varied. The range in which varying was done was chosen to encompass several avoided crossings, up to the one of the ground state of minimum (L) with the excited state of the higher mode in minimum (R) and the results are shown in Figure 6. For symmetric system, it can be seen that JFI method provides excellent agreement of the tunneling splitting with the quantum-mechanical values for the ground state and the excited mode 2. For the excited mode 1 the splitting is slightly overestimated, which is a consequence of a reduction of the effective barrier, caused by the fact that the mode 1 is longitudinal mode. Harmonic approximation overestimates the values of energy levels, while the VCI localized energies provide an excellent agreement with the quantum-mechanical data. As the asymmetry is increased, tunneling splittings obtained with the use of harmonic energies begin to deviate from the exact values, because the neglected anharmonicity in the two minima no longer cancels out. VCI energies, on the other hand, can accurately describe the tunneling splitting for a wide range of asymmetry, even as one approaches the avoided crossing of the excited mode 1 in minimum (R) and excited mode 2 in minimum (L), as shown in Figure 7. Even though the position of the minimum in the gap is slightly underestimated, the value of the splitting is in excellent agreement with the exact one. This indicates that the JFI theory yields an accurate value of the tunneling matrix element, while the error arises from the inaccurate VCI energies of localized states.

Similar results have been obtained for the asymmetry in the mode 2 and with $d > 0$, which is given in Supplement. It is worth noting that in the case of asymmetry imposed by $d > 0$, harmonic energies provide a reasonably good agreement with the exact values. This is a result of the construction of the potential energy surface, which is made so that the two wells have approximately the same shape, which results in a cancellation of errors in the neglected anharmonicity.
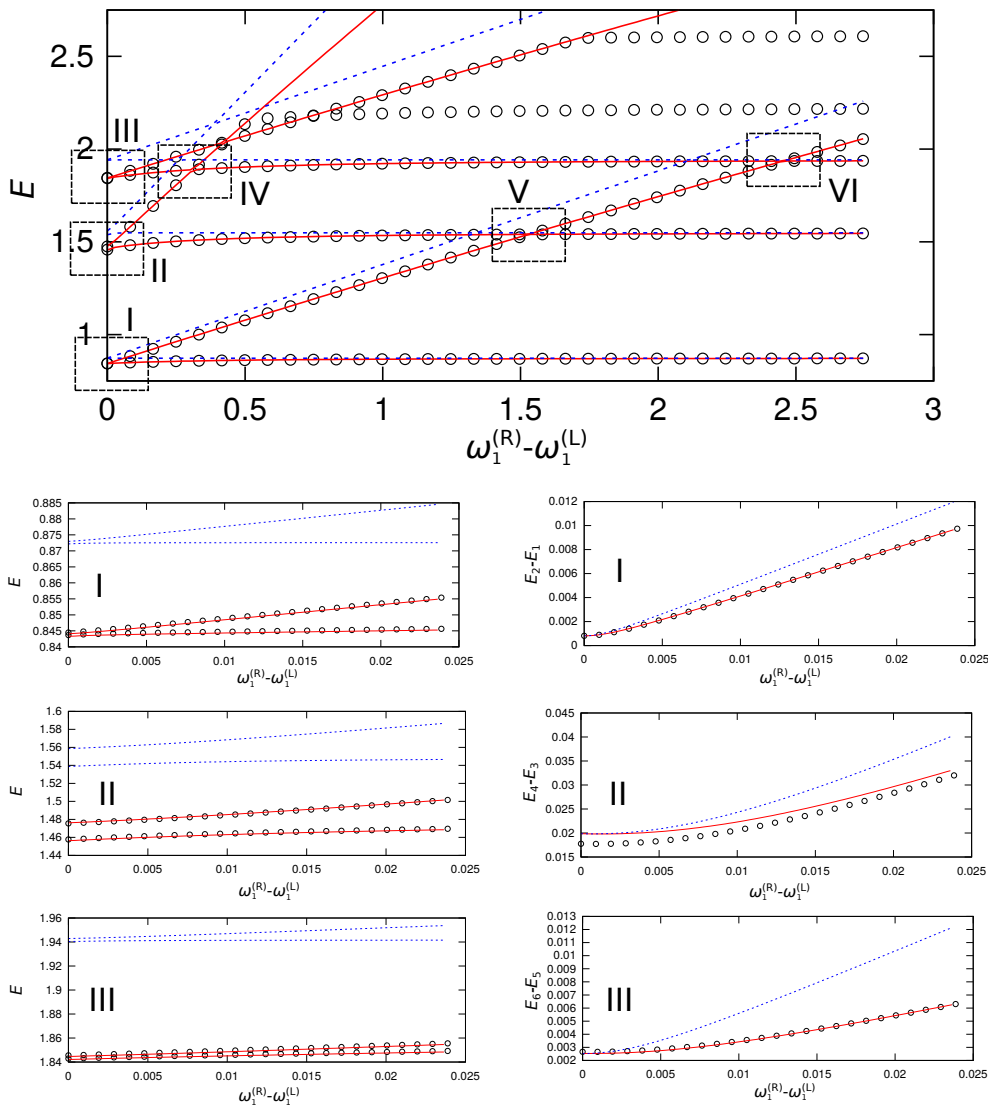
Figure 6. Dependence of vibrational energies of the lowest 6 states in the double-well potential given by equation (4.7) on the frequency of the lower mode $\omega_1^{(R)}$. Circles represent quantum-mechanical values, blue lines are obtained using instanton method with harmonic energies and red lines are obtained using a combined VCI/instanton approach. Frames I-III in the top panel are shown magnified in the left column panels below, and the dependence of the associated tunneling splittings on $\omega_1^{(R)}$ in the right column panels below.
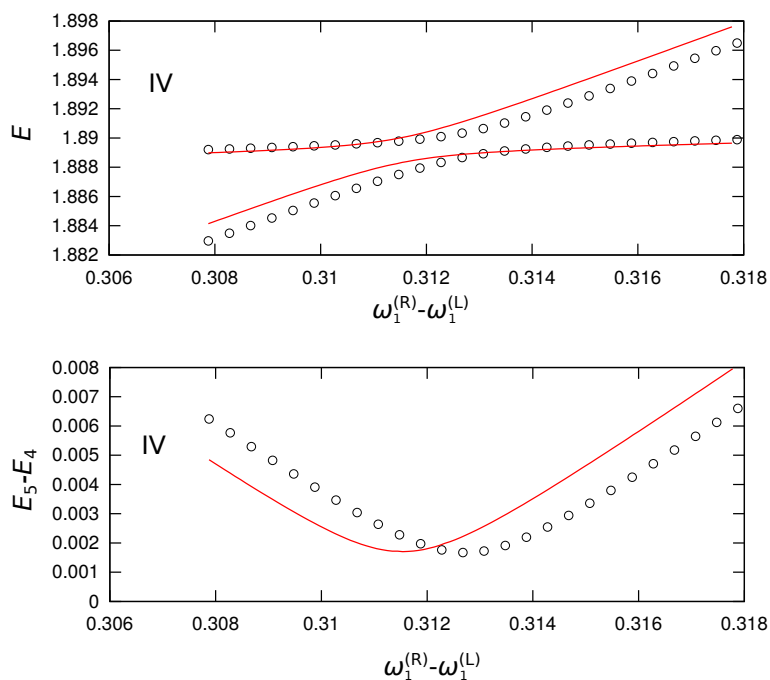
Figure 7. Dependence of vibrational energies and tunneling splittings in the 2D model potential given by equation (4.7) on the frequency $\omega_1^{(R)}$ in the region of the avoided crossing between the first ($\omega_1^{(R)}$-) excited state in minimum (R) and the second ($\omega_2^{(L)}$-) excited state in minimum (L), shown in frame IV in the top panel of Figure 6. Circles represent quantum-mechanical values, while red lines represent values obtained using a combined VCI/instanton approach.

4.2. Malonaldehyde

Malonaldehyde molecule was chosen to test the developed theory, because it has been extensively studied in the past, both using theoretical and experimental methods. For all calculations, the analytic potential energy surface by Wang et al.[10] has been used. JFI was used to compute tunneling splittings for the ground state and singly excited modes $1 - 5$ and $7, 8$, which have also been computed using MCTDH by Hammer et. al.[36] Calculations were performed using 201 beads to ensure convergence of the results, while the initial 'jump' was done at $\varepsilon = 0.25$ a.u. In the first approximation, tunneling splittings were computed by splitting degenerate energy levels of the two minima with the corresponding tunneling matrix elements. This is equivalent to the perturbation theory for degenerate systems. As can be seen in Table 5, the values of the tunneling splittings obtained using JFI method are in good agreement with the MCTDH results for all states except the excited modes 1 and 2. Differences in the values of splittings for other states are within the estimated errors of the MCTDH calculations, as reported by Hammer et al. Overestimation for the excited mode 2 is likely caused by the fact that it is the longitudinal mode for the hydrogen transfer, and that exciting it significantly reduces the effective barrier for the tunneling. Discrepancy in excited mode 1 is likely due to the neglected anharmonicity, which was noticed in both VCI calculations and from the shape of the potential energy along the MAP.

Table 5. Tunneling splittings in the ground-state and select singly excited states obtained using JFI method. Values obtained using MCTDH method are given for reference.

Mode	$\Delta(\text{JFI})/\text{cm}^{-1}$	$\Delta(\text{MCTDH})/\text{cm}^{-1}$
GS	24.60	23.5
1	13.40	6.7
2	88.40	69.9
3	17.06	16.3
4	15.64	18.8
5	24.4	21.1
7	39.5	33.3
8	15.6	14.6

Next, Hamiltonian matrix was constructed using the lowest 4 and 8 localized states in each minimum, for the purpose of testing the effect of adding additional states to the Hamiltonian matrix on the energies and tunneling splittings. These 8 states contain ground state, four singly-excited states, with excitations in modes $1 - 4$, two doubly excited states, in modes 1 and 2, and a combination state with simultaneously excited modes 1 and 2. The modes that were considered are depicted in Figure 8, along with the numbering of atoms. VCI calculations were performed to determine energies of localized states. Number of Gauss-Hermite DVR points used to fit the potential energy surface was $N_{\text{fit}} = 11$, while the order
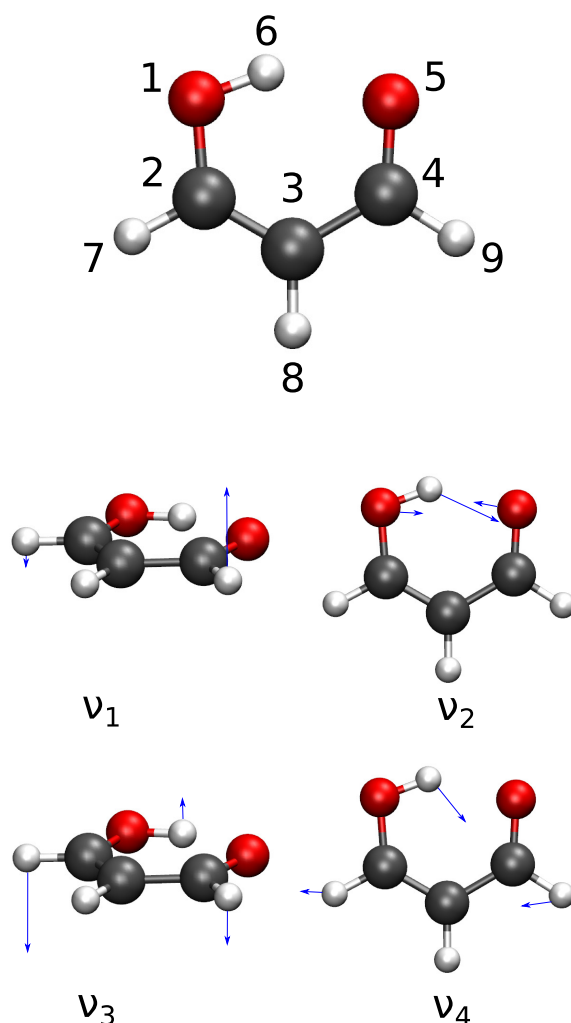
Figure 8. Annotated equilibrium geometry of malonaldehyde and schematic representation of four lowest-frequency normal modes.

of polynomials used for the fit was $N_{pol} = 8$. In the VSCF calculation, $N_{basis} = 16$ was used, which provided converged results. Tunneling matrix elements obtained using JFI method are given in Table 6.

As can be seen from the tunneling matrix elements, only the vibrational states of the same symmetry interact. In the model made from 4 states in each well, a noticeable interaction occurs between ground-state and the excited mode 2, which is a consequence of a relatively large tunneling matrix element, caused by the fact that mode 2 is the longitudinal mode. Energy levels shift by values $1.22 - 1.46 \text{ cm}^{-1}$, while the effect on the tunneling splittings in both states is negligible.

In the model made by considering 8 local states in each well, ground-state and excited mode 2 strongly interact with the doubly-excited mode 2. This interaction also causes a small change in the value of their tunneling splitting, from 24.85 cm^{-1} to 25.68 cm^{-1} and from 88.15 cm^{-1} to 89.4 cm^{-1}. A strong interaction is present between the doubly-excited mode 2

Table 6. Tunneling matrix elements connecting the first 8 localized vibrational states of different minima in malonaldehyde.

	$GS^{(R)}$	$v_1^{(R)}$	$v_2^{(R)}$	$v_3^{(R)}$	$(v_1+v_1)^{(R)}$	$v_4^{(R)}$	$(v_2+v_2)^{(R)}$	$(v_1+v_2)^{(R)}$
$GS^{(L)}$	-12.30	0.00	-21.94	0.00	-4.98	-4.62	-25.53	0.00
$v_1^{(L)}$	0.00	-6.70	0.00	6.85	0.00	0.00	0.00	-11.95
$v_2^{(L)}$	-21.94	0.00	-44.20	0.00	-8.87	-7.54	-55.97	0.00
$v_3^{(L)}$	0.00	6.86	0.00	8.53	0.00	0.00	0.00	12.22
$(v_1+v_1)^{(L)}$	-4.98	0.00	-8.88	0.00	-4.84	-1.87	-9.14	0.00
$v_4^{(L)}$	-4.61	0.00	-7.53	0.00	-1.87	7.82	-8.14	0.00
$(v_2+v_2)^{(L)}$	-25.53	0.00	-55.97	0.00	-9.14	-8.15	-75.86	0.00
$(v_1+v_2)^{(L)}$	0.00	-11.95	0.00	12.22	0.00	0.00	0.00	-21.31

and doubly-excited mode 1 as well. It should be noted that, as these are doubly-excited modes, the magnitude of these elements are only estimates made from the F and $\mathbf{U}$ terms obtained for the singly-excited states. It is interesting to note a relatively large interaction between the excited mode 4 and doubly excited mode 1, which changes the tunneling splitting in the excited mode 4 from 15.64 cm^{-1} to 17.27 cm^{-1}, bringing it closer to the MCTDH value of 18.8 cm^{-1}. Additionally, this interaction causes a component of the singly-excited mode 4 to mix with the doubly-excited state 1, which can be seen from the coefficients of the eigenstate, given in the Supplement. Such mixing might cause an increase in the IR intensity of the doubly-excited state 1. States further above were not taken into consideration, as at those energies the density of states begins to drastically increase, making it difficult to determine a reasonable cut-off.

Finally, the JFI theory was applied to non-symmetry related minima of malonaldehyde molecule in which one hydrogen atom at the position 7/9 is replaced with deuterium. As this atom does not occupy equivalent position in the two minima, zero-point energies differ, which induces asymmetry. This choice of deuteration was made because the particular system has been studied by Jahr et al.[37] using RPI method and experimentally by Baughcum et al.[117] Parameters of JFI and VCI calculations were the same as for the homoisotopic malonaldehyde. From the VCI calculations, it was found that deuteration lowers the localized zero-point energies of both minima. In the case of deuteration at position 7 (D7), zero-point energy drops from 14682.45 cm^{-1} to 13978.19 cm^{-1}, while in the case of deuteration at position 9 (D9), it drops to 14013.04 cm^{-1}. Furthermore, due to a larger mass, all vibrational frequencies decrease, which results in the decrease of the energy of excited states making them more closely spaced. Normal modes are qualitatively similar to the homoisotopic malonaldehyde and are labeled the same. Tunneling matrix elements are also very similar to the homoisotopic case, indicating that the shape of the wavefunction in the barrier is not significantly affected by the asymmetry in this system.

Tunneling matrix elements for partially deuterated malonaldehyde are given in Table

Table 7. Vibrational energy levels of malonaldehyde obtained using a combined VCI/instanton approach. $E^{(\text{pairs})}$, $E^{(4)}$ and $E^{(8)}$ are energies obtained from the 2×2, 8×8 and 16×16 matrix models, respectively. $E^{(\text{MCTDH})}$ are MCTDH energies.[36]

No.	$E^{(\text{pairs})}$	$E^{(4)}$	$E^{(8)}$	$E^{(\text{MCTDH})}$
1	14670.15	14668.69	14667.08	14671.3
2	14694.76	14693.54	14692.76	14694.8
3	14998.31	14999.77	14987.74	14941.5
4	15005.95	15005.60	15005.09	15008.2
5	15019.35	15018.91	15018.54	15014.9
6	15086.70	15087.92	15077.14	15005.4
7	15125.42	15125.86	15125.14	15108.3
8	15142.47	15142.82	15142.04	15124.6
9	15243.00	-	15249.04	-
10	15257.21	-	15263.41	-
11	15266.89	-	15266.12	-
12	15274.07	-	15273.84	15249.6
13	15289.71	-	15291.11	15268.4
14	15314.85	-	15316.14	-
15	15357.47	-	15358.55	-
16	15394.71	-	15407.27	-

Table 8. Vibrational energy levels of partially deuterated malonaldehyde obtained using a combined VCI/instanton approach. $E^{(\text{pairs})}$, $E^{(4)}$ and $E^{(8)}$ are energies obtained from the 2×2, 8×8 and 16×16 matrix models, respectively.

No.	$E^{(\text{pairs})}$	$E^{(4)}$	$E^{(8)}$
1	13974.27	13972.91	13971.48
2	14016.96	14015.52	14014.49
3	14296.86	14298.42	14286.79
4	14295.75	14295.44	14294.91
5	14314.69	14313.95	14313.54
6	14391.55	14392.78	14381.17
7	14383.28	14384.05	14383.32
8	14446.16	14446.45	14445.64
9	14540.00	-	14537.31
10	14549.82	-	14549.32
11	14541.38	-	14556.57
12	14560.53	-	14561.08
13	14597.33	-	14598.21
14	14596.99	-	14598.33
15	14641.54	-	14642.66
16	14696.90	-	14709.18
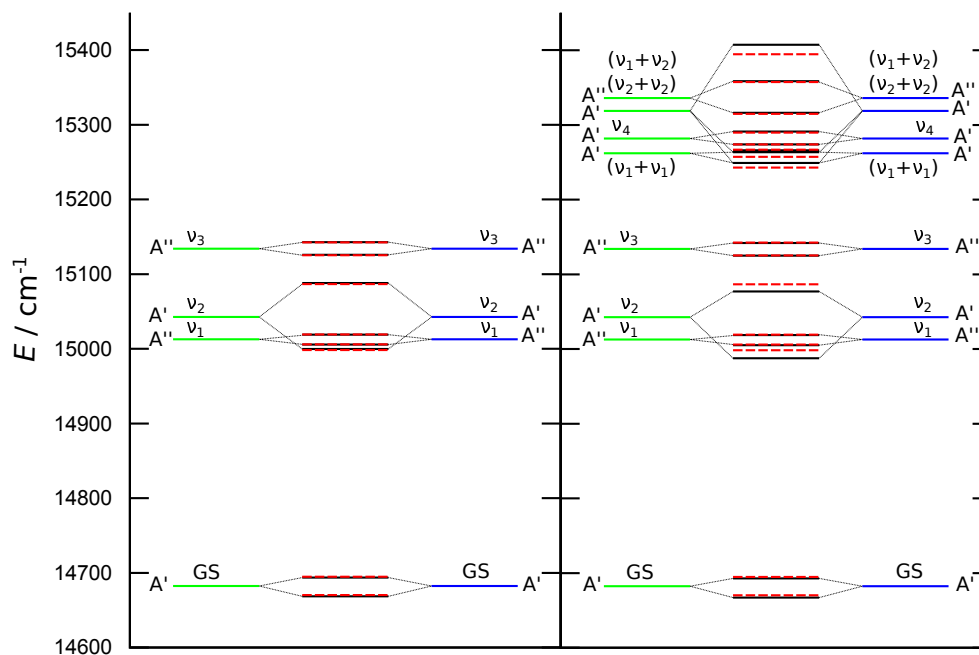
Figure 9. Vibrational tunneling spectrum of the lowest 8 (left panel) and 16 (right panel) states of malonaldehyde. Green and blue lines represent VCI energies of local wavefunctions. Dashed red lines are obtained using a 2×2 model. Black lines in the left panel represent energies from an 8×8 model, and in the right panel, they represent energies from a 16×16 model.

9. It can be seen that in the case of malonaldehyde, estimates of the errors introduced by neglecting the additional term (3.59) accounts for around 1% of tunneling matrix elements value in this case, meaning that it can be safely neglected. The tunneling matrix element for the ground-state, obtained using JFI, is 12.32 cm^{-1}, in close agreement with the RPI value 12.4 cm^{-1}, obtained by Jahr et al.[37] While the RPI method combined with harmonic energies overestimates the mixing angle for the ground-state, providing the value $\phi = 44°$ in comparison with $\phi = 41°$ obtained experimentally by Baughcum et al.,[117] use of VCI energies decreases the mixing angle to $\phi = 35.3°$, indicating that the anharmonicity is indeed important in the calculation of localized energies. Experimental value should be taken with caution, as it was obtained using several approximations. Namely, it was computed from the measured dipole moment, which was fitted to the linear combination of dipole moments of D7 and D9 molecules. As these cannot be measured experimentally, Baughcum et al. approximated them with the dipole moments of the D6D7/9D8 isomer, for which they assume both that the energy difference is sufficiently larger than the tunneling matrix element, making D6D7D8 and D6D9D8 localized and observable molecules, and that their dipole moments are the same.

As can be seen from Table 8 and Figure 10, inclusion of additional states removes the accidental degeneracy between states 3 and 4, while it induces a near-degeneracy between states 6 and 7. Furthermore, in the higher band of excited states, several states $(9 - 12)$ are very close in energy, with a significant mixing being present in the components of their

Table 9. Tunneling matrix elements connecting the first 8 local vibrational states of different minima in partially deuterated malonaldehyde. Values in parentheses refer to the estimated error introduced by the neglect of term (3.59), which is proportional to the overlap between L/R local states

|	$GS^{(D9)}$	$\nu_1^{(D9)}$	$\nu_2^{(D9)}$	$\nu_3^{(D9)}$	$(\nu_1+\nu_1)^{(D9)}$	$\nu_4^{(D9)}$	$(\nu_2+\nu_2)^{(D9)}$	$(\nu_1+\nu_2)^{(D9)}$
$GS^{(D7)}$	−12.32 (0.005)	0.00 (0.00)	−21.95 (0.133)	0.00 (0.00)	−5.04 (0.042)	−4.63 (0.034)	−25.54 (0.343)	0.00 (0.00)
$\nu_1^{(D7)}$	0.00 (0.00)	−6.86 (0.001)	0.00 (0.00)	6.52 (0.014)	0.00 (0.00)	0.00 (0.00)	0.00 (0.00)	−12.22 (0.077)
$\nu_2^{(D7)}$	−21.89 (0.109)	0.00 (0.00)	−44.12 (0.031)	0.00 (0.00)	−8.95 (0.037)	−7.52 (0.029)	−55.89 (0.452)	0.00 (0.00)
$\nu_3^{(D7)}$	0.00 (0.00)	7.37 (0.007)	0.00 (0.00)	8.64 (0.007)	0.00 (0.00)	0.00 (0.00)	0.00 (0.00)	13.14 (0.054)
$(\nu_1+\nu_1)^{(D7)}$	−5.16 (0.042)	0.00 (0.00)	−9.19 (0.034)	0.00 (0.00)	−4.58 (0.000)	−1.94 (0.001)	−9.45 (0.024)	0.00 (0.00)
$\nu_4^{(D7)}$	−4.44 (0.029)	0.00 (0.00)	−7.25 (0.021)	0.00 (0.00)	−1.82 (0.001)	7.97 (0.004)	−7.84 (0.010)	0.00 (0.00)
$(\nu_2+\nu_2)^{(D7)}$	−25.42 (0.304)	0.00 (0.00)	−55.79 (0.349)	0.00 (0.00)	−9.18 (0.015)	−8.10 (0.001)	−75.67 (0.090)	0.00 (0.00)
$(\nu_1+\nu_2)^{(D7)}$	0.00 (0.00)	−12.19 (0.072)	0.00 (0.133)	11.59 (0.037)	0.00 (0.00)	0.00 (0.00)	0.00 (0.00)	−21.72 (0.006)
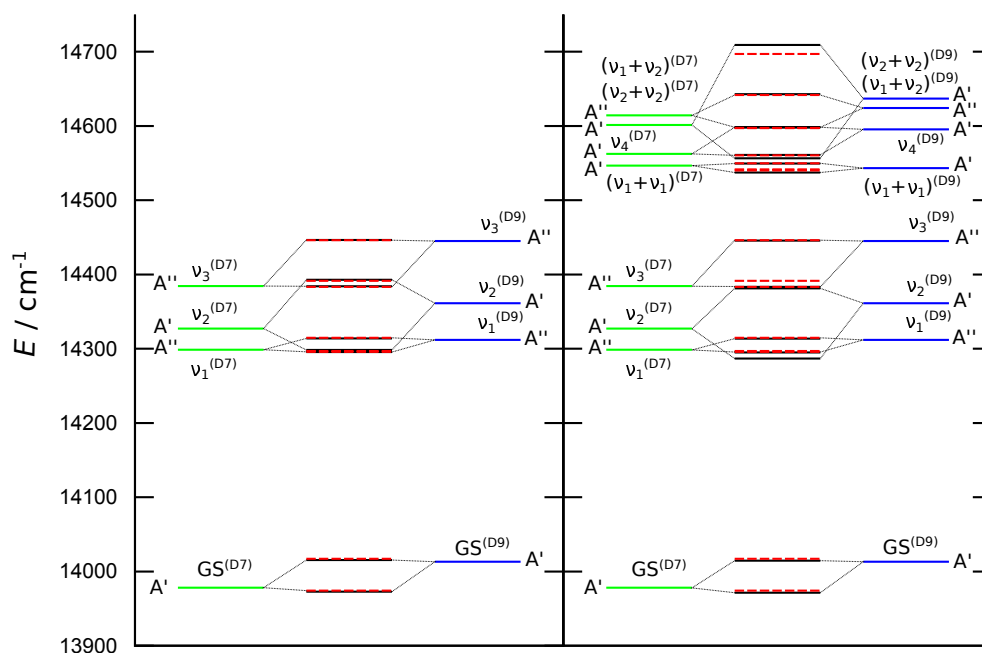
Figure 10. Vibrational tunneling spectrum of the lowest 8 (left panel) and 16 (right panel) states of partially deuterated malonaldehyde. Green and blue lines represent VCI energies of local wavefunctions in the D7 and D9 minima, respectively. Dashed red lines are obtained using a 2×2 model. Black lines in the left panel represent energies from an 8×8 model, and in the right panel, they represent energies from a 16×16 model.

corresponding eigenvectors. As one of those states corresponds to the singly excited mode 4, it is expected that a similar effect of the increase in the IR intensity of transitions to other, doubly-excited states in that range is expected.

4.3. Water Dimer

Water dimer is the smallest water cluster, and as such has been extensively studied using theoretical and experimental methods. RPI calculations have been used to identify 5 different types of MAPs that connect the total of 8 minima that form the molecular symmetry group. Minima that correspond to molecules in which hydrogen atoms are not covalently bonded to the same oxygen atom are assumed not to be connected by a tunneling motion, as MAPs that connect them describe covalent bond breaking, which results in high barriers and negligible tunneling matrix elements. Acceptor tunneling path is known to possess a small barrier for tunneling, resulting in the large tunneling matrix element and overestimation of its value using instanton methods. As vibrational excitation could rise the vibrational energy beyond the barrier height and increase inaccuracy of the calculations, the system that was considered was fully deuterated dimer, $(D_2O)_2$. Due to the larger mass of deuterium, vibrational energies of this dimer are smaller than in the case of homoisotopic dimer, leading to more accurate results. Instanton calculations were made on the MB-pol potential energy surface,[136–138] with the number of beads being $N = 600$, and the initial 'jump' made at $\varepsilon = 0.1$a.u.

Table 10. Tunneling matrix elements for different tunneling pathways in deuterated water dimer $(D_2O)_2$ obtained using instanton theory. Pathways described are acceptor tunneling (AT), geared interchange (GI), antigeared interchange (AI), bifurcation tunneling (BT) and donor exchange (DE). The excited-state splittings are, top to bottom, obtained using the F, and $F + U_i\xi_i$ prefactor, respectively. The splittings given in parentheses are experimental[38] (top) and quantum-mechanical[6] (bottom) results. For the ground state (GS), experimental values[39] are given in parentheses.

Mode	AT	GI	AI	BT	DE
GS	0.766	9.73(−3)	4.88(−4)	1.83(−4)	3.21(−6)
	(0.45)	(9.4(−3))	(3.7(−4))	(2.3(−4))	(−)
1	−11.8	−4.58(−2)	1.86(−2)	1.43(−9)	2.95(−6)
	−11.1	−5.07(−2)	1.83(−2)	−3.96(−5)	1.12(−5)
	(3.953)	(6.643(−2))	(1.561(−2))	(−)	(−)
	(3.92)	(6.63(−2))	(1.63(−2))	(−)	(−)
2	−0.502	−0.256	4.01(−3)	−6.17(−9)	−5.16(−5)
	−0.509	−0.254	4.98(−3)	−2.28(−4)	−4.38(−5)
	(0.634)	(0.109)	(1.375(−3))	(−)	(−)
	(0.758)	(0.140)	(4.25(−2))	(−)	(−)
3	1.15	0.147	2.13(−2)	5.47(−3)	3.27(−6)
	2.72(−2)	0.141	2.13(−2)	5.42(−3)	2.42(−6)
	(0.442)	(3.033(−2))	(2.427(−3))	(−)	(−)
	(0.45)	(2.88(−2))	(1.25(−3))	(−)	(−)
4	19.5	2.94(−2)	2.64(−2)	2.17(−3)	−2.43(−4)
	8.98	3.20(−2)	2.58(−2)	2.41(−3)	−3.70(−4)
	(−)	(−)	(−)	(−)	(−)
	(1.23)	(0.173)	(7.75(−2))	(−)	(−)

Acceptor tunneling (AT) matrix element is overestimated in the ground-state, which is a consequence of a small effective barrier, found to be only $V_{\text{eff}} = 77 \text{ cm}^{-1}$. Upon excitation of mode 1, which corresponds to the longitudinal mode for AT motion, the overestimation is amplified, as the corresponding rearrangement becomes over-the-barrier process. Similar overestimation was noticed for the excitation of mode 4, where it would seem that the change in the zero-point energy results in a reduction of the effective barrier. For the case of the excitation of mode 2, the obtained tunneling matrix element shows good agreement with the experimental value. In case of the excitation of mode 3, an interesting cancellation of contribution from F and $U_i \xi_i$ terms arises, resulting in a poor agreement with experimental value. This disagreement also indicates that the influence of anharmonicity becomes significant in this state, as anharmonic effects seem to account for the majority of the tunneling matrix element.

Geared (GI) and anti-geared (AI) interchange paths possess larger effective barriers in the ground-state, $V_{\text{eff}} = 188 \text{ cm}^{-1}$ and $V_{\text{eff}} = 227 \text{ cm}^{-1}$, respectively. Thus, the values of tunneling matrix elements in the ground-state are in good agreement with the experiment. Similarly, a good agreement is obtained for the case of the excitation of mode 1, with values differing by 24% and 17%, respectively. For the excitations of modes 2 and 3, tunneling matrix elements are overestimated. However, it should be noted that these states lie close in energy, and might interact, resulting in significant changes in the splitting, that are not accounted for in the JFI approach.

Bifurcation tunneling (BT) and donor exchange (DE) paths possess the highest barriers and, correspondingly, the smallest tunneling matrix elements. Due to this fact, their effect on the overall energy pattern is small and either difficult or impossible to measure experimentally. However, JFI theory could be used to compute these elements. It was found that their values increase significantly upon the excitation of mode 4, which could result in potentially observable shifts in future experiments.

4.4. Partially Deuterated Water Trimer

The developed JFI theory was used to compute the splitting pattern of partially deuterated water trimer $D_2O(H_2O)_2$, a system for which no theoretical or experimental results are currently available. Inclusion of one deuterated monomer induces a change in zero-point energies of some of the minima that are symmetry-related in the homoisotopic case. Thus, the selected water trimer possesses three types of minima, each corresponding to different position of the deuterated monomer, as can be seen in Figure 11. Consequently, JFI theory for the non-symmetry related minima must be used to compute the corresponding tunneling matrix elements. JFI calculations were made using MB-pol potential energy surface,[136–138] while the number of beads used for MAP optimizations was $N = 200$ and the value of the

initial 'jump' parameter $\varepsilon = 0.1$ a.u. Due to existence of three types of minima, there are
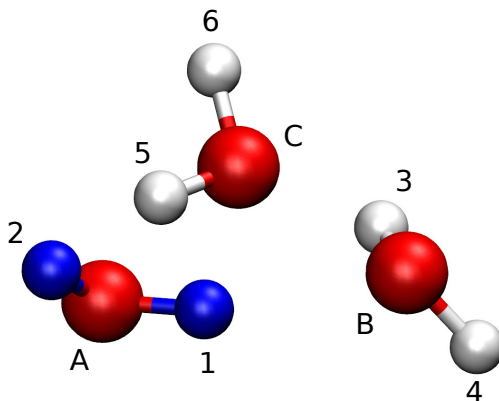
Figure 11. Annotated structure of partially deuterated water trimer at the geometry of one of the minima.

three tunneling matrix elements for each flip and bifurcation motion. MAPs corresponding to all of these motions can be seen in Figure 12. Tunneling matrix elements have been computed for all the MAPs and are given in Table 11, along with the zero-point energies of the three types of minima obtained in a harmonic approximation. It can be seen that the flip matrix elements are much larger than the ones corresponding to bifurcations, same as in the case of homoisotopic trimer.[101]

Flip tunneling matrix elements and zero-point energies can be used to construct a 6×6 flip matrix Hamiltonian, which is of the form

$$\begin{pmatrix} E_{\mathrm{A}} & 0 & 0 & h_{\mathrm{AB}}^{\mathrm{F}} & 0 & h_{\mathrm{AC}}^{\mathrm{F}} \\ 0 & E_{\mathrm{A}} & h_{\mathrm{AB}}^{\mathrm{F}} & 0 & h_{\mathrm{AC}}^{\mathrm{F}} & 0 \\ 0 & h_{\mathrm{AB}}^{\mathrm{F}} & E_{\mathrm{B}} & 0 & 0 & h_{\mathrm{BC}}^{\mathrm{F}} \\ h_{\mathrm{AB}}^{\mathrm{F}} & 0 & 0 & E_{\mathrm{B}} & h_{\mathrm{BC}}^{\mathrm{F}} & 0 \\ 0 & h_{\mathrm{AC}}^{\mathrm{F}} & 0 & h_{\mathrm{BC}}^{\mathrm{F}} & E_{\mathrm{C}} & 0 \\ h_{\mathrm{AC}}^{\mathrm{F}} & 0 & h_{\mathrm{BC}}^{\mathrm{F}} & 0 & 0 & E_{\mathrm{C}} \end{pmatrix}. \tag{4.8}$$

In the case of homoisotopic trimer, where $E_{\mathrm{A}} = E_{\mathrm{B}} = E_{\mathrm{C}}$ and all tunneling matrix elements are equal, eigenvalues of this Hamiltonian can be computed analytically and shown to form a quartet of states $(-2h, -h, h, 2h)$, of which states $\pm h$ are doubly degenerate, with the symmetry of states being described by C_{3h} group. The introduction of a deuterated monomer breaks the symmetry of Hamiltonian and lifts the degeneracies, resulting in a sextet of flip states. Symmetry operation C_3 no longer represents the exact symmetry in this case.

Each flip state is 8-fold degenerate, due to the existence of eight different flip manifolds, which are connected by bifurcations. The inclusion of bifurcation matrix elements results in a 48×48 tunneling matrix, whose eigenvalues correspond to the splitting pattern of the ground

Table 11. Tunnelling matrix elements and zero-point energies for $D_2O(H_2O)_2$ on MB-pol PES. The columns contain numbering, pathway symbol, initial and final structure labeled by the position of deuterated monomer, symbol for the matrix element, and the value of matrix elements in cm^{-1}.

no.	path	i	f	symb.	$D_2O(H_2O)_2$
1	F	A	B	h_{AB}^{F}	-21.0
2	A1	A	C	h_{AC}^{A1}	$-1.49(-3)$
3	A2	A	B	h_{AB}^{A2}	$-6.03(-3)$
4	A3	A	B	h_{AB}^{A3}	$-4.72(-5)$
5	B1	A	A	h_{AA}^{B1}	$-4.48(-3)$
6	B3	A	A	h_{AA}^{B3}	$-1.34(-4)$
7	F	B	C	h_{BC}^{F}	-51.8
8	A1	B	A	h_{BA}^{A1}	$-3.42(-3)$
9	A2	B	C	h_{BC}^{A2}	$-4.63(-3)$
10	A3	B	C	h_{BC}^{A3}	$-2.94(-3)$
11	B1	B	B	h_{BB}^{B1}	$-6.31(-3)$
12	B3	B	B	h_{BB}^{B3}	$-2.94(-3)$
13	F	C	A	h_{CA}^{F}	-46.9
14	A1	C	B	h_{CB}^{A1}	$-4.01(-5)$
15	A2	C	A	h_{CA}^{A2}	$-1.24(-4)$
16	A3	C	A	h_{CA}^{A3}	$-4.13(-3)$
17	B1	C	C	h_{CC}^{B1}	$-1.87(-4)$
18	B3	C	C	h_{CC}^{B3}	$-3.03(-3)$
min.				E_{ZPE}	
A					14598.39
B					14595.16
C					14591.35
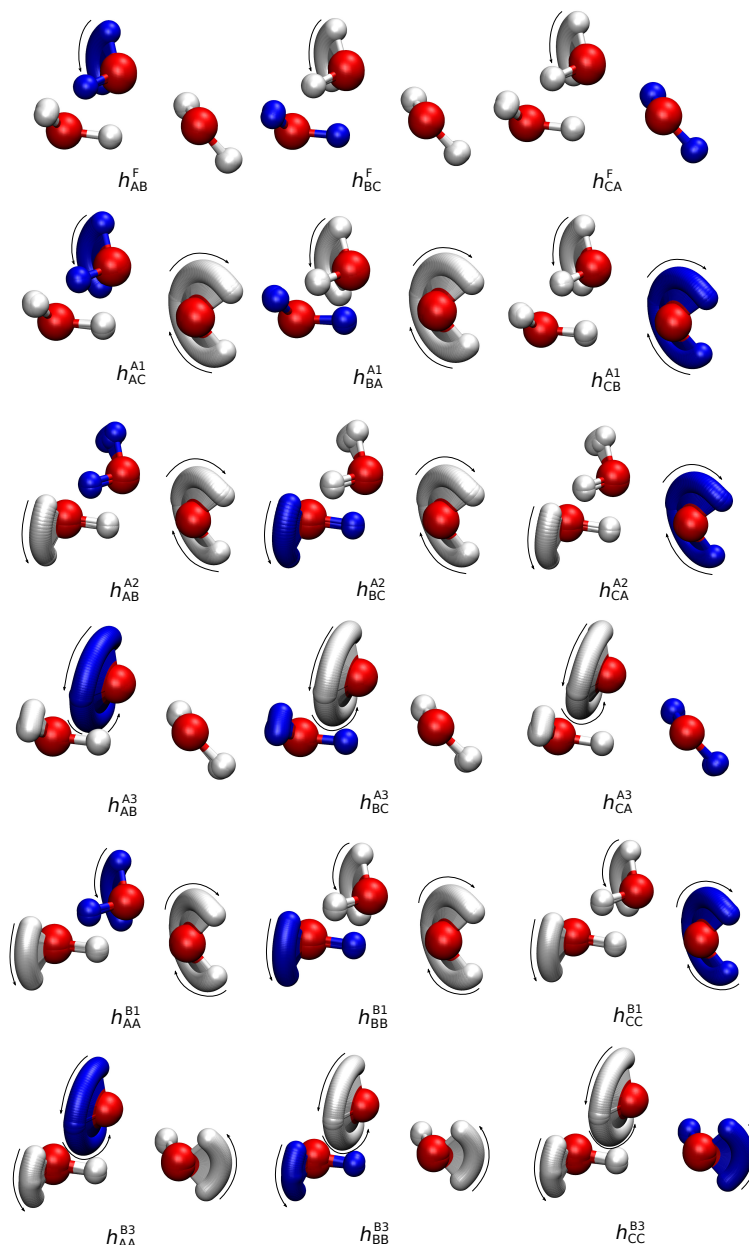
Figure 12. Minimum action paths corresponding to different tunneling motions in the partially deuterated water trimer $D_2O(H_2O)_2$.

vibrational state. The inclusion of bifurcations results in lifting of the degeneracy of each flip state, and produces a splitting pattern presented in Figure 13

Bifurcations of the partially deuterated water trimer were found to form $G_{16} = G_2 \otimes G_2 \otimes G_2 \otimes G_s$, with G_2 groups containing identity and permutation of hydrogens/deuteriums on the same oxygen atom, and C_s containing identity and inversion operation. Character table for this group was constructed and is presented in Supplement. To obtain symmetry labels, representation of localized states, which has character 16 for the identity operator and 0 for all others, was reduced using a known algorithm.[127] Furthermore, decomposition was made for the nuclear spin states as well, resulting in $\Gamma_{\text{nuc}} = 54A_1^+ \oplus 18A_2^+ \oplus 18A_3^+ \oplus 6A_4^+ \oplus 27B_1^+ \oplus$
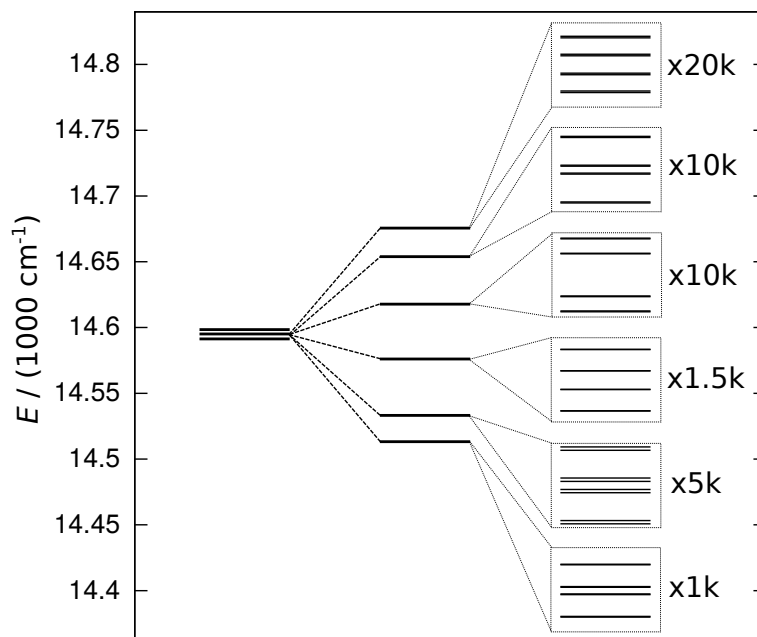
Figure 13. Splitting pattern of the partially deuterated water trimer $D_2O(H_2O)_2$.

$9B_2^+ \oplus 9B_3^+ \oplus 3B_4^+$. Spin weights of all states were found from the fact that overall nuclear wavefunction must belong to $A_4^\pm$ representations, given that protons are identical fermions and deuteriums identical bosons. The weights of the overall vibrational tunneling states thus obtained are $\Gamma_{\text{vib}} = 6A_1^\pm \oplus 18A_2^\pm \oplus 18A_3^\pm \oplus 54A_4^\pm \oplus 3B_1^\pm \oplus 9B_2^\pm \oplus 9B_3^\pm \oplus 27B_4^\pm$. Energy levels with corresponding weights and symmetry labels are given in Supplement.

4.5. Hydroperoxyl Radical

Hydroperoxyl radical was chosen to test the performance of the JFI theory for the calculation of tunneling matrix elements in rotationally excited states. Tunneling motion, which corresponds to migration of the hydrogen atom from one oxygen to the other, results in noticeable changes in the moments of inertia, which indicates a significant influence of rotational excitation on the tunneling splitting. As this radical consists of only three atoms, quantum-mechanical calculations could easily be done to provide the benchmark results. For this purpose, nuclear Hamiltonian was written in terms of Jacobi coordinates. Hamiltonian matrix was constructed for each value of J and divided into two blocks of different parity. Basis set functions were chosen to be potentially optimized DVR for two stretching coordinates, whose functions were obtained from one-dimensional potential energy curve obtained by changing one of the stretching variables, while keeping the other variables the same as in the minimum geometry. For the angular coordinate, Legendre DVR was used. All calculations were done on the DMBE-IV potential energy surface.[139] Instanton calculations were done using $N = 128$ beads with the initial 'jump' parameter $\varepsilon = 0.1$ a.u.. The path obtained, as well as the corresponding potential energy profile, are given in Figure 14.
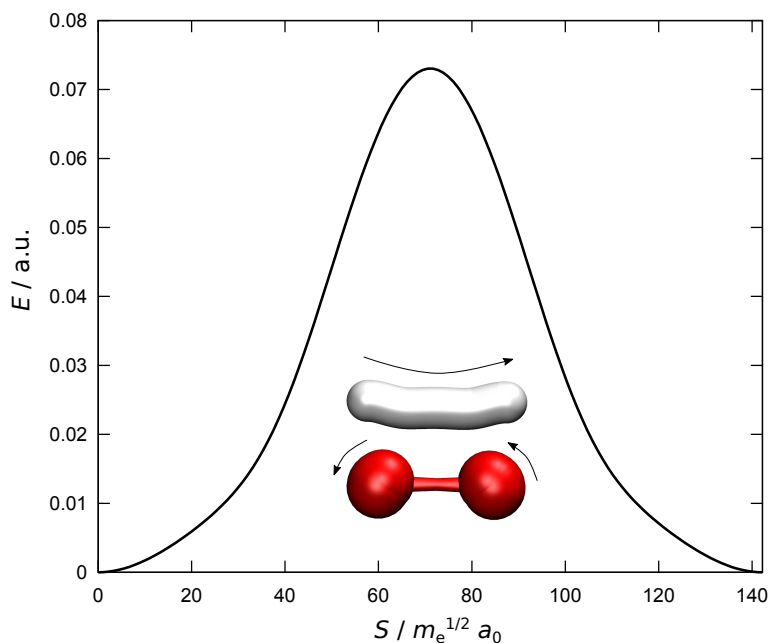
Figure 14. Minimum action path and corresponding potential energy profile for hydroperoxyl radical.
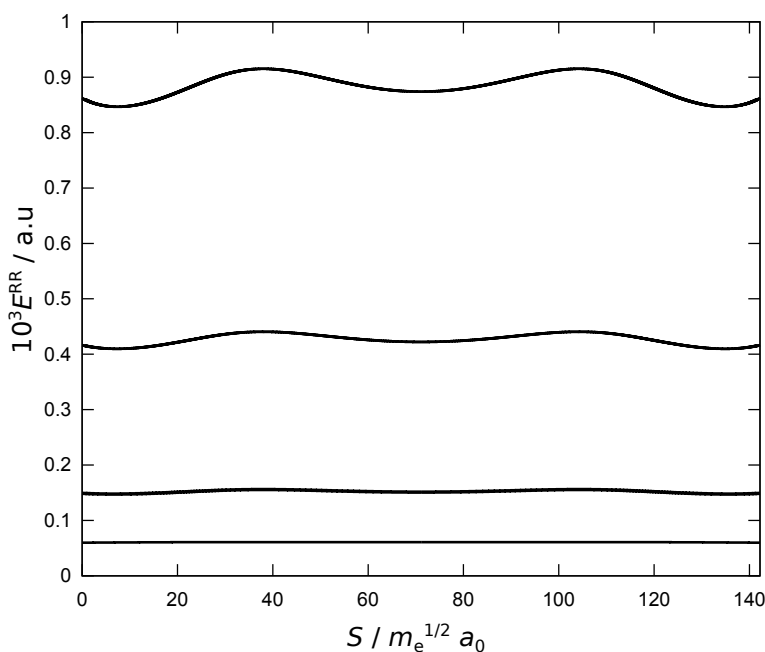
Figure 15. Rigid-rotor energies of hydroperoxyl radical along the MAP for $J = 3$. All lines except the one corresponding to the lowest energy state form closely spaced doublets, due to the similar rotational constants.

Hydroperoxyl radical is an asymmetric top at all points along the MAP. Due to the large masses of oxygen atoms compared to the hydrogen, one principal axis lies closely to the internuclear O-O axis, forming a small angle with it. Thus, hydroperoxyl radical is near the prolate symmetric top limit, and rotational energies form closely spaced doublets, as can be seen in Figure 15. MAP starts along the lowest-frequency mode, which corresponds to the

O-O stretch, in the direction which elongates O-O bond and causes a slight decrease of the rotational energies. This elongation forms a site for the hydrogen atom, which begins to move between the oxygen atoms. Such motion decreases moment of inertia corresponding to the axis resembling the bisector of O-O bond, which causes an increase in rotational energies. Finally, at the top of the barrier, hydrogen atom slightly moves toward the O-O moiety, causing a final decrease in rotational energies. As can be seen in Figure 14, O-O moiety rotates along the MAP, resulting in the rotation of principal axes between the two minima.

As can be seen from the results present in the Table 12, increase in the rotational quantum number J causes a small decrease of the tunneling splitting. This decrease becomes more prominent for larger values of J. It can also be noted that the change in rotational energy, which is accounted for using the adiabatic rotation approximation, has a virtually negligible effect on the tunneling matrix elements, which is well within the error of the JFI method. Such behaviour could be expected, as the magnitude of changes in rotational energies is less than 1% of the potential energy barrier. On the other hand, it can be seen that the change in principal axes between the two minima accounts for entire effect of rotational excitation on tunneling splitting. Thus, one can conclude that the non-adiabatic effects on the rotational states are entirely responsible for the changes in tunneling splitting. Furthermore, the correct relative orientation of one minimum with respect to the other, that accounts for the change in the splitting, is dictated by the MAP, a fact that can be used to model the coupling terms that are measured in high-resolution microwave experiments. Additionally, it is expected that the effects of rotational excitation are significant only in small molecules, in which tunneling motion causes significant changes in the orientation of principal axes, such as water dimer, HF dimer, hydroperoxyl radical, etc., while the effect in larger molecules, such as malonaldehyde and larger water clusters, becomes less significant.

Table 12. Tunneling splittings of hydroperoxyl radical in several rotational states relative to the splitting in $J = 0$. Given values correspond to the ones obtained using adiabatic rotation approximation (ARA) and considering changes of principal axes (PA). Quantum-mechanical value at $J = 0$ is $\Delta_{J=0} = 8.13(-13)$ eV, while the JFI value is $\Delta_{J=0} = 9.56(-13)$ eV

J	$\Delta(\text{QM})/\Delta_{J=0}(\text{QM})$	$\Delta(\text{ARA})/\Delta_{J=0}(\text{JFI})$	$\Delta(\text{PA})/\Delta_{J=0}(\text{JFI})$
	0.976	0.9999	0.976
1	0.977	0.9994	0.976
	1.000	0.9994	1.000
	0.931	0.9996	0.930
	0.903	0.9991	0.907
2	0.979	0.9991	0.976
	0.975	0.998	0.976
	0.977	0.998	0.977
	0.860	0.9992	0.862
	0.810	0.9987	0.806
	0.943	0.9987	0.942
3	0.908	0.997	0.907
	0.907	0.997	0.909
	0.964	0.995	0.965
	0.962	0.995	0.965

§ 5.   CONCLUSION

The aim of this doctoral thesis was the development of new methods for computation of split rovibrational energy levels in systems with multiple minima. For this purpose, several improvements of the efficient Jacobi field instanton theory have been developed, which is drastically more efficient than exact quantum-mechanical methods. The method is based on locating minimum action paths on the inverted potential energy surface, which connect two minima whose localized states interact via tunneling. To compute tunneling matrix elements using this method, it is necessary to compute only the minimum action path and a small number of potential energy Hessians along it, making it numerically efficient. The improvements made in this dissertation resulted in a method that can be used to compute tunneling matrix elements for systems with asymmetric minimum action paths, both in the ground and excited vibrational states. Additionally, the method was extended to compute tunneling matrix elements between vibrational states with different excitations, or states corresponding to two non-symmetry related minima. As a result, Jacobi field instanton method can now be used to compute energy levels of systems with an arbitrary number of potential energy wells, at a significantly reduced computational cost in comparison with quantum-mechanical methods. Finally, an approximate method for the inclusion of the effects of rotational excitation on the tunneling matrix elements has also been considered.

The generalization to treat systems with asymmetric minimum action paths was found by considering propagation of objects used in the Jacobi field theory from both minima to a connection point on the path, in contrast to the propagation of a single object from one minimum to the center. Additionally, it was proven that the choice of this connection point does not influence the values obtained. Generalization of the method to the excited vibrational states was made by considering a common form of the pre-exponential factor for the excited-state wavefunctions, instead of making a distinction between longitudinal and transversal excitations. The method thus obtained provides a good matching between the approximate wavefunction used and the harmonic oscillator wavefunction near minima, giving a consistent method. These generalizations were tested on a set of model potentials, tailored to examine the importance of the new factors that were added and test the limits of its applicability. It was found that the method yields results that are in good agreement with the quantum-mechanical values in the deep tunneling regime, while it tends to overestimate the tunneling matrix elements in the case of shallow tunneling or over-the-barrier processes. Furthermore, the method was tested on selected molecular systems, malonaldehyde, a relatively rigid molecule, with the exception of tunneling motion, and water dimer, a flexible molecular complex.

The results obtained for the malonaldehyde were found to be in excellent agreement with both quantum-mechanical results and the experiment, while the results for the flexible and anharmonic water dimer were either in good agreement with the experiment, or of the same order of magnitude in the worst cases.

The generalization of Jacobi field instanton method to systems with non-symmetry related minima was made by demonstrating that the approximate wavefunctions that appear in this method can be used to construct inter-well matrix elements of the molecular Hamiltonian in the basis of localized states. Diagonal matrix elements were approximated either by harmonic energies or with energies obtained using vibrational configuration interaction on a single potential energy well. This combined approach yields good vibrational energies of the system at the cost of an instanton calculation, if harmonic energies are used, or a single-well vibrational configuration interaction calculation. The method was tested on a specially tailored model potential and the results were obtained for different types of induced asymmetry. It was found that the instanton/VCI combination performs extremely well for a wide range of asymmetries, and can even be used to describe splitting in the resonances of different vibrational states of two potential energy wells. This method was used to compute ground-state splitting pattern in the partially deuterated water trimer and lowest 16 energy levels of partially deuterated malonaldehyde molecule, which are the first calculations on these systems to date.

Finally, an attempt was made to include effects of rotational excitation by considering change in the rotational energy along the minimum action path under the adiabatic rotation approximation. The method obtained was tested on the hydroperoxyl radical and was found to give a good prediction of the decrease in the values of tunneling splitting for higher rotational states, but underestimates the magnitude of this change. However, it was found that the majority of the effects of rotational motion are accounted for in the change of the principal axes system along the instanton path. Thus, a good treatment of the rotational excitations was found by expanding the tunneling matrix into block form corresponding to a rotational manifold of interest, taking into account different orientations of minima.

The developed method can be used to to gain valuable information on tunneling rearrangements in systems with multiple minima, such as water clusters, in full dimensionality. Due to the generalizations made, it is now possible to investigate effects of vibrational excitations, and thus the change in temperature, on these motions. Furthermore, as systems with non-symmetry-related minima can be treated with the developed method, it is possible to study the effects of heavier isotopes in the system. Additionally, it can be used to study tunneling in molecules adsorbed on surfaces or in cavities of materials, which can induce asymmetry between different minima. Due to the efficiency of the method and relatively small number of potential energy gradient and Hessian evaluations needed, it is possible to use on-the-fly

ab initio electronic structure calculations, which extends the number of systems that can be studied.

§ 6. LIST OF ABBREVIATIONS

Kratica	Pojam
AI	Antigeared interchange
ARA	Adiabatic rotation approximation
AT	Acceptor tunneling
BT	Bifurcation tunneling
CMD	Centroid molecular dynamics
CMF	Central mean-field
CNPI	Complete nuclear permutation-inversion symmetry group
DE	Donor exchange
DMC	Diffusion Monte Carlo
DMRG	Density matrix renormalization group
DVR	Discrete variable representation
GI	Geared interchange
HRMS	High-resolution microwave spectroscopy
IR	infra-red
JFI	Jacobi Field instanton
L-BFGS	Limited-memory Broyden-Fletcher-Goldfarb-Shanno
MAP	Minimum action path
MD	Molecular dynamics
MCTDH	Multiconfigurational time-dependent Hartree
MEP	Minimum energy path
PA	Principal axes
PES	Potential energy surface
PIMD	Path integral molecular dynamics
PODVR	Potential-optimized discrete variable representation
RPI	Ring-polymer instanton
RPMD	Ring-polymer molecular dynamics
TTNS	Tree tensor network states
VCI	Vibrational configuration interaction
VCISD	Vibrational configuration interaction with single and double excitations
VSCF	Vibrational self-consistent field

Kratica	Pojam
WKB	Wentzel-Kramers-Brillouin

§ 7. REFERENCES

1. F. Hund, *Zs. f. Physik* **43** (1927) 805–826.

2. R. P. Bell, *The Tunnel Effect in Chemistry*. Chapman and Hall, 1980.

3. F. N. Keutsch and R. J. Saykally, *P. Natl. Acad. Sci. USA* **98** (2001) 10533–10540.

4. U. Manthe, H.-D. Meyer, and L. S. Cederbaum, *J. Chem. Phys.* **97** (1992) 3199–3213.

5. Q. Wu, D. H. Zhang, and J. Z. H. Zhang, *J. Chem. Phys.* **103** (1995) 2548–2554.

6. C. Leforestier, K. Szalewicz, and A. van der Avoird, *J. Chem. Phys.* **137** (2012) 014305.

7. H.-G. Yu, H. Song, and M. Yang, *J. Chem. Phys.* **146** (2017) 224307.

8. T. Hammer, M. D. Coutinho-Neto, A. Viel, and U. Manthe, *J. Chem. Phys.* **131** (2009) 224109.

9. D. Blume and K. B. Whaley, *J. Chem. Phys.* **112** (2000) 2218–2226.

10. Y. Wang, B. J. Braams, J. M. Bowman, S. Carter, and D. P. Tew, *J. Chem. Phys.* **128** (2008) 224314.

11. S. Haberson, D. E. Manolopoulos, T. E. Markland, and T. F. Miller, *Annu. Rev. Phys. Chem.* **64** (2013) 387–413.

12. V. A. Benderskii, D. E. Makarov, and C. A. Wight, "Chemical Dynamics at Low Temperatures". *Advances in Chemical Physics, Vol. 88*. John Wiley & Sons, Inc., 1994.

13. J. O. Richardson and S. C. Althorpe, *J. Chem. Phys.* **134** (2011) 054109.

14. G. V. Mil'nikov and H. Nakamura, *J. Chem. Phys.* **115** (2001) 6881–6897.

15. G. V. Mil'nikov and H. Nakamura, *J. Chem. Phys.* **122** (2005) 124311.

16. G. V. Mil'nikov, O. Kühn, and H. Nakamura, *J. Chem. Phys.* **123** (2005) 074308.

17. W. Ritz, *J. Reine Angew. Math.* **135** (1909) 1–61.

18. B. A. Finlayson, *The Method of Weighted Residuals and Variational Principles*. SIAM-Society for Industrial and Applied Mathematics, 2014.

19. G. Avila and T. Carrington, *J. Chem. Phys.* **135** (2011) 064101.

20. A. Baiardi, C. J. Stein, V. Barone, and M. Reiher, *J. Chem. Phys.* **13** (2017) 3764–3777.

21. J. C. Light and T. Carrington, "Discrete-variable representations and their utilization". *Advances in Chemical Physics, Vol. 114*. John Wiley & Sons, Inc., 2000, pp. 263–310.

22. D. Heidrich, *The Reaction Path in Chemistry: Current Approaches and Perspectives*. Kluwer Academic, 1995.

23. M. A. Suhm and R. O. Watts, *Phys. Rep.* **204** (1991) 293–329.

24. M. H. Beck, A. Jackle, G. A. Worth, and H.-D. Meyer, *Phys. Rep.* **324** (2000) 1–105.

25. P. A. M. Dirac, *Phys. Z. Sowjetunion* **3** (1933) 64–72.

26. R. P. Feynman, *Rev. Mod. Phys.* **20** (1948) 367–387.

27. H. Kleinert, *Path Integrals in Quantum Mechanics, Statistics, Polymer Physics, and Financial Markets 3. ed.* World Scientific, 2004.

28. L. S. Schulman, *Techniques and Applications of Path Integration.* John Wiley & Sons, 1981.

29. D. Chandler and P. G. Wolynes, *J. Chem. Phys.* **74** (1981) 4078–4095.

30. E. Mátyus and S. C. Althorpe, *J. Chem. Phys.* **144** (2016) 114109.

31. E. Mátyus, D. J. Wales, and S. C. Althorpe, *J. Chem. Phys.* **144** (2016) 114108.

32. C. Herring, *Rev. Mod. Phys.* **34** (1962) 631–645.

33. A. Garg, *Am. J. Phys.* **68** (2000) 430–437.

34. S. Carter, J. M. Bowman, and N. C. Handy, *Theor. Chim. Acta* **100** (1998) 191–198.

35. K. M. Christoffel and J. M. Bowman, *Chem. Phys. Lett.* **85** (1998) 220–224.

36. T. Hammer and U. Manthe, *J. Chem. Phys.* **136** (2012) 054105.

37. E. Jahr, G. Laude, and J. O. Richardson, *J. Chem. Phys.* **153** (2020) 094101.

38. L. B. Braly, J. D. Cruzan, K. Liu, R. S. Fellers, and R. J. Saykally, *J. Chem. Phys.* **112** (2000) 10293–10313.

39. E. N. Karyakin, G. T. Fraser, and R. D. Suenram, *Mol. Phys.* **78** (1993) 1179–1189.

40. X.-G. Wang and T. Carrington, *J. Chem. Phys.* **148** (2018) 074108.

41. P. M. Felker and Z. Bačić, *J. Chem. Phys.* **151** (2019) 024305.

42. C. Šmydke, J. Fábri, and A. G. Császár, *Phys. Chem. Chem. Phys.* **21** (2019) 3453–3472.

43. A. Viel, M. D. Coutinho-Neto, and U. Manthe, *J. Chem. Phys.* **126** (2007) 024308.

44. L. N. Trefethen and I. Bau D, *Numerical Linear Algebra.* SIAM-Society for Industrial and Applied Mathematics, 1997.

45. W. Yang and A. C. Peet, *Chem. Phys. Lett.* **153** (1988) 98–104.

46. A. C. Peet and W. Yang, *J. Chem. Phys.* **90** (1989) 1746–1751.

47. M. Abramowitz and I. A. Stegun, *Handbook of Mathematical Functions.* 10th ed. NBS, 1972.

48. A. S. Dickinson and P. R. Certain, *J. Chem. Phys.* **49** (1968) 4209–4211.

49. J. Echave and D. C. Clary, *Chem. Phys. Lett.* **190** (1992) 225–230.

50. A. Nauts and D. Lauvergnat, *Mol. Phys.* **116** (2018) 3701–3709.

51. D. Lauvergnat, E. Baloitcha, G. Dive, and M. Desouter-Lecomte, *Chem. Phys.* **326** (2006) 500–508.

52. H. S. Lee and J. C. Light, *J. Chem. Phys.* **118** (2003) 3458–3469.

53. H. Larsson, *J. Chem. Phys.* **151** (2019) 204102.

54. K. Giese, H. Petković, and O. Kühn, *Phys. Rep.* **430** (2006) 211–276.

55. J. O. Richardson, *Phys. Chem. Chem. Phys.* **19** (2017) 966–970.

56. J. Huang, D. Yang, Y. Zhou, and D. Xie, *J. Chem. Phys.* **150** (2019) 154302.

57. D. H. Zhang, Q. Wu, J. Z. H. Zhang, M. von Dirke, and Z. Bačić, *J. Chem. Phys.* **102** (1995) 2315–2325.

58. H. Chen and J. C. Light, *J. Chem. Phys.* **110** (1999) 168–176.

59. C. Leforestier, L. B. Braly, K. Liu, M. J. Elrod, and R. J. Saykally, *J. Chem. Phys.* **106** (1997) 8527–8544.

60. C. Leforestier, R. van Harrevelt, and A. van der Avoird, *J. Phys. Chem. A* **113** (2009) 12285–12294.

61. A. Fick, *Annalen der Physik und Chemie* **170** (1855) 59–86.

62. J. B. Anderson, *J. Chem. Phys.* **63** (1975) 1499–1503.

63. M. H. Kalos, D. Levesque, and L. Verlet, *Phys. Rev. A* **9** (1974) 2178–2195.

64. J. B. Anderson, *J. Chem. Phys.* **73** (1980) 3897–3899.

65. J. B. Anderson and B. H. Freihaut, *J. Comp. Phys.* **31** (1979) 425–437.

66. D. Blume, M. Lewerenz, P. Niyaz, and K. B. Whaley, *Phys. Rev. E* **55** (1997) 3664–3675.

67. J. K. Gregory and D. C. Clary, *J. Chem. Phys.* **102** (1995) 7817–7829.

68. M. Quack and M. A. Suhm, *Chem. Phys. Lett.* **234** (1995) 71–76.

69. U. Manthe, H.-D. Meyer, and L. S. Cederbaum, *J. Chem. Phys.* **97** (1992) 9062–9071.

70. U. Manthe and A. D. Hammerich, *Chem. Phys. Lett.* **211** (1993) 7–14.

71. P. A. M. Dirac, *Proc. Cambridge Philos. Soc.* **26** (1930) 376–385.

72. A. Raab, *Chem. Phys. Lett.* **319** (2000) 674–678.

73. W. H. Press, S. A. Teukolsky, W. T. Vetterling, and B. P. Flannery, *Numerical Recipes in Fortran 77: The Art of Scientific Computing, Second Edition*. Cambridge University Press, 1992.

74. T. J. Park and J. C. Light, *J. Chem. Phys.* **85** (1986) 5870–5876.

75. H. Tal-Ezer and R. Kosloff, *J. Chem. Phys.* **81** (1984) 3967–3971.

76. C. Lanczos, *J. Res. Natl. Bur. Stand.* **45** (1950) 255–282.

77. U. Manthe and F. Matzkies, *Chem. Phys. Lett.* **252** (1996) 71–76.

78. U. Manthe, *J. Chem. Phys.* **128** (2008) 064108.

79. H.-D. Meyer and S. Pal, *J. Chem. Phys.* **91** (1989) 6195–6204.

80. U. Manthe, *J. Chem. Phys.* **128** (2008) 164116.

81. G. Worth and I. Burghardt, *Chem. Phys. Lett.* **368** (2003) 502–508.

82. H. Goldstein, C. P. Poole, and J. L. Safko, *Classical Mechanics, Third Edition*. Addison Wesley, 2001.

83. H. Duru and H. Kleinert, *Phys. Lett. B* **84** (1979) 185–188.

84. H. Duru and H. Kleinert, *Fortschr. d. Phys.* **30** (1982) 401–435.

85. R. P. Feynman, A. R. Hibbs, and D. F. Styer, *Quantum Mechanics and Path Integrals, Emended ed.* Dover Publications, 2017.

86. D. M. Ceperley and G. Jacucci, *Phys. Rev. Lett.* **58** (1987) 1648–1651.

87. G. C. Wick, *Phys. Rev.* **96** (1954) 1124–1134.

88. R. W. Hall and B. J. Berne, *J. Chem. Phys.* **81** (1984) 3641–3643.

89. D. Scharf, J. Jortner, and U. Landman, *Chem. Phys. Lett.* **130** (1986) 504–510.

90. M. Shiga and W. Shinoda, *J. Chem. Phys.* **123** (2005) 134502.

91. V. Kapil, J. Wieme, S. Vandenbrande, A. Lamaire, V. Van Speybroeck, and M. Ceriotti, *J. Chem. Theory Comput.* **15** (2019) 3237–3249.

92. M. Sugimoto, M. Shiga, and M. Tachikawa, *Comput. Theor. Chem.* **975** (2011) 31–37.

93. C. P. Herrero and R. Ramirez, *Phys. Rev. B* **97** (2018) 195433.

94. I. R. Craig and D. E. Manolopoulos, *J. Chem. Phys.* **121** (2004) 3368–3373.

95. J. S. Cao and G. A. Voth, *J. Chem. Phys.* **100** (1994) 5093–5105.

96. J. S. Cao and G. A. Voth, *J. Chem. Phys.* **100** (1994) 5106–5117.

97. J. S. Cao and G. A. Voth, *J. Chem. Phys.* **101** (1994) 6157–6167.

98. S. Jang and G. A. Voth, *J. Chem. Phys.* **111** (1999) 2371–2384.

99. T. J. H. Hele, M. J. Willatt, A. Muolo, and S. C. Althorpe, *J. Chem. Phys.* **142** (2015) 134103.

100. W. Mizukami, S. Habershon, and D. P. Tew, *J. Chem. Phys.* **141** (2014) 144310.

101. J. O. Richardson, S. C. Althorpe, and D. J. Wales, *J. Chem. Phys.* **135** (2011) 124109.

102. C. Zhu, R. H. Byrd, and P. Lu, *J. ACM. Trans. Math.* **23** (1997) 550–560.

103. M. Erakovic, C. L. Vaillant, and M. T. Cvitas, *J. Chem. Phys.* **152** (2020) 084111.

104. M. T. Cvitas and S. C. Althorpe, *J. Chem. Theory Comput.* **12** (2016) 787–803.

105. I. M. Gel'fand and A. M. Yaglom, *J. Math. Phys.* **1** (1960) 48–69.

106. G. J. Papadopoulos, *Phys. Rev. D* **11** (1975) 2870–2875.

107. T. Baba, T. Tanaka, I. Morino, K. M. T. Yamada, and K. Tanaka, *J. Chem. Phys.* **110** (1999) 4131–4133.

108. L. Evangelisti, P. Écija, E. J. Cocinero, F. Castaño, A. Lesarri, W. Caminati, and R. Meyer, *J. Phys. Chem. Lett.* **3** (2012) 3770–3775.

109. K. Tanaka, H. Honjo, T. Tanaka, H. Kohguchi, Y. Ohshima, and Y. Endo, *J. Chem. Phys.* **110** (1999) 1969–1978.

110. W. Li, L. Evangelisti, Q. Gou, W. Caminati, and R. Meyer, *Angew. Chem. Int. Ed.* **58** (2019) 859–865.

111. H. M. Pickett, *J. Mol. Spectrosc.* **148** (1991) 371–377.

112. T. R. Dyke, K. M. Mack, and J. S. Muenter, *J. Chem. Phys.* **66** (2001) 498–510.

113. F. N. Keutsch and R. J. Saykally, *Proc. Natl. Acad. Sci. U.S.A.* **98** (2001) 10533–10540.

114. C. J. Seliskar and R. E. Hoffmann, *J. Mol. Spectrosc.* **96** (1982) 146–155.

115. T. N. Wassermann, D. Luckhaus, and M. A. Suhm, *Phys. Chem. Chem. Phys.* **8** (2006) 2344–2348.

116. N. O. B. Lüttschwager, T. N. Wassermann, S. Coussan, and M. A. Suhm, *Phys. Chem. Chem. Phys.* **12** (2010) 8201–8207.

117. S. L. Baughcum, R. W. Duerst, W. F. Rowe, Z. Smith, and E. B. Wilson, *J. Am. Chem. Soc.* **103** (1981) 6296–6303.

118. T. D. Sewell, Y. Guo, and D. L. Thompson, *J. Chem. Phys.* **103** (1995) 8557–8565.

119. T. Taketsugu and D. J. Wales, *Mol. Phys.* **100** (2002) 2793–2806.

120. D. J. Wales, *J. Am. Chem. Soc.* **115** (1993) 11180–11190.

121. D. J. Wales, *J. Chem. Soc. Faraday. Trans.* **92** (1996) 2505–2517.

122. M. Takahashi, Y. Watanabe, T. Taketsugu, and D. J. Wales, *J. Chem. Phys.* **123** (2005) 044302.

123. M. Erakovic and M. T. Cvitas, *J. Chem. Phys.* **153** (2020) 134106.

124. J. M. Bowman, S. Carter, and X. Huang, *Int. Rev. Phys. Chem.* **22** (2003) 533–549.

125. G. Rauhut, *J. Chem. Phys.* **121** (2004) 9313–9322.

126. R. Berger, C. Fischer, and M. Klessinger, *J. Chem. Phys.* **102** (1998) 7157–7167.

127. P. R. Bunker and P. Jensen, *Molecular Symmetry and Spectroscopy, second edition.* NRC Research Press, 1998.

128. J. T. Hougen, P. R. Bunker, and J. W. C. Johns, *J. Mol. Spectrosc.* **34** (1970) 136–172.

129. J. Cioslowski, *J. Chem. Phys.* **145** (2016) 026102.

130. H. C. Longuet-Higgins, *Mol. Phys.* **6** (1962) 445–460.

131. E. A. Coutsias, C. Seok, and K. A. Dill, *J. Comput. Chem.* **25** (2004) 1849–1857.

132. C. F. F. Karney, *J. Mol. Graph. Model.* **25** (2007) 595–604.

133. W. Burnside, *Theory of Groups.* Dover, 1911.

134. S. Donkin, *J. Pure Appl. Algebra* **97** (1994) 281–301.

135. J. D. Dixon, *Num. Math.* **10** (1967) 446–450.

136. V. Babin, C. Leforestier, and F. Paesani, *J. Chem. Theory Comput.* **9** (2013) 5395–5403.

137. V. Babin, G. R. Medders, and F. Paesani, *J. Chem. Theory Comput.* **10** (2014) 1599–1607.

138. S. K. Reddy, S. C. Straight, P. Bajaj, C. Huy Pham, M. Riera, D. R. Moberg, M. A. Morales, C. Knight, A. W. Götz, and F. Paesani, *J. Chem. Phys.* **145** (2016) 194504.

139. M. R. Pastrana, A. M. Quintales, J. Brandao, and A. J. C. Varandas, *J. Chem. Phys.* **94** (1990) 8073–8080.

§ 8.   SUPPLEMENT
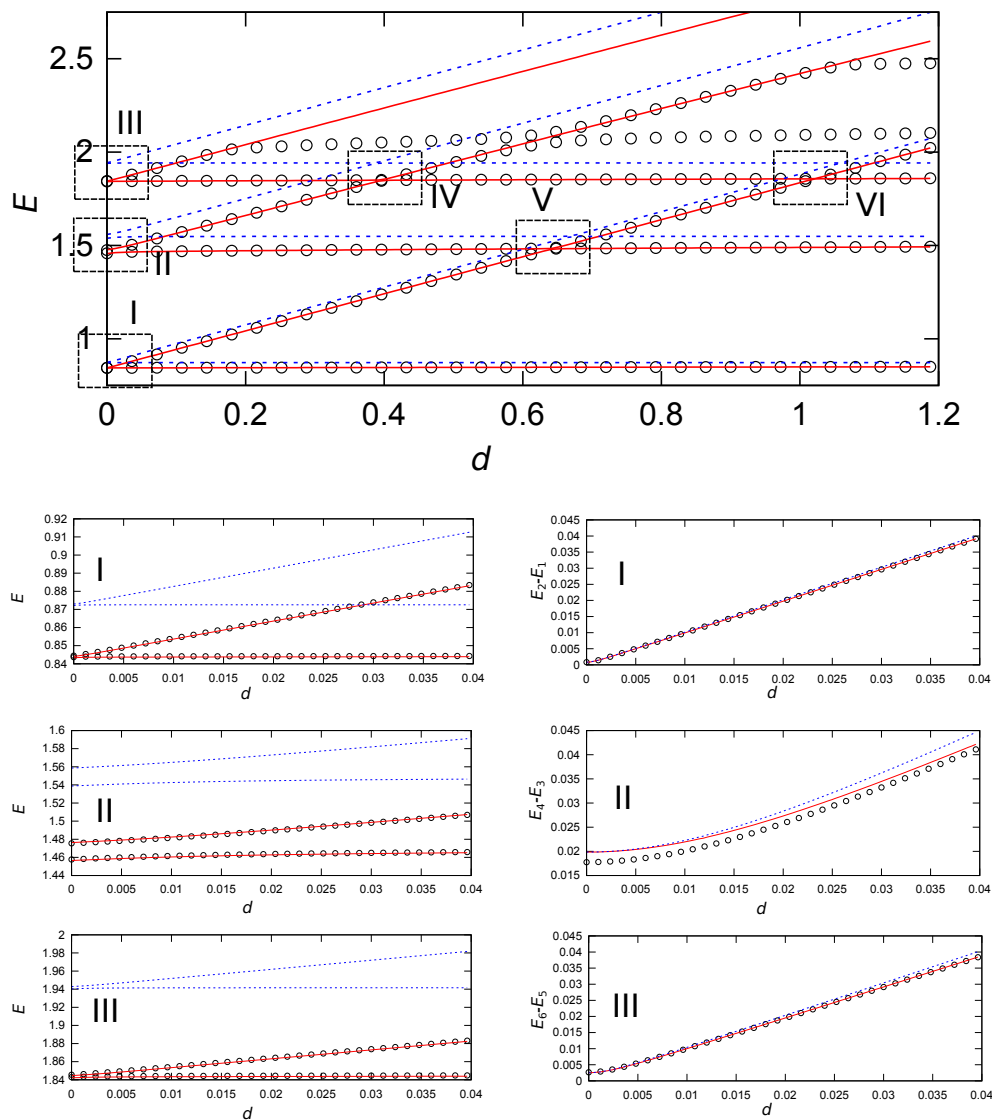
Figure S1. Dependence of vibrational energies of the lowest 6 states in the double-well potential given by (4.7) on the frequency of the energy d of the minimum (R). Circles represent quantum-mechanical values, blue lines are obtained using instanton method with harmonic energies and red lines are obtained using a combined VCI/instanton approach. Frames I-III in the top panel are shown magnified in the left column panels below, and the dependence of the associated tunneling splittings on d in the right column panels below.
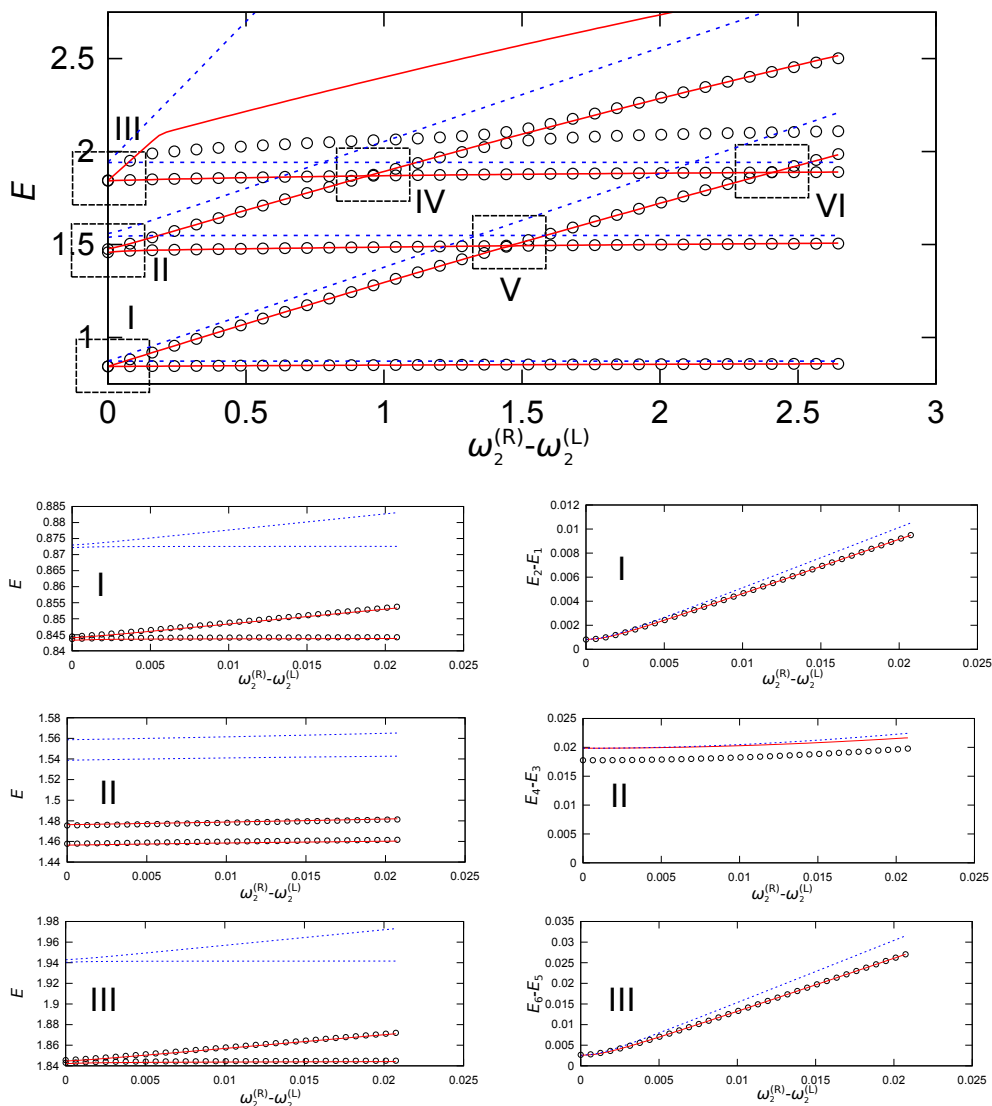
Figure S2. Dependence of vibrational energies of the lowest 6 states in the double-well potential given by (4.7) on the frequency of the higher mode $\omega_2^{(R)}$. Circles represent quantum-mechanical values, blue lines are obtained using instanton method with harmonic energies and red lines are obtained using a combined VCI/instanton approach. Frames I-III in the top panel are shown magnified in the left column panels below, and the dependence of the associated tunneling splittings on $\omega_2^{(R)}$ in the right column panels below.

Table S1. Dominant configurations of vibrational states of malonaldehyde, obtained as the eigenvectors of tunneling matrix in the 2×2 and 8×8 models.

| No.	Pairs	(8)
1	$0.707 \left|GS^{(L)}\right\rangle$ $0.707 \left|GS^{(R)}\right\rangle$	$0.704 \left|GS^{(L)}\right\rangle$ $0.704 \left|GS^{(R)}\right\rangle$
2	$0.707 \left|GS^{(L)}\right\rangle$ $-0.707 \left|GS^{(R)}\right\rangle$	$0.704 \left|GS^{(L)}\right\rangle$ $-0.704 \left|GS^{(R)}\right\rangle$
3	$0.707 \left|v_2^{(L)}\right\rangle$ $0.707 \left|v_2^{(R)}\right\rangle$	$0.688 \left|v_2^{(L)}\right\rangle$ $0.688 \left|v_2^{(R)}\right\rangle$
4	$0.707 \left|v_1^{(L)}\right\rangle$ $0.707 \left|v_1^{(R)}\right\rangle$	$0.706 \left|v_1^{(L)}\right\rangle$ $0.706 \left|v_1^{(R)}\right\rangle$
5	$0.707 \left|v_1^{(L)}\right\rangle$ $-0.707 \left|v_1^{(R)}\right\rangle$	$0.705 \left|v_1^{(L)}\right\rangle$ $-0.705 \left|v_1^{(R)}\right\rangle$
6	$0.707 \left|v_2^{(L)}\right\rangle$ $-0.707 \left|v_2^{(R)}\right\rangle$	$0.695 \left|v_2^{(L)}\right\rangle$ $-0.695 \left|v_2^{(R)}\right\rangle$
7	$0.707 \left|v_3^{(L)}\right\rangle$ $-0.707 \left|v_3^{(R)}\right\rangle$	$0.705 \left|v_3^{(L)}\right\rangle$ $-0.705 \left|v_3^{(R)}\right\rangle$
8	$0.707 \left|v_3^{(L)}\right\rangle$ $0.707 \left|v_3^{(R)}\right\rangle$	$0.704 \left|v_3^{(L)}\right\rangle$ $0.704 \left|v_3^{(R)}\right\rangle$
9	$0.707 \left|(v_2+v_2)^{(L)}\right\rangle$ $0.707 \left|(v_2+v_2)^{(R)}\right\rangle$	$0.447 \left|(v_1+v_1)^{(L)}\right\rangle$ $0.522 \left|(v_2+v_2)^{(L)}\right\rangle$ $0.447 \left|(v_1+v_1)^{(R)}\right\rangle$ $0.522 \left|(v_2+v_2)^{(R)}\right\rangle$
10	$0.707 \left|(v_1+v_1)^{(L)}\right\rangle$ $0.707 \left|(v_1+v_1)^{(R)}\right\rangle$	$0.547 \left|(v_1+v_1)^{(L)}\right\rangle$ $-0.436 \left|(v_2+v_2)^{(L)}\right\rangle$ $0.547 \left|(v_1+v_1)^{(R)}\right\rangle$ $-0.436 \left|(v_2+v_2)^{(R)}\right\rangle$
11	$0.707 \left|(v_1+v_1)^{(L)}\right\rangle$ $-0.707 \left|(v_1+v_1)^{(R)}\right\rangle$	$0.693 \left|(v_1+v_1)^{(L)}\right\rangle$ $-0.693 \left|(v_1+v_1)^{(R)}\right\rangle$
12	$0.707 \left|v_4^{(L)}\right\rangle$ $-0.707 \left|v_4^{(R)}\right\rangle$	$0.693 \left|v_4^{(L)}\right\rangle$ $-0.693 \left|v_4^{(R)}\right\rangle$
13	$0.707 \left|v_4^{(L)}\right\rangle$ $0.707 \left|v_4^{(R)}\right\rangle$	$0.693 \left|v_4^{(L)}\right\rangle$ $0.693 \left|v_4^{(R)}\right\rangle$
14	$0.707 \left|(v_1+v_2)^{(L)}\right\rangle$ $0.707 \left|(v_1+v_2)^{(R)}\right\rangle$	$0.705 \left|(v_1+v_2)^{(L)}\right\rangle$ $0.705 \left|(v_1+v_2)^{(R)}\right\rangle$
15	$0.707 \left|(v_1+v_2)^{(L)}\right\rangle$ $-0.707 \left|(v_1+v_2)^{(R)}\right\rangle$	$0.706 \left|(v_1+v_2)^{(L)}\right\rangle$ $-0.706 \left|(v_1+v_2)^{(R)}\right\rangle$
16	$0.707 \left|(v_2+v_2)^{(L)}\right\rangle$ $-0.707 \left|(v_2+v_2)^{(R)}\right\rangle$	$0.691 \left|(v_2+v_2)^{(L)}\right\rangle$ $-0.691 \left|(v_2+v_2)^{(R)}\right\rangle$

Table S2. Dominant configurations of vibrational states of partially deuterated malonaldehyde, obtained as the eigenvectors of tunneling matrix in the 2×2 and 8×8.

No.	Pairs	(8)
1	$0.953 \left\vert \mathrm{GS}^{(\mathrm{D7})} \right\rangle$ $0.303 \left\vert \mathrm{GS}^{(\mathrm{D9})} \right\rangle$	$0.946 \left\vert \mathrm{GS}^{(\mathrm{D7})} \right\rangle$ $0.313 \left\vert \mathrm{GS}^{(\mathrm{D9})} \right\rangle$
2	$-0.303 \left\vert \mathrm{GS}^{(\mathrm{D7})} \right\rangle$ $0.953 \left\vert \mathrm{GS}^{(\mathrm{D9})} \right\rangle$	$-0.316 \left\vert \mathrm{GS}^{(\mathrm{D7})} \right\rangle$ $0.946 \left\vert \mathrm{GS}^{(\mathrm{D9})} \right\rangle$
3	$0.826 \left\vert v_2^{(\mathrm{D7})} \right\rangle$ $0.564 \left\vert v_2^{(\mathrm{D9})} \right\rangle$	$0.797 \left\vert v_2^{(\mathrm{D7})} \right\rangle$ $0.560 \left\vert v_2^{(\mathrm{D9})} \right\rangle$
4	$0.919 \left\vert v_1^{(\mathrm{D7})} \right\rangle$ $0.394 \left\vert v_1^{(\mathrm{D9})} \right\rangle$	$0.914 \left\vert v_1^{(\mathrm{D7})} \right\rangle$ $0.401 \left\vert v_1^{(\mathrm{D9})} \right\rangle$
5	$-0.394 \left\vert v_1^{(\mathrm{D7})} \right\rangle$ $0.919 \left\vert v_1^{(\mathrm{D9})} \right\rangle$	$-0.403 \left\vert v_1^{(\mathrm{D7})} \right\rangle$ $0.909 \left\vert v_1^{(\mathrm{D9})} \right\rangle$
6	$-0.564 \left\vert v_2^{(\mathrm{D7})} \right\rangle$ $0.826 \left\vert v_2^{(\mathrm{D9})} \right\rangle$	$-0.573 \left\vert v_2^{(\mathrm{D7})} \right\rangle$ $0.794 \left\vert v_2^{(\mathrm{D9})} \right\rangle$
7	$0.990 \left\vert v_3^{(\mathrm{D7})} \right\rangle$ $-0.139 \left\vert v_3^{(\mathrm{D9})} \right\rangle$	$0.984 \left\vert v_3^{(\mathrm{D7})} \right\rangle$ $-0.138 \left\vert v_3^{(\mathrm{D9})} \right\rangle$
8	$0.139 \left\vert v_3^{(\mathrm{D7})} \right\rangle$ $0.990 \left\vert v_3^{(\mathrm{D9})} \right\rangle$	$0.138 \left\vert v_3^{(\mathrm{D7})} \right\rangle$ $0.987 \left\vert v_3^{(\mathrm{D9})} \right\rangle$
9	$0.566 \left\vert (v_1+v_1)^{(\mathrm{D7})} \right\rangle$ $0.824 \left\vert (v_1+v_1)^{(\mathrm{D9})} \right\rangle$	$0.505 \left\vert (v_1+v_1)^{(\mathrm{D7})} \right\rangle$ $0.293 \left\vert (v_2+v_2)^{(\mathrm{D7})} \right\rangle$ $0.761 \left\vert (v_1+v_1)^{(\mathrm{D9})} \right\rangle$ $-0.233 \left\vert (v_2+v_2)^{(\mathrm{D9})} \right\rangle$
10	$0.824 \left\vert (v_1+v_1)^{(\mathrm{D7})} \right\rangle$ $-0.566 \left\vert (v_1+v_1)^{(\mathrm{D9})} \right\rangle$	$0.830 \left\vert (v_1+v_1)^{(\mathrm{D7})} \right\rangle$ $-0.543 \left\vert (v_1+v_1)^{(\mathrm{D9})} \right\rangle$
11	$0.784 \left\vert (v_2+v_2)^{(\mathrm{D7})} \right\rangle$ $0.621 \left\vert (v_2+v_2)^{(\mathrm{D9})} \right\rangle$	$0.354 \left\vert v_4^{(\mathrm{D7})} \right\rangle$ $0.626 \left\vert (v_2+v_2)^{(\mathrm{D7})} \right\rangle$ $-0.349 \left\vert (v_1+v_1)^{(\mathrm{D9})} \right\rangle$ $0.537 \left\vert (v_2+v_2)^{(\mathrm{D9})} \right\rangle$
12	$0.975 \left\vert v_4^{(\mathrm{D7})} \right\rangle$ $-0.222 \left\vert v_4^{(\mathrm{D9})} \right\rangle$	$0.895 \left\vert v_4^{(\mathrm{D7})} \right\rangle$ $-0.299 \left\vert (v_2+v_2)^{(\mathrm{D7})} \right\rangle$ $-0.262 \left\vert v_4^{(\mathrm{D9})} \right\rangle$ $-0.161 \left\vert (v_2+v_2)^{(\mathrm{D9})} \right\rangle$
13	$0.222 \left\vert v_4^{(\mathrm{D7})} \right\rangle$ $0.975 \left\vert v_4^{(\mathrm{D9})} \right\rangle$	$0.236 \left\vert v_4^{(\mathrm{D7})} \right\rangle$ $0.961 \left\vert v_4^{(\mathrm{D9})} \right\rangle$
14	$0.782 \left\vert (v_1+v_2)^{(\mathrm{D7})} \right\rangle$ $0.624 \left\vert (v_1+v_2)^{(\mathrm{D9})} \right\rangle$	$0.778 \left\vert (v_1+v_2)^{(\mathrm{D7})} \right\rangle$ $0.622 \left\vert (v_1+v_2)^{(\mathrm{D9})} \right\rangle$
15	$-0.624 \left\vert (v_1+v_2)^{(\mathrm{D7})} \right\rangle$ $0.782 \left\vert (v_1+v_2)^{(\mathrm{D9})} \right\rangle$	$-0.623 \left\vert (v_1+v_2)^{(\mathrm{D7})} \right\rangle$ $0.780 \left\vert (v_1+v_2)^{(\mathrm{D9})} \right\rangle$
16	$-0.621 \left\vert (v_2+v_2)^{(\mathrm{D7})} \right\rangle$ $0.784 \left\vert (v_2+v_2)^{(\mathrm{D9})} \right\rangle$	$-0.612 \left\vert (v_2+v_2)^{(\mathrm{D7})} \right\rangle$ $0.764 \left\vert (v_2+v_2)^{(\mathrm{D9})} \right\rangle$

Table S3. Character table for $G_{16} = G_2 \otimes G_2 \otimes G_2 \otimes C_s$ group. Another 8 classes are not given in the table, but are obtained by applying inversion E^* to the classes that are given. The characters of all "+" irreps for them are the same as the characters of the corresponding classes given in the table. Eight irreps of "−" species have identical characters to the corresponding "+" species for classes given in the table and the characters of opposite sign to "+" species for the classes that involve inversion.

	E	(56)	(34)	(56)(34)	(12)	(56)(12)	(34)(12)	(56)(34) (12)
A_1^+	1	1	1	1	1	1	1	1
A_2^+	1	1	−1	−1	1	1	−1	−1
A_3^+	1	−1	1	−1	1	−1	1	−1
A_4^+	1	−1	−1	1	1	−1	−1	1
B_1^+	1	1	1	1	−1	−1	−1	−1
B_2^+	1	1	−1	−1	−1	−1	1	1
B_3^+	1	−1	1	−1	−1	1	−1	1
B_4^+	1	−1	−1	1	−1	1	1	−1

Table S4. Tunnelling-splitting pattern of $D_2O(H_2O)_2$ on MB-pol PES.[136–138] The energies are given relative to the pseudorotational flip states $1-6$. Symmetry labels correspond to irreps of G_{16} group, with the corresponding spin weights given as superscripts.

$D_2O(H_2O)_2$	E/cm^{-1}	$D_2O(H_2O)_2$	E/cm^{-1}
6	14675.59	5	14653.86
$^{18}A_3^-$	$1.07(-3)$	$^{9}B_3^+$	$2.53(-3)$
$^{9}B_3^-$	$1.01(-3)$	$^{18}A_3^+$	$2.45(-3)$
$^{6}A_1^-$	$3.90(-4)$	$^{3}B_1^+$	$3.41(-4)$
$^{3}B_1^-$	$3.30(-4)$	$^{6}A_1^+$	$2.62(-4)$
$^{54}A_4^-$	$-3.30(-4)$	$^{27}B_4^+$	$-2.62(-4)$
$^{27}B_4^-$	$-3.90(-4)$	$^{54}A_4^+$	$-3.41(-4)$
$^{18}A_2^-$	$-1.01(-3)$	$^{9}B_2^+$	$-2.45(-3)$
$^{9}B_2^-$	$-1.07(-3)$	$^{18}A_2^+$	$-2.53(-3)$
4	14617.81	3	14576.11
$^{3}B_1^+$	$2.80(-3)$	$^{6}A_1^-$	$1.56(-2)$
$^{6}A_1^+$	$2.74(-3)$	$^{3}B_1^-$	$1.55(-2)$
$^{9}B_2^+$	$1.65(-3)$	$^{18}A_2^-$	$4.75(-3)$
$^{18}A_2^+$	$1.60(-3)$	$^{9}B_2^-$	$4.68(-3)$
$^{9}B_3^+$	$-1.60(-3)$	$^{18}A_3^-$	$-4.68(-3)$
$^{18}A_3^+$	$-1.65(-3)$	$^{9}B_3^-$	$-4.75(-3)$
$^{27}B_4^+$	$-2.74(-3)$	$^{54}A_4^-$	$-1.55(-2)$
$^{54}A_4^+$	$-2.80(-3)$	$^{27}B_4^-$	$-1.56(-2)$
2	14533.21	1	14513.24
$^{18}A_3^-$	$5.85(-3)$	$^{27}B_4^+$	$2.01(-2)$
$^{9}B_3^-$	$5.34(-3)$	$^{54}A_4^+$	$1.96(-2)$
$^{6}A_1^-$	$1.12(-3)$	$^{9}B_2^+$	$3.05(-3)$
$^{3}B_1^-$	$6.12(-4)$	$^{18}A_2^+$	$2.53(-3)$
$^{54}A_4^-$	$-6.11(-4)$	$^{9}B_3^+$	$-2.53(-3)$
$^{27}B_4^-$	$-1.12(-3)$	$^{18}A_3^+$	$-3.05(-3)$
$^{18}A_2^-$	$-5.34(-3)$	$^{3}B_1^+$	$-1.96(-2)$
$^{9}B_2^-$	$-5.85(-3)$	$^{6}A_1^+$	$-2.01(-2)$

§ 9.   CURRICULUM VITAE

Opći podaci

Ime i prezime: Mihael Eraković

Datum rođenja: 18. svibnja 1994.

Mjesto rođenja: Rijeka, Hrvatska

Obrazovanje

2014. – 2017.   **Preddiplomski studij kemije**
Sveučilište u Zagrebu, Prirodoslovno-matematički fakultet

2017. – 2018.   **Diplomski studij kemije**
Sveučilište u Zagrebu, Prirodoslovno-matematički fakultet
Smjer: istraživački, grane: fizikalna i anorganska kemija

2018. – 2022.   **Doktorski studij kemije**
Sveučilište u Zagrebu, Prirodoslovno-matematički fakultet
grana: Fizikalna kemija

Radno iskustvo

2018. –   **Asistent**
Institut Ruđer Bošković, Grupa za teorijsku kemiju, Zavod za fizičku kemiju

Nastavne aktivnosti

2020. – 2022.   **Seminar**
Sveučilište u Zagrebu, Prirodoslovno-matematički fakultet
Diplomski studij kemije
Kolegij *Kvantna kemija*

2018. – 2020.   **Praktikumske vježbe**
Sveučilište u Zagrebu, Prirodoslovno-matematički fakultet
Preddiplomski studij kemije
Kolegiji *Praktikum fizikalne kemije 1*

Nagrade

2020. Nagrada Zavoda za fizičku kemiju za najbolje znanstvene radove objavljene u 2019. godini

2021. Nagrada za najbolji poster na konferenciji CECAM Flagship School "Path Integral Quantum Mechanics:From the Basics to the Latest Developments"

Znanstvene publikacije

1. M. Eraković, M. Cvitaš, *J. Chem. Theory Comput.* **18** (2022) 2785 – 2802.

2. N. Bedeković, T. Piteša, M. Eraković, V. Stilinović, D. Cinčić, *Cryst. Growth Des.* **22** (2022) 2644–2653.

3. M. Eraković, M. Cvitaš, *Phys. Chem. Chem. Phys.* **23** (2021) 4240–4254.

4. M. Eraković, M. Cvitaš, *J. Chem. Phys.* **153** (2020) 134106.

5. M. Eraković, C. L. Vaillant, M. Cvitaš, *J. Chem. Phys.* **152** (2020) 084111.

6. M. Eraković, D. Cinčić, K. Molčanov, V. Stilinović, *Angewandte Chemie* **58** (2019) 15702–15706.

7. M. Eraković, V. Nemec, T. Lež, I. Porupski, V. Stilinović, D. Cinčić, *Crystal Growth & Design* **18** (2018) 1182–1190.

Odabrana konferencijska priopćenja

1. Kratko usmeno priopćenje: 'Tunnelling splittings of vibrationally excited states via instanton approach', *Les Houches Workshop: Quantum Dynamics & Spectroscopy of Molecular Materials and Biological Photosystems*, 3.5. – 7.5.2021.

2. Postersko priopćenje: 'Vibrational spectrum of asymmetric well systems using a combination of VCI and instanton theory', *CECAM Flagship School 'Path Integral Quantum Mechanics:From the Basics to the Latest Developments'*, 14.6. – 18.6. 2021.

3. Usmeno priopćenje: 'Combined VCI and instanton approach for computation of vibrational spectrum in asymmetric well systems', 52nd *Conference of the European Group on Atomic Systems (EGAS)*, 6.7. – 8.7. 2021.

4. Usmeno priopćenje: 'Instanton theory for computation of tunneling splittings in excited vibrational states and asymmetric systems', *Workshop on Theoretical Chemistry, Exploring Chemical Space*, 23.2. – 26.2. 2021.